



BRNO UNIVERSITY OF TECHNOLOGY

VYSOKÉ UČENÍ TECHNICKÉ V BRNĚ

FACULTY OF CHEMISTRY

FAKULTA CHEMICKÁ

**INSTITUTE OF CHEMISTRY AND TECHNOLOGY OF
ENVIRONMENTAL PROTECTION**

ÚSTAV CHEMIE A TECHNOLOGIE OCHRANY ŽIVOTNÍHO PROSTŘEDÍ

**DEGRADATION OF HEAT TRANSFER FLUIDS IN
THERMAL SOLAR SYSTEMS AND PROPANE-1,3-DIOL AS
A NEW OPTION**

STÁRNUTÍ TEPLONOSNÝCH KAPALIN V TERMICKÝCH SOLÁRNÍCH SYSTÉMECH A PROPAN-1,3-DIOL
JAKO NOVÁ MOŽNOST

DOCTORAL THESIS

DIZERTAČNÍ PRÁCE

AUTHOR

AUTOR PRÁCE

Ing. František Mikšík

SUPERVISOR

ŠKOLITEL

prof. Ing. Josef Čáslavský, CSc.

BRNO 2018

Zadání dizertační práce

Ústav: Ústav chemie a technologie ochrany životního prostředí
Student: **Ing. František Mikšík**
Studijní program: Chemie a technologie ochrany životního prostředí
Studijní obor: Chemie životního prostředí
Vedoucí práce: **prof. Ing. Josef Čáslavský, CSc.**
Akademický rok: 2017/18

Název dizertační práce:

Stárnutí teplotnosných kapalin v termických solárních systémech a propan–1,3–diol jako nová možnost

Zadání dizertační práce:

1. Dlouhodobé sledování a analýza provozu experimentálního termického solárního systému.
2. Identifikace procesů stárnutí teplotnosných kapalin na bázi glykolů v termických solárních systémech, určení a charakterizace produktů degradace.
3. Analýza fyzikálních vlastností binární směsi propan–1,3–diolu s vodou.
4. Propan–1,3–diol jako moderní nemrznoucí teplotnosná kapalina.

Termín odevzdání dizertační práce: 8.6.2018

Ing. František Mikšík
student(ka)

prof. Ing. Josef Čáslavský, CSc.
vedoucí práce

doc. Ing. Jirí Kučerík, Ph.D.
vedoucí ústavu

V Brně dne 1.9.2017

prof. Ing. Martin Weiter, Ph.D.
děkan

ABSTRACT

Degradation of heat transfer fluids on an organic basis is a long-standing problem known since the beginning of their use. The first part of this dissertation is devoted to a case study of a functional experimental system that was filled with a propan-1,2-diol based heat transfer fluid upon construction and had been observed for a period of 7 years. Analysis of the fluid aging in this system was conducted by following the basic operating characteristics of the fluid, such as density, viscosity, freezing temperature, pH and metals content. Through these properties, the aging of the fluid was tracked indirectly. Direct observation of the degradation process was then performed by analysis of degradation products such as organic acids formation and changes in the composition of the mixture by isotachophoresis and mass spectrometry. For comparison, selected samples from several other systems filled with identical liquid with an evidently advanced form of degradation were also analysed. The second part of this thesis presents the basic physicochemical properties of aqueous propane-1,3-diol mixtures and their analytical evaluation and mathematical modelling for universal use as a new basis for antifreeze heat transfer fluid. Based on available information, the usability of this mixture is assessed. The advantage of propane-1,3-diol is seen mainly in the renewable production and certain physical and chemical properties, which outweigh the glycols used up to now in several areas.

ABSTRAKT

Stárnutí teplotnosných kapalin na organické bázi je dlhodobým problémom, ktorý je známy od počiatku ich používania. Prvá časť tejto dizertačnej práce je tak venovaná prípadovej štúdiu funkčného experimentálneho systému, ktorý bol ako nový naplnený teplotnosnou kapalinou na bázi propan-1,2-diol a pozorovaný po období 7 rokov. Pre analýzu stárnutia kapaliny v tomto systéme boli sledované základné provozní vlastnosti kapaliny ako sú hustota, viskozita, teplota tuhnutia, pH a obsah kovů. Skrz tieto vlastnosti tak bolo sledované stárnutie kapaliny nepriamo. Priame sledovanie stárnutia bolo posléze provedeno analýzou degradačných produktů, ako sú organické kyseliny a zmeny ve složení směsi pomocí izotachofórey a hmotnostní spektrometrie. Pro srovnání byly také analyzovány vybrané vzorky z několika dalších systémů plněných identickou kapalinou s prokazatelně pokročilou formou degradace. V druhé části práce jsou představeny základní fyzikálně-chemické vlastnosti směsi propan-1,3-diolu s vodou a jejich analytické hodnocení a matematické modelování pro univerzální použití jakožto nového základu pro nemrznoucí teplotnosné kapaliny. Na základě dostupných informací je pak hodnocena použitelnost této směsi. Výhoda propan-1,3-diolu je spatřována především ve výrobě z obnovitelných zdrojů a v některých fyzikálních a chemických vlastnostech, které dle dosavadních poznatků předčívají doposud používané glykolové směsi.

KEYWORDS

Heat transfer fluid; Antifreeze; Degradation; Thermal solar system; Propane-1,3-diol; Physicochemical properties

KLÍČOVÁ SLOVA

Teplotnosná kapalina; Nemrznoucí kapalina; Degradace; Termický solární systém; Propan-1,3-diol; Fyzikálně-chemické vlastnosti

MIKŠÍK, F. *Degradation of heat transfer fluids in thermal solar systems and propane-1,3-diol as a new option*. Brno: Brno University of Technology, Faculty of chemistry, 2018. 190 p. Supervisor of the doctoral thesis prof. Ing. Josef Čáslavský, CSc.

DECLARATION

Prohlašuji, že jsem tuto disertační práci vypracoval samostatně a že všechny použité literární zdroje jsem správně a úplně citoval. Disertační práce je z hlediska obsahu majetkem Fakulty chemické VUT v Brně a může být využita ke komerčním účelům jen se souhlasem školitele a děkana FCH VUT.

I declare that I have finished this doctoral thesis by myself and all the literature references are fully and correctly cited. The content of this doctoral thesis is a property of Faculty of Chemistry of Brno University of Technology and can be used commercially only with the consent of the supervisor of this thesis or the dean of the Faculty of Chemistry of Brno University of Technology.

.....
Podpis doktoranda / Sign of the Ph.D. student

ACKNOWLEDGEMENT

I would like to express my gratitude to my supervisor professor Čáslavský for valuable comments and advises for this thesis. My gratitude also belongs to my supervisor specialist Dr. Kotlík who had the patience to accept me under his wings and stayed with me until the very end.

CONTENT

1 INTRODUCTION	7
2 WORK OBJECTIVES	8
3 STATE OF THE ART	9
3.1 ENERGY SOURCES – RENEWABLE ENERGY SOURCES.....	9
3.1.1 <i>Planetary forces and movement</i>	10
3.1.2 <i>Nuclear energy</i>	11
3.1.3 <i>Solar energy – solar radiation</i>	12
3.2 TECHNOLOGIES FOR DIRECT USE OF SOLAR ENERGY	13
3.2.1 <i>Generating electricity</i>	13
3.2.2 <i>Generating thermal energy</i>	15
3.3 THERMAL SOLAR SYSTEMS	15
3.3.1 <i>Types of solar systems</i>	17
3.3.2 <i>Basic Components</i>	18
3.3.3 <i>Additional components</i>	23
4 THEORETICAL BACKGROUND	24
4.1 OVERVIEW OF HEAT TRANSFER FLUID IN THERMAL SOLAR SYSTEMS	24
4.1.1 <i>Air</i>	24
4.1.2 <i>Water</i>	24
4.1.3 <i>HTFs based on silicon oils</i>	24
4.1.4 <i>HTFs based on hydrocarbon oils</i>	25
4.1.5 <i>HTFs based on mono-alcohols</i>	25
4.2 HEAT TRANSFER FLUIDS BASED ON DIOLS	25
4.2.1 <i>Ethane-1,2-diol (CAS 107-21-1)</i>	27
4.2.2 <i>Propane-1,2-diol (CAS 57-55-6)</i>	27
4.2.3 <i>Propane-1,3-diol (CAS 504-63-2)</i>	27
4.2.4 <i>Propane-1,2,3-triol (CAS 56-81-5)</i>	27
4.2.5 <i>Ternary glycerol mixtures</i>	28
4.3 PROPERTIES OF HEAT TRANSFER FLUIDS IN THE THERMAL SOLAR SYSTEMS.....	28
4.3.1 <i>Desired properties</i>	28
4.3.2 <i>Physical properties</i>	29
4.3.3 <i>Flammability</i>	32
4.3.4 <i>Corrosion</i>	32
4.3.5 <i>Compatibility with sealing materials</i>	35
4.3.6 <i>Chemical and thermal stability</i>	35
4.3.7 <i>Environmental aspects</i>	35
4.3.8 <i>Production and applications</i>	36
4.4 AGEING OF HEAT TRANSFER FLUIDS IN TSS.....	38
4.4.1 <i>Acidic degradation of aqueous glycol mixtures</i>	38
4.4.2 <i>Stagnation process</i>	38
4.5 PROPANE-1,3-DIOL	40
4.5.1 <i>Basic physical and chemical properties</i>	41
4.5.2 <i>Production</i>	41
4.5.3 <i>Reactivity and degradability</i>	42
5 EXPERIMENT	43

5.1	SAMPLES AND THEIR PREPARATION.....	43
5.1.1	<i>Samples for estimation of ageing processes</i>	43
5.1.2	<i>Samples of propane-1,3-diol</i>	45
5.2	USED CHEMICALS AND MATERIALS.....	45
5.3	USED EQUIPMENT	48
5.4	METHODS	49
5.4.1	<i>Ageing of the heat transfer media and determination of degradation products</i>	49
5.4.2	<i>Analysis of properties of aqueous propane-1,3-diol</i>	50
5.4.3	<i>Isotachophoresis</i>	50
5.4.4	<i>Mass spectrometry</i>	53
5.4.5	<i>Karl Fisher Volumetric Titration</i>	57
5.4.6	<i>Atomic absorption spectroscopy</i>	59
5.4.7	<i>Determination of pH</i>	62
5.4.8	<i>Determination of conductivity</i>	64
5.4.9	<i>Density</i>	65
5.4.10	<i>Viscosity</i>	67
5.4.11	<i>Refractive index measurement</i>	73
5.4.12	<i>Freezing point measurement</i>	75
5.4.13	<i>Corrosivity quantification</i>	77
5.5	AUTOMATIC UBBELOHDE VISCOMETER.....	79
5.5.1	<i>Design</i>	79
6	RESULTS AND DISCUSSION.....	81
6.1	AGEING OF ANTIFREEZE MIXTURES BASED ON PROPANE-1,2-DIOL.....	81
6.1.1	<i>Long-term observation of experimental system in Vracov</i>	81
6.1.2	<i>Acidification of hydroxy groups in propane-1,2-diol based mixtures</i>	90
6.1.3	<i>Inhibitor additives depletion and other degradation products</i>	103
6.1.4	<i>Polymerization of propane-1,2-diol based mixtures?</i>	114
6.2	AQUEOUS PROPANE-1,3-DIOL CHARACTERISTICS	119
6.2.1	<i>Density</i>	119
6.2.2	<i>Viscosity</i>	125
6.2.3	<i>Refractive index</i>	139
6.2.4	<i>Freezing point</i>	142
6.3	HEAT TRANSFER FLUID BASED ON PROPANE-1,3-DIOL	143
6.3.1	<i>Thermal degradation processes</i>	143
6.3.2	<i>Corrosivity properties</i>	144
6.3.3	<i>Perspectives of utilisation of propane-1,3-diol as a novel antifreeze additive</i>	145
7	CONCLUSION.....	148
8	LITERATURE CITED.....	151
9	SYMBOLS, UNITS AND ABBREVIATIONS	172
9.1	SYMBOLS AND UNITS	172
9.2	ABBREVIATIONS.....	173
10	LISTS OF TABLES AND FIGURES	175
10.1	LIST OF TABLES	175
10.2	LIST OF FIGURES	176
11	LIST OF APPENDICES	179
12	APPENDICES.....	180

1 INTRODUCTION

Renewable energy sources (RES) continuously increase their share of primary energy sources due to the known limitations associated with exhaustible quantities of fossil fuels. The goal of developed countries thus largely lies in a diversification of basic energy sources and a gradual transition to renewable energy sources which will be able to ensure energy stability and self-sufficiency in the long run. This progress is further enhanced by social awareness and social pressure that places more and more emphasis on the environmental aspects of energy production and its use.

Similarly to fossil fuels, individual countries have limited prerequisites for the use of various RES, and of course, the Czech Republic is no exception. The location of the Czech Republic in the middle of Europe has a significant impact on the quantity and composition of RES which we are able to use efficiently on the basis of current technological state. For example, RES such as geothermal energy is virtually unusable on any larger scale in our location and it is limited to small-sized heat pumps. Situation is not better even in the case of harnessing wind power. The so-called wind farms can be built in our country with efficient energy gain only in carefully selected elevated locations where the air flow - wind throughout the year is sufficient. In the case of hydropower, we are again limited by the size of the rivers, which only spring in our country and then flow to other countries, and the volume of precipitation and suitable locations for their construction. Solar energy, however, can be used to some extent practically everywhere in the whole country.

But, even though the Sun shines evenly on the whole planet, the northern location of our country and a small number of actual sunny days in the year place great demands on the efficiency of solar technologies. In late years large areas of photovoltaic panels have been put into operation in the Central Europe, however, without generous state subsidies and guaranteed tariffs their operation would not be economically feasible. Therefore, we are forced to supplement their operation with other economic activities. The situation is slightly different in the case of modern thermal solar systems, when even in our conditions we can achieve energy outputs and results that are able to ensure the economic profitability of these systems. Nevertheless, this technology does not allow universal use in all locations and cases in our region and it is always necessary to assess the individual intended application. To expand this technology to environments where it has not yet been economically viable, further research is needed to improve its efficiency and usability and to increase its attractiveness as a modern renewable energy resource which will be able to compete with conventional energy sources. This work is focused on the heat transfer fluid which is responsible for transferring the thermal energy (heat) collected by the solar collectors to the place of consumption or accumulation. The main problem which will be discussed is the chemical stability of this fluid and possible alternative to the commonly used media.

2 WORK OBJECTIVES

- (1) Monitoring of experimental thermal solar system over long-period of time and its analysis.
- (2) Identifying principles for aging of heat transfer fluids based on glycols in solar thermal systems and the determination and description of degradation products.
- (3) Analysis of physical properties of propane-1,3-diol binary mixture with water.
- (4) Assessment of propane-1,3-diol in the context of modern antifreeze heat transfer fluid.

3 STATE OF THE ART

3.1 Energy sources – Renewable energy sources

The structure of energy is related to their source and use. From this perspective, we divide energy resources into renewable, non-renewable, exhaustible and inexhaustible. The terms themselves are fairly self-explanatory. Renewable sources of energy are sources of energy which are replenished over a time and can be used continuously or repeatedly. In this category we include solar energy, wind energy, hydropower and biomass/bioenergy. The non-renewable sources of energy are group which consists of energy sources which are not replenished over a time and sooner or later we will hit the bottom of their exploitation and run out with them. In this category we include all fossil fuels and nuclear fission materials. This category dividing system is sometimes expanded by subcategories as exhaustible and inexhaustible. Though similar in meaning, the significance of these terms lies more in the future and is more connected to the existence and capabilities of human species and sustainable development. In this manner, not all renewable sources of energy are considered inexhaustible and not all of the non-renewable sources of energy are exhaustible.

For example though biomass like trees is renewable, it is also, in case we chop off all the trees in the world, exhaustible^{1,2}, and non-renewable source, like nuclear fission materials, is in its practical manner of human existence inexhaustible³.

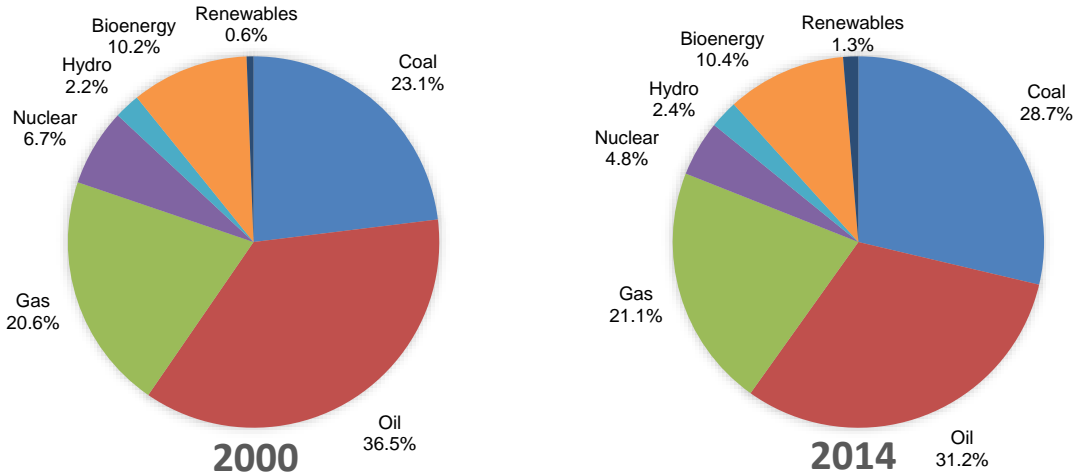


Fig. 3-1 Primary energy sources by fuel - global composition 2000 and 2014⁴.

The majority of the resources currently used are fossil fuels, which, in terms of the existence of the human species, are perceived as exhaustible, and above all non-renewable. Primary energy fuel global mix is shown on Fig. 3-1, and on Fig. 3-2 we can see the composition of primary energy sources used as source for producing electricity. The primary energy consumption in 2000 was around 10 043 Mtoe⁴ (420 480 PJ) and by the 2014 it rose to over 30 % to 13 684 Mtoe⁴ (572 922 PJ) and is steadily growing. A simple comparison of the graphs on Fig. 3-1 and Fig. 3-2 shows how large the difference between the structure of primary sources of energy and the production of electrical energy actually is, and how much we are dependant on the fossil fuels. The avoidance of the use of the word “still” in this context is deliberate, because except hydrogenation we are not any closer to be independent on the fossils fuels in the near future, whatsoever. Though the situation is significantly better in the case of

electricity generation, it is necessary to add that electricity represents only around 18.5 % (for 2015)⁴⁻⁶ of all the energy consumed in the world.

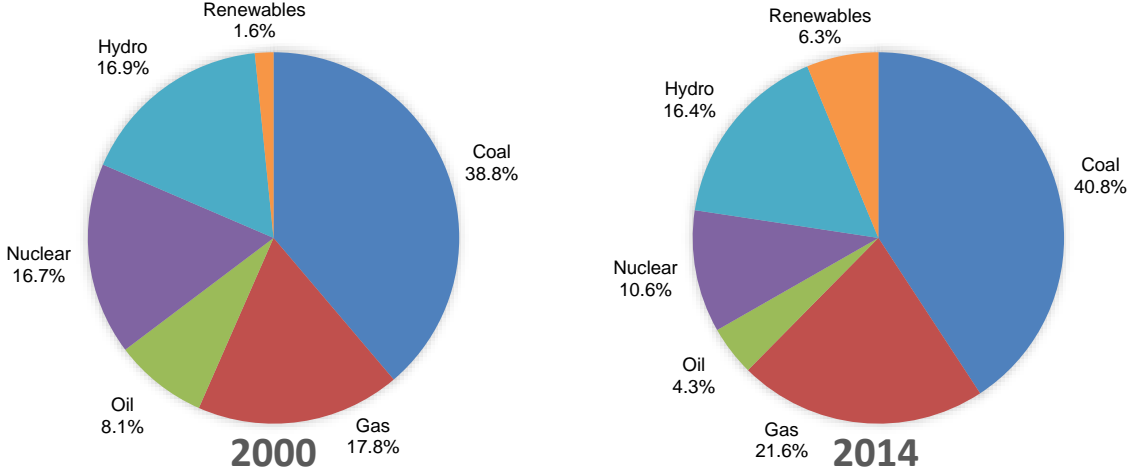


Fig. 3-2 Electricity sources - global composition⁴.

The currently used energy sources can be divided into three basic categories based on their origin as it is shown on Fig. 3-3.

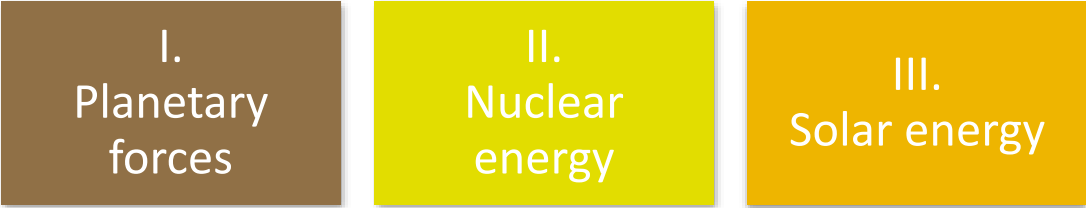


Fig. 3-3 Energy sources by their origin

3.1.1 Planetary forces and movement

Relatively interesting group consists of energy sources using the energy of planets, which can be divided according to the principle of origin to energy obtained from the motion of planets or the thermal energy of the planetary cores. Geothermal energy has been known since ancient times and thermal baths in the wild are also used by animals. The origin lies in the formation of our planetary system, though the continuous energy flow from the inside of the planet is sustained by radioactive decay⁷.

Although the planetary forces and energy are available from the entire surface of our planet, the problem remains in the concentration of this energy. To exploit the gravitational forces of the Moon and the Sun, the only option is oceans and seas where this energy is concentrated in the form of potential energy of a huge amount of water that moves around. Unfortunately, this applies only to coastal regions.

Geothermal energy is available everywhere on the mainland, however, there is again the problem of its concentration., This energy can be effectively used only in areas of current or past volcanic activity.

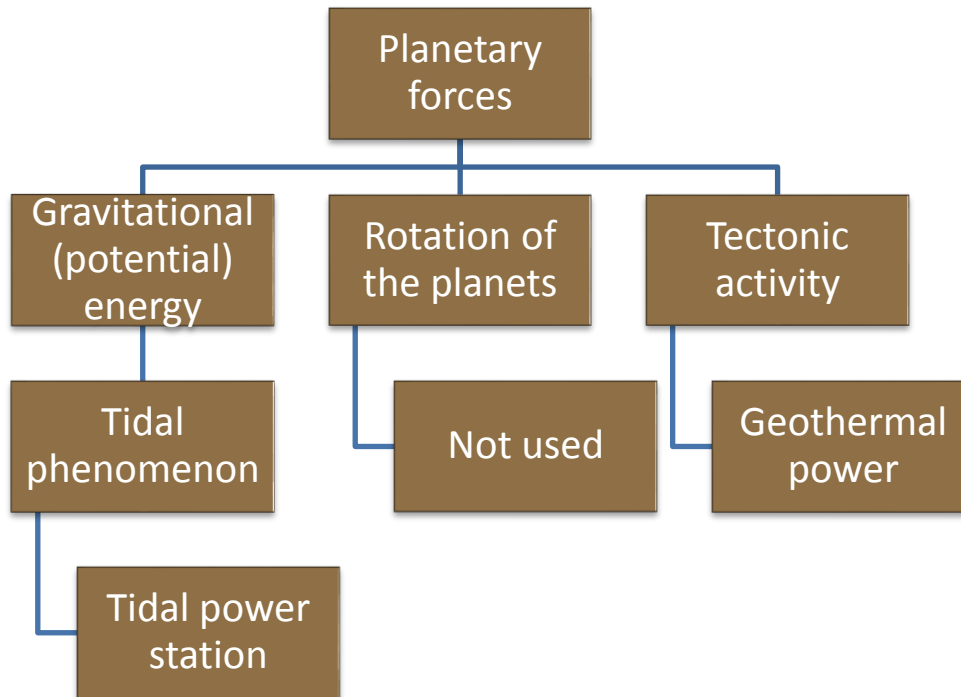


Fig. 3-4 Structure and use of planetary forces

3.1.2 Nuclear energy

Nuclear energy is the most concentrated energy source today. Obtaining energy from nuclear reactions can theoretically be divided into three processes, as shown on Fig. 3-5. At present, only nuclear fission is used in nuclear power plants and nuclear fusion is being experimented.

Although nuclear fusion technology is still in its infancy (even after several decades), the first steps to fully master this technology have already been taken. At present (2018), the largest TOKAMAK type (from Russian TORoidal'naya KAMERA s MAGnitnymi Katushkami) fusion reactor named ITER⁸ is being prepared to be the first reactor to burn hydrogen isotopes with a positive energy gain. The reactor is to be completed in 2021 and its experimental operation from 2025 is to confirm the basic assumptions for the first commercial reactors of the same type. If everything progress according to plan, it is assumed to start operating the first DEMO⁹ power supply fusion reactor by 2050.

The study on cold fusion, or LENR (Low-energy nuclear reactions) could be also perceived as highly interesting. Cold fusion is in general the same as the normal fusion, but due to much lower operating temperatures of up to 1 000 K (in TOKAMAK reactors the temperature of the reaction mixture is hundreds of millions of kelvin), it should be much safer. Its theoretical disadvantage is much lower conversion rate and hence much lower operating performance per unit weight of reactive substance. This makes this technology particularly suitable for small personal power plants. However, only a handful of scientists are interested in cold fusion and even when cold fusion is also studied in organizations such as NASA, the funds spent on cold fusion research are very small as well as the related scientific advances. Recently, however, the world scientific circles dealing with nuclear power had been shaken by the commercial project E-CAT^{10,11} from the workshop of inventor Andrea Rossi and his former colleague scientist Sergio Focardia (1932-2013). E-CAT is supposed to be a compact domestic appliance with a capacity of several kW of thermal energy and power consumption of up to 1 kW of electricity.

Its successor is then a power container with a capacity of 1 MW of electric power. The problem of this particular example of LENR technology remains, as with the rest of the LENR research, that the principle of its functioning has not yet been satisfactorily clarified. It is therefore a matter of time before this technology is proved to be a new breakthrough reality in the energy industry, or it will be rejected as another dysfunctional fraud¹².

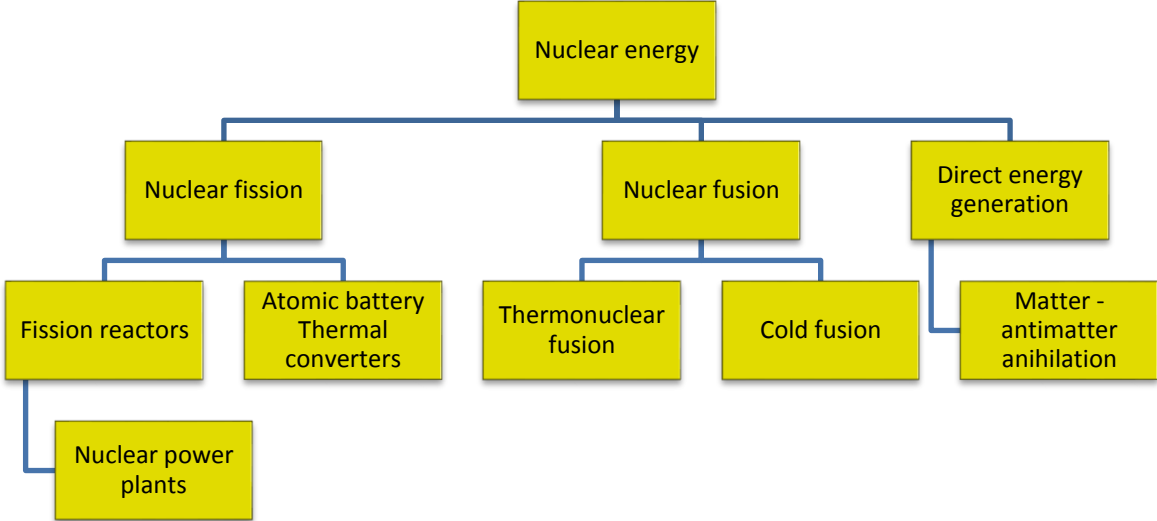


Fig. 3-5 Structure and use of nuclear energy

The last mentioned direct mass conversion of antimatter annihilation energy from the Fig. 3-5 still exists mainly as a physical theory and in the next few decades (or more likely centuries); it is not be expected to involve any significant shift towards practical use.

3.1.3 Solar energy – solar radiation

Sunlight is the primary source of energy available on our planet. Without the energy that the Sun has been transmitting to Earth for several billions of years, life on earth would not be possible. The Sun is the star of the main population and is about halfway through its active life. A major feature of the stars from the main population is the thermonuclear reaction of hydrogen to helium, while maintaining stable conditions over a long period of time. It is expected that the Sun will shine for another 5 billion years, and that is, from the point of view of the human species, unimaginably long. That is why we can consider the Sun as an inexhaustible source of energy. The structure of the main sources of energy which originate from the Sun is shown on Fig. 3-6.

As we can see in the diagram, solar energy can be used either directly or indirectly. The main difference between these two lies in the dependency on direct immediate sunlight. The efficiency of technologies that use direct sunshine are highly dependent on its intensity and duration. This is also the main limiting factor for using these technologies in different geographical locations. For example, systems that perform well in lower latitudes with abundance of direct everyday sunshine can only be used in our latitudes with difficulty and with low yearly efficiency and questionable payback period. A very important role as well is played by the microclimatic conditions at the location of use, especially when using these technologies under non-ideal conditions.

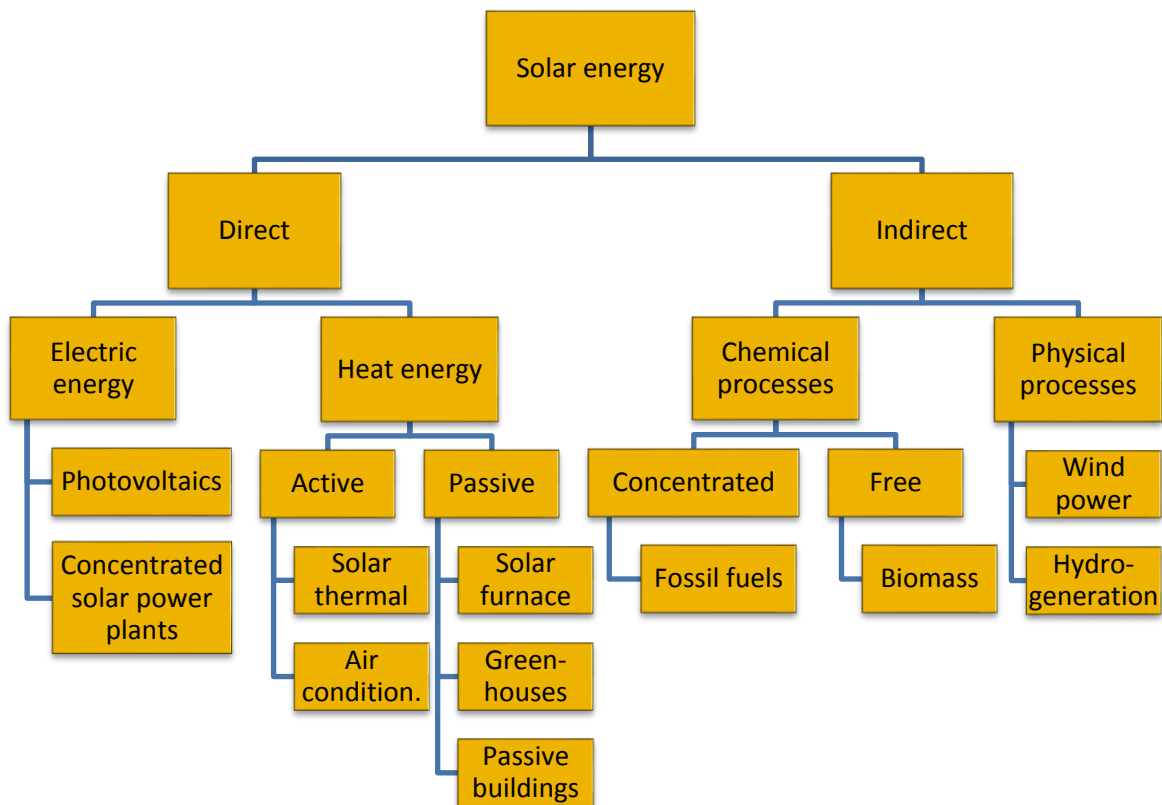


Fig. 3-6 Structure and use of solar energy

Since the wind power and water cycle are indirect manifestation of sunlight, solar energy is in fact the main source of for most of the renewable energy sources.

Although the nuclear energy is the main source of energy on the Sun, because it is neither manned nor influenced by man and, moreover, it is an entirely unique source of energy, the energy from the Sun is viewed as a separate source.

3.2 Technologies for direct use of solar energy

At the present, two ways of direct use of solar radiation are used: for generating electricity and for collecting heat energy. Even though other principles of direct use of solar radiation are known¹, only the two abovementioned are being practically used on the Earth's surface, mainly because of their relatively high efficiency.

The term "energy generation" means in this case to capture solar radiation, sometimes transform it with the possibility of accumulation and transfer to the point of consumption.

3.2.1 Generating electricity

3.2.1.1 Photovoltaics

The most used technology for generating electric energy directly from solar radiation is without any doubt the photovoltaic cell.

The direct transformation of electromagnetic radiation to electricity is called photovoltaic effect (closely related to photoelectric phenomenon), which was first observed in 1839 and

¹ Another possible use is for example use of solar wind for generating thrust for space probes and spacecrafts.

simply described by French scientist Alexandre-Edmond Becquerel. However, the phenomenon was not explained in detail until a few decades later when Albert Einstein won the Nobel Prize in 1921 for the theoretical explanation of the principle of photoelectricity.

The world's first PV cell constructed by Becquerel in 1839 did not have much to do with the modern panels that can be seen around us today. It was based on metal electrodes immersed in the electrolyte, as Becquerel had just been studying the effect of light on electrolytic processes.

Probably the first solid PV cell was built by Charles Fritts and it is dated back to 1883. The basis of the cell was a semiconductor of selenium covered with a transparent layer of gold. This PV cell, however, achieved efficiency only around 1 % and was therefore practically useless. Further research was mainly concerned with the possible materials in which the photovoltaic effect takes place, which was greatly supported by Einstein's explanation of the phenomenon.

With the advent of semiconductor devices and mastering the production of pure silicon, the sole base material for solar cells become silicon used in several configurations. One of the first applications of silicon photovoltaic cells was the space program where PV panels proved to be an ideal long-term power source for satellites and probes. Nowadays, PV cells can be found in almost all sectors of human activity. With advances in production technology and increasing energy conversion efficiency, PV cells are considered as one of the main sources for the future of "clean" electricity generation.

3.2.1.2 Concentrating power plants

Concentrating solar power plants are another way of directly using the solar radiation to generate electricity. Concentrating power plants use standard steam turbines with a generator for generating electricity the same way as they are used in conventional thermal power plants. However, the efficient production of steam by solar radiation requires a different technological solution than conventional thermal power plants or thermal solar collectors. To effectively capture sufficient solar energy, large areas are necessary. Because the amount of water required to collect heat from this area would be enormous, optical systems are used to concentrate solar radiation on a much smaller area from which heat energy can be collected more efficiently. In current time, there are basically two types of concentrating power plants with different arrangements of the concentrating optical system.

Fig. 3-7 presents a type that uses a single optical focus point located on the surface of the collector tower, where the solar rays converge reflected by the large mirror array called heliostats. The second type uses parabolic mirrors either in a line (gutter) or a spot (single dish) arrangement where the absorber is placed in the focus.

Because of the high temperatures that concentrator systems have to achieve for effective steam production, inorganic salts (most commonly a mixture of sodium and potassium nitrate) or oils are used as heat transfer fluids according to technology and temperatures instead of water.

Unique in terms of used technology is the project of three Andasol-1¹³, 2 and 3 concentrator power plants in Spanish Grenada (50 MWp each), which use as a heat transfer medium a mixture of potassium and sodium nitrate, and thanks to the system of storage, they able to produce electricity even at night for up to 7.5 hours.



Fig. 3-7 Concentrating solar power plant Planta Solar 10 (11 MWp) in Seville, Spain¹⁴

3.2.2 Generating thermal energy

As it is known from the photoelectric phenomenon, photovoltaic solar cells use mostly the visible spectrum of the light for their operation. Thermal solar systems (TSS) are on the other hand able to use almost the full range of electromagnetic radiation which is reaching the Earth's surface. The purpose of the thermal solar systems is to capture and convert solar radiation into thermal energy. The captured heat is then transferred to the point of consumption or accumulation.

In the Czech Republic, thermal systems are mostly used for heating domestic hot water (DHW) and for air-conditioning by heating in residential and commercial zones. The greatest potential of this technology in our country can be seen not only in the domestic use of small systems for DHW preparation but also as an additional element of the heating system and air-conditioning for commercial buildings.

3.3 Thermal solar systems

Electricity as the highest form of energy that can be easily transformed into other forms of energy, which is effectively the basis of the modern way of life and its availability is one of the factors for assessing the quality of life. It is no wonder then, that the consumption of electricity is a significant item in family budgets. On Fig. 3-8, we can see in detail the share of different energy consumption areas in European households and on the Fig. 3-9 the comparison between the European countries is shown. The figure Fig. 3-8 and Fig. 3-9 show the total energy demand of the household regardless of the type of energy (thermal, electrical). From the charts we can see that the energy used for hot water heating averages around 10-15 % of all household energy consumed in EU countries. This value roughly corresponds to the amount of energy consumed by lighting and home electronics. And since most of the households are using for DHW

preparation outside the heating season electricity, the living costs are rising with rising electric energy prices.

Recent trends are moving towards technologies that reduce energy consumption, due to high energy demands. These include, for example, LED lighting, modern high effective insulation, new building materials in construction, alternative energy technologies etc.

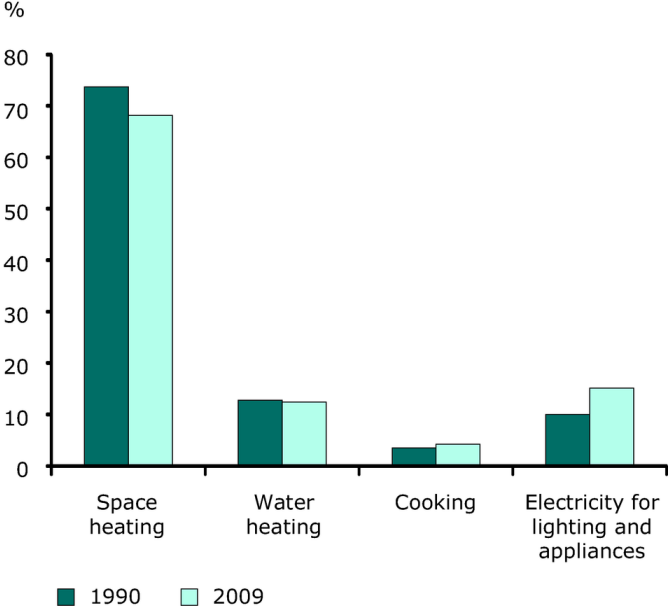


Fig. 3-8 Structure of energy consumption in the European household¹⁵

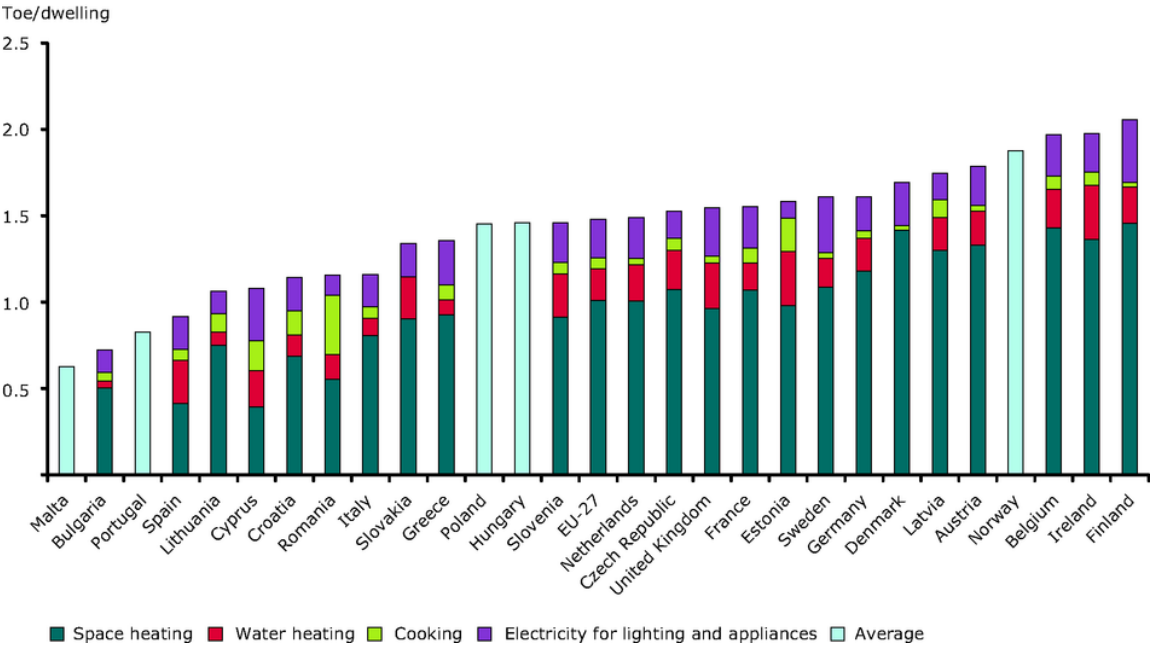


Fig. 3-9 Structure of energy consumption in the European households by country¹⁵

One of these alternative sources are thermal solar systems¹⁶. This technology is already advanced with many variations¹⁷ and can be used to save energy demands for preparing domestic hot water by around 60-70 % in average in the geographical conditions of the Czech Republic¹⁸. At present, this technology is especially useful for family houses where solar

systems are installed for spatial reasons on an unused roof area. According to statistics, more than 50 %¹⁹ of the population in the European Union lives in family houses or terraced houses with their own roof. Although it is not technically possible to occupy a roof area by the solar collectors in many cases (wrong direction of the roof, geographic conditions, technical design of the house or roof etc.), this area represents a significant potential for capturing solar energy.

The statistics show, that the installed area of solar collectors is growing rapidly. In Germany alone is annually installed over 1 million m² of solar collectors and other European countries are in trail with annual values normally accounted in hundreds of thousands of square meters²⁰.

3.3.1 Types of solar systems

Thermal solar systems can be logically divided by several criteria. Here, the division is based on the involvement of one-circuit systems and two-circuit systems that differ greatly from each another.

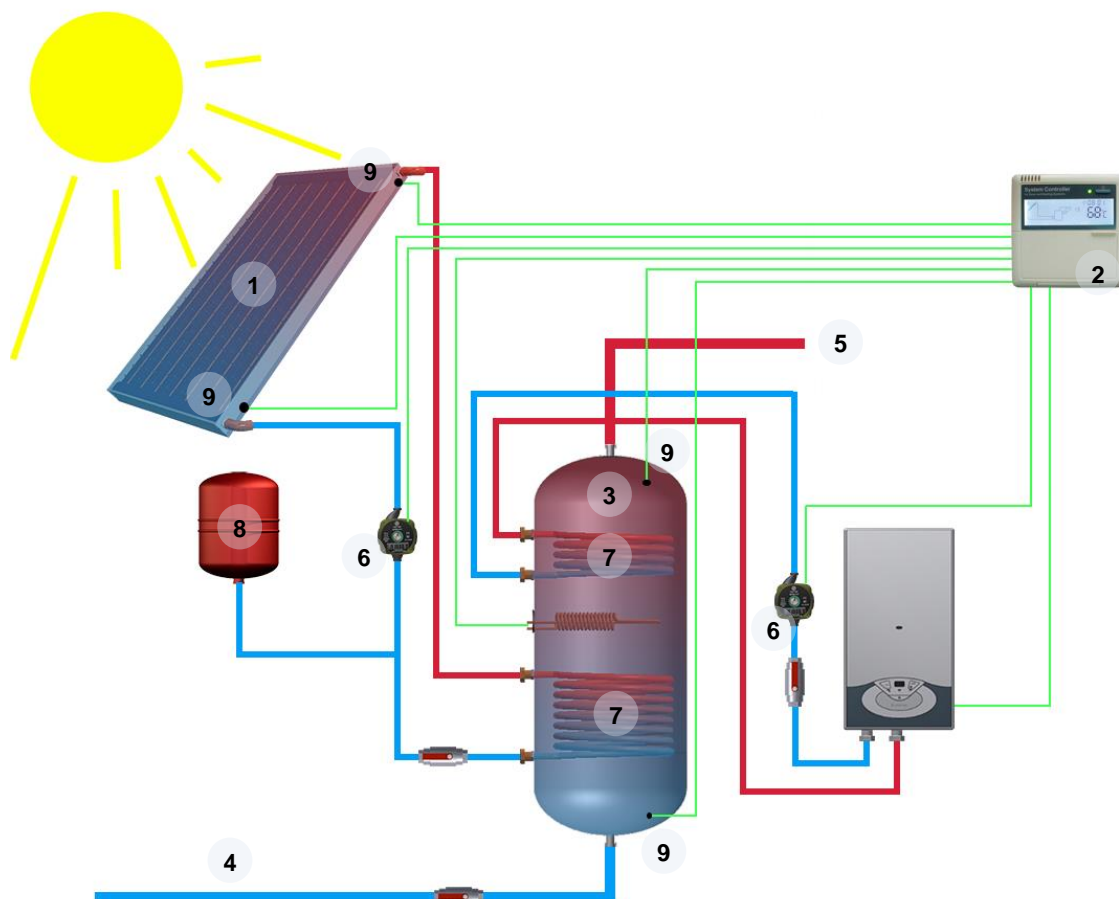


Fig. 3-10 Schema of a basic two-circuit thermal solar system

1-Solar collector, 2-Control unit, 3-DHW boiler, 4-Cold water inlet, 5-Hot water outlet, 6-Circulating pump, 7-Spiral heat exchanger, 8-Expander, 9-Sensors.

Heat transfer medium in the one-circuit system is a substance that is also intended for direct use. Thermal solar systems for swimming pools or outdoor thermal solar showers can serve as

a typical example. Their usage is usually only seasonal and heat transfer medium is usually plain water. The efficiency of these systems is small as the thermal insulation is basically non-existent and the collectors are also usually missing a selective layer. However, their low cost and very simple connectivity have made them widely available from home-based applications to public outdoor swimming pools.

Nowadays, the most advanced thermal solar systems have the solar circuit separated from the rest of the thermal system of the house, and thus creating at least two or more circuit systems with a thermal centre in a boiler or an accumulator tank. The second circuit in the solar system usually consist from the DHW itself. Other circuits may be represented by other heat energy sources such as boilers or heat pumps or consumption circuits in the form of central heating and underfloor heating. On Fig. 3-10 is a circuit diagram of the concept of a simple two-circuit thermal solar system, which in practice represents the most common solution while also showing the basic principles of the systems.

The base consists of a solar collector that absorbs solar radiation, thereby heating the absorber surface. From the surface, thermal energy is drained into a heat-carrying liquid, heat transfer fluid (HTF), which is pumped by the circulating pump into the boiler or storage tank. Through the heat exchanger the HTF transfers part of its thermal energy to the boiler or storage tank and returns to the collector in the circuit.

To evaluate all processes in the thermal solar system, a good knowledge of the design of these systems is necessary. The knowledge of the individual components of the system, their function and the material composition therefore represent the basic prerequisite for further work.

3.3.2 Basic Components

3.3.2.1 Solar collector

The basic design component without which the thermal solar system cannot be imagined is the solar collector. The most widespread type is currently a flat-type solar collector²⁰. On Fig. 3-10 is a solar collector shown under number 1. Composition of its individual parts then gives Table 3-1 with detailed structure shown on Fig. 3-11.

Although each manufacturer uses slightly different material composition, Table 3-1 summarizes the most commonly used materials for different parts of the solar collector. For the construction of the collector only materials that are able to withstand weather impacts for long period of time have to be used. In this respect, the most common material is aluminium and its alloys. The normal weight fraction of aluminium in the whole collector is usually around 35 %²¹. The main supporting components are made of aluminium including the anchoring to a suitable surface. Aluminium and its alloys used for the production of solar collectors are fully recyclable, and they excel by long-lasting corrosion resistance, low weight with sufficient strength and very easy machining.

Another integral part is cover glass. Here, the manufacturer tries to offer a glass that has the best solar radiation transmittance with minimal reflectivity and yet with sufficient strength. For the best permeability some quartz glass would be the best, however, it is too costly and its strength and flexibility is also insufficient for use in solar collectors that have to withstand in the horizontal position the power of rain, snow and sometimes hails, too. Therefore, the most common glass we can encounter with in solar collectors is hardened glass with low iron content (iron in the glass absorbs IR which is undesirable).

Table 3-1. Materials mostly used for the fabrication of the solar collectors.

Part	Material
Backsheet	Al, Al alloy
Frame	Al, Al alloy
Cover glass	Safety glass with low Fe content
Glazing rails	PA, ABS
Seal	EPDM, silicone
Piping	Copper
Absorbers	Copper or Aluminium
Selective layer	Titanium, Chromium, Nickel, Aluminium oxides
Insulation	PUR, mineral wool

*Reference^{22,23}.

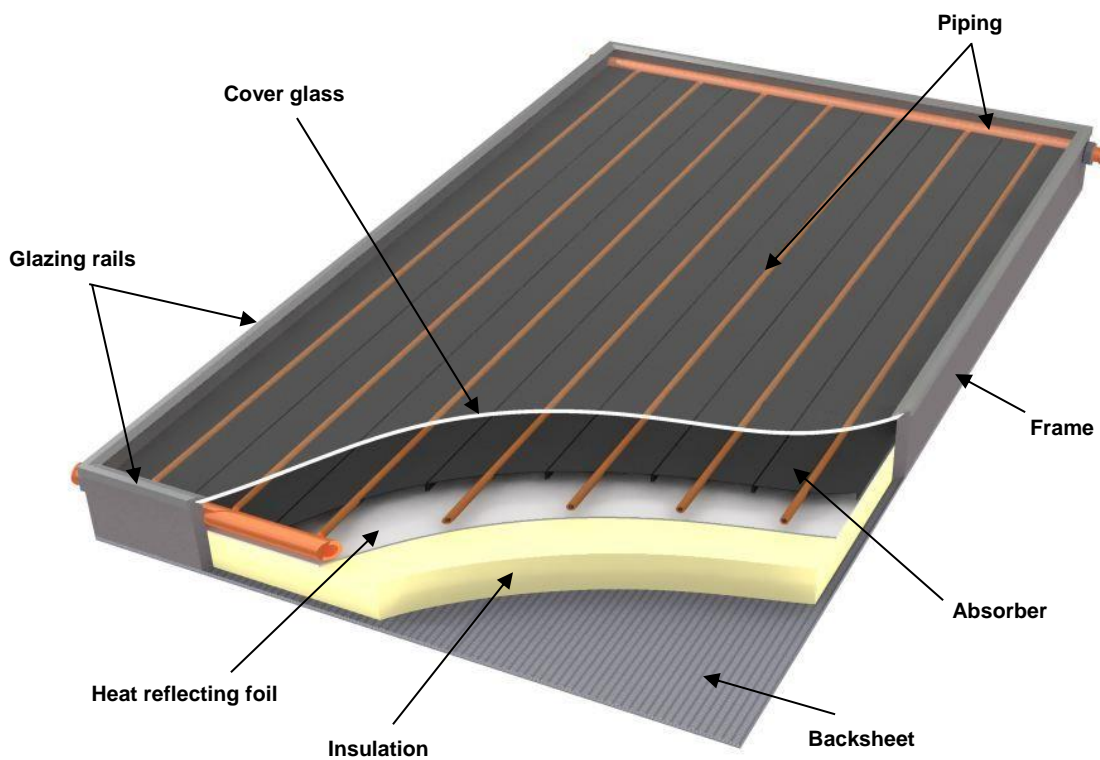


Fig. 3-11 The structure of a flat-type solar collector

The next most common element is represented in flat solar collectors by insulation material. Although, flat vacuum panels and tubular vacuum panels have already overgrown the older

insulated type in new installations, flat collectors with insulation are still the most widespread type of collector (especially in old installations)²⁰. The insulation materials used in solar collectors are different according to the manufacturer, though, the most used materials are usually insulation materials commonly used in construction. Above all, we can see in the collectors PUR foam, mineral wool, glass wool and, to a lesser extent, polystyrene. It should be noted that PUR foam and polystyrene are much more sensitive to high temperatures than mineral wool and glass wool, so they can only be used in systems where the temperature is not to be expected to exceed 130 °C.

3.3.2.2 Piping

Another essential part of the thermal solar system is pipeline system for leading the heat transfer medium. Recently, copper pipes and stainless steel pipes are used almost solely^{24,25} for high efficient two-circuit systems, however plastic piping can be commonly seen in one-circuit systems designed for operating temperatures under 80 °C.

In order to identify the processes inside the TSS, the knowledge of the processing of the metals and ways of joining is also important. In the basic, we can divide the ways of connecting the pipes to two types: *dismountable* and *permanent*. Each of these categories then has a large number of modifications of individual types of joints²⁶⁻²⁹:

- Connections by hard and soft soldering
- Press connections
- Connections with clamping rings
- Welding connections
- Connections over the flange
- Threaded connections with clamping ring
- Etc.

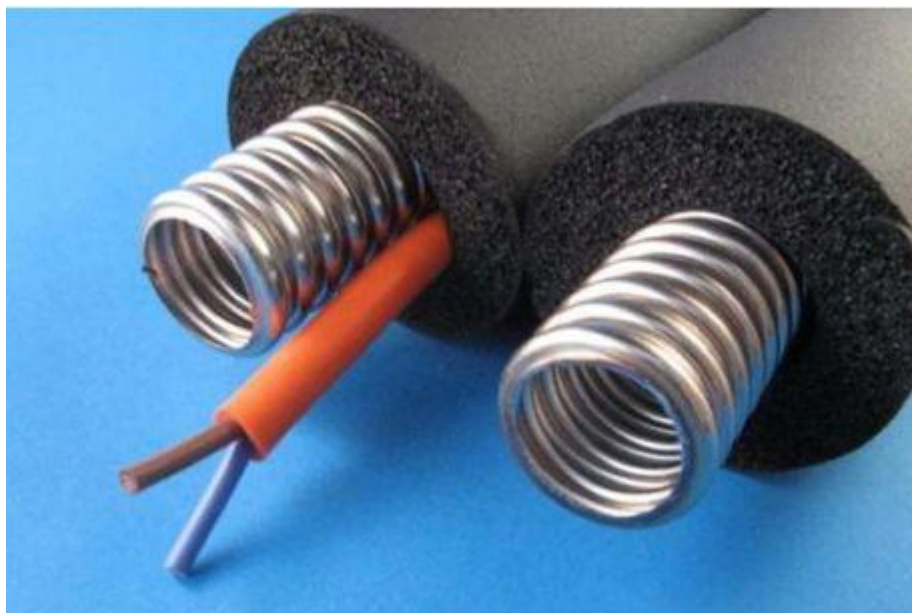


Fig. 3-12 Transfer pipe (corrugated stainless-steel pipe) encased in insulating material

From the point of view of the corrosion and degradation of heat transfer fluids, all soldering and welding methods are important for us, as they introduce new materials into the system that can create an electrochemical potential.

According to the German Institute for Copper DKI (Deutsches Kupferinstitut)²⁶, different soldering and melting agents can be used for soldering, however, they often contain toxic elements. Although their composition varies, the essential elements remain the same. These are tin, silver, phosphorus and zinc. In the case of welding, there is an additional material from the welding wire made of copper with a small addition of silver or tin, in case of copper welding. The main trends in solar technology are mainly the method of mechanical joining of pipes, especially by pressing and joining with clamping rings, which reduces the number of other materials and simplifies the installation processes. Welding and soldering is in particular the domain of older systems.

3.3.2.3 Exchanger

The heat exchanger is usually a simple piece of work. The most used types are plate and tube helix exchangers.

Modern plate heat exchangers are mainly made of non-corrosive steel – stainless steel. Plate heat exchanger design is illustrated on Fig. 3-13. As shown in the figure on the right, the plate exchanger consists of a series of individual plates separating two independent fluid flows when the individual plates act as a heat exchange surface for transferring thermal energy. In practice, we can meet with different designs and solutions. One of them is shown also on Fig. 3-13 on the left. The sheets are separated by a rubber seal and are then installed into a ready-to-install detachable structure pushing the plates together. Another often used construction is to simply weld the plates together. In solar applications, we can most often encounter with the first mentioned construction.

Another widespread type of heat exchanger is spiral heat exchanger with very simple design. The metal tube is spirally wrapped and placed directly in a medium container that we want to heat or cool down. The walls of the pipe itself act as a heat exchanging surface. Tubes are made of materials that conduct heat well, tolerate temperature differences and are corrosion resistant. The most common are copper and stainless-steel exchangers. Older types were made of iron and steel.

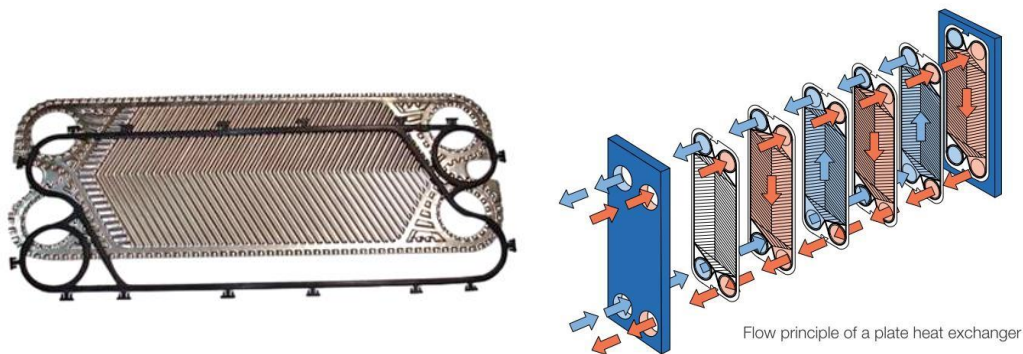


Fig. 3-13 Plate exchanger design.

Left - plate of exchanger with seal, Right - Standard plate exchanger design³⁰

3.3.2.4 Boiler

To prepare and store domestic hot water by using TSS, boiler is an important element. In most cases, it is a thermally insulated container in the shape of a cylinder with several inputs and outputs. For thermal solar systems, boilers are specially designed for maximum use of the low-potential heat. The design consists in installing the boiler upright and connecting the solar circuit to the lower colder part of the boiler in order to achieve the greatest possible temperature drop between the heat transfer medium and the boiler section to be heated. Boilers also provide separate inlets for other heat sources, such as furnace boiler or electric heater. The heat exchanger, through which the heat transfer fluid of the solar circuit is circulated, is a standard part of the boiler. In modern versions the exchanger is made of copper or stainless steel, although in the older systems is still common iron, exceptionally steel.

3.3.2.5 Storage tank

The storage tank is one of the additional elements of thermal solar systems, which are not usually used for small systems primarily designed only for DHW preparation. For large systems, which are also used for air-conditioning, the storage tank is a common feature.

Typically, this is a large, thermally insulated vessel filled with water as a storage medium and a number of inlets/outlets. As a reservoir of excess heat, the accumulation tank can significantly increase the overall efficiency of the TSS with the correct setting and selection of a suitable volume. Many inlets/outlets, which can be found on the storage tanks specifically designed for TSS systems, along the entire height of the tanks are used to maintain the correct and stable temperature stratification of storage media inside the tank, thereby further enhancing the efficiency of the entire system by utilizing more of the low-potential heat. The material composition corresponds to that of the boiler.

3.3.2.6 Pump

The basic moving part of the thermal solar systems is circulator pump. Its composition can be very variable according to different manufacturers, though the base is usually composed from asynchronous motor and radial centrifugal pump as shown on Fig. 3-14.

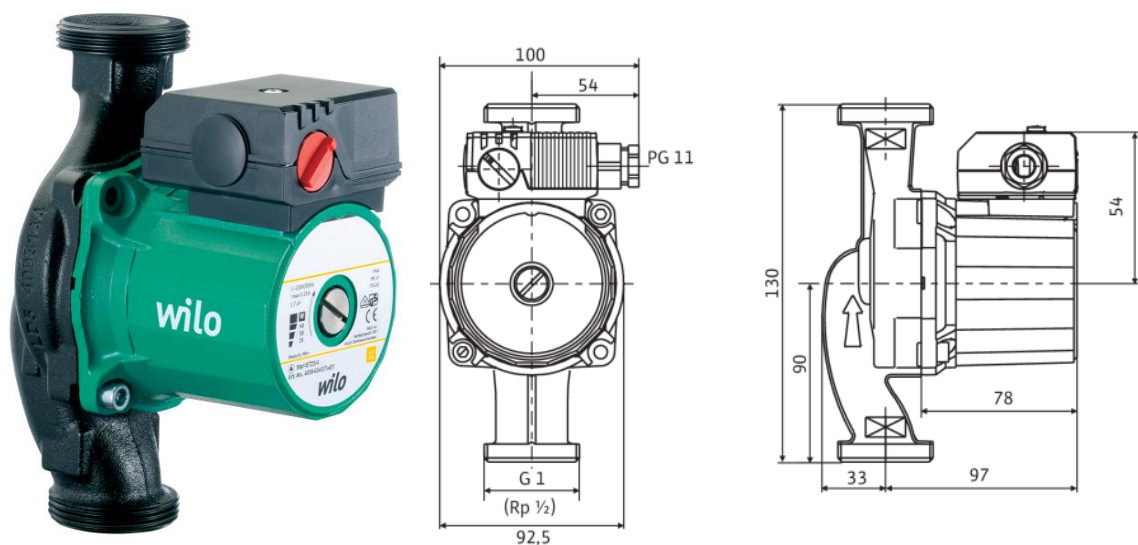


Fig. 3-14 The circulator pump³¹.

Circulator pumps used in solar systems are essentially identical to conventional circulating pumps for heating systems. Compared to them, however, they must withstand somewhat higher temperatures and have to cope with higher viscosity of antifreeze additives.

The body is almost entirely made of metal and we can mostly encounter with cast iron, bronze and stainless steel. Vanes of the pumps are largely made of polypropylene with glass fibre for higher durability. An integral part of circulator pumps is an asynchronous motor and mostly control electronics which enables the pump to operate at multiple speeds. Also with the recent development of photovoltaics (PV), more pumps compatible with direct connection to the PV systems are available^{32,33}.

3.3.2.7 Heat transfer fluid

The heat transfer fluid is the largest amount of material consumed during the operation of the thermal solar system. The consumption of the fluid depends on the size of the system and for common systems in houses of four members (the size of 2-4 panels) the filling of the heat transfer fluid differs from 5 to 10 litres. Naturally, other factors like the technology used and the distance from the collectors to the heat exchanger play an important role. Durability of one filling depends on the thermal load of the system, its material composition, system stagnation etc. Normally, the liquid is changed every five to seven years of operation. The most common heat transfer fluid is water and in case of colder climatic conditions water in mixture with antifreeze additives.

3.3.3 Additional components

3.3.3.1 Control electronics

For proper operation and maximum efficiency the thermal solar systems utilize advanced digital control electronics, which is based on measuring system properties and managing the system in real time. In the control electronics, all electronic equipment is included such as sensors and wiring. The essential part of the control electronics is composed of a control unit and the control and power electronic components. Wiring of the system is generally compact and does not require a separate power supply of the individual components of the system as they are fed with electricity through the control unit and power supply and are directly managed thereby. Thermal solar systems can also be utilised without an active control system driven just by hydrostatic forces caused by thermal expansion and change of density, however, such systems are not reflected in this work.

3.3.3.2 Other components

Besides the main components described in Section 3.3.2 and the control unit above, there is a number of other elements that have a direct impact on the operation of the system or are in immediate contact with the heat transfer fluid. That includes in particular: the manual valves, electromagnetic valves, automatic simple and multiway valves, check valves, pressure relief valves, degassing vessel, expansion tank/vessel etc. These element, however, represent only a small part of the system.

4 THEORETICAL BACKGROUND

4.1 Overview of heat transfer fluid in thermal solar systems

The main purpose of heat transfer fluids is, as stated in the name, to transfer heat energy from one place to another. For low-temperature systems (typically from -20 °C to 150 °C) water is usually the first choice as it is efficient and highly cost-effective fluid for transferring heat. Unfortunately, the basic properties of water and its typical behaviour at temperatures below 0.0 °C bring the necessity for antifreeze protection in form of additives to avoid damages to the system. The antifreeze additives are common in many industrial, home and automotive applications when there is a possibility for the temperatures to drop below freezing point of plain water. The protection against freezing is particularly used in outdoor systems like combustion engine cooling in vehicles or thermal solar systems and the extent of utilisation is usually connected to the specific climate conditions. Furthermore, thanks to profound standardisation in materials production and manufacturing processes, the antifreeze additives are also quite common in warm climate regions mostly in automotive. The most common group of chemicals which is used as an antifreeze additive for water is glycols, as a more common name for diols. Outside the antifreeze mixtures with water, however, in practice we encounter with a variety of other heat transfer fluids, which are successfully applied according to specific parameters and applications of the each TSS.

4.1.1 Air

Under normal temperature and pressure, the air is stable and inert. The problem poses only its very low thermal capacity which limits its use only for specific applications, such as passive applications where it takes advantage of its relatively easy spontaneous flow or direct air-conditioning where the Sun-heated air is used directly for the space heating. Good example would be double-skin façade used on many commercial building for passive air-conditioning³⁴ or solar thermal air collectors³⁵.

4.1.2 Water

From the viewpoint of viscosity and heat capacity water is almost ideal heat transfer medium. It is non-toxic and, in most countries, economically easily accessible. The greatest limitation for use in the thermal solar systems poses the point of fusion (melting point) and boiling point. Furthermore, in its pure form it is also very little corrosive, however, the pH must be kept neutral. Restrictions may present the dissolved minerals (hardness). Minerals and other substances occurring in plain water affect mainly its chemical properties and have a great influence on the actual pH and buffering capabilities of water. With decreasing temperature the solubility of minerals in the water also decreases, but the solubility of gases raises. This can cause their deposition on the contact surfaces and fouling of the heating system, which often leads to system malfunction and damage. For these reasons, even in mixtures primarily distilled or deionised water is used.

4.1.3 HTFs based on silicon oils

Although silicone oils have low fusion point, high boiling point, are practically non-corrosive and have high temperature durability, they are not a good candidate for heat transfer medium for the thermal solar systems. This is caused primarily by small heat capacity than that

of water, and very high viscosity, including comparatively higher price. These factors make high demands on the circulator pumps having a high energy consumption. Moreover, the silicon oils are known for their high capillarity, which puts high demands on the sealing of the pumps and on the entire system, where silicone oils can easily escape through any microscopic leaks. These properties are restricting the oils to be used in specially developed high-temperature systems, such as the concentrated solar power plants, which cannot use the common water-based mixtures as a heat transfer medium because of the high temperature. In addition, we can also encounter, to some extent, with the silicon oils in some home high-temperature thermal solar systems as well.

4.1.4 HTFs based on hydrocarbon oils

On a small scale in special TSS applications we can encounter with heat transfer mediums based on hydrocarbon oils. They have in general higher viscosity than water and lower heat capacity. The hydrocarbon oils are relatively inexpensive, non-corrosive and their fusion point and boiling point are more than sufficient for use in the most of the TSS with the possibility of being used in extreme conditions. Problematic, however, is their toxicity and flammability. Therefore, they can be found only in special applications where the circuits are strictly divided by double-walled protection against leakage. Their advantage is that they can last for the entire lifespan of the system, therefore, they can be found in systems where the exchange of the heat transfer fluid is problematic or difficult.

4.1.5 HTFs based on mono-alcohols

Mono-alcoholic heat transfer media with respect to their low fusion point can be found mainly in the primary circuits of heat pumps. The disadvantage is the very low heat capacity, which is almost 40 % lower than that of water. Thus, to transfer the same amount of energy substantially larger amount of the material has to be transferred. Limitations for use in solar systems also poses low boiling point. Methanol boils at 64 °C³⁶ and ethanol at 78 °C³⁶, which is too low compared to the normal operational temperatures obtained with conventional thermal solar systems. Their use in TSSs is therefore limited primarily to technologies such as vacuum solar tubes, where the mono-alcohols provide a heat transfer through phase change from the closed collector to the heat transfer medium in the system.

4.2 Heat transfer fluids based on diols

The biggest group of heat transfer fluids currently used in thermal solar systems and automotive industry is based on the same substances which are commonly known as glycols. From Ancient Greek “γλυκύς” (glukús, “sweet”) glycols are defined as any aliphatic di-alcohol with hydroxy groups on different carbon atoms³⁷. Because of the two hydroxy groups, glycols are often called simply diols, though having some specific differences unique to the group³⁸. Glycols are usually odourless, colourless and sweet tasting liquids at the standard temperature and pressure. The presence of two hydroxy groups is a reason for many typical properties of this group such high viscosity, hygroscopicity and unlimited miscibility with water³⁸⁻⁴⁰.

The main reason for using diols is protection against freezing in the mixture with water⁴¹ as so called antifreeze. Depending on the concentration of the binary mixture glycol/water, they can offer freezing protection up to -50 °C and at the same time rising the boiling point up to 110 °C (at normal pressure). Glycol mixtures used in thermal solar systems are derived from

the automotive industry and are available from 1920s⁴², when the first mixtures became available on the market.

The first glycol antifreeze mixture was based on ethane-1,2-diol, commercially known under the names ethylene glycol (EG) and monoethylene glycol (MEG). At that time the mixture was also referred to as "permanent antifreeze". MEG/water mixture was then used in the first water-cooled automobiles and gradually replaced ethanol and methanol-based water mixtures. With the advent of thermal solar systems MEG mixtures also began to be used in them. Later on, with the simplification of the production process of so far complicated propane-1,2-diol (commercial names: propylene glycol, monopropylene glycol, MPG), the mixture MPG/water also began to take the share of the market as a less toxic alternative to the MEG/water. Nowadays, the most used glycol mixtures used in automotive and thermal solar system are currently binary mixtures consisting of MEG/water and MPG/water⁴³. The propane-1,2-diol and ethane-1,2-diol are taking together over 90 % of the global market with antifreeze heat transfer fluids. A very small share is also taken by propane-1,2,3-triol (glycerol)^{41,44}, sometimes being incorrectly put into the glycol group as well. The structural formulas of ethane-1,2-diol, propane-1,2-diol and propane-1,2,3-triol are shown on Fig. 4-1.

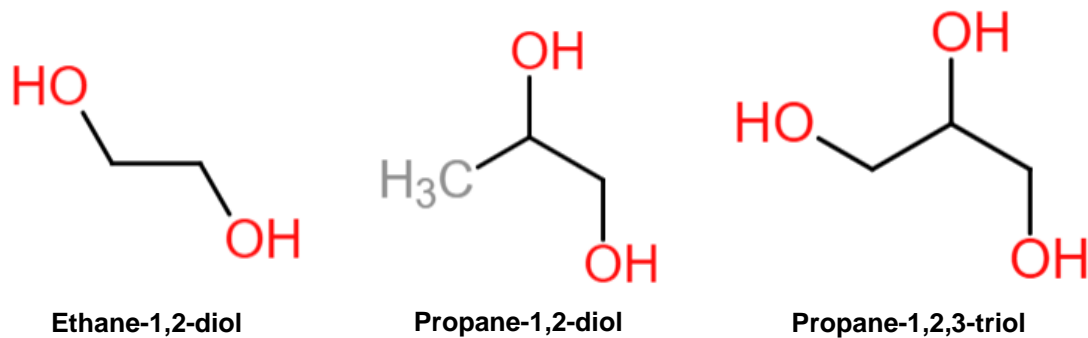


Fig. 4-1 Structural formula of selected glycols.

The TSS technology development saw a great progress in the efficiency of solar systems from its beginnings especially in the 70s of the last century. However, this development also marked the biggest deviation from the parameters of thermal systems in the automotive industry, especially in the rise of temperatures and pressures in the system⁴⁵. With the further development of the technology in the pursuit of higher energy gains this difference further increased and together with new materials the thermal solar systems are now fairly different and require somehow different approach than the thermal systems in the automotive. Consequently, that puts some increasing requirements on the heat transferring glycol mixtures, which changed only slightly, especially in the terms of their thermal stability and ecological aspects.

As it was discussed before, the most widespread basis for antifreeze heat transfer media thus consists of MEG and PEG. However, since these binary mixtures, and thereof the stabilizing components as well, were primarily prepared for car radiators, different thermal resistance was considered in their production. Mixtures in combustion engines operate at temperatures around 80 °C, whereas the conventional solar systems often work with temperatures around 100 °C and vacuum insulated systems far over 100 °C, at pressures around 150-300 kPa⁴⁶. The question is whether these mixtures, without additional treatment, are able to resist for a long period of time

at these conditions. The essential issue is also the ecological aspects of these compounds and their production.

4.2.1 Ethane-1,2-diol (CAS 107-21-1)

The ethane-1,2-diol is a colourless, moderately toxic, odourless substance with slight sweet smell that causes a methanol poisoning⁴⁷. For use as antifreeze additive ethane-1,2-diol is usually diluted with water in a dilution of approximately 40 to 50 wt%⁴⁸ and the corrosion inhibitors are also added according to the target properties of the system. Because of its toxicity, it can be used only in systems where the primary circuit is safely separated from the heated drinking water and systems are not in direct contact with food, leaving its most common application as antifreeze for combustion engines. The ethane-1,2-diol is also used in thermal solar systems for some time now, but it is gradually being removed and replaced by less toxic propane-1,2-diol. However, overall it is the most used antifreeze additive for water so far. Although the ethane-1,2-diol is used as antifreeze additive in large quantities, its primary usage (millions of tons, several times more than as the antifreeze additive) is as a precursor to polyester fibres and PET (polyethylene terephthalate)⁴⁹.

4.2.2 Propane-1,2-diol (CAS 57-55-6)

The second most used antifreeze additive for water is propane-1,2-diol. Because propane-1,2-diol is non-toxic⁵⁰⁻⁵², it is used instead of ethane-1,2-diol in applications, where the toxicity could be an issue, such as food industry and in places where contact with drinking water could occur. Like the MEG, the propane-1,2-diol is unlimitedly miscible with water with similar depression of fusion point and extension of boiling point, making it suitable antifreeze additive^{39,41}. In thermal solar systems are used primarily dilutions of about 50 wt%⁵³.

4.2.3 Propane-1,3-diol (CAS 504-63-2)

Propane-1,3-diol, commercially known also under the designation as PDO, is a structural isomer with propane-1,2-diol, and as such, it is similar in many ways. As well as MPG it is hygroscopic and completely miscible with water. It is slightly soluble in aromatic hydrocarbons and practically immiscible with aliphatic organic solvents⁵⁴. All of the production is used almost solely on the manufacturing of Polytrimethylene terephthalate polymer (PTT) used in carpet industry^{55,56}. But, thanks to its anti-freezing properties as the others diols, the possibilities of using it as a “green” substitute for almost exclusively crude oil based production of ethane-1,2-diol and propane-1,2-diol are currently studied^{57,58}. Due to the insufficient data on its long-term toxicity it has been not yet permitted for use in the food industry and for the production of medicines and cosmetics, though is it generally considered as safe according to several claims^{59,60} and short term studies⁶¹. From the available data and existing measurement results⁵³, the propane-1,3-diol is a promising substance as a new antifreeze additive⁴⁶. However, for widespread use of this substance some steps concerning the research on the physical and chemical properties of its aqueous solution are still necessary as well as rise of the quantity of production, which will be explained later.

4.2.4 Propane-1,2,3-triol (CAS 56-81-5)

Propane-1,2,3-triol, more know under its common names glycerol and glycerine, does not belong to the diol group but it is also consistently examined as a potential antifreeze

additive^{41,44,62}. Thanks to the third hydroxy group, the glycerol has much higher viscosity, boiling point and fusion point than the alkanediols⁶³. However, in the mixture with water it behaves similarly to the alkanediols. Glycerol is used in many industrial sectors, but its probably most famous application is as a precursor for nitro-glycerine production dynamite manufacturing process⁶⁴. Because of the very low toxicity of glycerol⁶⁵, it is used widely in food industry, pharmaceuticals and personal care products. Together with propane-1,2-diol it is also used as a solvent and delivery agent in e-cigarettes⁶⁶. For using it as an antifreeze additive its biggest disadvantage lies in its high viscosity in the target solution, slightly lower antifreeze capabilities and it is therefore more considered in ternary mixtures as a supplementary component⁵³.

4.2.5 Ternary glycerol mixtures

Ternary glycerol mixtures represent almost a completely separate issue and it is mainly due to the complexity of these systems and the large variety of possible dilution. Their availability in the market is currently very limited, mainly due to lack of thorough understanding of their behaviour in the TSSs. Data on their physical and chemical properties are also very limited and very often the individual sources disagree. Ternary mixtures are prepared using the conventional binary mixture of MEG/water and MPG/water as a base, when a portion of the alkanediol is replaced by glycerol. This solution could be particularly interesting because of the price of glycerol, which is a waste product of many industrial processes and depending on the market price can be economically advantageous⁵³.

4.3 Properties of heat transfer fluids in the Thermal Solar Systems

4.3.1 Desired properties

Quality and stable heat transfer fluids for the thermal solar systems must meet certain criteria, which are essential for its long-term and all-year use. Any proposed heat transfer fluid must pass a series of tests that demonstrate a suitability for its use as a heat transfer fluid. The fundamental properties that are observed in the design and evaluation of heat transfer fluids in the all-year thermal solar systems are^{43,53,67}:

- Low fusion point
- Good thermal and physical properties similar to water
- Low viscosity
- Low or none corrosivity
- Compatibility with sealing materials
- Non-flammability
- Environmental aspects (non-toxic, biodegradable)
- Long-term stability and heat resistance
- Affordability

4.3.2 Physical properties

Table 4-1. Physical properties of antifreeze additives in their pure state

Substance	Density ^{a,b} ρ [g·cm ⁻³]	Heat capacity ^{a,b} C_p [kJ·g ⁻¹ ·K ⁻¹]	Boiling point ^a T_{boil} [°C]	Melting point ^a T_{fus} [°C]	Viscosity ^{a,b} η [Pa·s]
Ethane-1,2-diol	1.113	2.41	197.3	-12.9	0.016
Propane-1,2-diol	1.036	2.48	188.2	-59.0	0.058
Propane-1,2,3-triol	1.261	2.43	290.0	17.8	1.412
Propane-1,3-diol	1.053	2.29	217.0	-27.0	0.052
Water	0.998	4.18	100.0	0.0	0.001

*References⁶⁸⁻⁷¹. ^aAt pressure $p = 101.325$ kPa. ^bAt temperature $T = 20$ °C.

4.3.2.1 Fusion point

For use of heat transfer fluid in the thermal solar systems in our latitudes it is important to fill the system with liquid medium that is capable of sustaining temperatures around -20 °C to -30 °C⁴³. Although water is an ideal heat transfer fluid, its use in systems for all-year operation is not possible. That is caused by the natural property of water for volumetric expansion during its freezing caused by process similar to crystallisation⁷². This process increases the volume of the water approximately by 9 %. This itself would not pose a big problem if the water would stay liquid. However, the process is accompanied by solidifying of the water, preventing it from any flow and creating localised high pressure on the equipment and in pipes, which ultimately leads to damage to the system, in many cases terminal. As has been explained earlier, to depress the fusion point and allow the water to be used as a heat transfer medium, even in environments where temperatures below the fusion point of water could occur, antifreeze additives have to be used. Because the usage of water is favourable in many cases, the antifreeze additives are chosen to be compatible with. That is also the case of alcohols and alkanediols. Thanks to the hydroxy groups, the organic molecules can interact with water molecules on a higher level creating kosmotropic mixtures⁷³. This unique interaction based on hydrogen bonds⁷⁴ grants the mixtures specific qualities which are apparent in many ways such as eutectic depression of fusion point. The comparison of the freezing temperature for most common antifreeze additives and their mixtures water is shown on Fig. 4-2.

The actual fusion point depression by the alcohols is in general dependent on two factors: (i) the number and position of the hydroxy group and (ii) the length of the carbon chain. These factors have different effect on the fusion point depression and are connected to the hydration capabilities of individual substances. As has been observed by Franks and Ives⁷⁵ the dissolution of alcohols in water is governed by two concurrent processes, namely hydrophilic and hydrophobic hydration. The hydrophilic hydration occurs for hydrogen bonds between water molecules and hydroxy groups of the alcohol and the hydrophobic hydration is a process where hydrogen bonded molecules cluster around the non-polar carbon chain part. The hydrophilic hydration has a favourable entropic structural effects and is exothermic opposite to the endothermic hydrophobic hydration⁷⁶. Therefore, the position and the length of the non-polar carbon stub plays an important role, which can be very easily seen on the mono-alcoholic group studied by Takaizumi and Wakabayashi⁷⁷. However, this effect can be also visible in the case of ethane-1,2-diol and propane-1,2-diol. The steric effect of the free methyl on propane-1,2-diol

and the connected hydrophobically hydrated water molecules does not allow creation of eutectic mixture unlike the ethane-1,2-diol. However, by attaching another hydroxy group to the molecule, creating propane-1,2,3-triol, the effect of the hydrophobic hydration will disappear⁷⁸. Similar process occurs in the case of α,ω -alkanediols (hydroxy groups in terminal positions), such as ethane-1,2-diol⁷⁹, and propane-1,3-diol studied in this work.

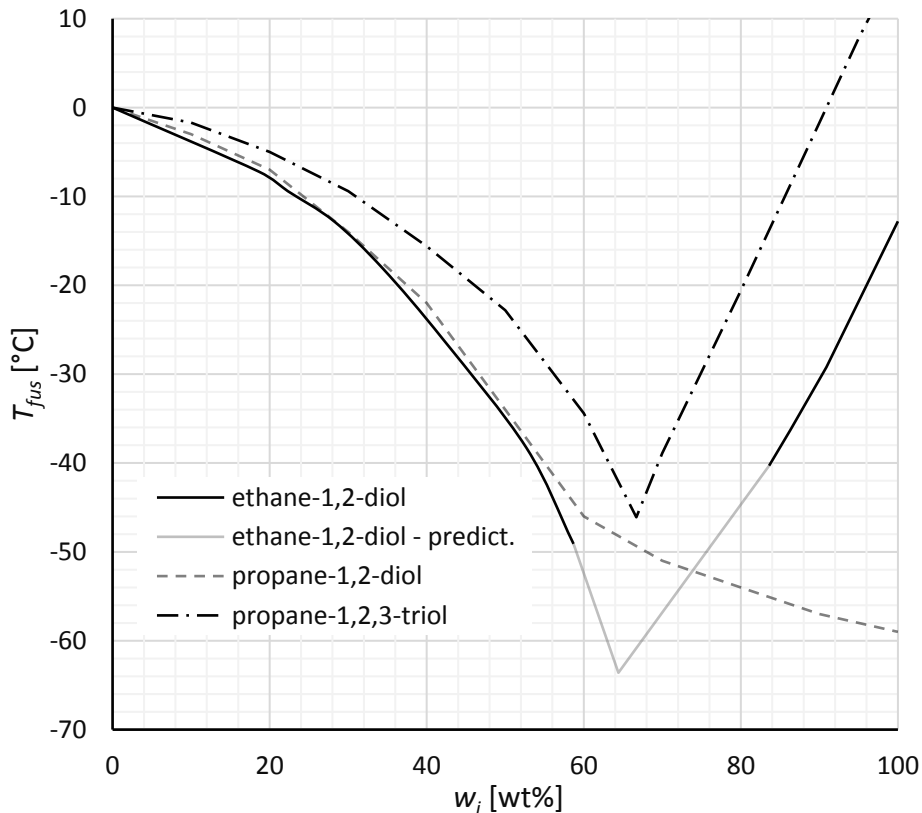


Fig. 4-2 Comparison of fusion point of some antifreeze additives.

4.3.2.2 Boiling point

By adding glycols into water, the boiling point of the resulting mixture is higher than that of the pure water. This feature is especially advantageous for newer systems with higher efficiency, where the temperature of the fluid commonly reaches 100 °C. Boiling point in the systems is also increased by pressure, which is normally maintained in TSS in the range of 2-3 bar. The increase in the boiling point of water by the addition of glycols is not that immense for the typically used solution of 50 wt%, but in the connection with the elevated pressure the temperature of the fluid can safely reach up to about 150 °C. However, heating the heat transfer medium to these temperatures increases the thermal stress on the organic base and accelerates aging. This is particularly noticeable when during the TSS stagnation the temperatures rises temporarily up to 200-300 °C^{67,80,81} and pressure up to 4.5-5 bar^{82,83} up to the set point of the pressure-relief safety valve.

4.3.2.3 Heat capacity

Although the glycols have positive effect on the boiling point of the water, their impact on the heat capacity of the mixture is quite opposite. At 50 % dilution the decrease of the thermal capacity is approximately 25 %. However, as shown in Fig. 4-3, the value of the overall system efficiency is dependent on the transfer medium only a little, and therefore the usage of the glycol

freezing point depressant on the heat transferring capabilities of the heat transfer medium is negligible.

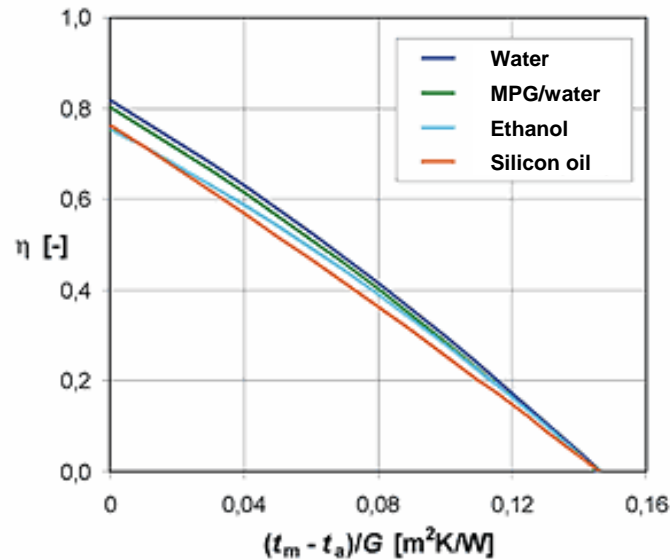


Fig. 4-3 Efficiency of solar systems, depending on the heat transfer medium⁴³.

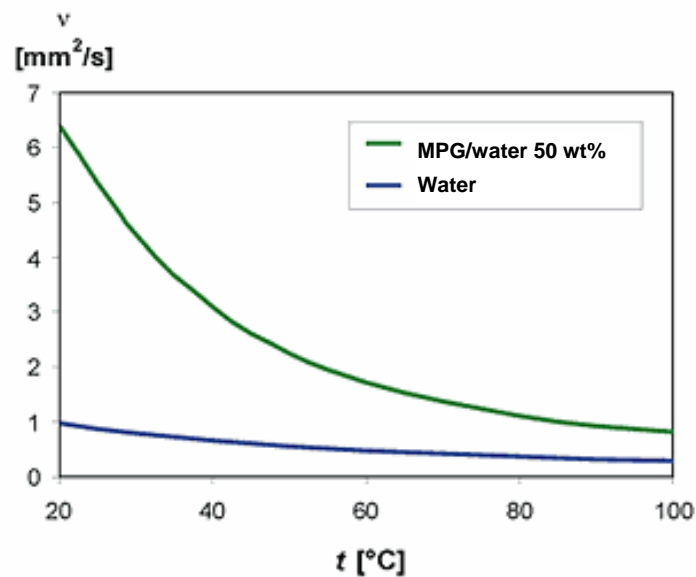


Fig. 4-4 Kinematic viscosity of binary mixture propane-1,2-diol/water⁴³.

4.3.2.1 Viscosity

One of the negative qualities of glycols mixtures is their high viscosity. Especially in the colder environment, this property puts high demands on the pump that drives the fluid in the system and the system has to be adequately designed. For correct design and sufficient safety margins the values of viscosity for possible dilutions have to be known and correctly applied. As can be seen on Fig. 4-4, a standard mixture of about 50 wt% of propane-1,2-diol in water is having up to 6 times higher viscosity than pure water at 20 °C. However, it is only two times higher than that of pure water at 80 °C. Therefore, the dependence on temperature is very important and the designing has to be carried out with that in mind. But comprehensive studies

that would have examined the burden of the undercooled highly viscous heat transfer fluid on active elements in the TSS and their electrical consumption are missing. That is caused mostly by the fact that most of the thermal solar systems works under those conditions only for a fraction of its running time and standard calculations are usually within satisfactory error margins. However, from previous measurements⁴⁶ was find out that the newly introduced propane-1,3-diol has at the same dilutions lower viscosity than other aqueous glycols at normal operating temperatures, although, the measured difference is not that significant.

4.3.3 Flammability

Equally important property of the substances circulating in the solar system is its low flammability or complete non-flammability^{39,43}. As the aqueous glycol mixtures are almost always used in a system together with a large quantity of water its decisive incombustibility plays important role for storage and transportation in pure form. Glycols and glycerol are generally considered as flammable substances, given their chemical structure with the hydrocarbon base and alcohol functional groups. Essential for their safety in use is their low vapor pressure above the surface, which puts them into less flammable class. However, this applies only to pure substances. The dilutions for use in the TSS as binary mixtures with water are generally considered as non-flammable³⁹.

4.3.4 Corrosion

Experience from practical use of the heat transfer media suggests that a vital element affecting the lifespan of the TSS are the corrosive properties of the heat transfer fluids. Manufacturers of heat transfer media and thermal solar systems are therefore trying to make a systems where the heat transfer medium and the materials used for the construction of the TSS interact with each other as little as possible⁸⁴.

Many research papers and reports show that the corrosive properties of glycol mixtures are greater than that of the pure substances⁸⁵⁻⁸⁸. This is due to the interaction of hydroxy group with water causing a change in pH, which subsequently leads to easier attack of oxidizing agents (hydroxy group, oxygen etc.) on the metallic surface. Therefore, the corrosive properties of the heat transfer fluids have to be artificially reduced by the addition of corrosion inhibitors^{87,88}. Since the inner part of the thermal solar system where the heat transfer medium flows is always made up of more than one type of material, it is necessary to use a mixture of inhibitors, where each component typically protects specific material, or a specific group of materials⁸⁸. At the present, there is no universal corrosion inhibitor which would be able to protect all materials, however there are several materials that are highly resistive against corrosion, though incomparably more expensive or thermally insufficient^{89,90}. Therefore, setting up the inhibitory system is very often a highly demanding process⁸⁴.

4.3.4.1 Corrosion inhibitors

In the previous sections it was explained that the first heat transfer media for thermal solar systems were derived from coolants used in the internal combustion engines. Since the pure water due to the high fusion point did not meet the requirements, the solution was to dilute water with substances which are able to adjust the fusion point and the solidification process itself. Relatively soon after the needs of these antifreeze agents at the beginning of the 20th century, the first glycol mixtures based on ethylene glycol were introduced. From the first mixture of the heat transfer media a century already passed and during that time countless

substances that could improve the properties of water as a heat transfer medium or completely replace it had been tried^{41,53,91}. Despite this long period of time and efforts of scientists, the glycol mixtures with water firmly hold their primacy as antifreeze heat transfer medium to the cooling systems of cars and thermal solar systems. It is caused primarily by long tradition, low price and still-sufficient properties. The biggest development so far can be then seen in the materials of the systems themselves, whether by car or TSS, rather than in the heat transfer fluids composition. However, corrosion processes still remain as the main reason for the systems' shutdown and damage.

Today, the applied mechanisms of the corrosion inhibition are based on one of the following processes⁹²:

- The inhibitor is chemically adsorbed (chemisorption) on the surface of the metal and forms a protective film with inhibitory effects or by combination of the inhibitor ions and the metallic surface.
- The inhibitor leads to a formation of a film by oxide protection of the base metal.
- The inhibitor reacts with a potential corrosive component present in the media and produces an inert complex.

The easiest way is based on a chemical reaction between the metal surface of the system^{87,89}, when on the surface of the material to be protected is created a protective film⁹², which aims to prevent the effects of aggressive substances from the heat transfer media. The treated surfaces have much higher resistance to various types of corrosion such as galvanic corrosion, pitting corrosion, crevice corrosion, erosion corrosion, cavitation corrosion and intergranular corrosion⁸⁷. A number of substances with similar capabilities is mentioned in the literature, but in practice only a few basic types of inhibitors proved by time are used on a larger scale^{87,89,92}.

The over-all aim is to create a system of inhibitors that would be able to protect all metal materials in the system. Since the first inhibitory systems were created for automotive cooling systems, corrosion inhibitors for aluminium, cast iron, silumin (aluminium–silicon alloy), brass, copper and solder were particularly used. After years of investigation antifreeze heat transfer fluid with anticorrosive non-foaming system based on ethane-1,2-diol and propane-1,2-diol was introduced. And this base, or most of it, is used in the majority of heat transfer fluids based on glycols. Very common composition is following^{93,94}:

- 0.015 wt% of a stabilizer selected from the group of ammonium salts of acrylic acid polymers with molecular weight from 10 000 to 20 000, or their alkali metal salts
- 0.05 to 0.15 wt% sodium nitrate
- 0.10 to 0.20 wt% sodium nitrite
- 0.15 to 0.25 wt% of benzotriazole
- 0.50 to 1.50 wt% of sodium benzoate
- 1-3 wt% of sodium tetraborate
- 0.005 to 0.015 wt% of polydimethylsiloxane
- 0.05 to 0.15 wt% of pentahydrate or nonahydrate sodium metasilicate

Sodium salts of acrylic acid polymer stabilize the system and prevent polymerization of the silicic acid anion and its elimination from the solution, thereby increasing the lifespan of the antifreeze. This system ensures that even when using lower additions of sodium tetraborate of

about 2 wt%, sodium benzoate of about 1 wt% and sodium metasilicate at about 0.1 wt%, the system will have still sufficient alkaline reserve of about 12 % (of equivalent amount of calcium carbonate) that is necessary to neutralize the acids formed from degradation products of the glycols. These additions are also sufficient to maintain the pH within the specified range 7.5 to 8.5. By using 0.2 wt% of benzotriazole as an effective and stable corrosion inhibitor of copper and brass, the liquid gives other possibility of inhibition of tetra sodium salts, benzoic acid and metasilicate supplemented further by addition of sodium nitrate and nitrite. Thus, a fixed combination of inhibitors, that are active on other metals as well. Without the use of benzotriazole, however, these inhibitors would be too aggressive towards copper and brass. To reduce foaming, small amounts of polydimethylsiloxane is also added to the mixture. A certain variability of properties enables us to use other salts of alkali metals and ammonium rather than just sodium salts^{93,94}.

The inventions by Holub et al.^{93,94} are based on using ethane-1,2-diol or propane-1,2-diol only, however, the physical and chemical properties of pure glycol are unsatisfactory and thus designed antifreeze would also be, thanks to the cost of the glycols themselves, expensive. If we take into consideration the physical properties of pure glycol, it is necessary to mention a few facts. At high concentrations the glycols are very viscous, especially at low temperatures, which would impose high requirements on the circulation system and is low heat capacity. Efforts to solve this problem have led to the production of multicomponent mixtures according to the invention which comprises of some 5 to 30 wt% of primary alcohol, 2-20 wt% diol, sometimes also with glycerol, and 40-75 wt% of water. Addition of about 4 wt% corrosion inhibitors then provides sufficient stabilization of the system. However, when using multi-substance mixture, problems arise in the terms of use of common corrosion inhibitors. Altogether, properly setting of the inhibitors in the mixture of so many materials and substances presents a difficult matter however good the other properties of the mixture could be, such as low viscosity, high thermal conductivity, high temperature of boiling and low fusion point^{93,94}.

Despite the undeniable quality of these multicomponent mixtures the manufacturers decided to follow a simpler way and founded their antifreeze mixtures purely on individual glycols. Until recently, the most widely used MEG in the thermal solar systems is already in most systems replaced with the less toxic MPG⁴³. The inhibitors used in these 'clean' diluted mixtures, as described above, formed the basis of modern inhibitory systems, which are gradually replaced by new and more efficient replacements. Besides those inhibitors, we can now encounter with inhibiting additives based on Organic Corrosion Inhibitors (OCI) such as amines, urea, mercaptobenzothiazole (MBT), benzotriazole, tolyltriazol, various aldehydes, heterocyclic nitrogen compounds, sulphur-containing compounds and acetylenic compounds, ascorbic acid, succinic acid, sebacic acid, tryptamine, pyridine, caffeine and several extracts of natural substances^{92,95,96}. With minor modifications, these inhibitors are able to work well even in diluted solution of various glycols⁵³.

It should be noted that the efforts of manufacturers of thermal solar systems and automobiles has led to a reduction in the number of different metal materials in these systems²³. Anticorrosive surface treatment of materials is then seen mainly on components of the thermal solar systems, since the life of the solar system should be around 20 years. With that aspects more expensive materials, such as stainless steel, are starting to be used. Although, for the heat exchangers, and in particular for the construction of the collector absorber, the more thermally conductive copper is still preferred. Even though, the thermal solar systems are using some

different materials than in automotive, the basic amount of said inhibitors for both systems are practically identical with some specialties for the TSS.

4.3.5 Compatibility with sealing materials

Since glycols are also polar chemicals with the possibility of forming hydrogen bonds and donating protons, their solvent properties are similar to water as polar protic solvents. They are thus compatible with most sealing materials that are commonly used in water distribution systems. This also applies to binary mixtures of propane-1,3-diol and water, although this mixture is still not so well known and proven.

4.3.6 Chemical and thermal stability

For long-term use of glycol mixtures in TSS the stability of their chemical and physical properties is essential. Long-term thermal stress of glycol mixtures in the thermal systems causes a change in their properties and forming of some new substances that are depleting the corrosion inhibitor systems, which finally leads to the termination of their activity and necessity for replacement.

Under normal conditions glycols are chemically relatively stable substances. That is, however, only in case that they are not exposed to direct sunlight or to high temperatures in oxidative environment. In the original application, where the glycol mixtures were used as coolant for automotive internal combustion engines, the common operating temperature is about 80-90 °C. This temperature ensures proper engine operation without excessive strain on the heat transfer fluid, although, some gradual chemical changes due to thermal stress also occur. Modern TSS, unlike cars, however, can often reach much higher temperatures and thus cause accelerated chemical destabilization of the used glycol mixtures. For glycol mixtures the destabilization can be in particular seen in the formation of organic acids which attack the inner surface of the systems with which they are in contact^{22,46,57}.

Chemical stability of the entire composition can be provided in terms of alkaline capacity/reserve which is able to compensate for the formation of acids and prolong the life of the fluid media in the system. From this point of view, it appears that the most susceptible to degradation is propane-1,2-diol which is little bit less stable than ethane-1,2-diol. The newly introduced propane-1,3-diol is then assumed to be the most stable, which is slightly inconsistent with its structure as a terminal α,ω -alkanediol⁵⁷.

4.3.7 Environmental aspects

4.3.7.1 Toxicity

Toxicity and ecotoxicity are among the key environmental aspects that are defining the security of using the chemical agents in the relation to the environment. This toxicity is also one of the reasons why the ethane-1,2-diol is being partially replaced by less toxic propane-1,2-diol. In Table 4-2 are summarized some basic ecotoxicological data that could give an idea of the hazardousness of the substances. In the case of ethane-1,2-diol, propane-1,2-diol and propane-1,2,3-triol large amount of valid data are available, due to the large number of comparative studies and long-term mass adoption and use of these substances. But the situation for propane-1,3-diol is much more complicated. Although it is also long-known substance, it has never been produced and used to the extent that it was necessary to determine the toxicological properties in a large scale. The small utilisation of the propane-1,3-diol and generally small amount of available information is also supported by the current absence of it

in the International Programme on Chemical Safety (IPCS) database⁹⁷, The International Chemical Safety Cards (ICSC) database⁹⁸ and only a note in the OECD database⁹⁹.

Table 4-2. LD₅₀ of the selected substances

Substance	Orally	Dermal	Inhalation
	mg/kg	mg/kg	Exposure/concentration
Ethane-1,2-diol	2125 - 4700 ^(R)	3300 ^(H)	> 4000 ppm/4h ^(R)
Propane-1,2-diol	20 000 ^(R)	20800 ^(H)	N/A
Propane-1,3-diol	10,500 - 15,789 ^(Rd)	N/A	> 1800 mg/m ^{3(H)}
Propane-1,2,3-triole	12 600 ^(R)	10000 ^(H)	> 570 mg/m ^{3(R)}

*References^{51,59,65,100}. (R) – rat, (H) – rabbit, (Rd) – rodents.

4.3.7.2 Biodegradability

Glycols degradability in the environment is not in most cases a serious problem. This is due to their good solubility in water and the very nature of the compounds, as the majority of organisms is capable of decomposing alcohols. However, it is necessary to add that the degradability in the environment is greatly limited by the concentration in which they are found and ambient temperature¹⁰¹. Diluted glycols in the environment degrade much faster than in the concentrated form and this also crucially contributes to the effects of acute toxicity as listed in Table 4-2.

Toxic substances are generally biodegraded more slowly because of their decomposition involving only organisms which are resistant to their toxicity. However, in general the glycols are broken down in the environment very fast, including for the human being toxic ethane-1,2-diol¹⁰². That is caused by the fact that the ethane-1,2-diol is mostly toxic only for mammals, but the aquatic organisms and less complex organisms are not affected^{47,50,100}. In the area of biodegradability an extensive research in particular on ethane-1,2-diol, propane-1,2-diol and propane-1,2,3-triol was undertaken, and all were identified by the OECD standards (OECD Test No. 301: Ready Biodegradability¹⁰³) as "rapidly biodegradable"^{51,65,100}. Propane-1,3-diol is still waiting for such research, however, available data indicates that propane-1,3-diol does not remain in the environment for a long time and can be readily degraded in the environment⁵⁹. Also, for the storage of glycols in their concentrated form it is not necessary to introduce any specific measures for assault by microorganisms, as the biodegradability is entirely dependent on water. However, it is necessary to protect them from direct sunlight and high temperatures, because they are susceptible to chemical changes as most of the organic compounds.

4.3.8 Production and applications

The production of the most used ethane-1,2-diol and propane-1,2-diol is based on crude oil derivatives. Ethane-1,2-diol is most often produced by hydration of ethylene oxide, which is generated from ethene by direct oxidation with air or oxygen. The simplified equation of the process is shown on Fig. 4-5. Another production method, which is gaining some attention is production of ethane-1,2-diol from methanol or carbon monoxide through methanol oxidative carboxylation to dimethyl oxalate which is then hydrogenated using copper or ruthenium catalyst to ethane-1,2-diol^{104,105}. Other production methods are not used as they are not

particularly developed or industrially interesting. However, constant research to improve current methods or development new methods is ongoing, including possible bioproduction⁴⁹.

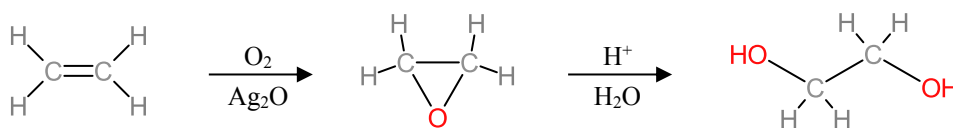


Fig. 4-5 Ethane-1,2-diol production from ethene

The propane-1,2-diol is almost solely produced by direct hydrolysis of propylene oxide with water, when the process is similar to the production of ethane-1,2-diol in many ways including the fractioning distillation following the production process⁵⁴. Propylene oxide (2-methyloxirane) is then gained from propene through hydrochlorination or oxidation by organic peroxides¹⁰⁶. The simplified reaction of 2-methyloxirane to propane-1,2-diol is shown on Fig. 4-6. The reaction is conducted at 200 °C without catalyst or around 150-180 °C in the presence of ion exchange catalyst or small amount of sulphuric acid. Although alternative routes for propane-1,2-diol production have been also investigated, thanks to very good availability of propylene oxide and low waste generation by the standard method none of them gained any important practical application⁵⁴.

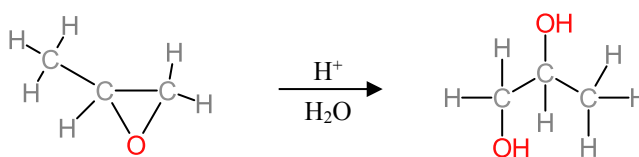


Fig. 4-6 Propane-1,2-diol production from 2-methyloxirane

As was explained earlier, even though the glycols are used in great quantities as antifreeze, it is not their primary field of application. Thanks to the two hydroxy groups, glycols are primarily used for manufacturing of polyesters. Ethane-1,2-diol is one of the main precursors for PET (polyethylene terephthalate) production and propane-1,2-diol is an important chemical feedstock for copolymers used for PU (polyurethane) production. Furthermore, because the propane-1,2-diol is practically non-toxic for mammals, it is also used in many products for human consumption as food additive, tobacco preservative, humectant and solvent for pharmaceuticals. All these applications have created an impressive market over the years and thanks to their mass use in the polymer industry the glycols become very accessible to other sectors. Outside the polymer production and use in antifreeze as a component in heat transfer fluids, important use of the ethane-1,2-diol and propane-1,2-diol lies in their application as aircraft de-icers^{50,107-109} where they are also used in large quantities.

Glycerol is produced mainly as a waste product in the production of biofuels from renewable sources, and this fact is the deciding factor for its price. However, since the production of biofuels depends directly on the political situation and actual government subsidies, the price fluctuates over the years as its use according to the price^{110,111}. Also, since its properties for direct use are poor, it is mainly used for further industrial production or it is considered as a part of the mixtures with ethane-1,2-diol and propane-1,2-diol⁵³.

4.4 Ageing of heat transfer fluids in TSS

The development of the thermal solar systems is constantly rising the operating temperatures and the transferred energy amount for the purpose of increasing the efficiency. That results in faster aging of the glycol-based heat transfer fluids and deterioration of their chemical and physical properties. This can be especially seen in the formation of organic acids, which attack the materials inside the system and cause corrosion damage.

Although the aging of the heat transfer fluid based on glycol is one of the decisive factors affecting the life of the system, the amount of available scientific data is relatively modest and larger studies come from the 80s of the last century, when the production of TSS used a slightly different materials and have a completely different operating conditions¹¹²⁻¹¹⁴. In addition, the in-depth analysis of aging heat-transfer fluids is nowadays conducted only in laboratory simulations of expected conditions and data from real systems are virtually non-existent.

So far, carrying out laboratory tests of products of aging heat transfer fluids based on glycol are primarily addressing the questions of forming acid and the general corrosiveness as recommended by the ASTM D1384¹¹⁵. However, the forming of organic acids does not fully explain the change of physical properties which are evidently occurring. It is therefore a question of what reactions are ongoing in the fluids circulating in the TSS and what compounds are formed. Knowledge of the processes and products of aging in modern TSS can then be authoritative guide for the design considerably improved stabilization system that will be able to resist changes much longer and leads to considerably increase of the usability of the glycol heat transfer fluid and the whole system. This will generally improve the economic parameters and competitiveness of technology as such.

4.4.1 Acidic degradation of aqueous glycol mixtures

Laboratory research conducted under simulated aging glycol mixtures in the laboratory have shown the formation of organic acids in MEG and MPG. These include simple monohydric organic acids generated by partial thermal decomposition of the primary glycol and subsequently its oxidation. As the most common organic acid degradation products are usually stated acetic, glycolic, lactic, pyruvic, oxalic, and formic acid. This topic will be fully explained in the following experimental part of the thesis.

Since PDO has not yet been extended as a heat transfer fluid, any information about its aging or acidic degradation are very rare and will be also discussed in the experimental part of the thesis.

4.4.2 Stagnation process

At present, the stagnation of solar systems is a serious problem that reduces the service life of the heat transfer medium and the system itself. The basic principle is the overheating of the heat transfer medium in the collectors and its subsequent evaporation. This is usually caused in hot-sunny days with insufficient circulation of heat transfer media, bad dimensioning or bad management of the system. During stagnation, there is high thermal strain on the heat transfer fluid, which stresses the organic part of the fluid and significantly reduces the life of the media and, as a result, reduces the lifetime of the whole system. The issue of stagnation can be partly solved by the construction of collectors with good evacuation ability. The designs of collectors with good evacuation ability is shown on Fig. 4-7 (top). As soon as the temperature in the collector exceeds the boiling point, the fluid starts to evaporate, and the produced overpressure

pushes the remainder of the liquid from the collector to prevent the evaporation of a larger amount of heat transfer fluid. The whole process can be divided into five distinguishable phases⁸⁰:

1. Liquid expansion.
2. Forming of saturated steam, which pushes the liquid out of the collectors.
3. The collectors are emptying by saturated steam from boiling of the heat transfer fluid. The pressure in the system is rapidly increasing. The steam expands to other parts of the system transporting the energy in form of condensation. The pressure reaches its maximum at the end of this phase.
4. The collectors are emptied by saturated and overheated steam and an equilibrium is reached. In case a lot of steam is created, the safety valve vents some of the pressure outside to protect the system from bursting. The stagnation reaches its equilibrium and this state can continue for long time.
5. By restoring the sufficient energy transport or decreasing of the energy input (reduction of the solar irradiation) the steam/vapour condenses back to its liquid form and the collectors are refilled. The stagnation ends.

During the stagnation the system is exposed to considerably high temperatures and pressures, though the actual values are highly dependent on the system design as has been demonstrated by several works^{80,83,116}. The approximate stagnation temperatures for some collectors are listed in Table 4-3.

Table 4-3. Approximate stagnation temperatures for different collector types^{17,67}

Open collector with no cover glass	65-100 °C
Non-selective collector with cover glass	100-120 °C
Selective collector with cover glass	180-200 °C
Vacuum tube collector	250-300 °C

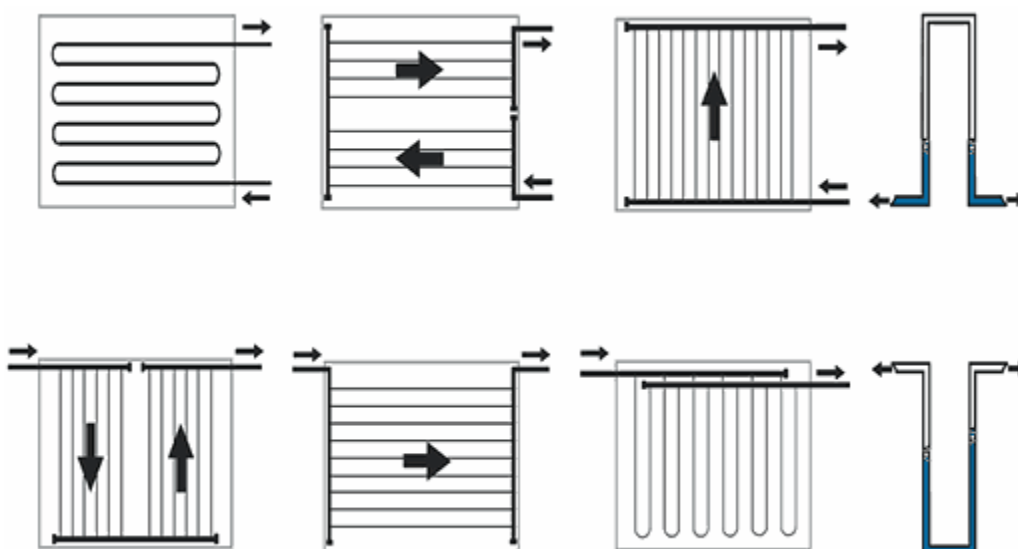


Fig. 4-7 Evacuation ability of different design solution, good (top), bad (bottom)⁸²

The problem of bad evacuating ability as it is shown on Fig. 4-7 (bottom) is mostly concern of older installation as modern systems are usually built differently and don't suffer from this lack of design. On the other hand, even with good evacuation ability, the fact that part of the system and part of the heat transfer fluid is exposed to some critical temperatures and pressures remains unchanged. The stagnation process was studied in detail in the work of Quiles et al.¹¹⁷, and many of the logical predictions were positively proven. One of them is that basically any system is susceptible to overheating and subject of potential stagnation regardless the design. The reason is that most of the systems are completely isolated and do not work with waste energy release. Especially high risk is for small systems with limited accumulation capacity and irregular use of the prepared domestic hot water.

To reduce the stagnation frequency or completely prevent it many designs have been tested. As the more advanced can be classified special thermochromics absorber coatings^{118,119} or special prismatic cover structures¹²⁰. The thermochromics coatings work with changing absorptive capabilities through change of colour based on the surface temperature. When the system enters the third phase, as explained earlier, the temperature rises dramatically. By the change of the temperature the absorptive layer of the collectors with thermochromics coating changes its colour and rejects most of the solar irradiation. The prismatic structure works differently and focuses on the part of the day with the highest risk of stagnation. By adjusting the prism on top of the absorber and its correct positioning, the system automatically reflects most of the energy back to atmosphere without absorbing it. Unfortunately, these physical systems are still quite new and not yet significantly widespread.

Thermal shocks resulting from the stagnation contribute to the degradation processes of the heat transfer fluid and degradation of the whole system. Another problem is caused by the evaporation of the heat transfer fluid and the elimination of stabilizing systems such as corrosion inhibitors and pH stabilizers from the fluid. If these substances are not adapted to be reconstituted in the cooled, re-condensed heat transfer fluid after stagnation, the concentration gets lower and the system is later less protected against corrosion. Naturally, the designers and manufacturers of the heat transfer fluids and inhibitor mixtures are fully aware of this problematic and the majority of new heat transfer fluids are equipped with inhibitor systems which are capable of dissolving upon exclusion. However, the elimination of inhibitory systems is not the only thing that causes degradation of heat transfer media. Glycols that are contained as a main base in antifreeze mixtures for thermal solar systems suffer by the high temperature themselves. Several researchers reported results from laboratory studies on the thermal degradation of the glycolic mixtures and their degradation and the effects of high temperatures is indisputable. However, the cumulative effect of continuous stagnation was not studied in such detail yet.

4.5 Propane-1,3-diol

In the late years a new liquid is discussed as a possible freezing point depressant for water. The fluid propane-1,3-diol belongs to the group of di-alcohols and glycols and shares many similar properties with other substances with the other chemicals from the same group including its possible applications.

4.5.1 Basic physical and chemical properties

The basic chemical and physical properties of pure propane-1,3-diol are very similar to those of propane-1,2-diol. The structural differences are apparent from the Fig. 4-8. The position of both of the hydroxyl groups in terminal position on the molecule is playing an important part in the interaction with water, which will be explained in more detail in the experimental part of this thesis. The most important data on pure propane-1,3-diol are summarized in Table 4-4. Although most of the important data on pure propane-1,3-diol are already available in good quantity and sufficient quality, the most important data on its aqueous form are rare.

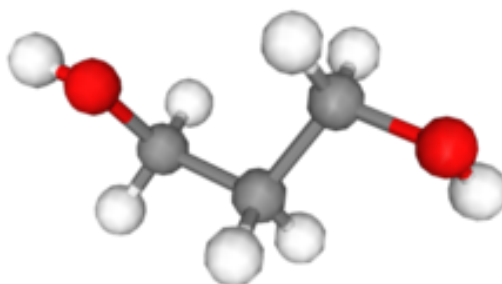


Fig. 4-8 Propane-1,3-diol 3D structural model

Table 4-4. Basic physical and chemical data on propane-1,3-diol

CAS Number	504-63-2
Names	Propane-1,3-diol (IUPAC); 1,3-Propanediol; 1,3-Dihydroxypropane; Trimethylene glycol; PDO
Chemical formula	C ₃ H ₈ O ₂
Molar mass (<i>M_r</i>)	76.095 g·mol ⁻¹
Density (at 25 °C) (<i>ρ</i>)	1.0597 g·cm ⁻³
Melting/Fusion point (<i>T_F</i>)	-27 °C
Boiling point (<i>T_B</i>)	210-212 °C
Viscosity (at 20 °C) (<i>η</i>)	52.007 mPa·s
Vapour pressure	4.5 Pa
Refractive index (<i>n_D</i>)	1.440
pH (50 % aqueous solution at 25 °C)	6.544

References^{36,68,121,exptl.}

4.5.2 Production

Most of the propane-1,3-diol produced at the moment is used for producing of poly(trimethylene terephthalate), also known as PTT¹²². This versatile polymer is mostly used in carpet production⁵⁶ but thanks to its unique properties it is also considered for many other applications such as clothes and functional sportswear^{56,58}.

The main synthesis routes for producing propane-1,3-diol are hydroformylation from ethylene oxide and hydrolysis followed by hydrogenation of acrolein. These two techniques are

the most used for the current production⁵⁶ with the raw source of material for the synthesis being crude oil. Another synthetic route was also developed from now abundantly available glycerol, produced as a by-product from bio-fuel/bio-diesel production¹²³. Together with the classical synthetic routes, new bio-approaches are investigated to answer the global demand for clean and environment-friendly technologies. The bio-transformation of glycerol through bacteria was thoroughly investigated by several researchers^{124,125} and it is still under investigation. Though, this simple bio-transformation route employs common glycerol available from bio-fuel production¹²⁶, other more direct approaches of bio-production of propane-1,3-diol are also investigated. Some of the processes are patented and were already commercialized⁵⁸, like the DuPont's Bio-PDO™ for Sorona® PTT production by its own corn sugar fermentation method. Other big producer of propane-1,3-diol, the Shell company, is producing propane-1,3-diol mainly from the oil-based ethylene oxide for production of its PTT's polyester version Corterra™. Including the fermentation process of corn sugar by DuPont, other processes of biomass fermentation are also investigated like in the case of two-stage fermentation of wheat-based thin stillage reported by Ratanapariyanuch in 2017¹²⁷. Many other methods are then summarised in the microbial production of propane-1,3-diol review put together by Saxena¹²⁸.

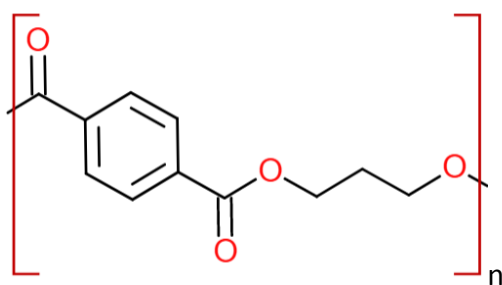


Fig. 4-9 Poly(trimethylene terephthalate)

4.5.3 Reactivity and degradability

One of the first mentions of the propane-1,3-diol to be used as an antifreeze additive with improved thermal stability was prepared by Eaton and his coworkers⁵⁷ in 2001. Their experiment was designed to prove the lower reactivity and degradability of the propane-1,3-diol in the system compared to other commonly used glycols, propane-1,2-diol and ethane-1,2-diol. The experiment was conducted in accordance with ASTM D3306¹²⁹ and D6210¹³⁰, but to fully explore the possibilities of the fluid the experiments were conducted at significantly elevated temperature of 150 °C. Although, the above-mentioned research provides some interesting data on reduced corrosivity of the aqueous solution of propane-1,3-diol, it cannot be deemed as a conclusive in terms of chemical stability of the propane-1,3-diol as any further analysis of degradation products and their quantities was not conducted as will be discussed later.

The antifreeze mixture with propane-1,3-diol can already be found as a green alternative to the present antifreeze, but studies on the reactivity and degradation of aqueous propane-1,3-diol are still scarce. Some of the recent studies on the degradation of propane-1,3-diol are provided in the experimental section together with detailed analysis of its physical properties.

5 EXPERIMENT

5.1 Samples and their preparation

5.1.1 Samples for estimation of ageing processes

5.1.1.1 System Vracov

The experimental system Vracov is located in South Moravia region in the Czech Republic, Fig. 5-1. The system started its operation on 4. 4. 2007. During the whole time only one heat transfer fluid *Solaren* was used. The manufacturer of the heat transfer fluid is VELVANA a.s., Velvary, Czech Republic. The main characteristics of the system are summarized in Table 5-1 and the main components are listed in Table 5-2.

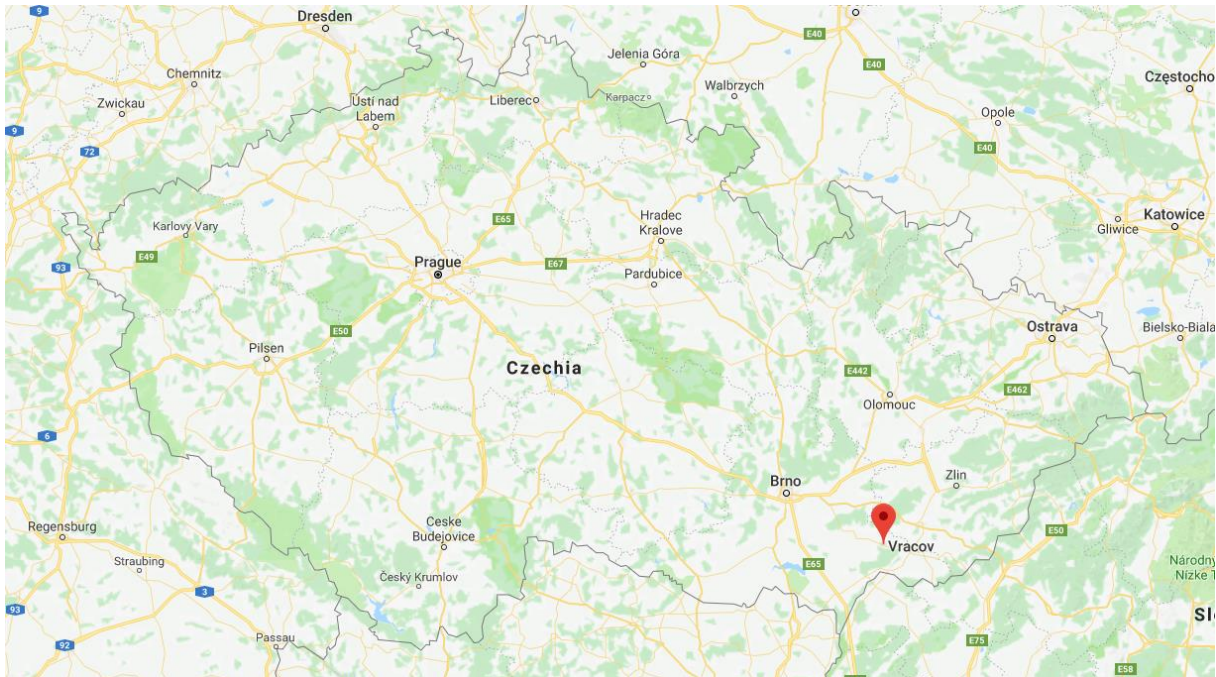


Fig. 5-1 Position of Vracov, Czech Republic

Table 5-1. Characteristics of the experimental system Vracov

Number of thermal collectors	6
Type of thermal collectors	Heliostar H400
Absorption area (sum)	10.6 m ²
DHW cylinder volume	0.3 m ³
Accumulator volume	1.3 m ³
Total length of piping	~80 m
Usage	DHW preparation + partial space heating

Table 5-2. Main components of the experimental system Vracov

Component	Material (contact with HTF)	Inner area	Volume
Heliostar H400 x6	Copper	1.8 m ²	7.8 L
Boiler cylinder Antikor SPE 300	Stainless-steel	2.0 m ²	0.8 L
Plate heat exchanger SWEP	AISI 316	2.4 m ²	0.9 L
Copper piping + soldered joints	Copper, Solder(Pb:Sn-1:1)	2.5 m ²	4.3 L
Circulator pumps (2 pumps)	Cast iron	0.3 m ²	0.4 L

The stated components from Table 5-2 are in direct contact with the heat transfer fluid constantly. The system also contains some other components such as valves and expansion tank, but their contact with the fluid is minimal and it is not expected for them to have any negative effect on the ageing process. The effective volume and contact inner area of such components is therefore negligible.

Table 5-3. Samples from experimental thermal solar system in Vracov

Sample designation	Sampling date	Description
VO2007	2006 (manufactured)	Original heat transfer fluid used or the first filling of the system in 2007. The fluid is a mixture of propane-1,2-diol at 48 wt% and water plus stabilizing and anticorrosion additives.
VO2014	10. 11. 2009 (manufactured)	It is heat transfer fluid, which was used to fill-up loses caused by continuous sampling. The filling up of the system was conducted only once in year 2014. The composition is identical to VO2007 with minor changes in the receipt of the anticorrosion system. The ratio between water and propane-1,2-diol remained the same.
V2007	18. 6. 2007	Sample from the working experimental system in Vracov.
V2008	21. 4. 2008	Sample from the working experimental system in Vracov.
V2009	1. 6. 2009	Sample from the working experimental system in Vracov.
V2011	27. 3. 2011	Sample from the working experimental system in Vracov.
V2012	27. 3. 2012	Sample from the working experimental system in Vracov.
V2013	1. 4. 2013	Sample from the working experimental system in Vracov.
V2014	13. 4. 2014	Sample from the working experimental system in Vracov.
V2014N	13. 4. 2014	Another sample was taken after filling of 1 litre of new HTF to compensate for the losses due to sampling.

After sampling from the system, the samples were kept in 250 mL big transparent polypropylene flasks in a refrigerator. That applies also for the sample of the original unused fluid from 2007. The sample VO2014 of the newer fluid used to toping-up the system in 2014 was kept in its original container made of opaque blue polyethylene, also in refrigerator.

During the years the samples were used by several graduate students for their research, but unfortunately, due to their careless handling of the samples, and despite the all well-intended

recommendations from the supervisors, some of the samples were completely depleted before measuring all of the necessary properties.

5.1.1.2 Highly degraded sample selection

To compare the results with the experimental system in Vracov several other samples of the HTF Solaren were obtained from other systems in different stages of destabilization of the HTF.

Table 5-4. Selected samples of highly degraded HTF

Sample designation	Sampling date	Description
SP	12.4.2014	Sample of a spent HTF <i>Solaren</i> from system in Petrov, Czech Republic. The filling of the system was conducted in 2010 and from that time, the system went through several cycles of stagnation.
SJ	11.3.2014	Sample of a spent HTF <i>Solaren</i> from a home-sized system localized in South Moravia. System went through a several cycles of stagnation.
SD	2014	Sample of a spent HTF <i>Solaren</i> from a middle-sized system from city Ostrava, Czech Republic. Due to the faulty pump, the system was undergoing a cyclic stagnation for several days, until discovered by a technician.
TS	14.3.2014	Sample of a spent HTF <i>FSV</i> from original filling by supplier of the system Sonnekraft. This HTF is also based on propane-1,2-diol, like in the case of <i>Solaren</i> , however, different inhibitor system was used to withstand higher temperatures of the vacuum tube collector. The freezing protection is stated up to -28 °C. System is localized in the region of South Moravia.

5.1.2 Samples of propane-1,3-diol

Table 5-5. Samples of propane-1,3-diol

Sample designation	Sampling date	Description
PDOC	2010	Pure (≥ 99 %) propane-1,3-diol from a Chinese manufacturer
PDOD	2015	Pure (≥ 99.8 %) propane-1,3-diol from DuPont Tate&Lyle BioProducts™

5.2 Used chemicals and materials

Table 5-6. Chemicals used for isotachopheresis

Chemical	CAS No.	State	Purity	Manufacturer
H ₂ O (Mili-Q)	7732-18-5	Liquid	Ultrapure	
Formic acid	64-18-6	Liquid	≥ 98 %	Sigma-Aldrich/France
Acetic acid	64-19-7	Liquid	≥ 99 %	Sigma-Aldrich/Germany
2-hydroxyethanoic acid	79-14-1	Solid	AR grade	Sigma-Aldrich/Germany

Table 5-6. Chemicals used for isotachophoresis (continuing)

Chemical	CAS No.	State	Purity	Manufacturer
Oxalic acid - dihydrate	6153-56-6	Solid	≥ 99.5 %	Penta Chrudim/CZ
2-hydroxypropanoic a. 80%	79-33-4	Liquid	AR grade	Penta Chrudim/CZ
Hydrochloric acid 35%	7647-01-1	Liquid	AR grade	Penta Chrudim/CZ
Hexanoic acid	142-62-1	Liquid	≥ 99 %	Sigma-Aldrich/Germany
6-aminohexanoic acid	60-32-2	Solid	≥ 99 %	Sigma-Aldrich/Germany
Hypromellose	9004-65-3	Solid	N/A	Sigma-Aldrich/Germany

Table 5-7. Chemicals used for mass spectrometry

Chemical	CAS No.	State	Purity	Manufacturer
H ₂ O (Mili-Q)	7732-18-5	Liquid	Ultrapure	
Methanol	67-56-1	Liquid	HPLC	Sigma-Aldrich/France
Acetic acid	64-19-7	Liquid	HPLC	Sigma-Aldrich/Germany

Table 5-8. Chemicals used for Karl Fisher titration

Chemical	CAS No.	State	Purity	Manufacturer
H ₂ O (Mili-Q)	7732-18-5	Liquid	Ultrapure	
Methanol	67-56-1	Liquid	≥ 99.8 %, Anhyd.	Sigma-Aldrich
HYDRANAL Methanol dry		Liquid		Sigma-Aldrich/Fluka/Germany
HYDRANAL Composite 5 K		Liquid		Sigma-Aldrich/Fluka/Germany

Table 5-9. Chemicals used for atomic absorption spectrometry

Chemical	CAS No.	State	Purity	Manufacturer
H ₂ O (Mili-Q)	7732-18-5	Liquid	Ultrapure	
Ethanol	64-17-5	Liquid	≥ 96 %, Tech. grade	
Cu aq. calibration standard 1.000 g·L ⁻¹		Solution	± 0.002	
Fe aq. calibration standard 1.000 g·L ⁻¹		Solution	± 0.002	
Pb aq. calibration standard 1.000 g·L ⁻¹		Solution	± 0.002	

Table 5-10. Chemicals used for determination of pH

Chemical	CAS No.	State	Purity	Manufacturer
H ₂ O (Mili-Q)	7732-18-5	Liquid	Ultrapure	
Ethanol	64-17-5	Liquid	≥ 96 %, Tech. grade	
Potassium tetraoxalate dihydrate	6100-20-5	Solution	12.6 g/L, pH=1.679 (25 °C)	Centipur
Potassium hydrogen phthalate	877-24-7	Solution	50.0 g/L, pH=4.005 (25 °C)	Centipur
di-Sodium tetraborate decahydrate	1303-96-4	Solution	47.0 g/L, pH=9.180 (25 °C)	Centipur

Table 5-11. Chemicals used for determination of conductivity

Chemical	CAS No.	State	Purity	Manufacturer
H ₂ O	7732-18-5	Liquid	Deionized	
Ethanol	64-17-5	Liquid	≥ 96 %, Tech. grade	

Table 5-12. Chemicals used for pycnometry

Chemical	CAS No.	State	Purity	Manufacturer
H ₂ O	7732-18-5	Liquid	Distilled	
Ethanol	64-17-5	Liquid	≥ 96 %, Tech. grade	

Table 5-13. Chemicals used for Oscillating U-tube Densitometry

Chemical	CAS No.	State	Purity	Manufacturer
H ₂ O	7732-18-5	Liquid	Deionized	
Ethanol	64-17-5	Liquid	≥ 96 %, Tech. grade	

Table 5-14. Chemicals used for Capillary Viscometry

Chemical	CAS No.	State	Purity	Manufacturer
H ₂ O	7732-18-5	Liquid	Distilled	
Ethanol	64-17-5	Liquid	≥ 96 %, Tech. grade	

Table 5-15. Chemicals used for Rotational Viscometry

Chemical	CAS No.	State	Purity	Manufacturer
H ₂ O	7732-18-5	Liquid	Deionized	
Ethanol	64-17-5	Liquid	≥ 96 %, Tech. grade	

Table 5-16. Chemicals used for refractive index measurement

Chemical	CAS No.	State	Purity	Manufacturer
H ₂ O	7732-18-5	Liquid	Deionized	
Ethanol	64-17-5	Liquid	≥ 96 %, Tech. grade	

Table 5-17. Chemicals used for freezing point measurement

Chemical	CAS No.	State	Purity	Manufacturer
H ₂ O	7732-18-5	Liquid	Deionized	
Ethanol	64-17-5	Liquid	≥ 96 %, Tech. grade	

Table 5-18. Chemicals used for corrosivity quantification

Chemical	CAS No.	State	Purity	Manufacturer
H ₂ O	7732-18-5	Liquid	Deionized	
Ethanol	64-17-5	Liquid	≥ 96 %, Tech. grade	

5.3 Used Equipment

Table 5-19. Machine and Equipment used according to method

Method	Machine/Equipment	Manufacturer
Isotachophoresis	Isotachophoretic analyser EA 100	Villa LABECO s.r.o., Spišská Nová Ves, SK
Mass spectrometry	Agilent 6320 Series Ion Trap LC/MS	Agilent Technologies, USA
-	Syringe infusion pump KDS 100	KD Scientific Inc., USA
Karl Fisher Volumetric Titration	852 Titrando with generator electrode without diaphragm	Metrohm AG, Switzerland
Atomic absorption spectrometry	AAS SpectrAA 30	Varian Techtron, Australia
pH determination	inoLab pH Level2	WTW, Svitavy, CR
-	Hotplate stirrer	
Conductivity determination	inoLab Cond Level3	WTW, Svitavy, CR
-	Hotplate stirrer	
Pycnometry	25mL glass pycnometer	
-	Insulated vessel	BUT, CR - (Self-produced)

Table 5-19. Machine and Equipment used according to method (continuing)

Method	Machine/Equipment	Manufacturer
Oscillating U-tube Densitometry	Anton Paar Stabinger SVM 3000	Anton Paar, Germany
-	Cryostat Julabo F-34	Julabo, Germany
Capillary Viscometry	Ubbelohde U-type viscometer	
-	Insulated vessel	BUT, CR - (Self-produced)
-	Automatic Ubbelohde Viscometer - Prototype	BUT, CR - (Self-produced)
-	Immersion Cooler Huber TC40E	Huber, Germany
Rotational Viscometry	Anton Paar Stabinger SVM 3000	Anton Paar, Germany
-	Cryostat Julabo F-34	Julabo, Germany
Refractive Index	Anton Paar Abbemat 350 Automatic Refractometer	Anton Paar, Germany
Freezing point	Immersion Cooler Huber TC40E	Huber, Germany
-	Isolation Box	BUT, CR - (Self-produced)
Corrosivity	Hotplate stirrer	
	Set of standard metal samples according to ASTM D1384	

In all cases was also used various laboratory glassware such as beakers, flasks, volumetric flasks, Erlenmeyer flasks, gas-tight syringes, Hamilton syringes, coolers etc. The actual used glassware is described in individual methods. For weight measuring analytical balances with resolution of 0.0001 g with standard deviation / repeatability of ± 0.1 mg were used. The balances are periodically tested and standardized and are situated on antivibration analytical balances table. For preparation of ultrapure water (Mili-Q) a purification system from MilliporeTM was used. The resistivity of the prepared ultrapure water was $R = 18.2$ M Ω .

5.4 Methods

Systematically, the methods used in this work can be divided into two categories according to the target application and sample group. The two categories are in accordance with the goals of this work and are following systematic analysis of prepared samples to reach comprehensible and clear conclusions. Because some of the methods were used simultaneously for both categories in the same manner, the description of the methods is stated individually to avoid double description.

5.4.1 Ageing of the heat transfer media and determination of degradation products

The first group covers methods used to analyse and determine the ageing processes in the heat transfer fluids based on glycols. Selected and used methods to determine the degradation products and the ageing processes were as follows:

- Isotachopheresis
- Mass spectrometry
- Karl Fisher volumetric titration
- Atomic absorption spectrometry
- Determination of pH
- Determination of conductivity
- Viscosity
- Freezing point measurement

5.4.2 Analysis of properties of aqueous propane-1,3-diol

- Density
- Viscosity
- Refractive index measurement
- Freezing point measurement
- Corrosivity quantification

5.4.3 Isotachopheresis

Isotachopheresis (ITP) belongs to the group of electromigration methods¹³¹ dating to the end of 19th century¹³² and it is a nonlinear technique used for separation of ionic compounds. The compound can be almost any charged molecules from a small metal ion to large proteins^{133,134}. The meaning of nonlinear technique lies in the self-concentrating and self-sharpening of the analytes originally present in the sample. This makes ITP very powerful tool for analysing samples of very low concentration or quantity¹³⁵.

The basic working principle is based on two base electrolytes with different electrophoretic mobility. The electrophoretic mobility μ [$\text{m}^2 \cdot \text{s}^{-1} \cdot \text{V}^{-1}$] describes the ability of charged particle – ion to move inside an electric field. It is described as an observed rate of migration of a component (v [$\text{m} \cdot \text{s}^{-1}$]) divided by electric field strength (E [$\text{V} \cdot \text{m}^{-1}$]) and it is specific for a given medium, in this case an electrolyte solution. The base electrolyte with higher electrophoretic mobility is called Leading Electrolyte (LE) and the base electrolyte with lower electrophoretic mobility is called Terminating Electrolyte (TE). The main parts of a typical ITP are shown on Fig. 5-2. The basic parts are the cells filled with leading electrolyte and terminating electrolyte. The cells are connected by hollow tube or capillary and the cells with electrolyte are equipped with pair of electrodes connected to a regulated DC current source creating together a closed circuit.

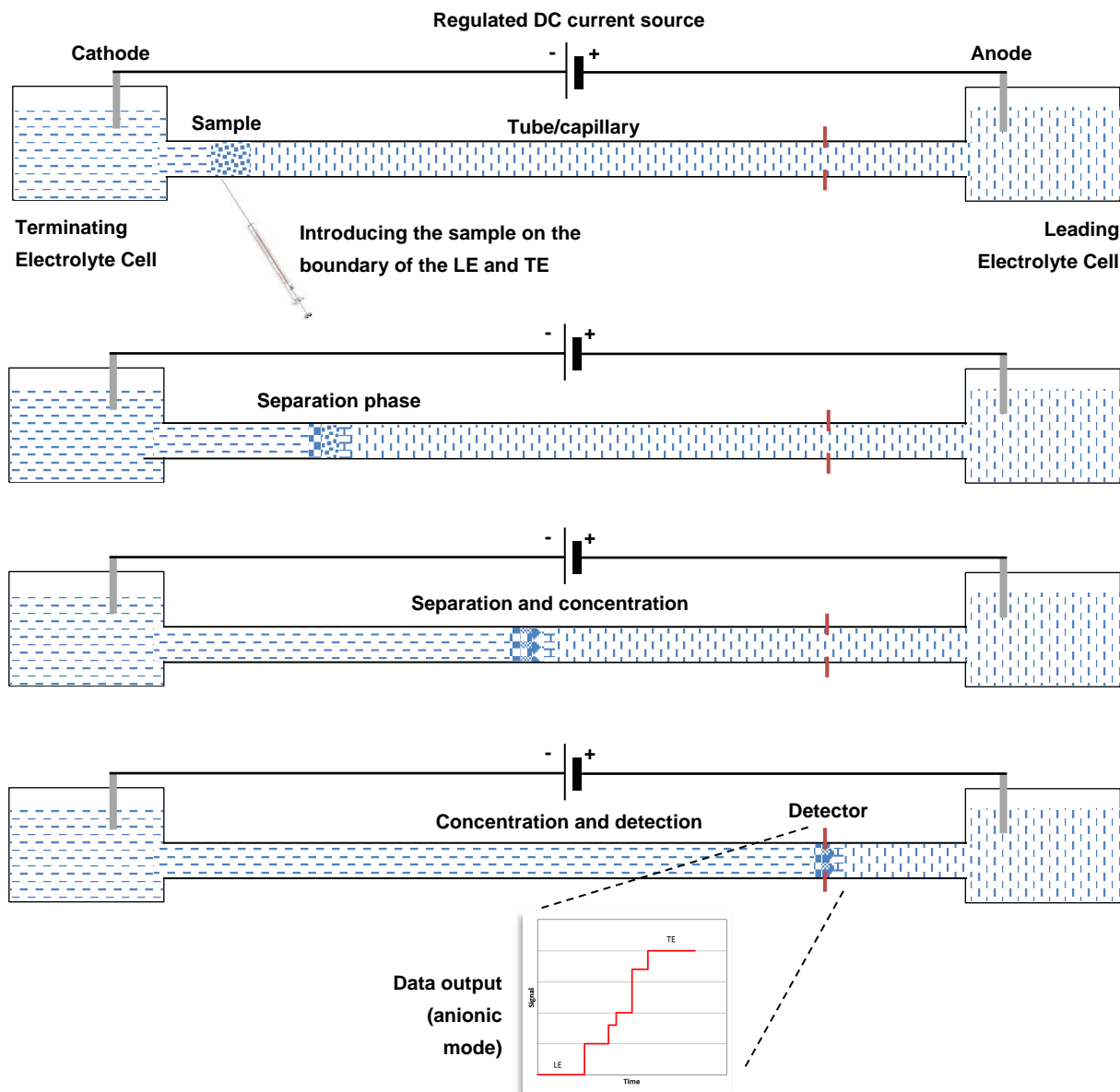


Fig. 5-2 Isotachopheresis - principle diagram

The process of electrophoretic separation in case of ITP starts with filling the system with leading electrolyte into the cell for leading electrolyte (on the right on Fig. 5-2) and the tube/capillary. The terminating electrolyte is also filled into its designated cell creating practically a boundary in the tube/capillary between leading electrolyte and terminating electrolyte. The sample is introduced into the system exactly in the boundary, therefore separating the leading and terminating electrolyte creating a so called sample zone or plateau. By applying a constant current to the electrodes submerged in the electrolytes in the cells, the ions start to move towards the appropriate electrodes. Anions towards anode and cations towards cathode. By carefully choosing the electrolytes and mode of analysis the whole sample zone will start to move towards the detector and separating and concentrating the samples analytes in the process thanks to the different electrophoretic mobilities. To be able to analyse the samples analytes it is necessary to choose leading electrolyte with higher electrophoretic

mobility than of the sample's analytes and terminating electrolyte with lower electrophoretic mobility than of the sample's.

The self-concentrating ability based on different electrophoretic mobilities can be described by the following Kohlrausch equation, describing the theoretical concentration in a plateau of the analyte in the created zone of the sample:

$$c_{plateau} = c_{LE} \frac{z_{LE}(|\mu_{LE}| + |\mu_{counter-ion}|)\mu_{analyte}}{z_{analyte}(|\mu_{analyte}| + |\mu_{counter-ion}|)\mu_{LE}}, \quad (5.4.1)$$

where $c_{plateau}$ is the sample concentration in the theoretical plateau, c_{LE} is the concentration of the leading electrolyte, z_{LE} and $z_{analyte}$ are the charges of the leading electrolyte and analyte, and μ_{LE} , $\mu_{analyte}$ and $\mu_{counter-ion}$ are the respective electrophoretic mobilities¹³⁶. The self-concentration effect is very strong and during the process can be enhanced up to million times¹³⁷. This allows us to detect precisely analytes in even very diluted samples.

ITP method is generally used for quantitative analysis. Because during the measurement the electrophoretic mobilities are constant as long as the applied current is constant, we can precisely measure the amount of the analytes by comparing them to the standards. The comparison is done through the fact that at the time of the detection, according to the Eq. (5.4.1), the concentration of the analyte is the same as of the standard and by simply comparing the time of passing the substances through the detector we can easily calculate the unknown amount of the analyte from known concentration of the standard.

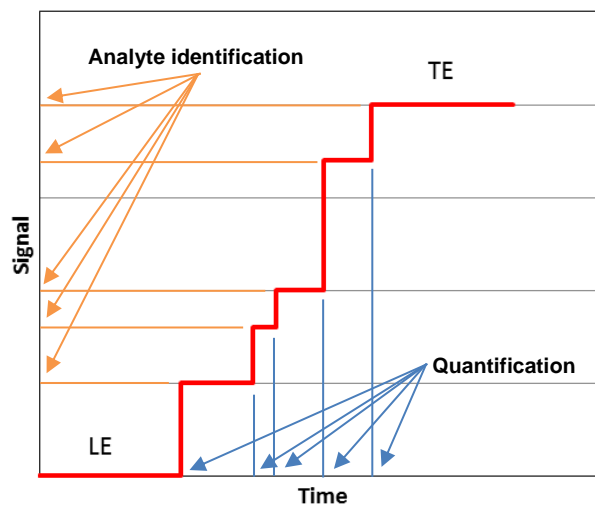


Fig. 5-3 Isotachophoresis - quantitative and qualitative analysis

To calculate the amount of analyte it is also necessary to correctly identify it and compare it to the correct standard. That is done on the basis of the signal output. As it is shown on Fig. 5-3 there is a difference between the leading and terminating electrode signal value represented by the lowest and the highest signal output. Each step then represents different plateau in the sample zone, therefore accordingly different analyte. In the example on Fig. 5-3 is used typical output from conductivity detector, but ITP can be also equipped with detectors such as UV detector or gradient detector.

5.4.3.1 Sample preparation

Before application the samples were filtered through a filtration paper to eliminate any solid impurities and to avoid clogging of the system. No other preparations were conducted and the samples were used in their undiluted - original form.

5.4.3.2 Measurement procedures

The basis for the measurement was taken from application bulletin No. 13 (RECMAN Laboratorní technika¹³⁸) used for determination of organic and some inorganic acids in sugar and sugar solutions. The first step before actual measuring was to prepare the leading and terminating electrolyte and stock solutions of the standards used for qualitative and quantitative analysis of organic acids. The leading and terminating electrolyte were prepared as it is described in Table 5-20. The standard stock solutions of the organic acids were prepared in concentrations of 10 mmol·L⁻¹. The standard solutions were prepared for formic acid, acetic acid, 2-hydroxyethanoic acid, oxalic acid and 2-hydroxypropanoic acid.

Table 5-20. Isotachophoretic analysis setting

Capillary size	0.8 mm
Analysis mode	Anionic
Analysis time	20 minutes
Leading Electrolyte	10 mmol·L ⁻¹ hydrochloric acid, 10 mmol·L ⁻¹ 6-aminohexanoic acid, 0.2 % hypromellose
Terminating Electrolyte	5 mmol·L ⁻¹ hexanoic acid
Working current – starting (I_S)	50 μ A
Working current – terminating (I_T)	250 μ A

Before the actual measurement the separation capillary was thoroughly washed three times with the prepared electrolytes to eliminate any influence of previous measurement. The cleaning process was done ultimately the same way as the actual measurement, but instead of injecting of the sample on the boundary of leading and terminating electrolyte only leading electrolyte was injected. The amounts of standards and sample injections are then described with the results.

5.4.4 Mass spectrometry

Mass spectrometry (MS) is a detection method used to detect molecules and atoms based on proportion between the weight of the particle and its charge. This ratio is generally described as m/z ratio and for ions with the charge of ± 1 (describes the number of electrons in terms of deficiency or abundance) is usually equivalent to the value of the relative atomic or molecular mass¹³⁹. MS is often used as a tandem technique with separation methods. Typical combinations are with gas or liquid chromatography, or less commonly with supercritical fluid chromatography or capillary electrophoresis¹⁴⁰. MS systems can also be used independently if the settings allow it. In this work, the MS system is used without a separation method, therefore, the separation part of the system is not explained in here. The whole MS system schematic used

in work is shown on Fig. 5-6. The MS system can be divided into basic parts based on what gradually happens to the analyte. These parts are ion source, analyser and detector.

The ion source of the MS system is responsible for creating ions from so far neutral molecules and atoms. The MS system used in this work is Ion Trap Agilent 6320 equipped with electrospray. The diagram and basic principle of operation of electrospray is pictured on Fig. 5-4. One of the biggest advantages of the electrospray is its capability to work under atmospheric pressure. The ionization of the molecules by electrospray can be described by a two-step process as Nebulization and Desolvation¹⁴⁰. In the first phase due to the effect of sheer force of the nebulizing gas and high voltage (2-10 kV)¹⁴¹, applied between the spraying capillary and the end plate at the entrance to analyser, the sample solution is forced out of the spraying capillary forming small droplets containing ions of chosen polarity. Due to the electrostatic repulsion forces in the droplets, the ions of one polarity migrate to the droplet surface. In the second phase the droplets are gradually dried by the drying gas (in this case by nitrogen) heated up to 300 – 400 °C. The principle is depicted on the lower part of the Fig. 5-4. By evaporating of the solvent, the volume and surface area of the droplet is reduced which leads to increase of the charge density on the surface until the Rayleigh limit¹⁴² is reached. By additional evaporation of the solvent the Rayleigh limit is exceeded, which means that the Coulomb repulsion forces become bigger than the surface tension and the droplet divides. This process is then repeated until an individual droplet contains only one molecule with remaining charge on at least some of them. The ions are then lead into the dielectric capillary. The ions are then accelerated and focused through series of instruments such as skimmers and octopoles and transferred to analyser.

The analyser of MS system used in experimental part is spherical ion trap with ring type electrode. The great importance of this device is emphasized by the Nobel prize in physics in 1989 for its invention for Hans Dehmelt and Wolfgang Paul. The spherical ion trap is constructed from three electrodes of a hyperbolic profiles positioned in a unique geometry. The purpose of the ring electrode and end cap electrodes is to create a stable quadrupolar field which is then capable to interact with ions¹⁴³.

The spherical ion trap works in cycles containing from filling the trap with ions, their stabilization and ejection/scanning. In the first step the endcap electrodes are grounded and on the ring electrode a high AC voltage at radio frequencies (RF) (781 kHz¹⁴⁰) is applied. The ions are then trapped inside the quadrupolar electric field based on their mass and the level of voltage of the applied RF. The trapped masses range is typically wide enough and allows to scan spectrum in a wide range at high sensitivity. The trapping capabilities are dependent on the speed of the ions from the ion source and the immediate phase of the RF voltage. If the ions are too fast and the RF phase is near the middle, the ions just fly through the trap without being caught inside the dynamic field. To slow down the ions and allow them to be affected by the dynamic field, the ion trap is filled with helium atoms (buffer gas) which absorb part of the kinetic energy of the entering ions. That allows longer residence time of the ions inside the trap, long enough for them to be affected by the field.

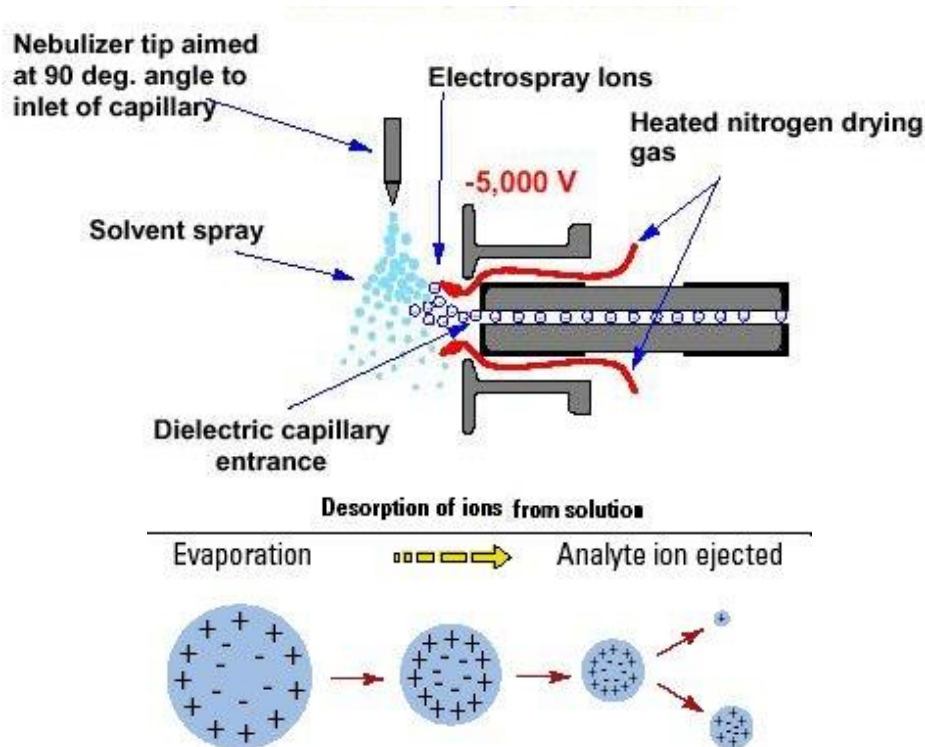


Fig. 5-4 MS – Electro spray ionization diagram and principle (Agilent)¹⁴⁴

Once the ions are inside the trap, their actual trapping depends on voltage of the RF and on the auxiliary AC voltage between the endcap electrodes. This process is described by the Mathieu stability diagram shown on Fig. 5-5 (right). The spherical ion trap is operated in the RF-only mode without additional DC voltage. The stability of the ions then follows the red arrow (q_z axis) depicted on the Fig. 5-5 (right) at $a_z = 0$.

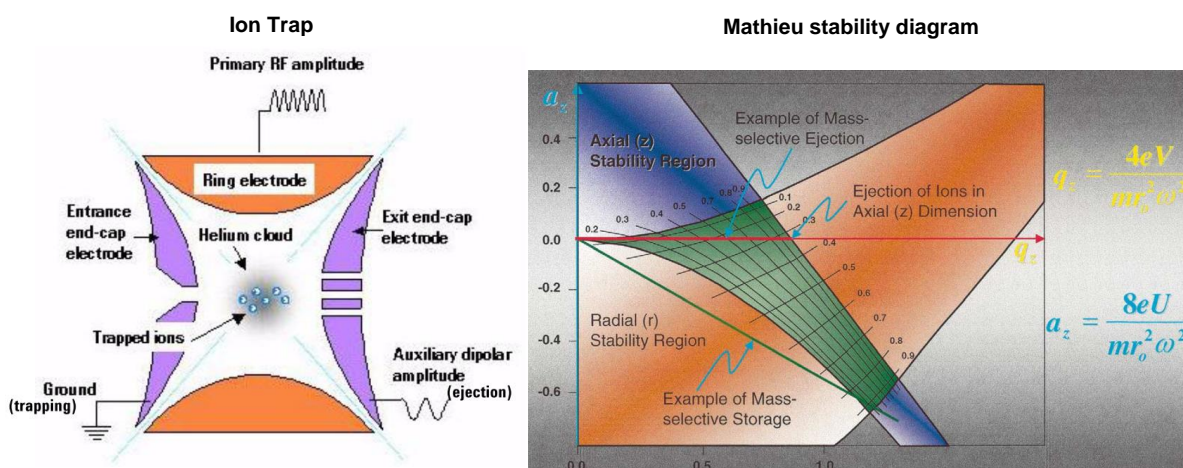


Fig. 5-5 MS – Spherical Ion Trap schema¹⁴⁰ and Mathieu stability diagram¹⁴³

What makes this method so powerful, is the capability of trapping only ions in the selected m/z range, allowing for concentrating of the analytes with very low concentration (trace analysis). Furthermore, once are the ions trapped, the ion trap allows isolation of selected ion –

precursor, which can be fragmented by application of additional resonant AC voltage on endcap electrodes. This increases intensity of ion – helium collisions leading to fragmentation of the trapped ions which allows detailed elucidation of their structure¹⁴⁰. Then the product ions could be either ejected from the ion trap (registration of product spectrum), or another precursor could be isolated and subjected to further fragmentation. This could be repeated several times. This method is commonly known as tandem mass spectrometry in time (MSⁿ). To detect the trapped ions, it is necessary to eject them from the trap to the detector. That is done by increasing of the ring electrode RV voltage and applying supplementary AC voltage to the endcap electrodes. This results in controlled destabilization of ion path inside the trap towards the detector. The ejection of ions with certain m/z ratio is dependent on the amplitude and frequency of the applied AC voltages. The ions take up the energy from the electric field very fast and leave the trap before further destabilization. This fast energy transfer with the precise and fast scan ramp generator controls allows very fast scan speed up to 38 microseconds per 1 mass unit¹⁴⁰.

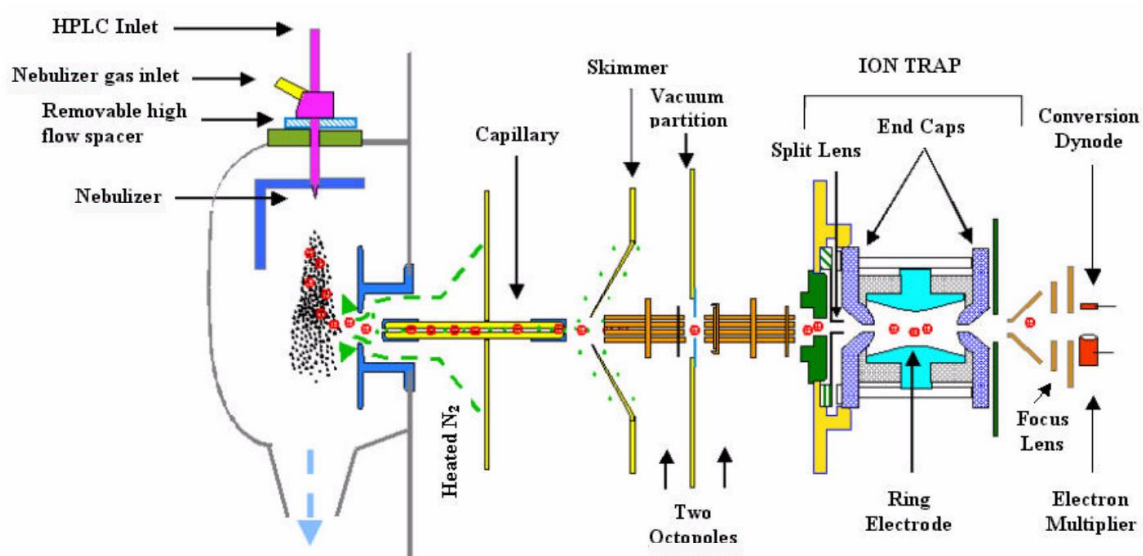


Fig. 5-6 Mass spectrometry – Agilent 6300 series system diagram¹⁴⁰

Last part of the MS system is detector which registers ejected ions from the ion trap. Based on the actual state of the ion trap and the strength of the detector signal (number of detected ions converted to signal intensity) the m/z spectrum is created and send as data stream to the computer for analysis¹⁴⁰. The detector in this case is a conversion dynode/electron multiplier and includes also a lens system to focus the ions towards the detector. The detector can work in two separate modes to detect cations or anions. The conversion makes also use of a calibration file to ensure good mass accuracy.

Table 5-21. Mass spectrometer analysis setting

Nebulizing gas pressure	15 psi/103.4 kPa
Drying gas flow	7 L·min ⁻¹
Drying gas temperature	325 °C
Scanning range m/z	50 – 1,500
Scanning mode	Anions or cations

5.4.4.1 Sample preparation

The original samples of HTFs were diluted to the 1 vol% and 3 vol% volumetric solutions by a solvent consisting of 80 vol% of ultrapure water and 20 vol% of methanol. To examine the effect of pH on the measurement, two more sets of the same dilution were created and spiked with 1 microliter of acetic acid. Altogether four sets of samples were prepared.

5.4.4.2 Measurement procedures

Though the used Agilent 6320 Series Ion Trap LC/MS instrument is equipped with liquid chromatograph for analyte separation before detection, in this work only the MS detector with direct infusion of the sample in different scanning modes was used.

For each sequence of measurements around 100 μL from the individual prepared samples was sucked into a 250 μL gas-tight syringe, which was connected to the spraying capillary of electrospray ion source. The continuous flow of the sample was achieved by a syringe infusion pump (on Fig. 5-7) in the mode of constant flow of $q = 5 \mu\text{L}\cdot\text{min}^{-1}$. Each sample was scanned in both anion and cation detection mode for basic target m/z ratios of 100, 500 and 1,000. To further examine the structure of the analysed HTFs, the fragmentation method was used in the MS/MS mode and MS^3 mode with helium as a collision gas.



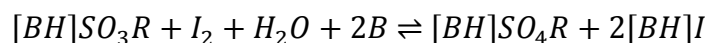
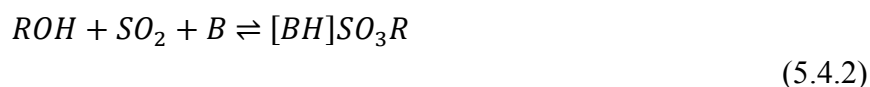
Fig. 5-7 Syringe infusion pump KDS 100¹⁴⁵

5.4.5 Karl Fisher Volumetric Titration

In 1935 the German chemist Karl Fisher published a paper¹⁴⁶ on a new method how to determine water content in liquids and solids. The Karl Fisher (K-F) titration, as the method is called commonly, builds on a highly selective reaction between alcohol (ROH), a base (B), SO_2 and I_2 with water as is depicted on Eq. (5.4.2). As the alcohol usually methanol, ethanol or 2-(2-ethoxyethoxy)ethanol is used. As the base variety of organic bases such as imidazole or pyridine can be used.

The processes occurring during the K-F titration can be described by two chemical reaction (Eq. (5.4.2)). In the first step the alcohol reacts with the sulphur dioxide and the base forming an alkylsulfite ($[\text{BH}]\text{SO}_3\text{R}$) intermediate. This intermediate then reacts directly with the iodine and water. Because the reaction of water and iodine is equimolar, we can easily estimate the content of water from the amount of consumed iodine during the titration. The titration is at its end when iodine (I_2) persist in the solution in its molecular state causing a persistent yellow

colouring of the solution. Because estimating the end of the titration just by the colour change is not very precise, especially with coloured samples, the modern Karl Fisher Titration uses for detecting of the endpoint potentiometric or bipotentiometric¹⁴⁷ titration method.



The titration can be proceeded by two different ways, the coulometric and volumetric way. The main difference between these two approaches is based on the way how the iodine is generated. In case of coulometric titration the I_2 is generated at the electrode and in case of the volumetric titration the I_2 is included in the reagents¹⁴⁸. Because the coulometric titration is more sensitive it is more suitable for low concentrations of water, with the sample containing usually 0.001-0.1 % of water. The volumetric titration is then used for samples with 0.1-100 % of water content. Because the samples in this work have high water content, only the volumetric way of Karl Fisher titration will be considered further.

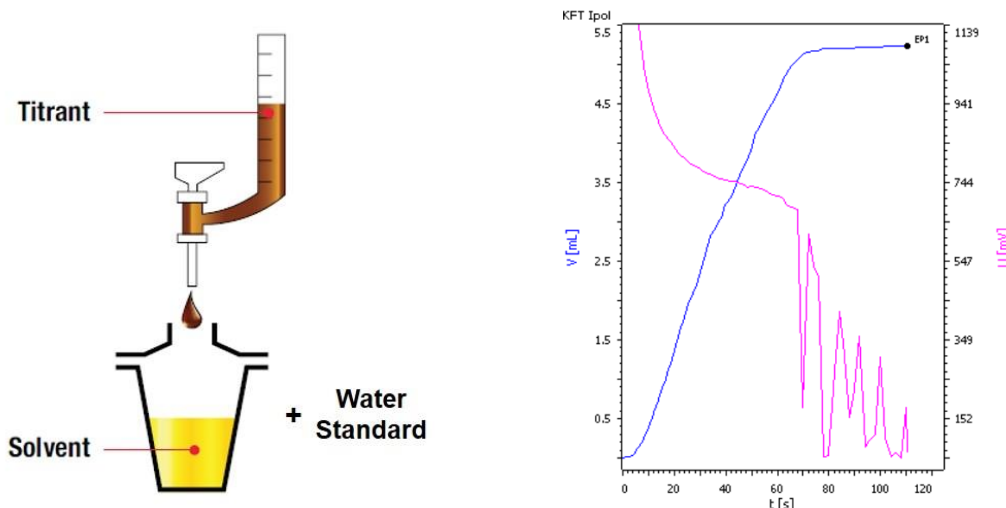


Fig. 5-8 Karl Fisher titration – basic apparatus¹⁴⁹ and titration progress diagram¹⁵⁰

The volumetric titration used in this work is based on simplified and fully automated process of two working mixtures. In the apparatus shown on Fig. 5-8 (left) the bottom mixture designated as solvent usually contains alcohol, SO_2 , base and supporting chemicals to stop any side reaction which could lead to false results. The titrant is then only alcoholic solution of iodine. There is also possible solution with only the alcohol and supporting chemicals in the solvent mixture which offers better stability and better protection against side reactions, though it is somehow slower in respect to speed of the titration¹⁴⁹. The end point of the titration is determined by drop of the conductivity of the solution like can be seen on the Fig. 5-8 (right) where a typical curve of volumetric Karl Fisher titration is shown. The determination of the end point is strongly dependent on pH of the solution as a governing factor for dissociation of the present molecules and speed of the reaction. The ideal pH for the Karl Fisher titration is $pH = 5.5-8$, where the reaction rate is constant with minimum side reactions¹⁵¹.

5.4.5.1 Sample preparation

The samples were used in their untreated – original form.

5.4.5.2 Measurement procedures

The measurement procedures and results of the process described in here are in compliance with the international standard ASTM D1123¹⁵². First, the sealed measuring cell was filled with 20 mL of the methanol solvent (Hydranal Methanol dry) and the sequence before measuring was started. The sample was inserted into a micro-syringe with capacity of 200 μL and the syringe with sample (about 150 μL) was weighted. In the meantime, the automatic titration system conducted a pre-titration to eliminate any moisture inside the cell. After the pre-titration was finished, around 100 μL of the sample was injected into the titration cell and the syringe was weighted again. The difference of the two weightings was then the actual sample amount. The information about the amount was inserted into the automatic titrator and the actual measurement of the sample started. Measurement of each sample was conducted 3 times. After each measurement the titration cell was emptied and washed out together with the syringe by new solvent. For each measurement a report with information about the titrant consumption, time and water content was printed out.

5.4.6 Atomic absorption spectroscopy

To analyse the content of selected metals in the HTFs atomic absorption spectrometry (AAS) was used. AAS is a spectro-analytical method to quantitatively determine chemical elements by the absorption of electromagnetic radiation in UV and in the visible range by free atoms in gaseous state¹⁵³. The origins of practical AAS dates to the second half of 19th century when the basic principles were for the first time put together by Robert Wilhelm Bunsen and Gustav Robert Kirchhoff¹⁵⁴. The typical setup of a modern AAS is described on Fig. 5-9.

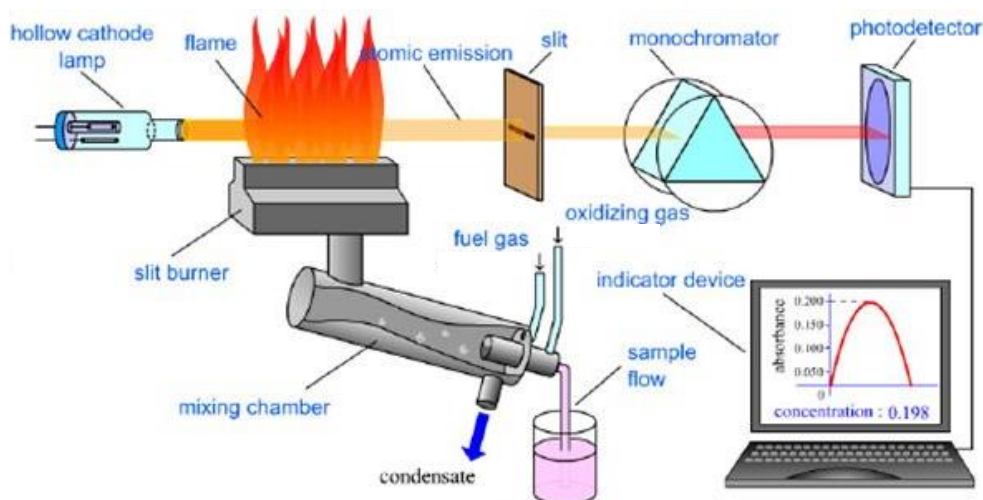


Fig. 5-9 Atomic Absorption Spectroscopy – system diagram¹⁵⁵

The principle comes from the fact that electromagnetic radiation of a certain wavelength is absorbed by present free ground state atoms in gaseous state. By absorbing radiation of a given wavelength λ which exactly corresponds to the specific energy necessary for the electron excitation in the particular element's atom, the atoms are excited (electrons of the atom are promoted to higher orbitals) and the passing radiation is weakened. The energy of photon and therefore energy of excitation is specified as:

$$E = \frac{hc}{\lambda} \quad (5.4.3)$$

where h is Planck's constant, c is the speed of light and λ is the wavelength of the photon. The high selectivity of this method is based on the fact that each wavelength corresponds usually to just one element and the width of the effective irradiation wavelength is very narrow, typically only a few picometers. The correlation between the concentration and light intensity is then explained by the Beer-Lambert law^{156,157}.

The Beer-Lambert law builds on the definition that the transmittance of the material T is related to its optical depth τ and to its absorbance A :

$$T = \frac{\Phi_e^t}{\Phi_e^i} = e^{-\tau} = 10^{-A}, \quad (5.4.4)$$

where Φ_e^i is the radiant flux received by the material and Φ_e^t is the radiant flux transmitted by the material. The absorbance of a given material is then given as a relationship between intensity of light transmitted through a sample with the material I and intensity of a reference - blank sample I_0 :

$$A = \log_{10} \frac{I_0}{I}. \quad (5.4.5)$$

With the absorbance as a method for assessing the change in the intensity of transmitted light, the Beer-Lambert law explains this change based on the optical path length l and the sum of the N individual parts of the material which affect the transmitted intensity through their concentration c_i and molar absorptivity ε_i :

$$A = \log_{10} \frac{I_0}{I} = l \sum_{i=1}^N \varepsilon_i c_i. \quad (5.4.6)$$

Because the molar absorptivity ε_i vary for each medium, the typical method for quantification by AAS is creation of calibration curve from solutions with known amount (concentration) of pursued element.

5.4.6.1 Sample preparation

The samples were used in their untreated – original form.

5.4.6.2 Measurement procedures

In the beginning, the calibration solutions of Cu, Fe and Pb were prepared into 25 mL big volumetric flask with the concentrations listed in Table 5-22. The calibration solutions were prepared from highly precise and clean stock solutions of concentration $1.0 \pm 0.002 \text{ g}\cdot\text{L}^{-1}$. Before measurement of each element, the calibration of the instrument for that element was conducted. For measuring of each element corresponding hollow cathode lamp as a source of light was selected. After selecting the correct lamp for current element measurement,

the heat-up time of approximately 10-30 minutes was allowed to stabilize the signal from the photodetector.

Table 5-22. Atomic absorption spectroscopy analysis setting

Atomizer	Acetylene flame atomizer
Flame temperature	>2200 °C
Ratio of acetylene/air	3.5/1.5
Set wavelength to detect Fe atoms λ [nm]	248.3 nm
Set wavelength to detect Cu atoms λ [nm]	324.8 nm
Set wavelength to detect Pb atoms λ [nm]	217.0 nm

The calibration dependence was created from the calibration solutions in the manner from the lowest concentrations to the highest in ordered manner. The resulting calibration lines of all elements are presented on Fig. 5-10. After completion of the calibration, the calibrated element was measured for all samples. For measuring different element, different light source had to be chosen and the whole process of calibration was repeated.

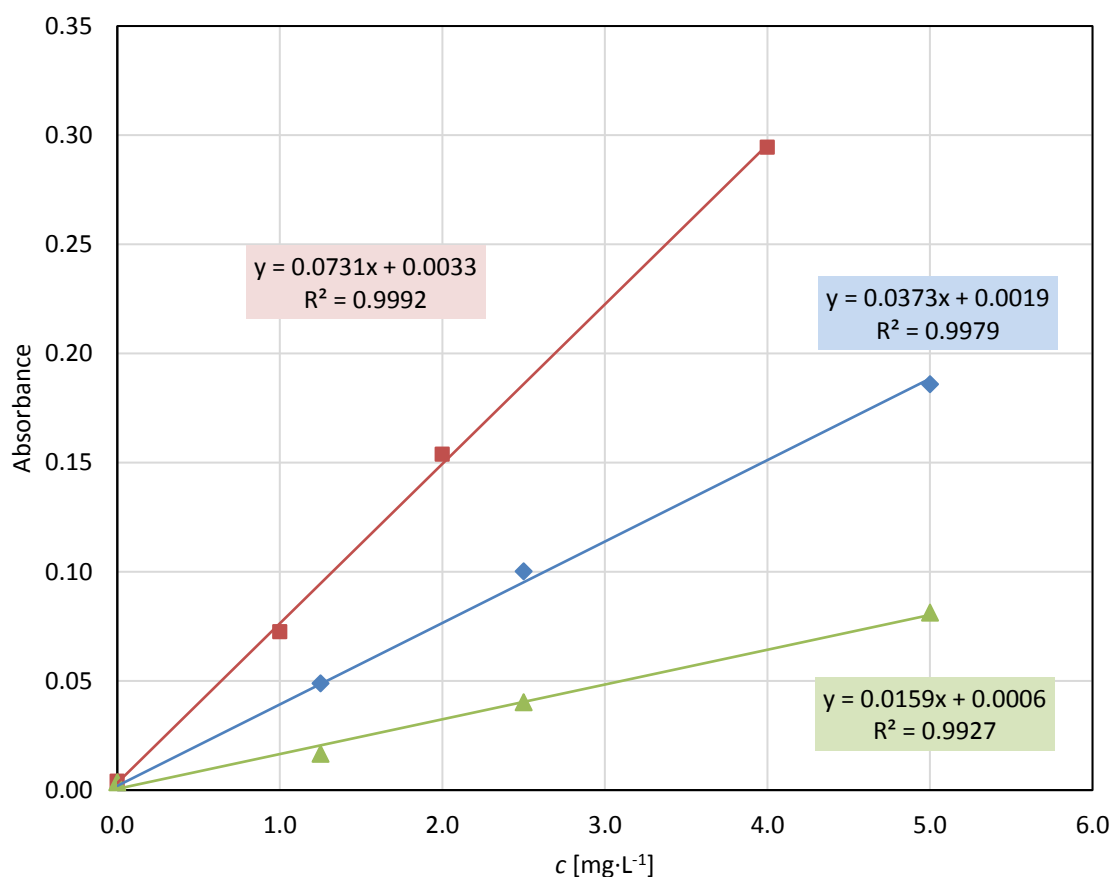


Fig. 5-10 AAS - calibration dependences for Cu, Fe and Pb

Table 5-23. Absorbance of the calibration solutions

Cu - concentration c [mg·L ⁻¹]	0.0 mg·L ⁻¹	1.0 mg·L ⁻¹	2.0 mg·L ⁻¹	4.0 mg·L ⁻¹
Absorbance (Cu) A	0.004	0.0725	0.1538	0.2944
Fe, Pb - concentrations c [mg·L ⁻¹]	0.0 mg·L ⁻¹	1.25 mg·L ⁻¹	2.5 mg·L ⁻¹	5.0 mg·L ⁻¹
Absorbance (Fe) A	(0.0000)	0.0489	0.1002	0.1859
Absorbance (Pb) A	0.0036	0.0166	0.0402	0.0813

5.4.7 Determination of pH

The concept of the potential of hydrogen – pH was for the first time introduced as negative logarithm of the base 10 of the hydrogen ion concentration¹⁵⁸ c_{H^+} [mol·L⁻¹]:

$$pH = -\log_{10} c_{H^+}. \quad (5.4.7)$$

Later, in the definition it was more specified and recommended by IUPAC as negative logarithm of the base 10 of the hydrogen ion relative activity¹⁵⁸ a_{H^+} :

$$pH = -\log_{10} a_{H^+} = \log_{10} \frac{1}{a_{H^+}}. \quad (5.4.8)$$

The definition of activity was selected over the concentration because the ion-selective electrodes respond and are defined on the basis of activity rather than concentration. This also better describes and allows to explain the dependency on temperature. For example, water has pH of 7.47 at 0 °C, 7.00 at 25 °C and 6.14 at 100 °C. For measurement with the ion-selective electrodes, we can describe the electrode potential based on Nernst equation (in ideal state) for the hydrogen ion as:

$$E = E^0 + \frac{RT}{F} \ln a_{H^+} = E^0 - \frac{2.303RT}{F} pH, \quad (5.4.9)$$

where E is the measured potential, E^0 is the standard electrode potential, R is the gas constant, T is temperature and F is Faraday constant. The international standard ISO 80000-9¹⁵⁹ describes the precise measurement of pH in a way of a measure of electromotive force between reference electrode and an electrode sensitive to hydrogen ion activity (a form of a galvanic cell). For the purpose of practical measurement, it is universally agreed that the definition pH is an operational one, thus, in practice, it is compared to defined standards. Therefore, according to the agreement (IUPAC recommendation)¹⁵⁸ the $pH(X)$ of a given solution X with electromotive force $E(X)$ in the measured cell, comprised of reference electrode with KCl solution (not less than 3.5 mol·kg⁻¹)¹⁶⁰ and hydrogen electrode (H₂/Pt), compared to standard, is given as:

$$pH(X) = pH(S) + \frac{E(S) - E(X)}{\frac{RT}{F} \ln 10}, \quad (5.4.10)$$

provided the known $pH(S)$ and the electromotive force of the standard $E(S)$ measured under the same conditions as the solution X . Thanks to this definition, the hydrogen electrodes, which are difficult to handle, can be replaced by other electrodes sensitive to hydrogen ions, such as glass electrode used in this work. The typical combined glass electrode is shown on Fig. 5-11.

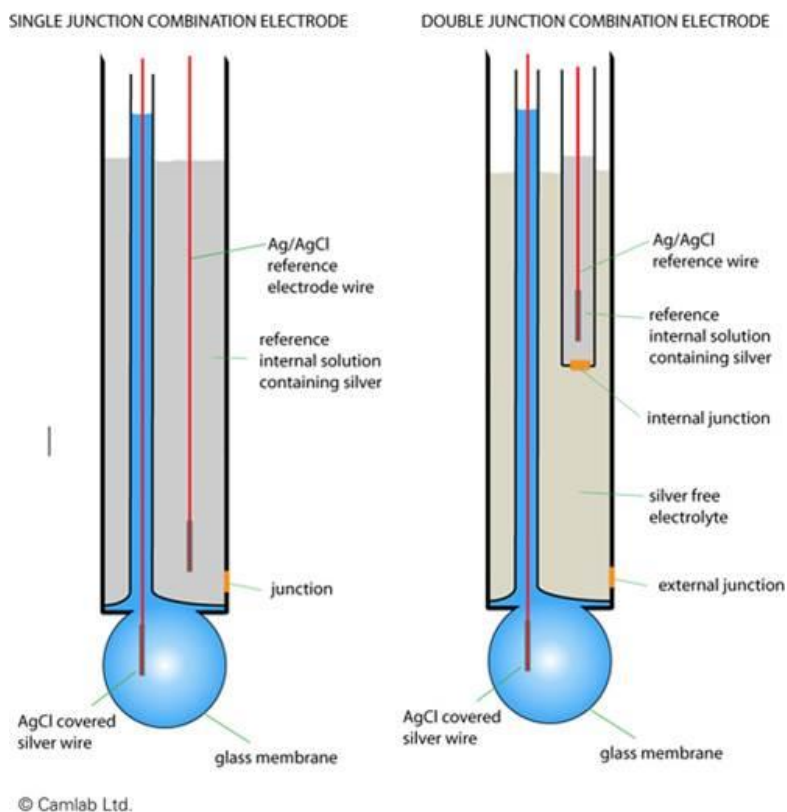


Fig. 5-11 Schema of a typical combined glass electrodes for pH determination¹⁶¹

5.4.7.1 Sample preparation

The samples were used in their untreated – original form.

5.4.7.2 Measurement procedures

In the beginning, the calibration of the pH meter was conducted according to the operating manual¹⁶². For the automatic calibration of pH meter were used three different solution according to DIN standards, the types A, B and F with pH values 1.679, 4.005 and 9.180, respectively. The electrode was thoroughly washed by ultrapure water and dried between each measurement of standard solutions as well as between the measurements of the samples. The calibration and the measurement were conducted under the same standard temperature setting of $T = 25.0$ °C. Because the target temperature was above the ambient temperature, to rise the temperature of the solutions an electric heater with magnetic stirrer was used. First, the measured solution was heated up to the target temperature under continuous stirring in a beaker. When the temperature reached the target value, the stirring was stopped, and the pH electrode

was immersed into the measured solution in a manner that glass membrane of the glass electrode and the junction of the reference electrode were fully submerged. The pH was read when the stability of the signal didn't change more than ± 0.02 of the pH value in 30 s. Three successive measurements for each sample at the same temperature were conducted.

5.4.8 Determination of conductivity

Conductivity κ [$\text{S}\cdot\text{m}^{-1}$] – Siemens per meter) is property of matter/material describing the ability to conduct electric current. From the general definition of electric current, therefore, the conductivity is described as a property of how readily the material is capable of moving electric charge in an electric field³⁶:

$$\kappa = \frac{1}{\rho} = \frac{J}{E}. \quad (5.4.11)$$

In the above equation the conductivity κ is expressed as inverse value of resistivity ρ . That leads to conductivity to be expressed as magnitude of current density J over the magnitude of electric field E .

The charge in materials can be transferred in several ways. The solid materials transfer the charge mostly through dissociable electrons. That applies especially for metals and semimetals which have abundance of electron states near the Fermi level¹⁶³. For the semiconductors and insulators, the electrons are further from the Fermi level, in a band gap, and under normal circumstances the conductivity is negligible. By doping the semiconductors with different atoms with electrons at suitable energy levels, we can change the characteristics of the material and make them conductive¹⁶⁴.

The ionic liquids and electrolytes lead the electric current not through the band electrons nor holes, but rather by the whole atomic and molecular species. Therefore, by measuring the conductivity we can assess the amount of ion content¹⁶⁵. Furthermore, elevated conductivity of the HTF could lead to galvanic corrosion, especially if the system is constructed from several different metals with different electrochemical potentials. The conductivity is measured by conductivity meter using alternating current to avoid electrolysis. Typical frequency used for the measurement in electrolytes is usually in single units of kHz¹⁶⁶.

5.4.8.1 Sample preparation

The samples were used in their untreated – original form.

5.4.8.2 Measurement procedures

For the measurement was used the probe TetraCon 325. The probe is equipped with two carbon electrodes spaced exactly 1 cm from each other. The conductivity was measured at set temperature of $T = 25\text{ }^\circ\text{C}$ similarly to the determination of pH. Firstly, the samples were poured into a beaker and heated up on a plate heater while stirred with magnetic stirrer. After the temperature reached the set value, the stirrer was stopped, and the probe was lowered into the sample while making sure that both electrodes are fully submerged and without bubbles. Before each measurement and in the end, the probe was thoroughly washed by deionized water until the shown conductivity was zero and then dried by clean laboratory wipes.

5.4.9 Density

5.4.9.1 Pycnometry

Determination of density of liquids by pycnometer is a simple method using a very precise glass flask of certain volume called pycnometer, thus the short name pycnometry. The determination is done through comparison of a sample with unknown density to a standard liquid with known density under the same conditions. Advantage of this method is its simplicity with sufficient reproducibility and precision when following proper steps¹⁶⁷.

Table 5-24. Constants for pycnometry at $T = 20\text{ }^{\circ}\text{C}$

ρ_w (Density of water)	0.9982 g·cm ⁻³
ρ_{air} (Density of air)	0.0012 g·cm ⁻³
m_p (Weight of the pycnometer)	18.0955 g
m_{p+w} (Weight of the pycnometer with water)	43.8125 g

The density of a sample ρ_s [g·cm⁻³] is determined by pycnometry as:

$$\rho_s = \frac{m_{p+s} - m_p}{m_{p+w} - m_p} (\rho_w - \rho_{air}) + \rho_{air} , \quad (5.4.12)$$

where ρ_w , ρ_{air} , m_p , m_{p+w} are the constants from Table 5-24 and m_{p+s} represents the weight of the pycnometer filled with sample.



Fig. 5-12 Pycnometer – 25 mL/20 °C¹⁶⁸

5.4.9.2 Sample preparation

The samples were used in their untreated – original form.

5.4.9.3 Measurement procedures

First, a clean and dry pycnometer, such as on Fig. 5-12, with volume of 25 mL was weighed. Then it was filled with distilled water and tempered for 30 minutes in a water bath at temperature $T = 20\text{ }^{\circ}\text{C}$. After the 30 minutes the pycnometer was removed from the water bath, dried and immediately weighted. The care was taken that the whole volume of the pycnometer was filled including the calibrated capillary in the tip. This was repeated three times to establish basic constants for further measurements. The basic constants are shown in Table 5-24. To measure the sample, the pycnometer was again rinsed with distilled water and ethanol and dried with compressed air. The clean and dry pycnometer was filled with sample liquid and its weight was measured under the same conditions as distilled water. After each weighing, the pycnometer was thoroughly washed and dried. Each sample was weighed this way three times.

5.4.9.4 Oscillating U-tube Densitometry

The technique of oscillating U-tube is based on the law of harmonic oscillation, or we can also say resonance, of a U-tube cell completely filled with a measured sample. The basic experimental setup is shown on Fig. 5-13.

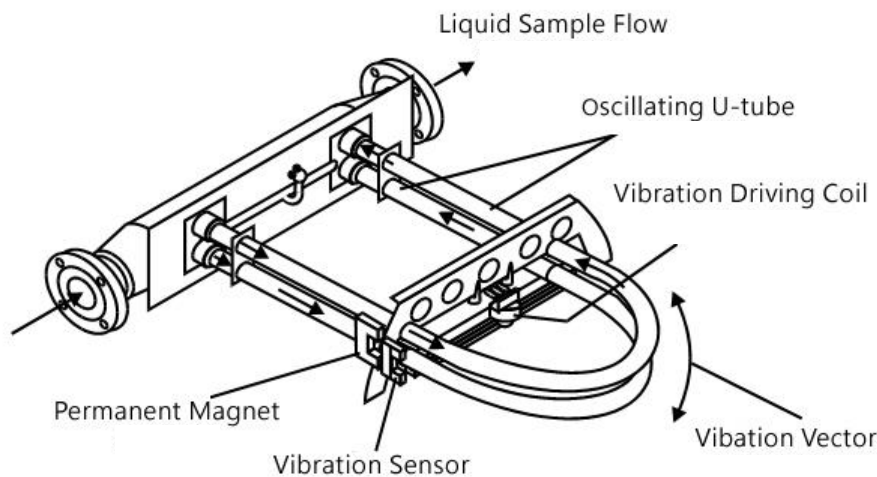


Fig. 5-13 Oscillating U-tube density meter – principle of function¹⁶⁹

The measurement of density is based on Mass-Spring Model¹⁷⁰, where through inducing a natural vibration to a measuring U-shape cell the frequency of vibration is measured. The dependency of frequency on the density of measured sample is then given as:

$$\tau = 2\pi \sqrt{\frac{\rho V + m}{C}}, \quad (5.4.13)$$

where τ is the oscillation period, ρ is the sample density, V is the cell volume, m is the mass of the cell and finally C is the spring constant. By square of the Eq. (5.4.13) we can substitute the present constants creating two combined constants $A = \frac{4\pi^2 m}{C}$ and $B = \frac{4\pi^2 v}{C}$ giving one simple equation for calculating the density by oscillating U-tube density meter:

$$\rho = \frac{\tau^2 - A}{B}. \quad (5.4.14)$$

5.4.9.5 *Sample preparation*

The samples were used in their untreated – original form.

5.4.9.6 *Measurement procedures*

Measuring the density by the Anton Paar Stabinger SVM 3000 used in this method is fully automatic procedure and requires only a minimal setting. After filling a syringe with the sample, the syringe was attached to the device input. The temperature of measurement was set on the instrument and the sample was injected into the device and the measurement started. After the measurement finished, the tubing was washed thoroughly with washing solution and several times with deionized water. For measuring at temperatures below 0 °C, the density meter was used in the combination with the Julabo cryostat.

The measurements was conducted in accordance with ISO 15212¹⁷¹. The density meter is periodically calibrated by technicians of the instrument's manufacturer, who also issue a certificate of calibration. The machine is calibrated by standard liquids according to ISO 17025¹⁷² / ISO Guide 34¹⁷³ and complies to ASTM D1480¹⁷⁴.

5.4.10 *Viscosity*

Viscosity can be described as a physical expression of internal fluid friction or it is also explained as the fluid resistance to gradual deformation caused by shear stress or tensile stress. The numerically expressed viscosity then expresses its rate or magnitude. The higher the viscosity, the greater the friction inside the fluid, and the greater the resistance to the force applied on it. By a simple observation, the higher the viscosity, the worse is how the fluid flows.

The basic relationship for determining the viscosity of these substances is based on Newton's viscosity law, which establishes the relationship between shear stress and velocity. Newton's viscosity law describes this relationship as a direct relation, and we talk about the rate of shear deformation. The Newtonian shear velocity is expressed by dynamic viscosity as a constant of proportionality and from that expression we can define the shear stress τ [Pa] in the fluid as:

$$\tau = \eta \frac{du}{dy} \quad (5.4.15)$$

where η is the dynamic viscosity, $\frac{du}{dy}$ represents the local shear velocity, and y is the coordinate in the direction perpendicular to the flow velocity direction u . For better understanding a graphical representation of this relation of a flow inside a pipe (or any flat surface) is given on Fig. 5-14. For a given temperature, the viscosity or internal friction coefficient is constant.

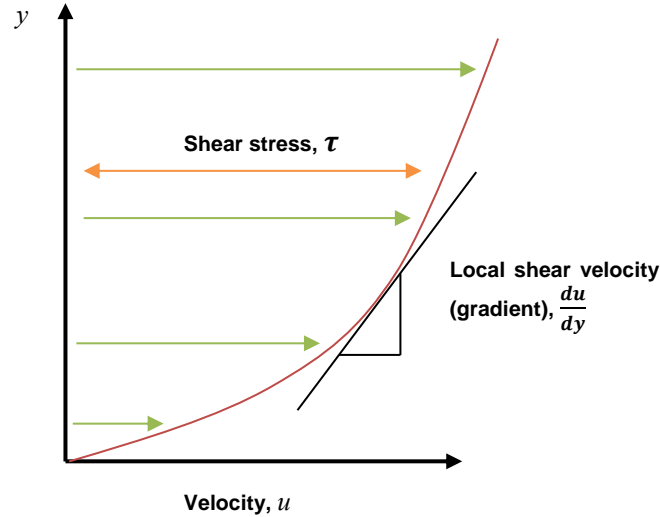


Fig. 5-14 Parallel flow in a straight pipe

The viscosity is usually expressed as dynamic viscosity η (from the Eq. (5.4.15)) or kinematic viscosity ν . The relation between dynamic viscosity and kinematic viscosity given by the ratio of its density as:

$$\nu = \frac{\eta}{\rho} \quad (5.4.16)$$

The respective viscosities have also different units. The dynamic viscosity η [$\text{N}\cdot\text{s}\cdot\text{m}^{-2}$] which is Newton-second per square meter and the kinematic viscosity is ν [$\text{m}^2\cdot\text{s}^{-1}$] which is reciprocally square meter per second. For practical reasons, the SI units stated above are rarely used and are commonly replaced by η [$\text{mPa}\cdot\text{s}$] (millipascal second) and η [cP] (centipoise) for dynamic viscosity. The relation between these units is:

$$1 \text{ mPas} = 1 \text{ cP} \quad (5.4.17)$$

In case of kinematic viscosity we can encounter more likely with ν [mm^2s^{-1}] (square millimetre per second) and ν [cSt] (centistokes), when the relation is:

$$1 \text{ mm}^2\text{s}^{-1} = 1 \text{ cSt} \quad (5.4.18)$$

For example, distilled water has a dynamic viscosity³⁶ at 20 °C: $\eta = 0.001 \text{ N}\cdot\text{s}\cdot\text{m}^{-2}$, which is $\eta = 1 \text{ mPa}\cdot\text{s}$ (1 cP), and a kinematic viscosity of $\nu = 1.016 \cdot 10^{-6} \text{ m}^2\text{s}^{-1}$ being $\nu = 1.016 \text{ mm}^2\text{s}^{-1}$ (or 1.016 cP).

In this work are used two different methods for measuring viscosity, which will be explained further in the work. The used methods are capillary viscometry and rotational viscometry.

5.4.10.1 Capillary Viscometry

Capillary viscometers are types of U-tube viscometers. In practical use, the most common are the Ostwald viscometer, Cannon-Fenske viscometer and Ubbelohde viscometer. The viscometers are shown on Fig. 5-15.

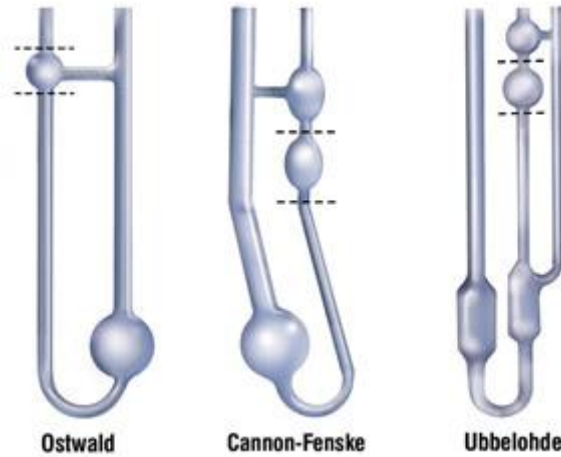


Fig. 5-15 Common U-tube viscometers¹⁷⁵

Although, in this work was used only Ubbelohde viscometer¹⁷⁶, shown in detail on Fig. 5-16, which will be further described in this section, most of the theoretical background is identical to all capillary viscometers. The determination of viscosity by capillary viscometers is based on Hagen-Poiseuille's law and can be written as:

$$\frac{dV}{dt} = v\pi R^2 = \frac{\pi R^4}{8\eta} \frac{|\Delta P|}{L}, \quad (5.4.19)$$

where $\frac{dV}{dt}$ represents the change of the volume V of the liquid through time t (volume flow) when passing through the capillary and equals to a combination of v as mean flow velocity, π constant pi and R which is the capillary radius. In the following expansion, η is the dynamic viscosity, ΔP is average applied pressure and L is the length of the capillary. The applied pressure ΔP is expressed as

$$\Delta P = \rho g \Delta H, \quad (5.4.20)$$

where ρ is density of the liquid, g is the standard gravity constant and ΔH is the average head of the liquid. By rearranging the equations (5.4.19) and (5.4.20) we get an expression which gives directly the dynamic viscosity:

$$\eta = \frac{\rho \pi R^4 g \Delta H}{1} \frac{t}{8LV}. \quad (5.4.21)$$

Because the density is not always known, in case of Ubbelohde viscometer we usually encounter with the form of the Eq. (5.4.21) that gives kinematic viscosity in accordance with Eq. (5.4.16) as the measurements results:

$$v = \frac{\eta}{\rho} = \frac{\pi R^4 g \Delta H}{8LV} t. \quad (5.4.22)$$

In practice the constants from the right side of Eq. (5.4.22) are usually brought together to give one combined constant K . The Eq. (5.4.22) will then take this very simple form:

$$v = Kt. \quad (5.4.23)$$

However, the Eq. (5.4.22) gives only a theoretical background for the actual measurement. Because the ideal conditions are not very likely to be achieved in the real world, the constant K from Eq. (5.4.23) is typically adjusted and calibrated by measuring standardized liquids such as distilled water or pure chemicals¹⁷⁷.

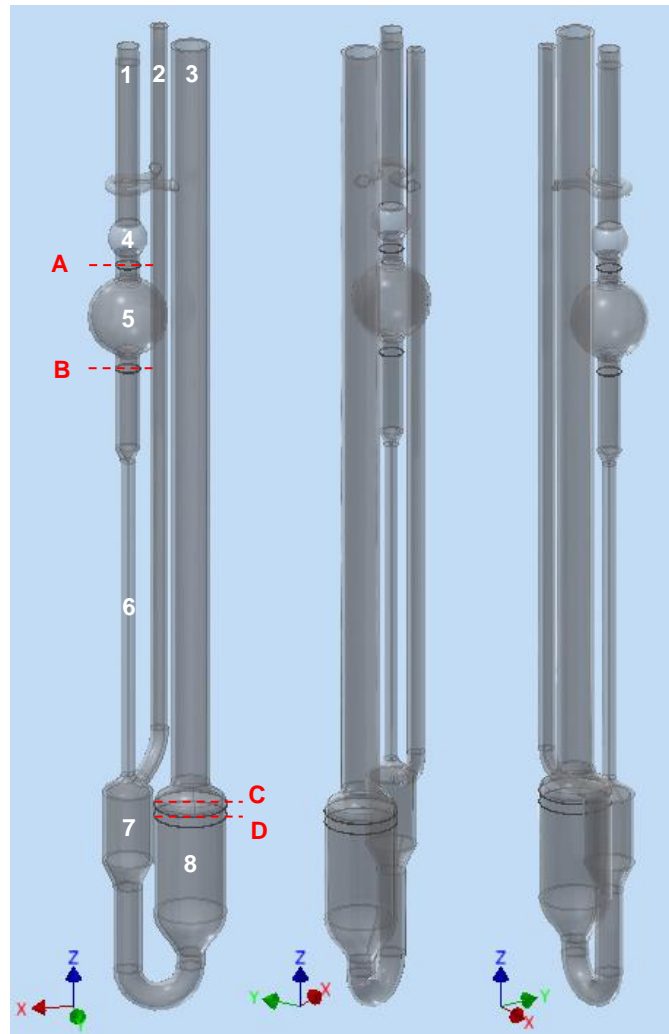


Fig. 5-16 Ubbelohde viscometer according to DIN 51 562 Part 1 and ISO DIS 3105

1-Suction tube; 2-Venting tube; 3-Filling tube; 4-Pre-run sphere; 5-Measuring sphere; 6-Capillary; 7-Levelling bulb; 8-Storage bulb; A,B-Measurement marks; C,D-Filling marks

5.4.10.2 Sample preparation

The samples were used in their untreated – original form.

5.4.10.3 Measurement procedures

The insulated container was filled with antifreeze fluid and the submersible part of the chiller Huber was inserted together with temperature sensor creating a thermo bath. The bath was tempered to set temperature. To evenly spread the temperature, an external stirrer was also submerged in the bath. The quality of the isothermal bath was periodically tested by a calibrated ethanol thermometer in different depths. The sample was poured inside the Ubbelohde viscometer to the point between the filling marks and this way prepared viscometer was immersed in the prepared bath. The viscometer filled with liquid was tempered for 30 minutes before start of the measurement. The process of the measurement was as follows. By a laboratory suction ball attached to the suction tube (Fig. 5-16: 1) the measured liquid was elevated through the both measurement marks and the measurement was started. The measurement time was taken when the liquid surface passed through the measurement marks - starting the time when passing the top mark and stopping when passing the bottom one. During the whole time the viscometer was submerged, and slightly retracted above the surface of the thermo bath only to check the level and to take the time in the beginning and in the end. Every measurement was repeated 3 times and the resulting values were averaged. After each set new temperature setting was established. After the bath reached the new temperature, the viscometer was again tempered for 30 minutes before starting next set of measurements.

5.4.10.4 Rotational Viscometry

The basic principle of measurement of the rotational viscometers is based on transfer of force through the liquid between two cylindrical bodies. As it is shown on the Fig. 5-17, one cylindrical body is a container (a cup or outer tube, from the picture description) and other cylindrical body is a rotor (a bob). The force can be transferred from one body to another based on the two principles¹⁷⁸. The Searle principle¹⁷⁹ transfers the force from the rotor to the container (from bob to cup) and in Couette principle¹⁸⁰ the force is transferred from the container to the rotor (from cup to bob). The instrument used in this work, Anton Paar Stabinger SVM 3000, works on the modified Couette principle, where the force originates from the containing cylinder.

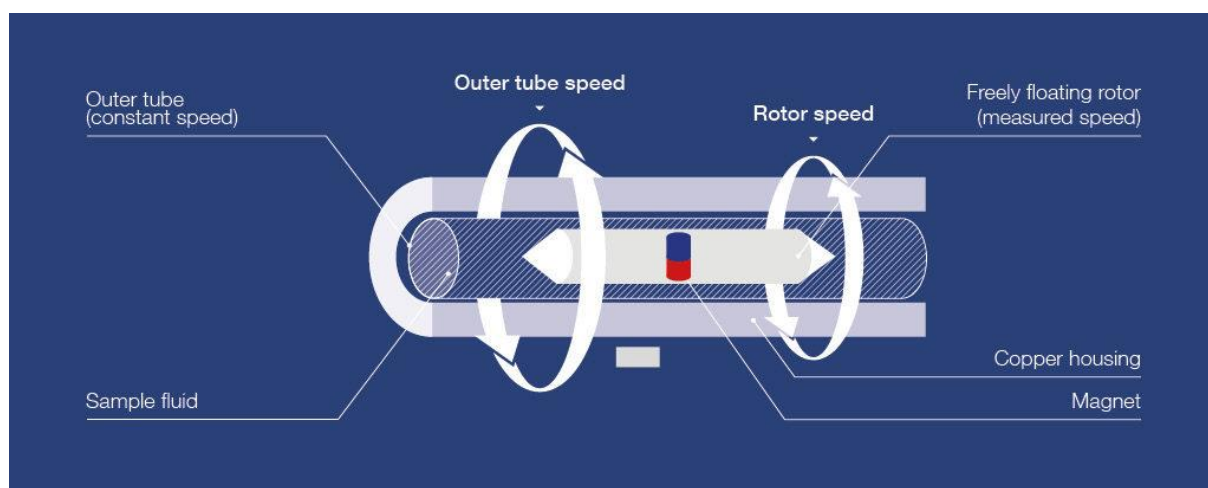


Fig. 5-17 Stabinger Viscometer™ viscosity measuring principle¹⁸¹

Though the basic principle of the rotational viscometry is more or less simple, the application of in case of Stabinger Viscometer is quite complex and advances the technique quite a bit,

especially in terms of precision and measuring range. As the speed of rotation of the container cylinder is constant, with the lower viscosity the slower the rotor will turn and the speed difference between these two bodies will be greater. The dynamic viscosity η is then expressed as approximately the inverse value of the difference between the speeds:

$$\eta \sim \frac{1}{n_c - n_r}, \quad (5.4.24)$$

where n_c and n_r are the speeds of the container and the rotor, respectively. To calculate the dynamic viscosity precisely we need to understand more about the dependency of the rotor speed in the liquid. For the equilibrium, when the rotor speed is stable and stays constants applies:

$$M_D = M_R, \quad (5.4.25)$$

where M_D represents driving torque and M_R represents retarding torque. We know that the driving force (torque) is proportional to the viscosity and the speed difference between the container cylinder and rotor. Other properties of the driving force are for simplicity expressed by a single system constant K_D and the whole equation of the driving torque will take this form:

$$M_D = K_D \eta (n_c - n_r). \quad (5.4.26)$$

Even though the position of the system is horizontal, thanks to the fast spinning fluid around and iron centred ring (in combination with magnetic core of the rotor), the rotor is fully suspended in the fluid in centred position by centrifugal forces and hydrodynamic lubrication effect¹⁸². This way, any other friction than through the fluid is avoided.

The retarding force (torque) is mainly dependent on the speed of the rotor n_r and the system itself. The main retarding force are considered eddy currents arising from the rotating magnetic field of the rotors magnet in the copper housing. All the factors that are influencing the retarding torque are then combined in one constant K_R giving out a simple equation:

$$M_R = K_R n_r. \quad (5.4.27)$$

Then, by combining Eq. (5.4.26) and Eq. (5.4.27) we can get the expression for the final constant K :

$$K = \frac{K_R}{K_D}, \quad (5.4.28)$$

and the resulting equation for calculating of the dynamic viscosity will be written like this:

$$\eta = \frac{K}{\frac{n_c}{n_r} - 1} = \frac{K}{\frac{n_c - n_r}{n_r}}. \quad (5.4.29)$$

The final constant K is combination of many factors and simplifies the whole process. In the practical application it is dependent on calibration process of the machine.

5.4.10.5 Sample preparation

The samples were used in their untreated – original form.

5.4.10.6 Measurement procedures

The system for measurement is fully automatic and requires only minimal preparations. First, the sample was filled into a syringe and attached to the capillary input of the instrument. The temperature of measurement was set on the viscometer and the sample was injected into the measuring device and the measurement started. After the measurement finished, the measuring cell was washed thoroughly with washing solution and several times with deionized water. For measuring at temperatures below 0 °C, the viscometer was used in combination with the Julabo cryostat.

The measurements was conducted in accordance with ASTM D7042¹⁸³. The viscometer is periodically calibrated by technicians of the instrument's manufacturer who also issue a certificate of calibration. The viscometer is calibrated by standard liquids according to ISO 17025¹⁷² / ISO Guide 34¹⁷³ and complies to ASTM D2162¹⁸⁴.

5.4.11 Refractive index measurement

The refractive index also written as index of refraction is defined as a ratio between the speed of light in vacuum and inside a given medium¹⁸⁵:

$$n_D = \frac{c}{v}, \quad (5.4.30)$$

where n_D is the dimensionless refractive index, c is speed of light (in vacuum) and v is speed of light inside the given medium. To describe the ratio in terms of two different environments which none of them is vacuum the Snell's law (also known as Snell–Descartes law or the law of refraction) is typically used:

$$\frac{\sin \theta_2}{\sin \theta_1} = \frac{v_2}{v_1} = \frac{n_2}{n_1}. \quad (5.4.31)$$

The refractive index of water is $n_D^{20} = 1.333$ at 20 °C³⁶ and the refractive index of air is $n_D^{20} = 1.0003$ at 20 °C³⁶ which means that according to Snell's law, when the light is entering the water from air at the entering angle of 60° the refracted light will have angle of 40.6° against the normal as can be seen on Fig. 5-18.

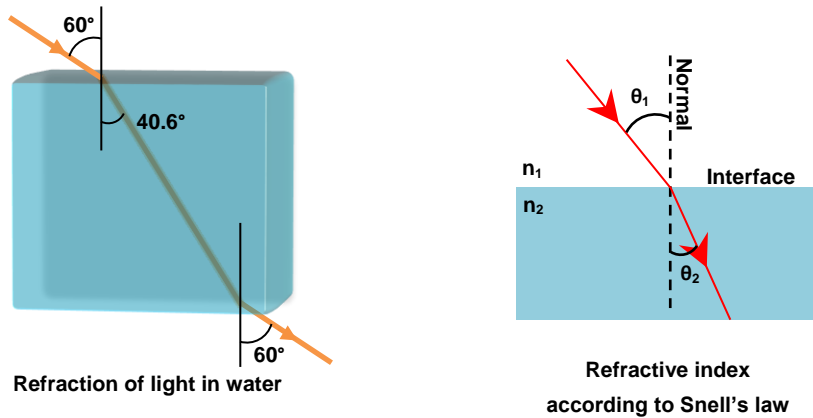


Fig. 5-18 Refraction in water and Refractive index definition

It is important to add that the actual refractive index is also dependent on the wavelength of the light¹⁸⁵. That is given by a simple fact of the dependency of photon frequency f on its speed v and wavelength λ :

$$f = \frac{v}{\lambda}. \quad (5.4.32)$$

From experiments we know that the frequency of light is not changed by traveling through a specific environment (the energy of photon is conserved: $E = hf$) but as the speed changes the wavelength will have to change accordingly. From the original equation for refractive index (5.4.30) we can assume:

$$n_D = \frac{f_0 \lambda_0}{f \lambda}, \quad (5.4.33)$$

where f_0 and λ_0 are the frequency and wavelength of light in vacuum and f and λ are the frequency and wavelength of light in a given environment. If the frequency is constant $f_0 = f$, thus:

$$n_D = \frac{\lambda_0}{\lambda}. \quad (5.4.34)$$

From the Eq. (5.4.34) is apparent that for clear information about the refractive index the wavelength information is an important factor. For the technique of refractometry if not stated otherwise, the wavelength is standardized at $\lambda = 589.3 \text{ nm}$ ³⁶ which is the wavelength of sodium D line originating from sodium vapor lamp. The principle of measurement of refractive index is shown on Fig. 5-19.

The refractive index of water is then dependent on the temperature (as the density and permittivity changes), on the wavelength, and finally, it is dependent on the other substances dissolved in water¹⁸⁶, if they have different refractive index. Therefore, through this very simple method, we can assess the concentration of dissolved substances in water binary mixtures to a certain degree of precision. However, this method is usually used where high precision is not

necessary, such as assessing the concentration of antifreeze of HTFs for automotive and TSS. The values is dependent on many factors like temperature, ion activity, impurities¹⁸⁷ etc. Because of that, proper experimental data are usually necessary, especially for substances actively interacting with water molecules like other polar liquids such as alcohols.

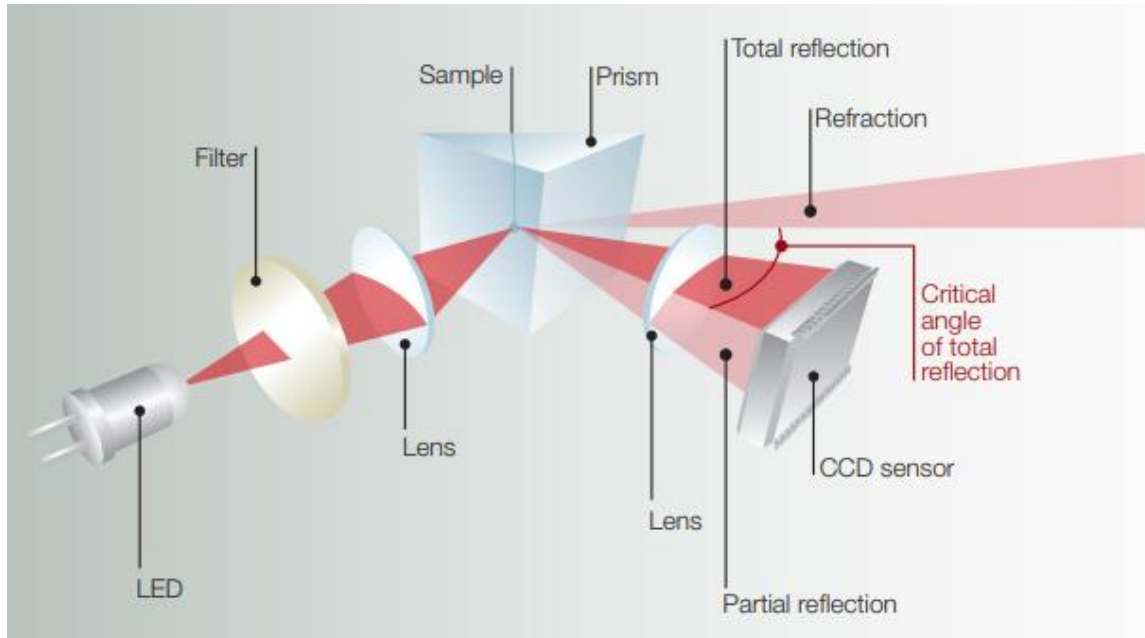


Fig. 5-19 Refractometry – principle of measurement¹⁸⁸

5.4.11.1 Sample preparation

The samples were used in their untreated – original form.

5.4.11.2 Measurement procedures

Because the Anton Paar Abbemat 350 Automatic Refractometer is fully automatic device, the procedures of measurement were very simple. It employs the standard measuring wavelength of $\lambda = 589 \text{ nm}$ ¹⁸⁹. After setting the temperature of the measurement the sample was put into the measurement cell and inserted into the instrument. After tempering of the sample and stabilizing the temperature, the refractive index was measured. The refractive index was measured for several different temperatures for the same sample. Between each measurement and in the end the measurement cell was thoroughly cleaned, rinsed with distilled water several times and dried. The method and use of the instrument was in compliance with international standard method ASTM D3321¹⁹⁰.

5.4.12 Freezing point measurement

Freezing point, melting point and fusion point are all describing the same temperature of changing the physical state between solid and liquid, though, not necessarily equal at all times.

For a liquid to freeze, heat loss is required to drop the temperature, a thermodynamic property of matter, to its freezing point. From a thermodynamic point of view during the process of physical state change (phase change) the Gibbs free energy ΔG remains constant, and only the enthalpy ΔH and entropy ΔS are changing:

$$\Delta S = \frac{\Delta H}{T}. \quad (5.4.35)$$

The zero change of Gibbs free energy gives the process some specific properties. One of them is, that the process proceeds under normal condition (if not supercooled) in a very small temperature range when releasing or consuming considerably big amount of energy which we call latent heat. On the Fig. 5-20 are shown typical measurements of freezing point with the visible phase change as the temperature remains constant for prolonged period of time.

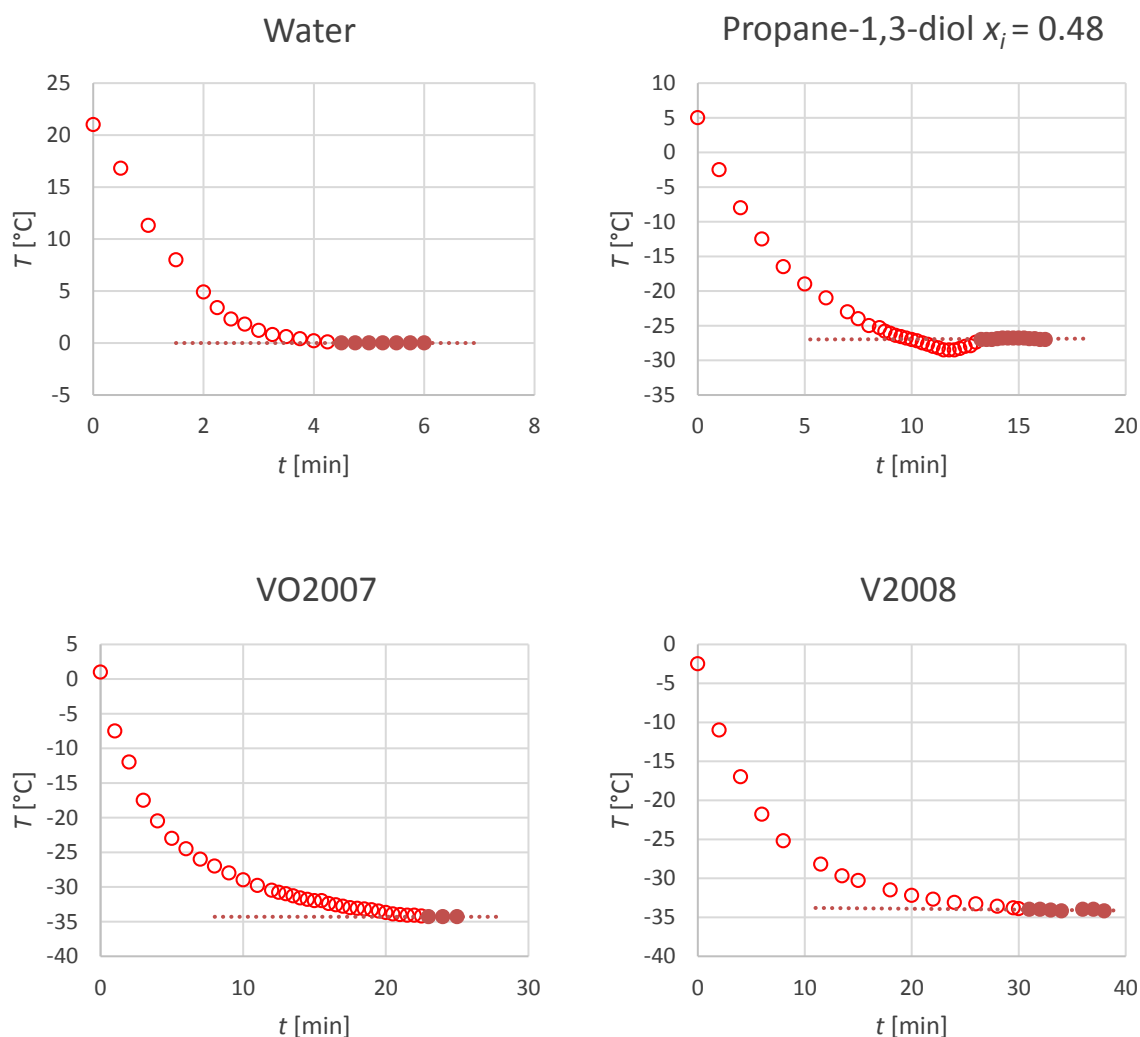


Fig. 5-20 Freezing point measurement – temperature development over time

5.4.12.1 Sample preparation

The samples were used in their untreated – original form.

5.4.12.2 Measurement procedures

For the measurement of the freezing point the method ASTM D1177¹⁹¹ was modified according to the technical capabilities of available laboratory and instead of Dewar's vessel a self-prepared insulated vessel was used. Inside the insulated vessel a glass beaker was inserted

and it was fastened immobile. Before the start of the measurement, the insulated vessel was filled with 4 litres of coolant and tempered to $-37\text{ }^{\circ}\text{C}$ by the immersible cooler. A sample with volume of 70 mL was poured into the beaker which was partially submersed in the cooled coolant liquid. The beaker was sealed with a lid with two openings. The openings were used to introduce a stirrer and a thermometer. Stirring was set to about 60 rpm and temperature was recorded at minute intervals. When approaching the expected freezing temperature, the time intervals for temperature reading were shortened to 15 seconds and the mixing was switched off. To avoid local overcooling, thin copper wire was present in the cooled sample to evenly spread the migrating heat energy. The freezing point was established on the basis of Eq. (5.4.35), when the temperature stopped dropping and the released energy was completely provided by the phase change. The correct temperature was always also confirmed by visual means, when the solidification of the samples was directly observed.

5.4.13 Corrosivity quantification

The corrosivity quantification was conducted in accordance with ASTM standard D1384 – Standard Tet Method for Corrosion Test for Engine Coolants in Glassware¹¹⁵. The corrosivity quantification by the means of ASTM D1384 is very simple method based on the practical applications. The used apparatus is depicted on Fig. 5-21 and it is composed from glass beaker as a container for the test and set of different metals strips fully submersed in the tested fluid. For the test are used six different metals: copper, solder, brass, steel, cast iron and cast aluminium. Exact composition of the metals is also provided in this method with more details stated in other standards listed in the original ASTM D1384. The metals are conductively connected to avoid galvanic corrosion. The test is conducted in two different temperature settings ($88\text{ }^{\circ}\text{C}$ or $71\text{ }^{\circ}\text{C}$) based on intended application of the liquid. The test is conducted continuously over period of 336 hours (14 days) and the temperature should be maintained within $\pm 2\text{ }^{\circ}\text{C}$ from the original temperature settings. Although the method described in ASTM D1384 is intended for propane-1,2-diol and ethane-1,2-diol mixtures, according to new standard ASTM D7518¹⁹², describing mixture of propane-1,3-diol for engine coolants, the method can be used for propane-1,3-diol as a reference method as well.

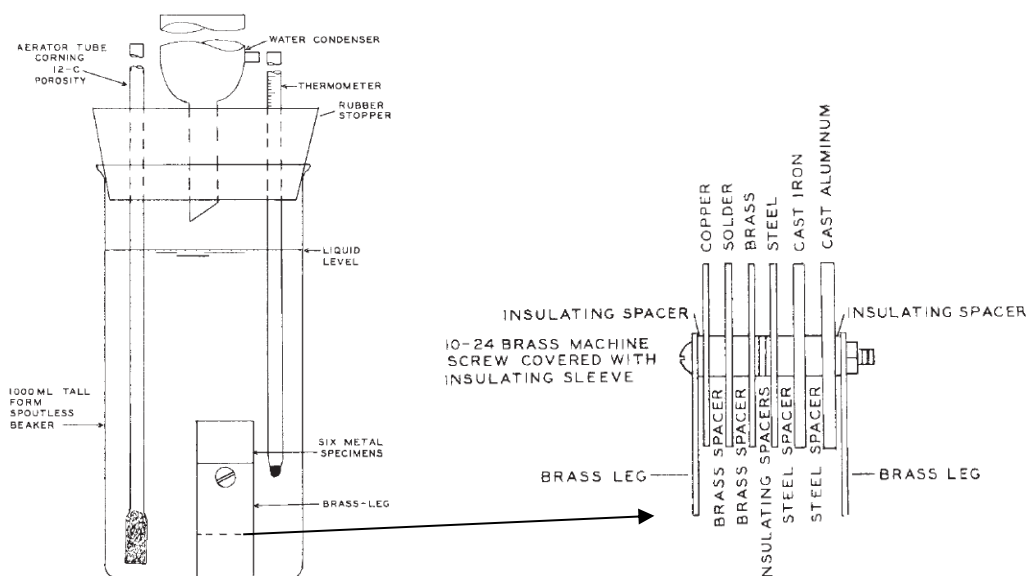


Fig. 5-21 Corrosion test apparatus as described in the ASTM D1384¹¹⁵

The idea of the method is direct measurement of weight loss of the tested metals by corrosion. Before the measurement, the metals strips are neatly cleaned and weighed. The corrosion is then estimated by repeated weighting of the strips after the test is finished. For a mixture to pass the test and be applicable as a heat transfer fluid / coolant liquid certain limits must be achieved. Some of the more common limits as stated by standard ASTM D3306¹²⁹ (Standard Specification for Glycol Base Engine Coolant for Automotive and Light-Duty Service) are shown in Table 5-25.

Table 5-25. Corrosion limits expressed as weight loss according to ASTM D3306

Metal	Corrosion limit
Copper	10 mg
Solder	30 mg
Brass	10 mg
Steel	10 mg
Cast iron	10 mg
Cast Aluminium	30 mg

Although this method is very simple and provide only an overview results it can serve as a very good estimation for the corrosion properties of new liquids. More profound method is then provided by standard ASTM D2570¹⁹³. Full simulation of the corrosion in engines under laboratory conditions is described by ASTM D2758¹⁹⁴. Even though all of the above mentioned standard methods are intended to test heat transfer fluids based on glycols for combustion engines, the universality and simplicity of these methods can be in general used for HTFs for thermal solar systems as well.

5.4.13.1 Sample preparation

The samples were used in their untreated – original form.

5.4.13.2 Measurement procedures

As a first step was prepared the metal strips. Individual metal strips were washed and cleaned as described in the method ASTM D1384. That encompasses rinsing with diluted acids such as HCl and HNO₃ and brushing with brass and bristle brush. Every metal was treated in a different way and the exact step by step procedures are written in the ASTM D1384. After proper cleaning all samples were thoroughly dried and then weighted. The metal stripes were assembled together as shown on Fig. 5-21 (right) and put into a 1000 mL beaker. The prepared samples of heat transfer fluid were poured into the beaker with the metal specimens in volume of 750 mL. The beaker was then assembled as shown on Fig. 5-21 (left). The beaker was closed by a rubber stopper with several holes for necessary equipment. Into the necessary equipment belongs thermometer, aeration output and reflux cooler. After assembling everything, the heater was set to 88 °C and the aeration was opened to 100 mL·min⁻¹. Next to the actual sample another set of metal stripes was prepared as a blank reference. The experiment setting was maintained for 336 hours with the cooled reflux. After the time period was finished, the metal samples were removed from the HTF sample and immediately disassembled. Another cleaning was performed the same way as in the preparation stage. After final drying the metal stripes were weighted. The final loss of material caused by corrosion m_{loss} was calculated as:

$$m_{loss} = (m_{start} - m_{finish}) - (m_{blank\ start} - m_{blank\ finish}), \quad (5.4.36)$$

where m_{start} and m_{finish} are the weights of cleaned metal stripes before and after test and $m_{blank\ start}$ and $m_{blank\ finish}$ are weights of the blank set of metals which was treated (cleaned) the same way as the tested set.

5.5 Automatic Ubbelohde viscometer

For the purpose of data verification and validation another viscometer was prepared in parallel for some of the viscosity measurement. The design of this automatic viscometer is based on the use of Ubbelohde capillary viscometer, which is used worldwide for measurement of viscosity of petroleum products and other Newtonian fluids. The advantage of such solution lies in use of the Ubbelohde viscometer itself, because it is part of a number of international standards for viscosity measurements, and the constructed device is in full agreement with them.

The automatic Ubbelohde viscometer was constructed in the scope of cooperative project TH01031303 “Teplonosné nemrznoucí kapaliny pro energetiku a automotive” with Classic Oil s.r.o. and it was financed by Technological Agency of the Czech Republic.

5.5.1 Design

The basic part is made from custom IR sensor pair attached to the Ubbelohde viscometer, on Fig. 5-22, which detects the level of the measured fluid as it is passing through the marked control points on the viscometer as a common industrial solution¹⁹⁵. The unique part of the instrument is then responsible for precise temperature management and automatic filling and measuring process. The viscometer is constructed from several separate modules responsible for individual tasks for measurement, control and data acquisition. The main part with control unit made of ATmega32¹⁹⁶, is responsible for basic control, data acquisition and connection to a PC. The temperature control is checked by series of resistance temperature detectors (RTDs) Pt1000 (1/3DIN grade) with readable accuracy of 0.005 °C and repeatability of 0.1 °C (according to the standard). The time readability of the IR sensors is set to 100 Hz by default.

The system is equipped with custom firmware on the machine side and control software on the PC side. The system design and programming on both sides was fully developed by author of this thesis.

Because the device is subject of an industrial design protection the details cannot be part of the public work before the finishing of the patent procedures (subjected to industrial patent protection in 2018). The photo documentation of the machine is available in appendix A-5.

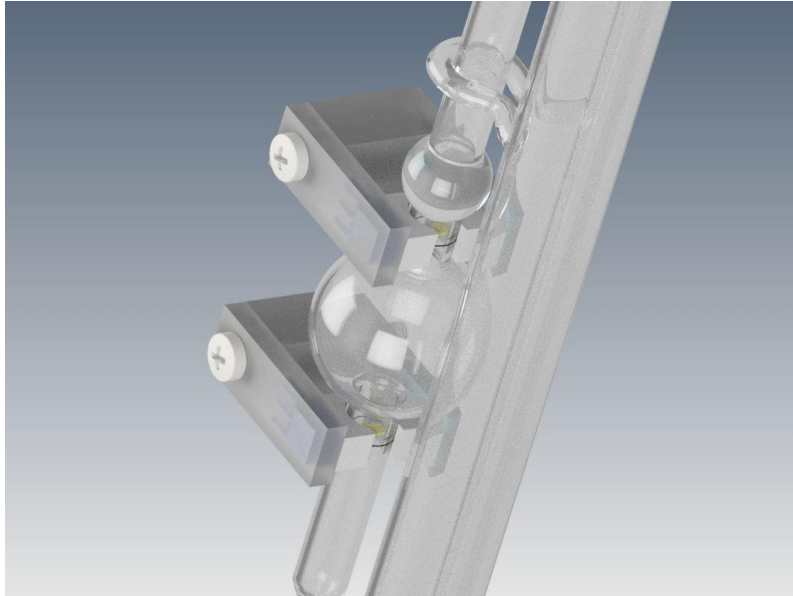


Fig. 5-22 Automatic Ubbelohde viscometer – IR pair sensor positioning

6 RESULTS AND DISCUSSION

6.1 Ageing of antifreeze mixtures based on propane-1,2-diol

6.1.1 Long-term observation of experimental system in Vracov

As it was described before, the system in Vracov was established in 2007 and it was continuously observed with sampling the heat transfer fluid every year except 2010. The system was topped up in 2014 due to the constant sampling and resulting pressure drop by insufficient fluid volume. From the perspective of changing properties pH, conductivity, content of Cu, freezing point, density and viscosity were monitored.

To fully understand what was happening with the fluid over the long period of time a certain energy balance analysis is necessary. Detailed data on energy conversion (how much energy was prepared and transported by the heat transfer medium from solar irradiation) are available for the whole operating time of the system.

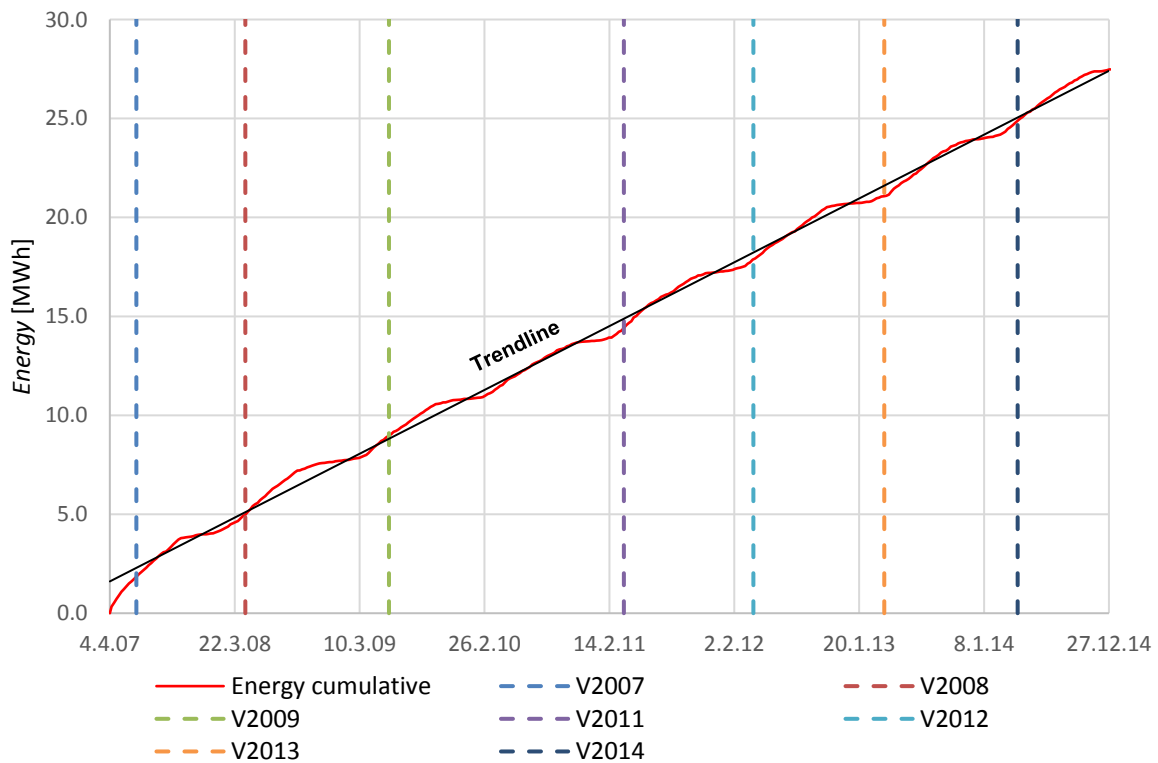


Fig. 6-1 Cumulative energy production (transported) in Vracov system

On the Fig. 6-1 is shown cumulative energy accumulation over the sampled period of time. The energy Q was calculated by a simple formula based on known amount of transported heat transfer fluid V and the difference between the inlet T_{in} and outlet T_{out} temperature of the collector as described in Eq. (6.1.1).

$$Q = (T_{in} - T_{out}) \cdot V \quad (6.1.1)$$

The transported amount of heat transfer fluid was automatically recalculated from flow sensor and the system made all necessary calculations in real time providing with the resulting energy production. It can be seen on the Fig. 6-1 that the amount of transported energy is nearly linear with only small seasonal differences. The influence of season is much better visible on Fig. 6-2. The difference between winter and summer is easily distinguishable when the highest energy flow can be usually encountered in late spring.

The cumulative data shows that the system was very stable during the whole time without any significant thermal load. This is an important premise for the samples from Vracov system, which can be therefore considered as an ideal chronological sequence of samples. No stagnation or serious thermal load was not detected during the whole observed period of time.

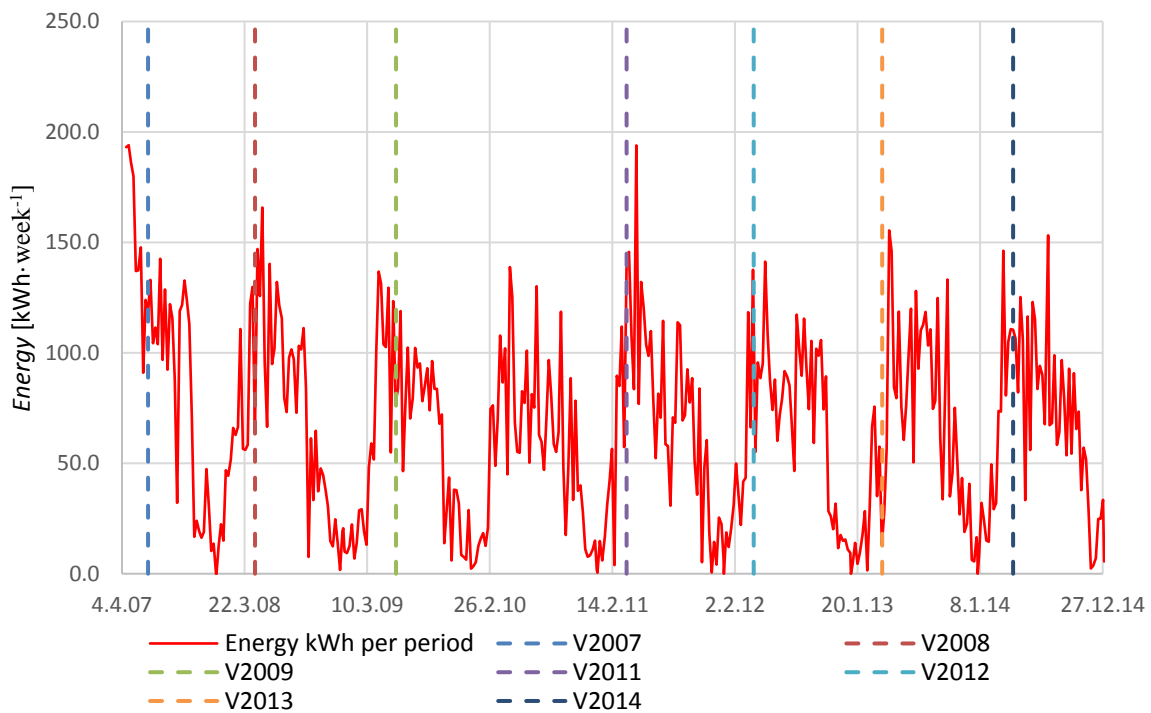


Fig. 6-2 Weekly energy production (transported) in Vracov system

The basic and most simple information about the state of the HTF is provided by its pH. The collected data on the pH values of the samples from the experimental system in Vracov and the original manufactured fluids are provided in the Table 6-1. The comparison of the pH values between the spent and original HTFs are then visualized on Fig. 6-3. The data show gradual drop of the pH over the time, though, the change is only minimal. The original fluid had $\text{pH}(\text{VO2007}) = 8.144$ which dropped to $\text{pH}(\text{V2014}) = 8.000$ during the seven years in work. It can be seen, that the most rapid change was recorded during the first years of service and during the last two years the change was practically zero. For comparison the value after addition of new fluid in 2014 was also added. The addition was only 2 litres and did not lead to any notable change in the pH value nor of any other values of the monitored properties. The drop in pH is connected to organic acid degradation products, which have been extensively studied in the 80s of the last century, some 30 years ago, by Rossiter, Brown and Galuk on propane-1,2-glycol and ethane-1,2-diol mixtures^{112-114,197,198}. The specific acidic degradation products and their formation will be explained later.

Table 6-1. pH measurement results

Sample	pH	Temperature T [°C]
VO2014	8.011	24.8
VO2007	8.144	24.6
V2007	8.147	25.2
V2008	8.047	24.9
V2009	8.080	24.9
V2011	8.041	24.9
V2012	8.019	24.8
V2013	8.001	25.0
V2014	8.000	24.9
V2014N	8.001	25.1

When comparing the data, we can notice a certain difference between the values of pH of VO2007 and VO2014. According to the interview with the product manager from the manufacturer (Velvana a.s.), the receipt for the fluid was slightly changed between the years 2006 and 2009 to better accommodate the needs of the modern systems. Adjusting the mixture led also to a certain drop of the basicity from pH = 8.144 to pH = 8.011, however, this change did not mean any drop in the free alkalinity as stated in the Technical lists of the original fluids¹⁹⁹⁻²⁰¹. The main aim of this change was possibly to adjust the pH more towards the neutral values to further limit the degradation process.

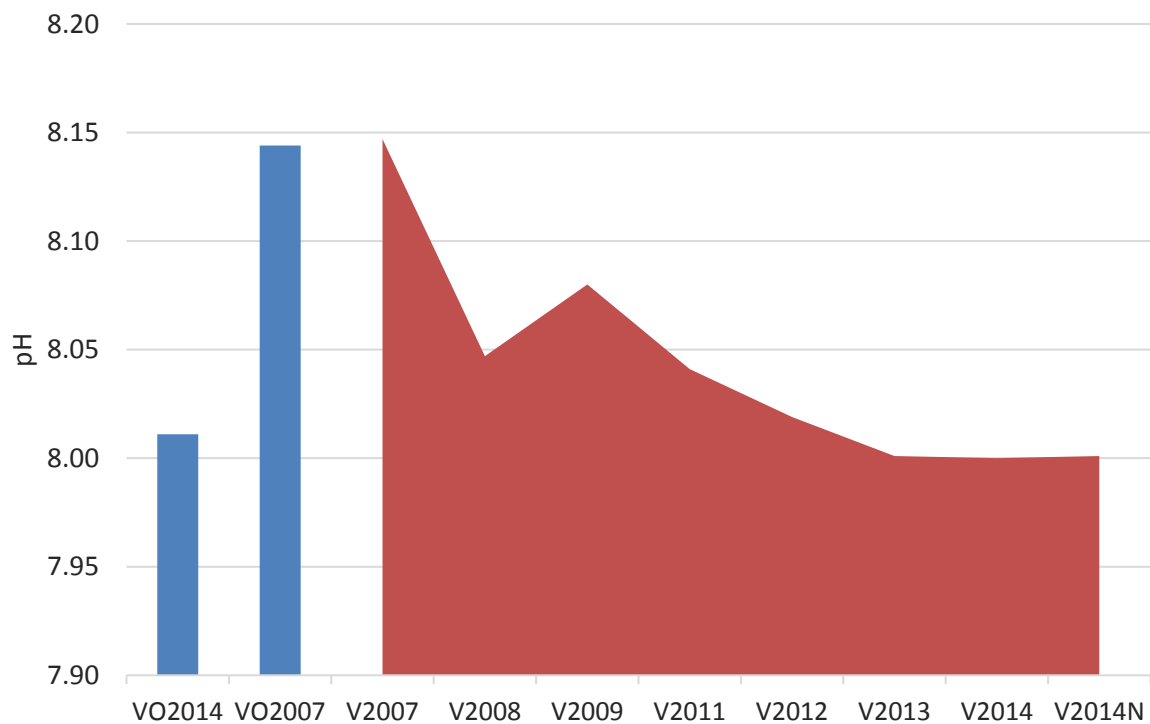


Fig. 6-3 pH comparison of unused and used HTFs from experimental system

Naturally, with the decreasing pH the conductivity of the fluid was rising following very similar trend as the pH. The data on the fluid conductivity are summarised in Table 6-2 and graphically represented on Fig. 6-4.

Table 6-2. Conductivity measurement results

Sample	Conductivity κ [mS·cm ⁻¹]	Temperature T [°C]
VO2014	2.15	24.8
VO2007	2.03	24.6
V2007	2.08	25.2
V2008	2.07	24.9
V2009	2.16	24.9
V2011	2.21	25.1
V2012	2.22	24.9

The rise in conductivity is directly connected to the acidity of the fluid and it is affected by the dissociation constants of the present chemicals. By lowering the pH some of the substances are dissociating into individual ions which leads to rise of the conductivity. From the definition described in capture 5.4.8 we know, that the conductivity describes the capability of the solution to carry charge from one place to another. In the system where different materials with different electrochemical potential are present, this property can be critical to propagate the galvanic corrosion^{202,203}. However, thanks to switching to fully stainless-steel systems in the late decade, the importance of this property is now slightly less important than it was before.

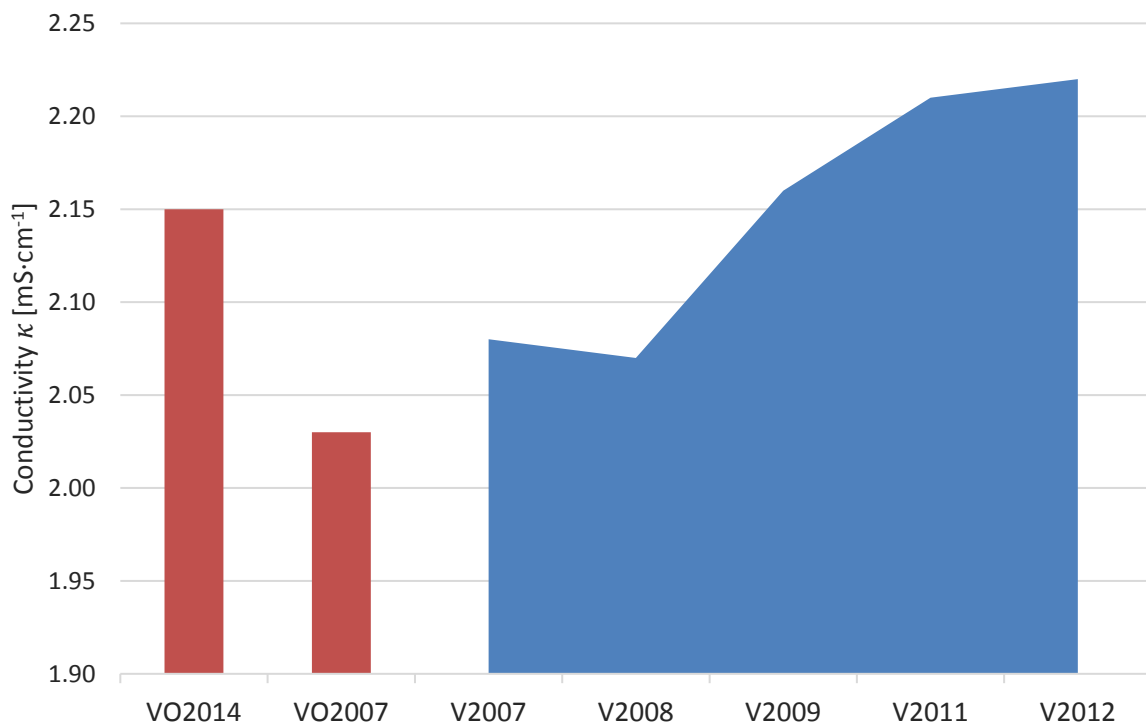


Fig. 6-4 Conductivity comparison of unused and used HTFs from experimental system

The measured values in this case indicate medium/low conductivity. In comparison, the conductivity of sea water, which is considered as fairly conductive, is stated as high as $\kappa_{Seawater}(25\text{ }^{\circ}\text{C})^{36} = 0.053\text{ S}\cdot\text{cm}^{-1}$, which is about 20 times more than the measured values in this case. To the general conductivity the propane-1,2-diol adds only a little as its electrical conductivity is very small $\kappa_{MPG}(25\text{ }^{\circ}\text{C})^{36} \sim 1\cdot 10^{-6}\text{ S}\cdot\text{cm}^{-1}$ and does not dissociate. The main substances affecting the resulting conductivity are various salts added to the mixture as anticorrosion additives and buffers. Among them are chemicals such as sodium benzoate in concentrations $< 0.5\%$ ^{199–201}. Hence, paradoxically, by their addition the risks of galvanic corrosion are enhanced.

Another observed property indicating the changes inside the heat transfer fluid is the density and viscosity. The results of measured density for the samples from the Vracov system are summarised and shown in Table 6-3 and on Fig. 6-5 and the viscosity change on Fig. 6-6. The data shows that the dependency on time is almost linear. That could mean, in comparison with other indicators such as pH and conductivity, that the decrease of density could be connected to some other processes in the system. From the density tables of the aqueous propane-1,2-diol^{39,204,205} (the density graph is listed as appendix A-1²⁰⁶) is apparent, that the drop of density can mean increase of the water content. This applies for the weight fraction of propane-1,2-diol with water from zero up to some 80 wt% where the density rises with the addition of the glycol.

Table 6-3. Density measurement results

Sample	Weight m_{p+s} [g] (pycnometer + sample)	Sample density ρ_s [g·cm ⁻³]
VO2014	45.0597	1.0466
VO2007	45.0325	1.0455
V2007	45.0781	1.0473
V2008	45.0402	1.0458
V2009	45.0251	1.0452
V2011	44.9781	1.0434
V2012	44.9449	1.0421

For higher concentrations the trend switches and by adding more of the glycol the density drops again until it reaches the value of the pure propane-1,2-diol. This density anomaly is typical for all glycols and it is in detail explained in the work of Rhys et al.²⁰⁷. However, the initial concentration of the glycol in the Solaren antifreeze from this work is 48 wt% and it follows natural order of an ideal mixture. Therefore, the question is, where does the drop of density comes from inside a sealed system?

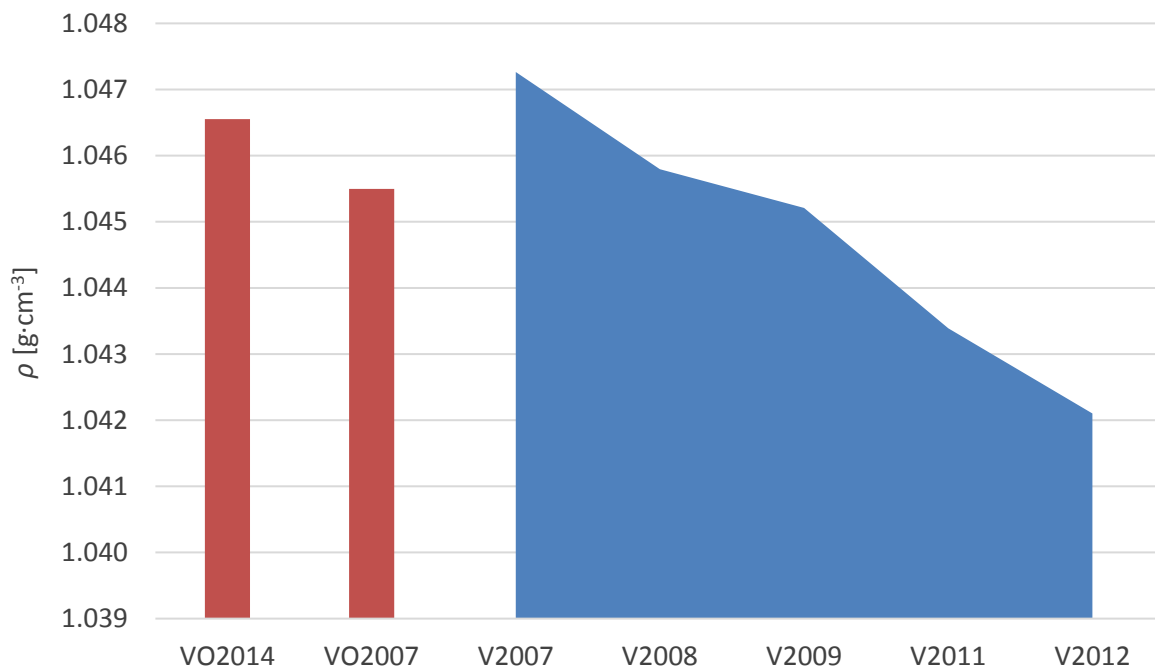


Fig. 6-5 Density comparison of unused and used HTFs from the experimental system

In the beginning, we can root out the possibility of sample manipulation error as all of the samples were treated in the same way and it would not explain the gradual decrease of the density like the data displays (even with the gap in 2010). One of the possible explanation could be gradual condensation of the glycol to its etheric form. The three isomeric products of the alcoholic condensation process of propane-1,2-diol, often called by a collective name dipropylene glycol⁵⁴, are shown on Fig. 6-7.

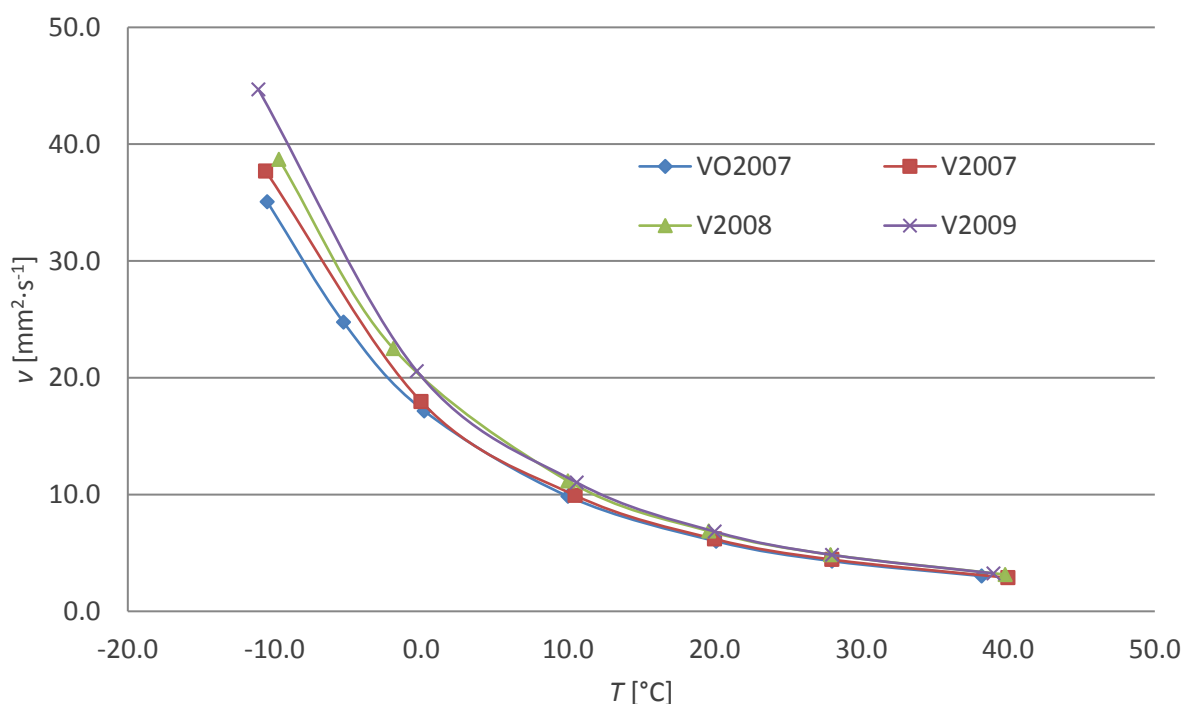


Fig. 6-6 Kinematic viscosity of the unused and used HTFs from the experimental system

Density of these products is also lower than the density of propane-1,2-diol, although, still higher than water ($\rho_{dg} = 1.0206 \text{ g}\cdot\text{cm}^{-3}$)³⁶. The formation of the etheric form was also supported by mass spectrometry (MS) analysis, where the dipropylene glycols ($M_r = 134.0943 \text{ g}\cdot\text{mol}^{-1}$) were found mostly as protonated or sodium adduct ions.

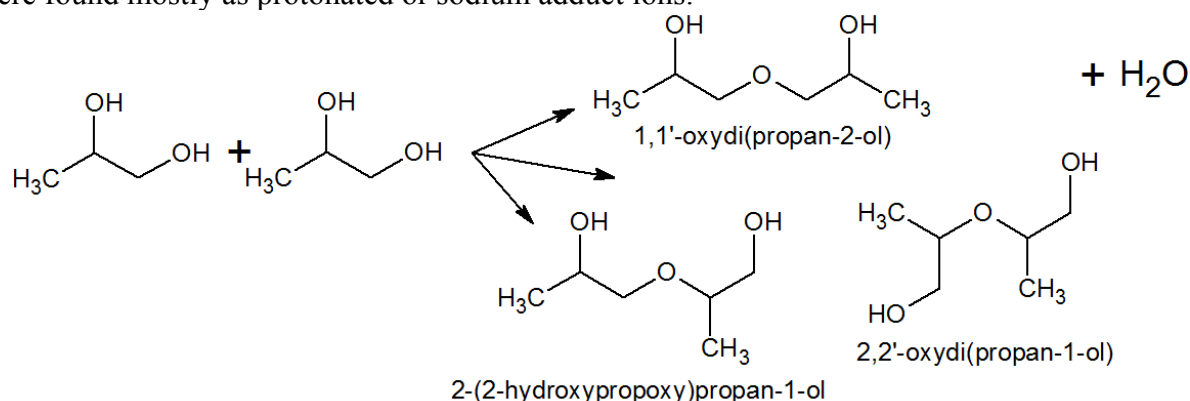


Fig. 6-7 Dipropylene glycol isomers - products of condensation reaction of MPG

On the Fig. 6-8 is displayed mass spectrometry peak of the dipropylene glycol as a sodium adduct. Furthermore, on the same picture (down) is shown the calculated isotopic pattern as a red line corresponding to the actual spectrogram.

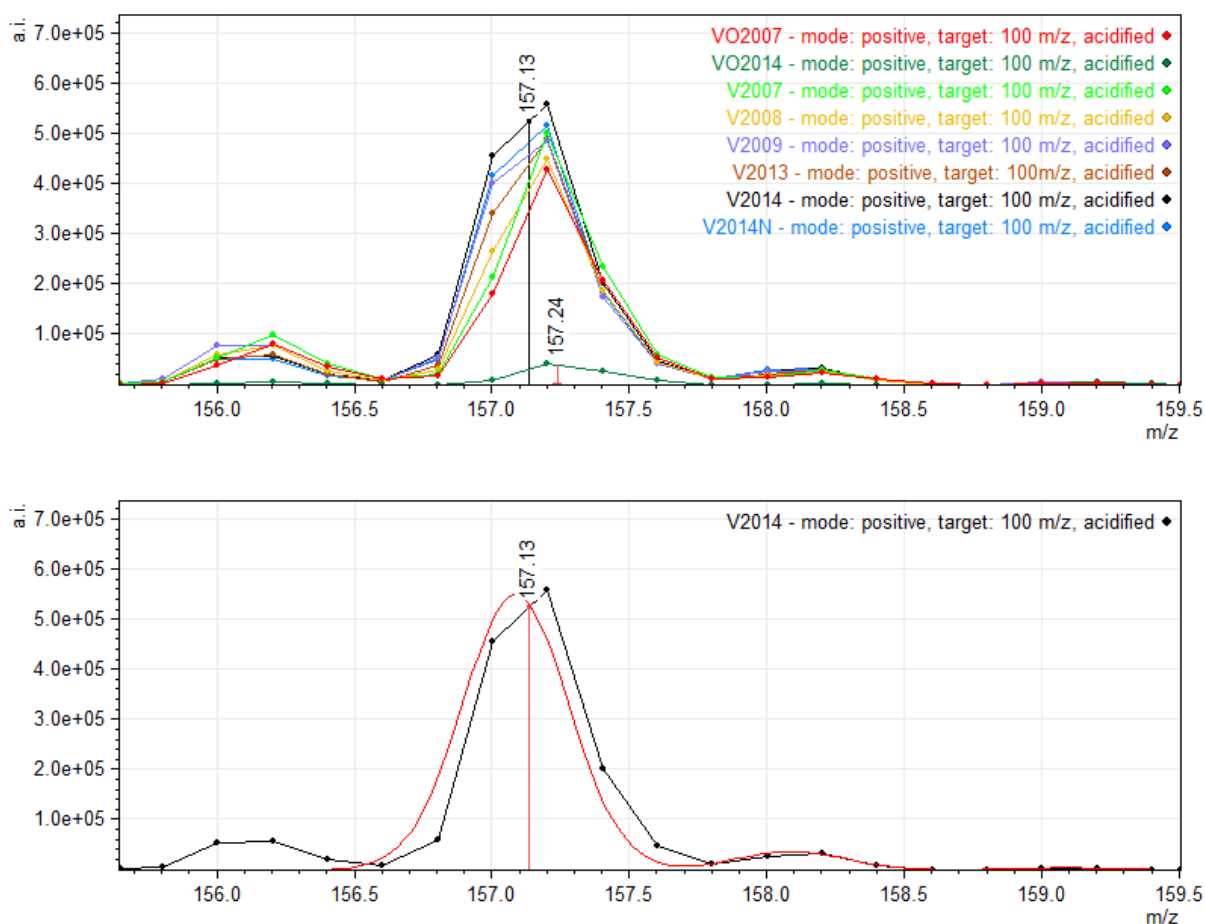


Fig. 6-8 MS peak of dipropylene glycol (top) and its isotopic pattern (bottom)

The intensity of the peaks is rising through the samples according to operation time inside the system, suggesting rise in concentration, with anomaly high intensity of sample V2007. Interesting is also comparison between the VO2007 and VO2014 where the intensity of the dipropylene glycol peak is in case of VO2014 ten times lower, although it must be noted, that a simple comparison of MS spectra is not a sufficient method for sound concentration estimation. That could mean different source or better refined propane-1,2-diol in the newer fluid. The very low concentration would also explain the drop in the concentration between V2014 and V2014N when the fluid in the Vracov system was topped (in 2014) with the VO2014 and therefore diluting the dipropylene glycol in the whole system. Furthermore, the higher content of dipropylene glycol would also explained the lower density of VO2007 compared to VO2014.

Connected to the measurement of the density was establishing of the freezing point. Through the standard measurement of freezing point was find out that the freezing protection was not affected and if it was, it is on the verge of the method detection limits. The freezing point of the original mixture VO2007 was measured as -33 °C and for all of the other measured samples were -34 °C or -33 °C. The different results are most likely product of measurement error and it is necessary to add that this method of measurement is not very precise together with the difficulty of measuring the freezing point aqueous glycols and alcohols^{77,79,207}.

The presence of metallic ions can also significantly enhance the rate of degradation. This fact was proved by several researchers which were studying the degradation processes in the presence of copper^{113,198,203}, aluminium²⁰⁸ and their combinations^{87,112–114,203,208,209}. The results were very unfavourable towards copper ions dissolved in the solution, when the most rapid degradation occurred just only in the presence of the copper. As the copper is deemed to work as a catalyser, it is not necessary for it to be dissolved inside the solution. However, these research were conducted several decades ago and the corrosion protection for copper has significantly advanced. The modern organic corrosion inhibitors such as sebacic acid, benzotriazole and tolyltriazole^{88,92,96,210,211} are not only inhibiting the corrosion of the aluminium and copper but also actively preventing the reaction on the surface of the metals, therefore, also inhibiting the influence of these metals on the degradation process.

Table 6-4. Copper concentration Results

Sample	Absorbance	Copper content c [mg·L ⁻¹]	Relative growth
VO2014	0.0202	0.236	-
VO2007	0.0169	0.191	-
V2007	0.0216	0.255	33.5 %
V2008	0.0259	0.314	23.1 %
V2009	0.0459	0.587	86.9 %
V2011	0.0607	0.791	36.1 %
V2012	0.0967	1.284	62.8 %

The progressing deterioration of the system stabilizing agents can be therefore observed by the presence of metal ions gradually appearing in the fluid. The results of the measurement of the copper content in the samples from Vracov system are summarised in Table 6-4 and plotted on Fig. 6-9. From the graph on the Fig. 6-9 it may seem that the rate is gradually increasing,

however, the relative growth between the samplings increasing only a little, with average about ~50 %. This means that the concentration of copper is increasing steadily by doubling its concentration between every sample in a chronological way.

From all the observation is apparent that heat transfer fluid in the observed experimental system in Vracov is still in a good condition even after 7 years in work. That is already above the recommended time of operation for most of the manufacturers, who recommend to change the fluid every 5 years (warranty time of the fluid under standard conditions)²¹². The factors that allowed for the fluid to be in this good shape may be several, however, two of them are deemed as predominant.

The first and probably the most important factor is that the system was never exposed to a stagnation process. As it was explained in the chapter 4.4.2, the stagnation process has a very strong impact on the degradation process and in many cases can be seen as an initiator for irreparable changes that can occur even after the stagnation is over. However, the exact process is not fully described, because of the complexity of the reactions and possible pathways.

The second factor is sustainably low operating temperature of this particular system. The system is equipped with generously built storage tank (1.3 m³) and boiler cylinder. When the boiler cylinder is fully charged the excess energy is released and accumulated in the storage tank. This combination guarantees that the temperature of the heat transfer fluid inside the system and especially inside the solar collectors does not exceed 100 °C, which is generally considered as a bordering temperature for rapid degradation processes by several researchers^{87,197,203}. Although, the modern thermal solar systems can easily reach operating temperatures above 100 °C by a proper design of the system and correct dimensioning we can significantly slow down the degradation processes, however, it is impossible to stop them completely.

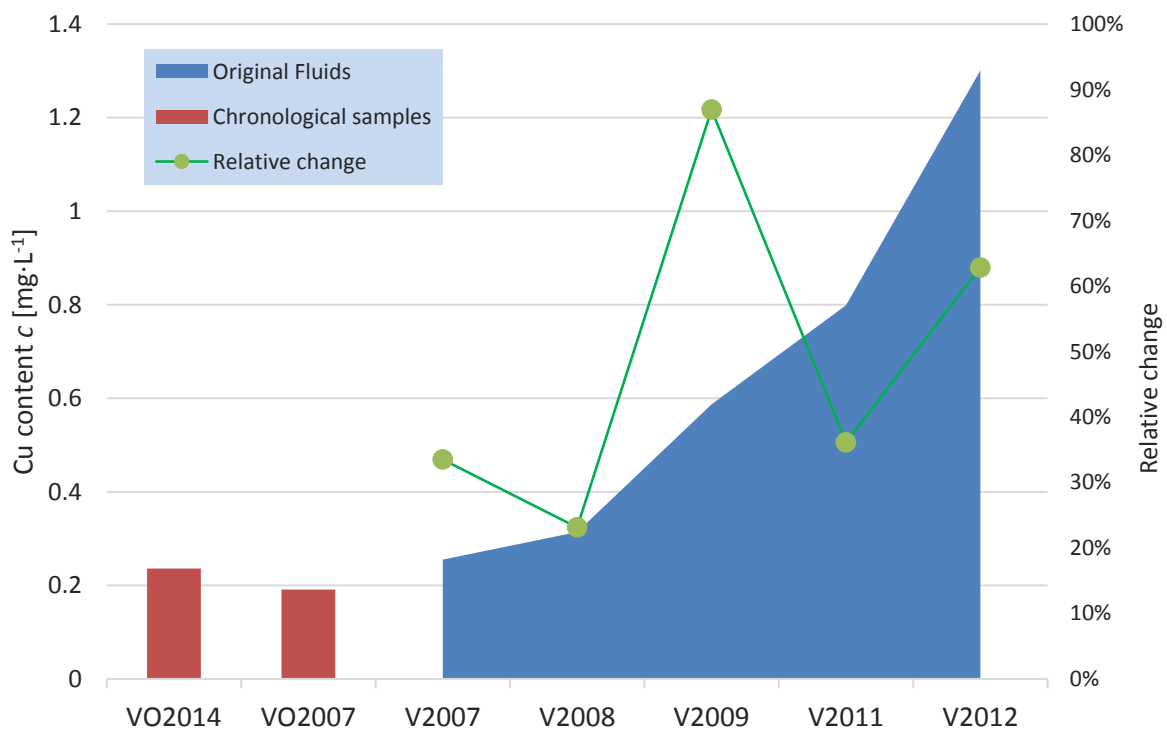


Fig. 6-9 Development of copper concentration and comparison to unused samples

6.1.2 Acidification of hydroxy groups in propane-1,2-diol based mixtures

It has been reported by extensive research of Rossiter and his colleagues^{112-114,197,198} on the topic of propane-1,2-diol and ethane-1,2-diol degradation, that another important factor, especially for formation of acidic degradation products, is the presence of oxygen. The modern systems are usually completely sealed, and therefore it is to be expected that the composition of the acidic degradation will lead to different production rates of the organic acids if ever. For that reason, several visibly degraded heat transfer fluids from various systems were selected and the content of acidic products were measured by isotachopheresis (ITP).

To correctly identify the intended chemical individua through ITP the Relative Step Height (RSH) method was used as a typical method for ITP applications²¹³⁻²¹⁶. The RSH method is described as a ratio of differences in height (electric potential) of the signal of the analyte and the leading and terminating electrolyte this way:

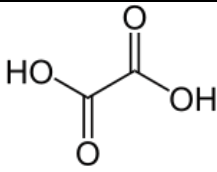
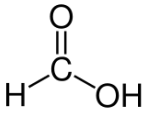
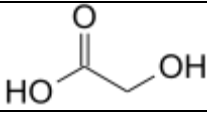
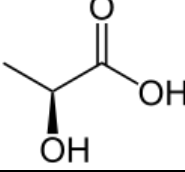
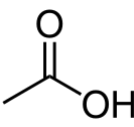
$$RSH_A = \frac{h_A - h_L}{h_T - h_L}, \quad (6.1.2)$$

where RSH_A is the Relative step height of an analyte, h_A is the signal height (potential) of the analyte and the h_L and h_T are signal heights of the leading and terminating electrolyte, respectively.

To establish the basic dataset for qualitative analysis, several different organic acids were measured separately and the RSH was then calculated according to their isotachophoregrams. The isotachophoregrams of the pure standard of the selected organic acids are presented on Fig. 6-10. The RSH of the standards are then summarized in Table 6-5 including the experimental parameters from measuring of the standards.

To check the compatibility between the acids and their possible mutual influence, several combined runs were conducted with only standards of organic acids. The combined runs were also used together with the original standards as a base for quantitative analysis calculation. The combined runs are shown on Fig. 6-11. Three mixtures of standard organic acids were prepared mixing the original $10 \text{ mmol}\cdot\text{L}^{-1}$ stock solutions of the organic acids. The mixture No. 1 was prepared by mixing $200 \mu\text{L}$ of formic acid, $400 \mu\text{L}$ of acetic acid, $600 \mu\text{L}$ of oxalic acid and $800 \mu\text{L}$ of 2-hydroxypropanoic acid. The mixture No. 2 and No. 3 were prepared practically in identical way but $1000 \mu\text{L}$ of 2-hydroxyethanoic acid was added above that to the mixtures. Sample volume of the mixtures was $5 \mu\text{L}$ for mixtures No. 1 and No. 2 and $2 \mu\text{L}$ for mixture No. 3.

Table 6-5. Selected acidic products and their Relative Step Height (*RSH₀*) coefficients

Acid name (IUPAC)	CAS number	Dissociation constant pK_a^*	Structure	Alternative names
Oxalic acid	144-62-7	$pK_{a1}=1.25$; $pK_{a2}=3.81$		Ethanedioic acid
Formic acid	64-18-6	3.75		Methanoic acid
2-hydroxyethanoic acid	79-14-1	3.83		Glycolic acid Hydroxyacetic acid Hydroacetic acid
2-hydroxypropanoic acid	50-21-5	3.86		Lactic acid
Acetic acid	64-19-7	4.756		Ethanoic acid
Signal voltage and Relative Step Height coefficients				
Acid name (IUPAC)	U_{LE} [V]	U_{TE} [V]	U_o [V]	RSH_o
Oxalic acid	1.323	5.335	1.878	0.117
Formic acid	0.979	5.857	2.022	0.215
2-hydroxyethanoic a.	0.955	5.906	2.627	0.325
2-hydroxypropanoic a.	1.267	5.020	2.974	0.427
Acetic acid	0.962	5.386	3.877	0.616

*Reference³⁶

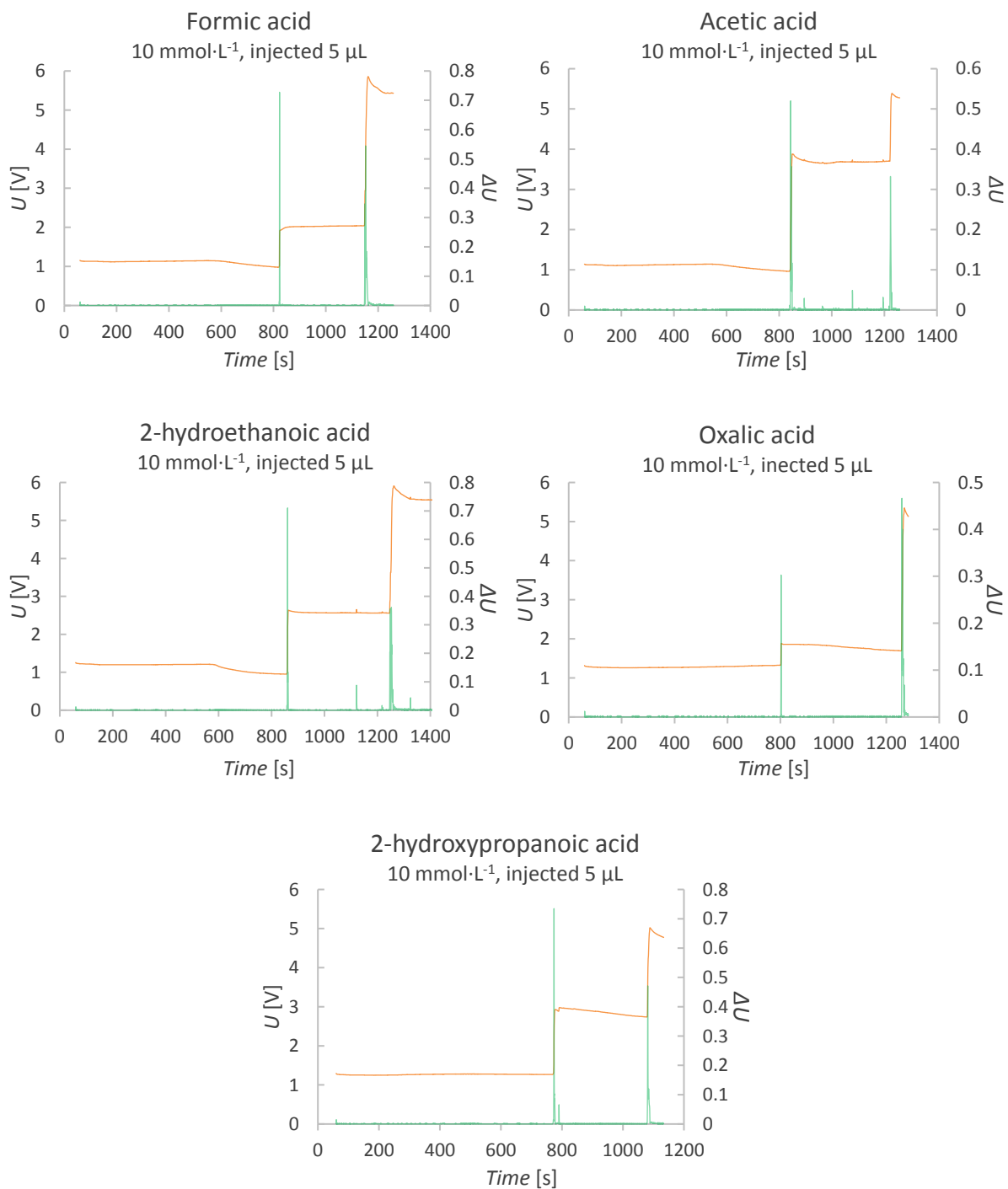


Fig. 6-10 Isotachporegrams of individual standards of organic acids for analysis

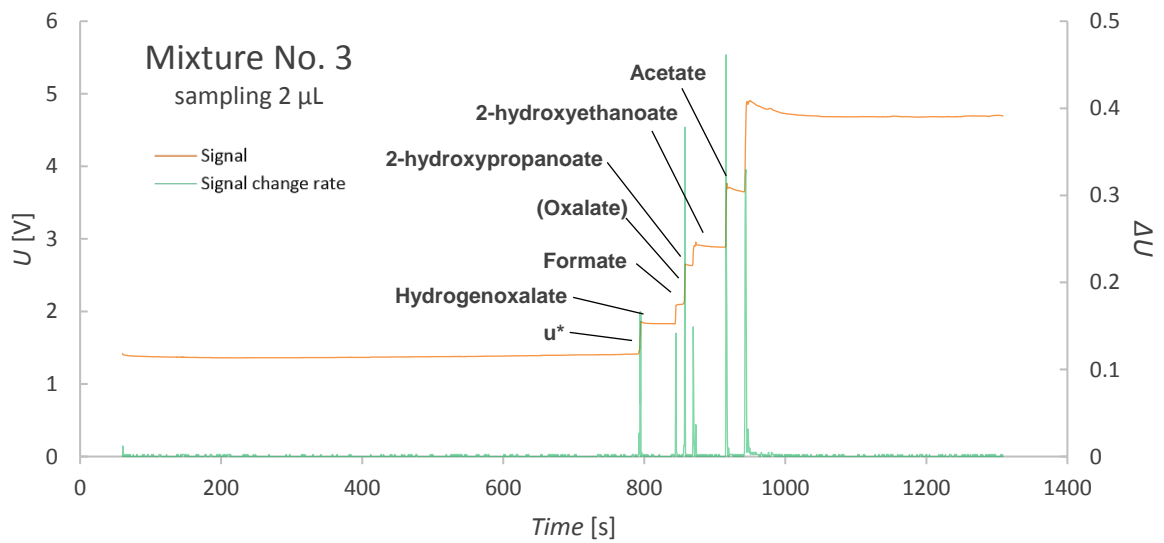
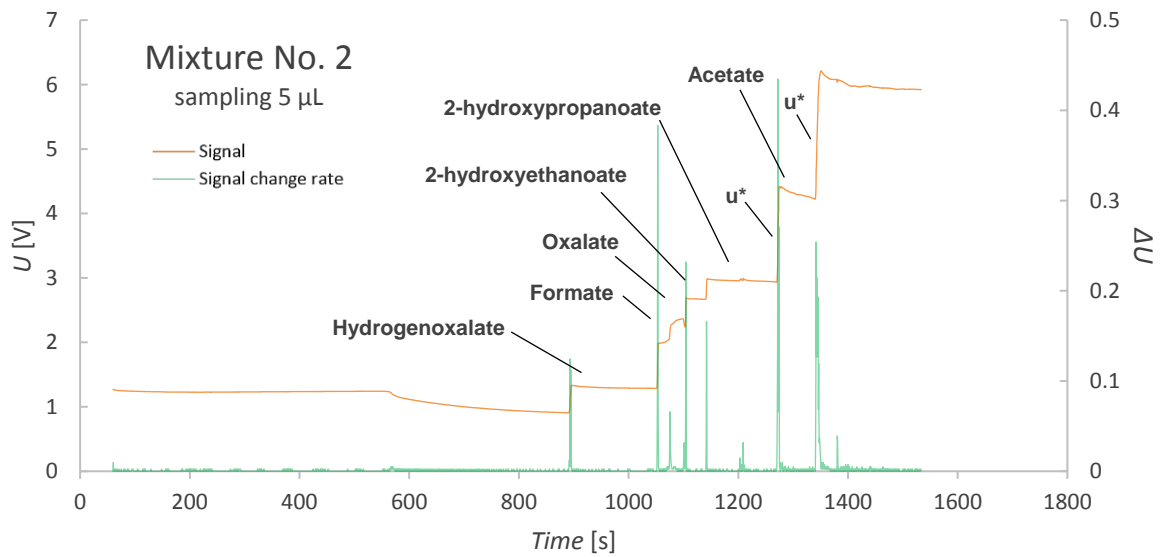
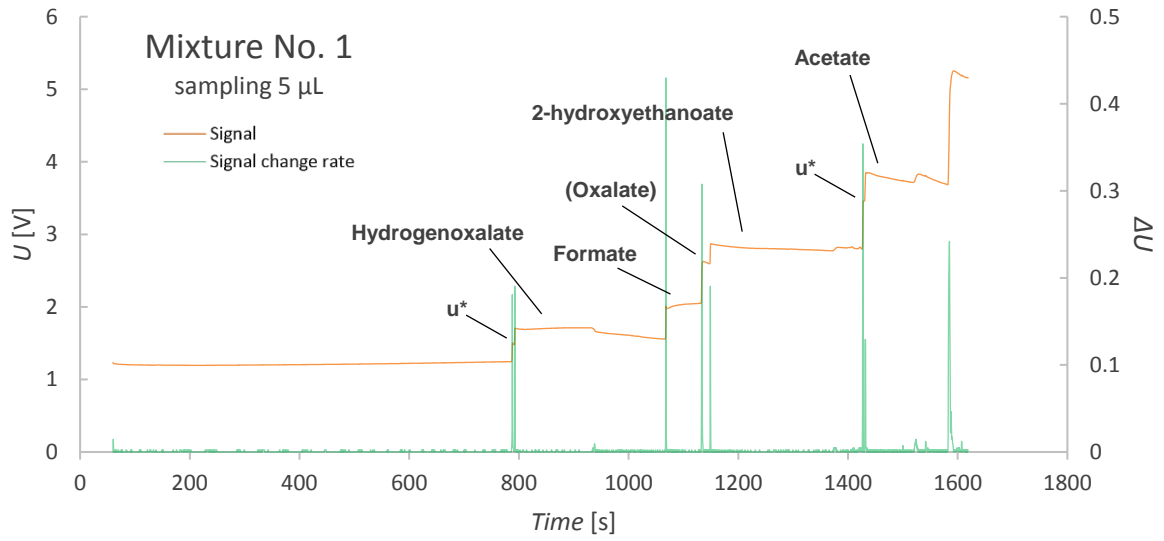


Fig. 6-11 Isotachopherograms of mixed standard, u^* - unknown/impurities

Table 6-6. Results of quantitative and qualitative analysis of standard mixtures

Standard Mixture No. 1						
Sample volume 5 μ L						
$U_{LE} = 1.245 \text{ V} / U_{TE} = 5.254 \text{ V}$						
Step No.	U_A [V]	RSH_A	Identified component	t_1 [s]	t_2 [s]	Δt
1	1.421	0.044	-	787.90	792.30	4.40
2	1.704	0.114	Hydrogenoxalate	792.30	1067.90	275.60
3	2.012	0.191	Formate	1067.90	1133.15	65.25
4	2.603	0.339	Oxalate	1133.15	1148.80	15.65
5	2.871	0.406	2-hydroxypropanoate	1148.80	1426.95	278.15
6	3.179	0.482	-	1426.95	1431.80	4.85
7	3.848	0.649	Acetate	1431.80	1583.10	151.30
Standard Mixture No. 2						
Sample volume 5 μ L						
$U_{LE} = 0.908 \text{ V} / U_{TE} = 6.189 \text{ V}$						
Step No.	U_A [V]	RSH_A	Identified component	t_1 [s]	t_2 [s]	Δt
1	1.333	0.086	Hydrogenoxalate	893.10	1052.80	159.70
2	2.002	0.221	Formate	1052.80	1075.15	22.35
3	2.366	0.295	Oxalate	1075.15	1104.10	28.95
4	2.678	0.358	2-hydroxyethanoate	1104.10	1141.90	37.80
5	2.981	0.419	2-hydroxypropanoate	1141.90	1272.30	130.40
6	3.926	0.610	-	1272.30	1273.85	1.55
7	4.390	0.704	Acetate	1273.85	1341.70	67.85
8	5.227	0.874	-	1341.70	1345.15	3.45
Standard Mixture No. 3						
Sample volume 2 μ L						
$U_{LE} = 1.414 \text{ V} / U_{TE} = 4.907 \text{ V}$						
Step No.	U_A [V]	RSH_A	Identified component	t_1 [s]	t_2 [s]	Δt
1	1.834	0.187	Hydrogenoxalate	794.65	844.55	49.90
2	2.085	0.238	Formate	844.55	857.40	12.85
3	2.651	0.353	2-hydroxyethanoate	857.40	869.30	11.90
4	2.908	0.404	2-hydroxypropanoate	869.30	915.75	46.45
5	3.779	0.581	Acetate	915.75	943.10	27.35

As it was explained before, the quantitative analysis is based on the time of elution of the steps that represent the individual analytes. To precisely determine the amount of an unknown analyte in a sample, extensive preparations are necessary. Comparison of standard mixtures No. 1, 2 and 3 gives away an overview of relative step height and time of elution in relation to the concentration of the analyte. This data were used as a base for analyte recognition together with

the relative step time according to standard additions of individual organic acid with the sample. To calculate the actual concentration of an organic acid c_a the following equation was used:

$$c_a = \frac{t_a c_{std} V_{std}}{t_{a+std}(V_S + V_{std}) - t_a V_S}, \quad (6.1.3)$$

where t_a and t_{a+std} are time-lengths of the analyte and the analyte and standard steps, respectively, and V_S and V_{std} are the volumes of a sample and the standard addition. The example of data analysis is shown on Fig. 6-14. The data peaks, shown in green on the isotachophoregrams, were created by simple assessing the rate of change defined as a change of the output voltage ΔU per time unit. The time unit in this case was selected the smallest possible as 0.05 second. This time difference was selected based on the unit capabilities of acquiring raw data. The step time was then selected as a difference between peaks creating a base for the quantitative analysis.

The collected and analyzed raw data are summarized in Table 6-8. The data are organized in a way where corresponding substances are in the same column. All the analytes were recognized positively in the samples with standard deviation being between 0.6 – 2.7 % with 1.9 % on average.

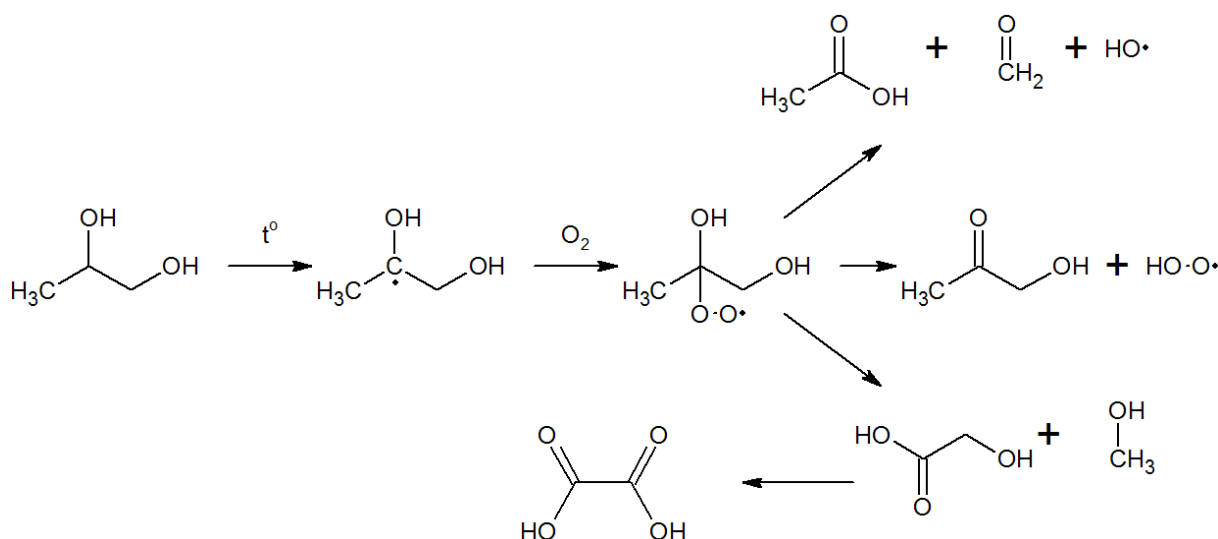


Fig. 6-12 Degradation process of propane-1,2-diol through C_2 thermal oxidation

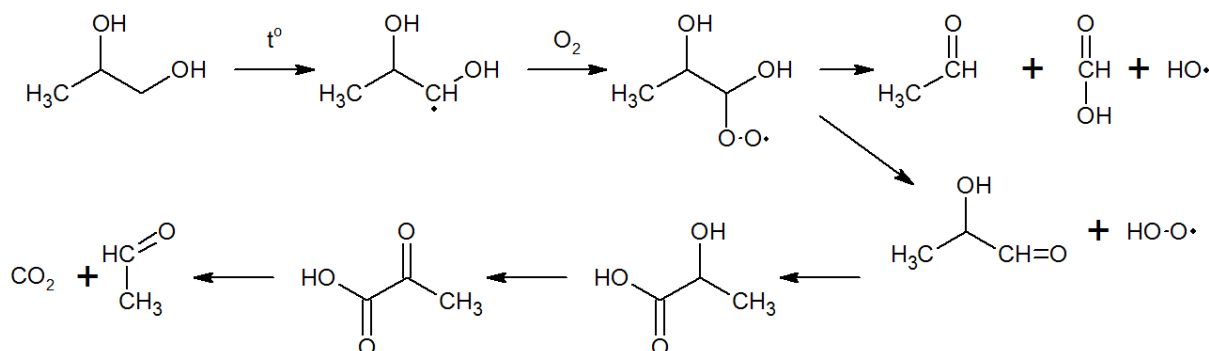


Fig. 6-13 Degradation process of propane-1,2-diol through C_1 thermal oxidation

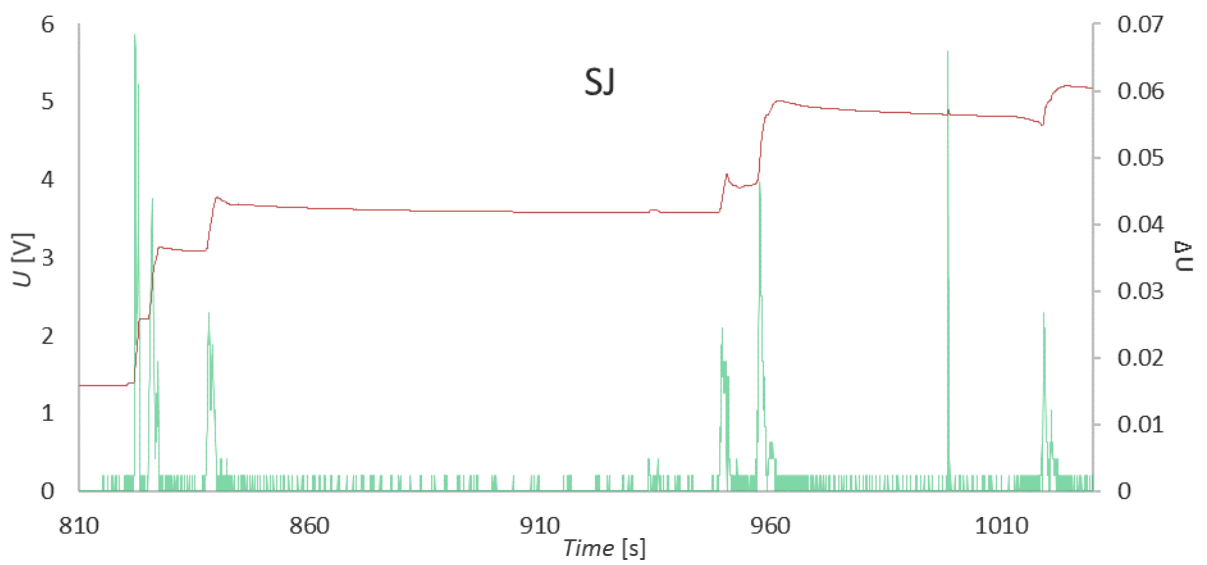
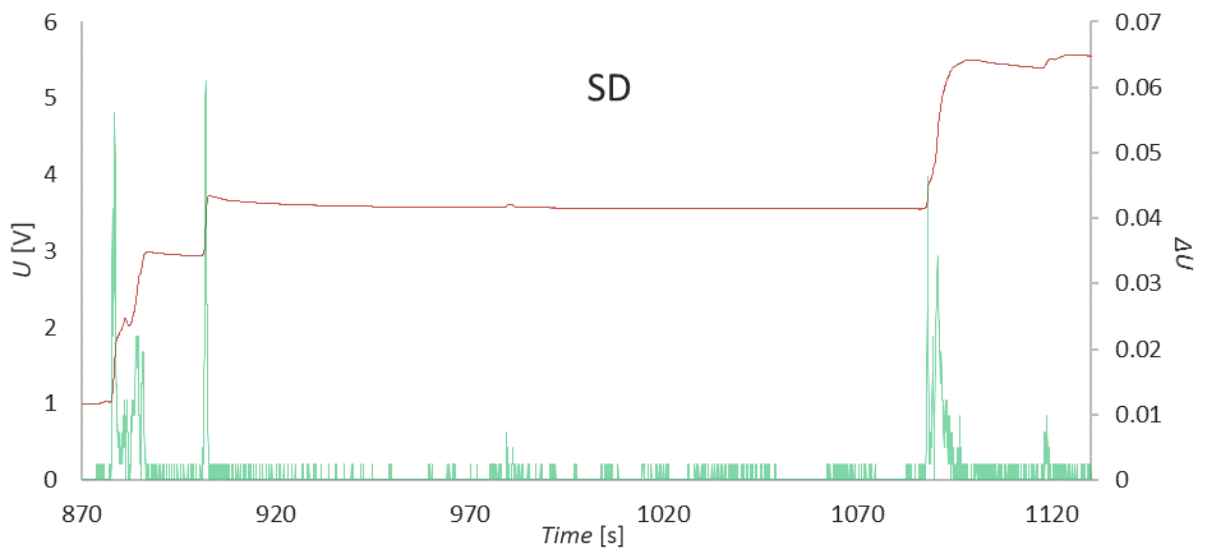
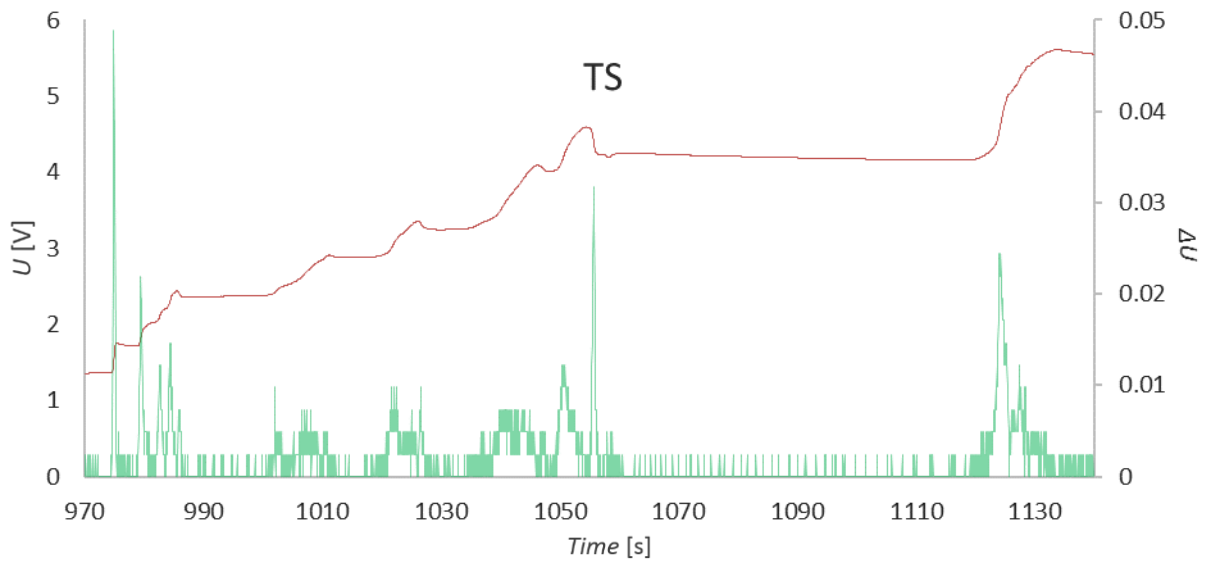


Fig. 6-14 Examples of real samples analysis results

Table 6-7. pH measurement for highly degraded samples SD, SJ, TS and SP

Sample	pH	Temperature T [°C]
SD	7.23	23.1
SJ	7.81	22.8
TS	5.83	24.6
SP	7.79	23.1

In the Table 6-8 the data are distinguishable easily by colour. The colour definition is following:

Oxalate	Formate	2-hydroxy-ethanoate	2-hydroxy-propanoate	Sebacate	Acetate
---------	---------	---------------------	----------------------	----------	---------

In the samples SD and SJ also sebacic acid in the form of sebacate was positively confirmed. In the more degraded SJ the amount of sebacate is dramatically reduced, which is also visible in the case of MS spectra in the next chapter.

When comparing these data to the literature, it is apparent that the amounts of acidic degradation product formation is much smaller than stated in literature. According to literature (Rossiter et al.¹¹⁴ and DOW²⁰⁹) sources the dominant product for aqueous propane-1,2-diol degradation should be 2-hydroxypropanoic acid (lactic acid). That is, in case of oxidative environment and presence of copper. Although in the observed system copper was abundant, the systems were completely sealed without oxygen supply. But even without the oxygen the dominant degradation product in case of samples SJ and SD was indeed 2-hydroxypropanoic acid. Different results, however, show sample TS. As previously described, the sample TS was taken from a vacuum tube system and it was subjected to much higher stagnation temperatures than samples SD and SJ. That taken in account can lead to a conclusion that the temperature can be a deciding factor to which degradation product will predominate in anoxic environment.

For comparison the samples V2007, V2008, V2009, V2013 and V2014 were also tested on the presence of acidic degradation products. From the pH change would seem that some acidification occurs even in stable systems. But the results for the presence of organic acid were negative in all cases. The only positively identified acid inside the samples was sebacic acid from the corrosion inhibitor system.

Table 6-8. Collected data and step finding results of isotachopheric analysis

Sample	Injection	Std. add	RSH ₁	Δt_1 [s]	RSH ₂	Δt_2 [s]	RSH ₃	Δt_3 [s]	RSH ₄	Δt_4 [s]	RSH ₅	Δt_5 [s]	RSH ₆	Δt_6 [s]	RSH ₇	Δt_7 [s]	RSH ₈	Δt_8 [s]	RSH ₉	Δt_9 [s]	RSH ₁₀	Δt_{10} [s]	RSH ₁₁	Δt_{11} [s]	RSH ₁₂	Δt_{12} [s]	RSH ₁₃	Δt_{13} [s]
SD	2 μ L	0 μ L	-	-	0.205	2.70	0.269	0.90	0.328	1.70	-	-	0.430	16.25	0.563	186.15	-	-	0.641	1.35	0.701	1.35	-	-	0.979	28.00	-	-
SD	2 μ L	100 μ L	-	-	0.230	3.35	-	-	0.334	1.30	0.450	1.25	0.456	25.45	0.581	163.60	0.647	0.75	0.670	3.20	-	-	0.891	2.00	0.911	23.90	0.944	2.00
SD	2 μ L	100 μ L	0.167	0.35	0.222	2.80	-	-	0.329	1.25	-	-	0.454	14.45	0.582	164.70	-	-	0.675	17.70	0.838	1.20	-	-	0.913	25.40	0.940	1.65
SD	2 μ L	100 μ L	0.077	17.55	0.213	2.95	-	-	0.335	1.15	-	-	0.400	15.05	0.537	169.45	0.629	1.55	0.645	2.50	-	-	0.882	4.45	0.957	23.65	-	-
SD	2 μ L	100 μ L	0.144	0.90	0.213	15.80	0.279	0.40	0.348	0.95	-	-	0.414	15.35	0.546	170.00	0.641	1.75	0.654	2.70	0.806	1.00	0.884	2.90	0.970	23.25	-	-
SD	2 μ L	100 μ L	-	-	0.208	5.05	-	-	0.329	14.15	-	-	0.398	15.20	0.531	167.60	0.630	2.10	0.641	2.35	0.775	0.80	0.876	3.25	0.969	23.35	-	-
SD	2 μ L	300 μ L	-	-	0.227	3.35	-	-	0.333	1.10	0.450	2.40	0.448	40.00	0.576	135.85	0.632	0.60	0.662	4.00	0.845	1.50	0.899	1.00	0.912	19.10	0.955	2.75
SD	2 μ L	300 μ L	-	-	0.226	3.05	0.336	1.10	0.396	0.60	-	-	0.460	14.95	0.578	140.50	0.627	0.65	0.653	34.70	0.875	2.20	-	-	0.909	19.85	0.949	2.80
SD	2 μ L	300 μ L	-	-	0.226	2.75	0.336	1.00	0.369	34.35	-	-	0.444	11.45	0.573	138.70	0.623	0.60	0.655	3.80	0.819	1.05	0.902	1.20	0.913	19.95	0.945	1.95
SD	2 μ L	300 μ L	0.122	25.80	0.203	2.15	0.308	1.05	0.388	1.10	-	-	0.446	10.90	0.573	131.10	-	-	0.650	3.75	0.831	1.00	0.902	1.30	0.912	18.50	0.937	2.00
SD	2 μ L	300 μ L	0.146	0.35	0.234	30.65	-	-	0.362	1.00	0.424	0.85	0.494	12.10	0.620	138.60	-	-	0.704	4.25	0.841	0.65	0.910	1.55	0.966	20.10	0.981	1.50
SJ	2 μ L	0 μ L	-	-	0.130	0.70	0.235	3.10	-	-	-	-	0.437	1.20	0.476	10.95	0.612	110.75	-	-	0.696	8.15	0.949	3.20	-	-	-	-
SJ	2 μ L	300 μ L	-	-	0.188	1.80	0.231	0.90	0.335	3.80	0.384	0.50	-	-	0.422	40.10	0.559	88.70	0.655	1.75	0.661	8.40	0.873	3.05	0.964	44.45	0.934	2.70
SJ	2 μ L	300 μ L	-	-	-	-	0.228	2.90	0.346	0.20	0.395	0.70	-	-	0.435	9.80	0.561	90.80	-	-	0.641	42.60	-	-	0.936	47.25	0.911	2.45
SJ	2 μ L	300 μ L	-	-	0.145	0.90	0.233	2.15	-	-	0.370	34.70	-	-	0.441	10.15	0.581	95.25	0.705	0.95	0.685	8.40	0.892	2.65	-	-	-	-
SJ	2 μ L	300 μ L	0.076	0.45	0.134	37.25	0.220	3.90	-	-	-	-	0.407	0.90	0.458	10.30	0.589	86.95	0.671	1.20	0.665	10.55	0.915	3.50	0.917	44.25	0.868	1.15
SJ	2 μ L	300 μ L	-	-	0.149	0.50	0.233	33.20	-	-	-	-	0.429	1.00	0.478	10.25	0.609	90.00	0.708	1.40	0.692	10.45	-	-	0.916	50.35	0.868	0.95
SJ	2 μ L	100 μ L	-	-	0.148	0.35	0.261	4.45	-	-	-	-	0.460	0.95	0.515	11.85	0.647	105.65	0.743	1.65	0.729	21.75	0.927	1.05	0.975	57.35	1.008	2.05
SJ	2 μ L	100 μ L	-	-	0.119	0.40	0.231	4.10	-	-	-	-	0.441	2.10	0.461	23.25	0.590	104.55	0.676	1.45	0.678	11.60	0.895	2.35	0.930	55.90	0.939	1.95
SJ	2 μ L	100 μ L	-	-	0.117	0.40	0.237	4.40	-	-	0.380	11.90	-	-	0.451	12.25	0.586	105.30	0.666	1.35	0.678	11.25	0.902	1.30	0.941	54.85	0.928	1.95
SJ	2 μ L	100 μ L	-	-	0.113	0.30	0.232	16.10	-	-	0.344	0.70	0.409	0.60	0.453	12.40	0.588	105.85	0.673	1.45	0.685	11.20	0.912	2.30	-	-	-	-
SJ	2 μ L	100 μ L	0.062	0.80	0.111	16.25	0.221	3.95	0.328	0.85	0.396	0.60	-	-	0.438	12.85	0.577	107.60	-	-	0.676	12.70	0.898	2.80	-	-	-	-
TS	2 μ L	0 μ L	0.096	1.85	0.157	1.55	0.203	0.60	0.238	9.70	-	-	-	-	0.359	5.60	0.446	8.45	-	-	0.630	3.35	0.673	26.45	-	-	-	-
TS	5 μ L	0 μ L	0.094	4.35	0.162	3.35	0.208	1.65	0.246	16.00	0.288	6.10	-	-	0.367	14.00	0.461	17.80	-	-	0.635	6.50	0.675	68.45	-	-	-	-
TS	2 μ L	100 μ L	0.082	1.85	0.142	2.15	-	-	0.245	6.05	0.277	3.80	-	-	0.334	8.25	0.430	19.55	0.587	2.95	0.687	3.40	0.670	23.30	0.745	1.25	0.855	2.25
TS	2 μ L	100 μ L	0.076	1.95	0.129	2.20	0.211	1.25	0.257	6.35	-	-	-	-	0.327	6.25	0.428	8.25	0.584	2.95	0.685	3.50	0.668	37.95	0.736	1.15	0.820	1.60
TS	5 μ L	100 μ L	0.071	4.20	0.118	3.60	0.148	1.70	0.258	23.50	-	-	-	-	0.323	13.85	0.427	19.50	0.583	9.45	0.708	4.25	0.662	99.05	0.799	2.95	-	-
TS	5 μ L	100 μ L	0.102	3.80	0.172	2.25	-	-	0.250	52.95	0.336	2.35	-	-	0.383	11.70	0.462	16.45	0.584	3.65	0.642	5.55	0.684	71.90	0.817	1.10	0.877	2.40
TS	5 μ L	100 μ L	0.096	4.05	0.164	2.25	0.213	1.45	0.251	22.50	0.323	2.70	0.374	10.50	0.389	39.25	0.457	15.30	0.614	6.00	0.637	3.40	0.678	73.55	0.875	3.80	0.949	1.40
TS	5 μ L	300 μ L	0.093	3.35	0.154	2.70	0.197	1.00	0.255	19.30	0.329	2.50	-	-	0.368	20.30	0.446	85.15	0.625	8.15	0.731	3.05	0.676	58.55	0.868	2.95	0.946	3.55
TS	5 μ L	300 μ L	0.082	3.95	0.137	2.90	0.174	1.50	0.255	16.30	0.293	6.50	-	-	0.348	11.15	0.449	15.25	0.611	7.75	0.716	3.20	0.665	145.7	0.783	0.60	0.846	1.85
TS	5 μ L	300 μ L	0.080	3.90	0.136	4.35	-	-	0.256	21.55	0.339	9.20	-	-	0.372	96.45	0.440	13.60	0.599	7.55	0.716	3.55	0.676	58.30	0.832	2.35	0.921	3.20
TS	5 μ L	300 μ L	0.076	3.90	0.118	1.60	0.154	1.55	0.250	93.75	0.272	11.95	-	-	0.338	10.55	0.439	16.10	0.593	9.15	0.717	3.55	0.683	60.00	0.780	0.50	0.844	2.05
TS	5 μ L	300 μ L	0.070	115.0	0.145	2.00	0.174	1.25	0.232	23.35	-	-	-	-	0.303	12.75	0.409	16.60	0.564	9.00	0.697	3.90	0.668	59.75	0.802	1.40	0.862	1.80

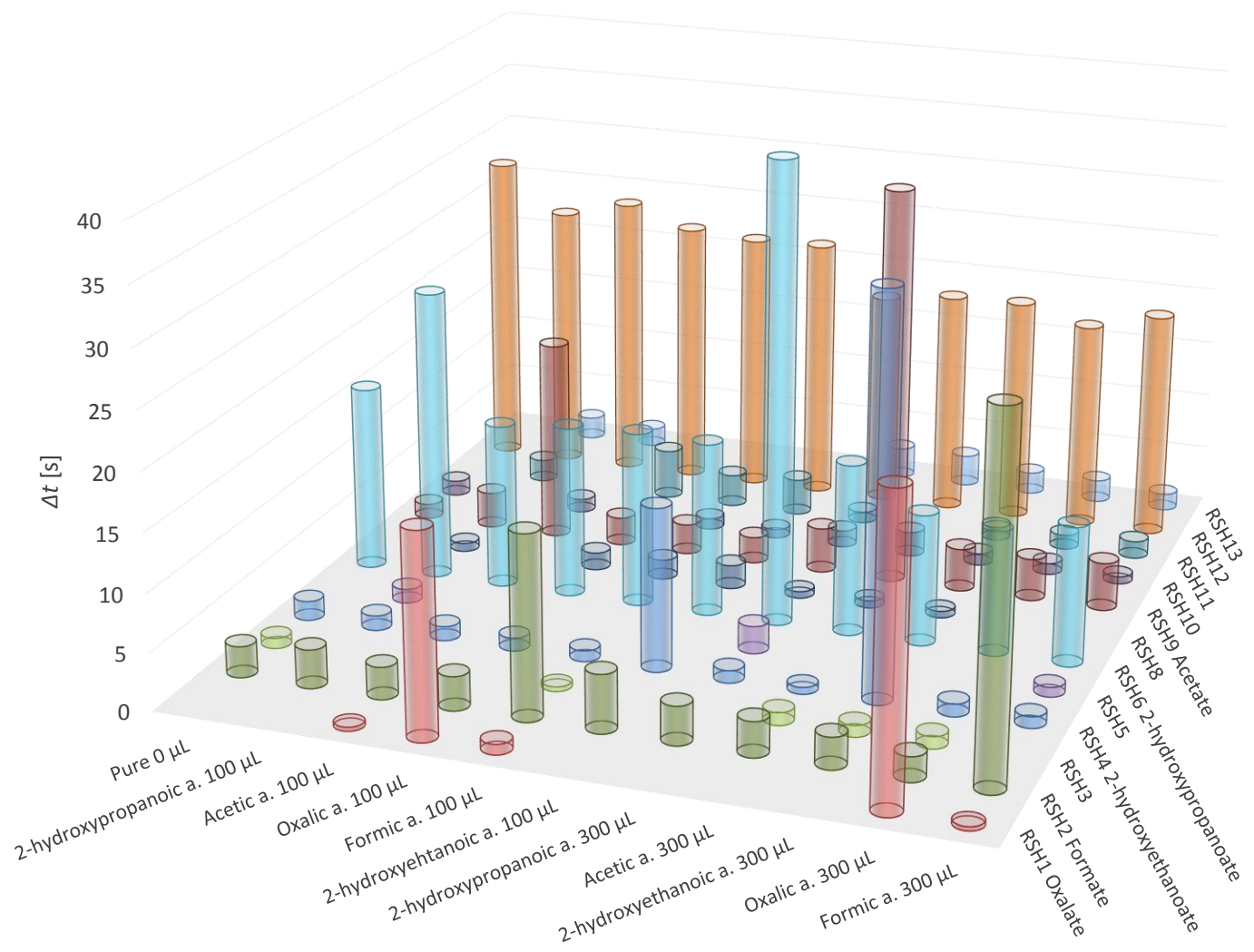


Fig. 6-15 ITP step detection times of sample SD for different standard additions

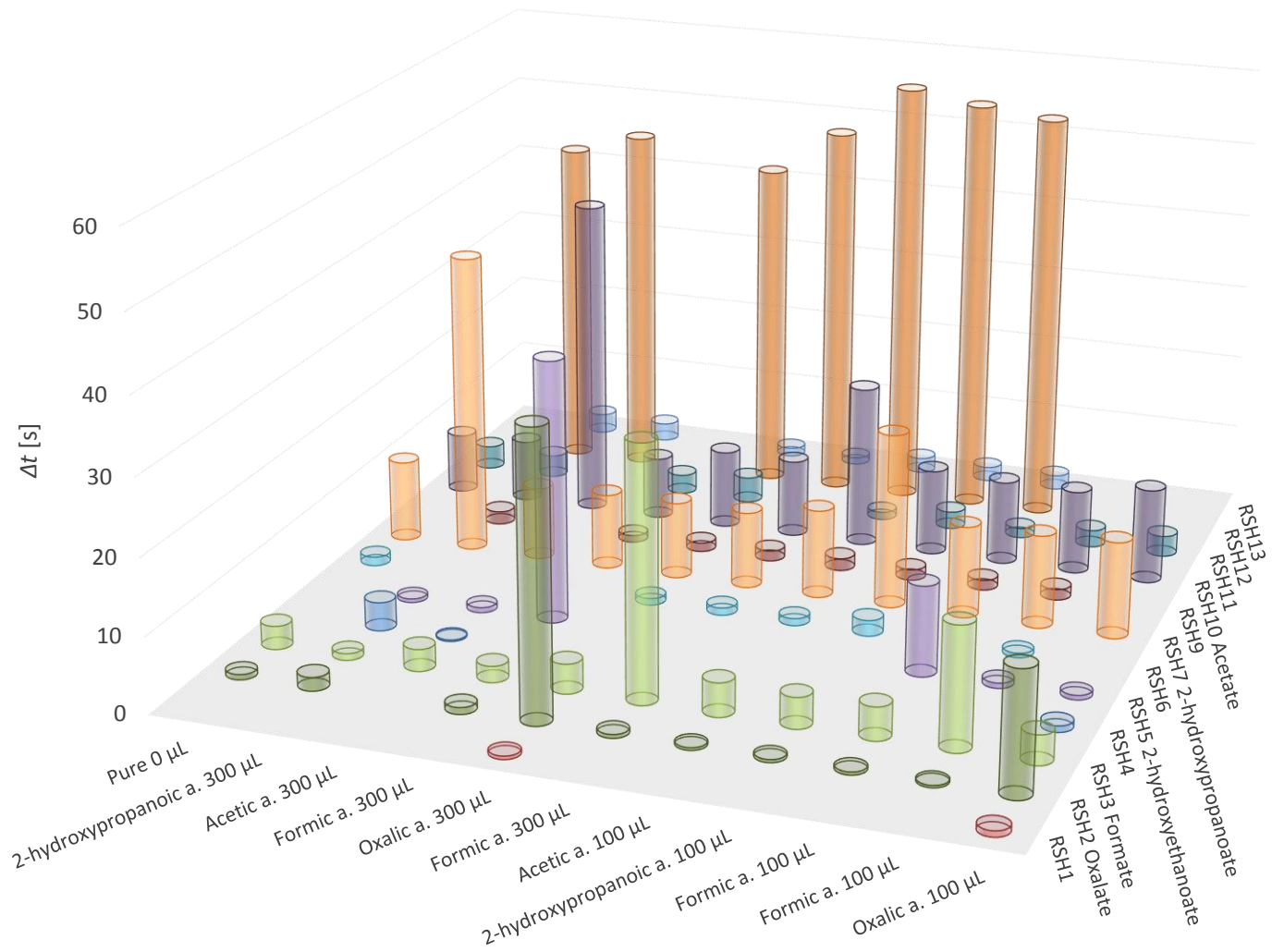


Fig. 6-16 ITP step detection times of sample SJ for different standard additions

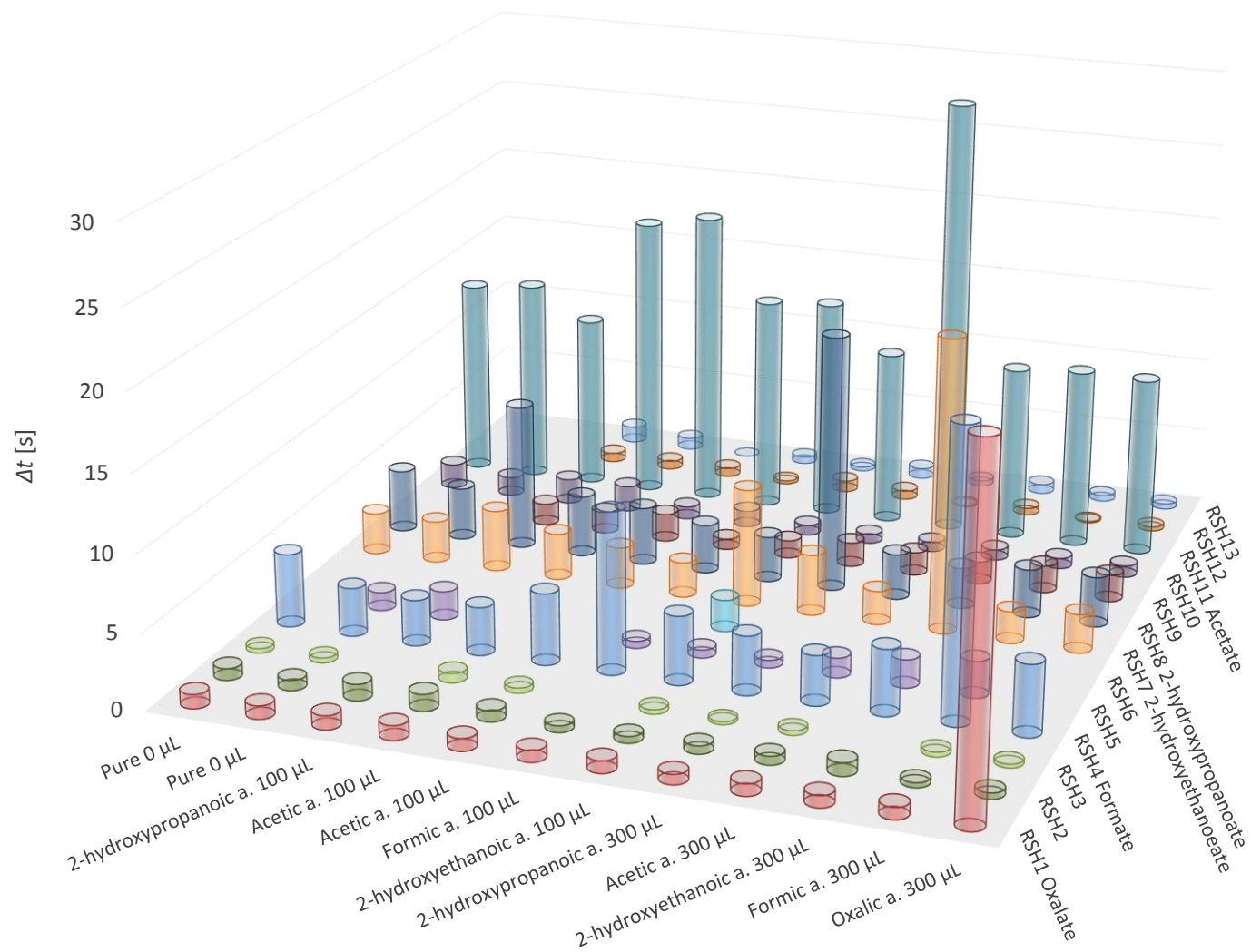


Fig. 6-17 ITP step detection times of TS for different standard additions (to 1 μL)

Table 6-9. Isotachophoretic quantitative analysis - results

Sample SD							
Organic acid	t_a (avr) [s] (100uL)	t_a (avr) [s] (300uL)	t_{a+std} [s] (100uL)	t_{a+std} [s] (300uL)	c_a [g·L ⁻¹] (100uL)	c_a [g·L ⁻¹] (300uL)	c_a [mg·L ⁻¹]
Oxalic acid	0.62	0.35	17.55	25.80	0.0030	0.0028	2.93
Formic acid	3.54	3.27	15.80	30.65	0.0118	0.0123	12.05
2-hydroxyethanoic acid	1.16	0.95	14.15	34.35	0.0061	0.0050	5.55
2-hydroxypropanoic acid	15.01	12.35	25.45	40.00	0.1042	0.0842	94.17
Acetic acid	2.69	3.95	17.70	34.70	0.0096	0.0173	13.45
Sample SJ							
Organic acid	t_a (avr) [s] (100uL)	t_a (avr) [s] (300uL)	t_{a+std} [s] (100uL)	t_{a+std} [s] (300uL)	c_a [g·L ⁻¹] (100uL)	c_a [g·L ⁻¹] (300uL)	c_a [mg·L ⁻¹]
Oxalic acid	0.36	1.35	16.25	37.25	0.0019	0.0077	4.80
Formic acid	4.22	2.46	16.10	33.20	0.0144	0.0084	11.39
2-hydroxyethanoic acid	0.65	0.60	11.90	34.70	0.0040	0.0031	3.52
2-hydroxypropanoic acid	12.34	10.12	23.25	40.10	0.0840	0.0651	74.55
Acetic acid	11.69	9.45	21.75	42.60	0.0574	0.0371	47.21
Sample TS							
Organic acid	t_a (avr) [s] (100uL)	t_a (avr) [s] (300uL)	t_{a+std} [s] (100uL)	t_{a+std} [s] (300uL)	c_a [g·L ⁻¹] (100uL)	c_a [g·L ⁻¹] (300uL)	c_a [mg·L ⁻¹]
Oxalic acid	4.02	3.77	-	115.00	-	0.0070	7.00
Formic acid	23.00	20.13	52.95	93.75	0.0300	0.0273	28.67
2-hydroxyethanoic acid	12.77	11.48	39.25	96.45	0.0320	0.0230	27.48
2-hydroxypropanoic acid	17.08	15.39	48.88	85.15	0.0420	0.0436	42.79
Acetic acid	72.72	59.35	99.05	145.70	0.1205	0.0822	101.38

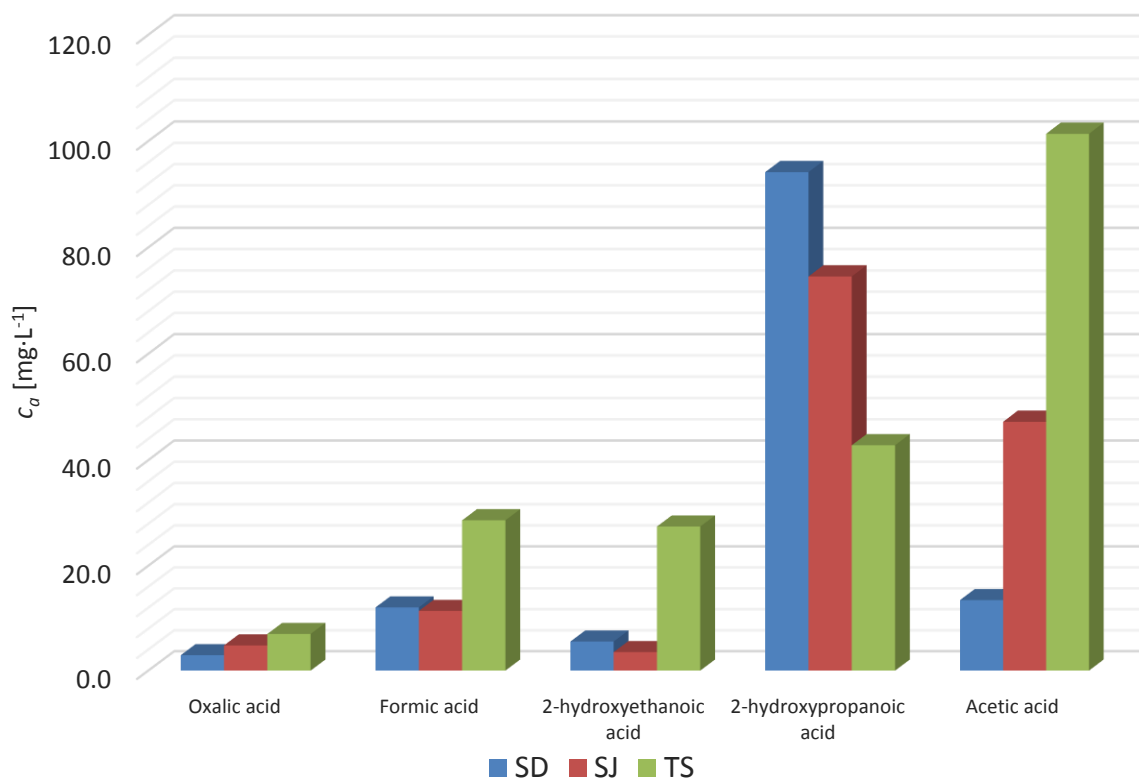


Fig. 6-18 Organic acid content - comparison of analysed samples

6.1.3 Inhibitor additives depletion and other degradation products

During the operation time of the heat transfer fluids based on propane-1,2-diol and ethane-1,2-diol in the thermal systems, many different chemical products are created. That is caused by organic nature and the number of possibilities how the glycols can react with themselves, other substances in the medium and with the materials of the system. On the search for a reason for the physical properties to be changed during the operation time, like it was discussed in case of density and viscosity of the samples from the experimental system in Vracov, a more basic approach was chosen. To fully analyse all of the products, a mass spectrometry analysis was conducted on most of the available samples. The analysis of available samples by mass spectroscopy uncovered several aspects, which are not discussed in the literature. The mass spectra were analysed by an open source program mMass²¹⁷⁻²¹⁹.

The data were acquired in both positive and negative modes for three different target m/z : 100 m/z , 500 m/z and 1000 m/z . In the positive mode most of the substances were found as an $[M+Na]^+$ adducts, as the most common contamination cation in MS is sodium²²⁰, and $[M+H]^+$ adducts. These adducts make the analytes to be found according to their molecular mass in the area of $m/z = M_r + 22.99$ in case of the sodium adducts and $m/z = M_r + 1.008$ in the case of protonated adducts. Several others adducts were also identified such as $[M+K]^+$, $[M+CH_3OH+H]^+$ or $[M+H_2O+H]^+$. Naturally, the signal intensity and therefore the abundance of these adducts was significantly reduced compared to the two abovementioned and they were used only to confirm the original ions. The overview of some common adducts is listed in Table 6-10 for both positive and negative modes.

inhibitor system. Because the used ionizing technique was ESI (electrospray), which is soft ionizing method, most of the analytes were found in their full molecular state and the problem was achieving sufficient intensity and variability of ionized adducts to positively and fully identify selected components.

The low intensity of the signal of some substances was solved by adding a small amount of acetic acid (as a proton source) to the prepared sample solutions. That was especially effective in case of sebacic acid, shown on Fig. 6-20, which is present in the *Solaren* in a relatively high concentration and can serve as a very good starting point. Especially because it can be easily found in both positive and negative mode. This could lead to a conclusion that other organic acids, which are created through the degradation process, can be detected better by additional source of H^+ . However, because the created organic acids have low molecular weight, the detection proved to be difficult with the used MS instrument, which is generally used for the region of 100-2000 Da. The overview of the searched organic acids is provided in Table 6-12. To positively confirm the substances from Table 6-11, search for other adducts and isotopic peak analysis was also performed. Furthermore, comparison to spectra without the addition of acetic acid was also tried as shown on Fig. 6-19. The acidification enhanced the intensity for several ions but at the same time some of them disappeared as the primary ionisation process was changed. Because this method was intended only as a screening, only known chemicals and high intensity peaks were studied. The number of additional detected ions was far beyond any reasonable analysis.

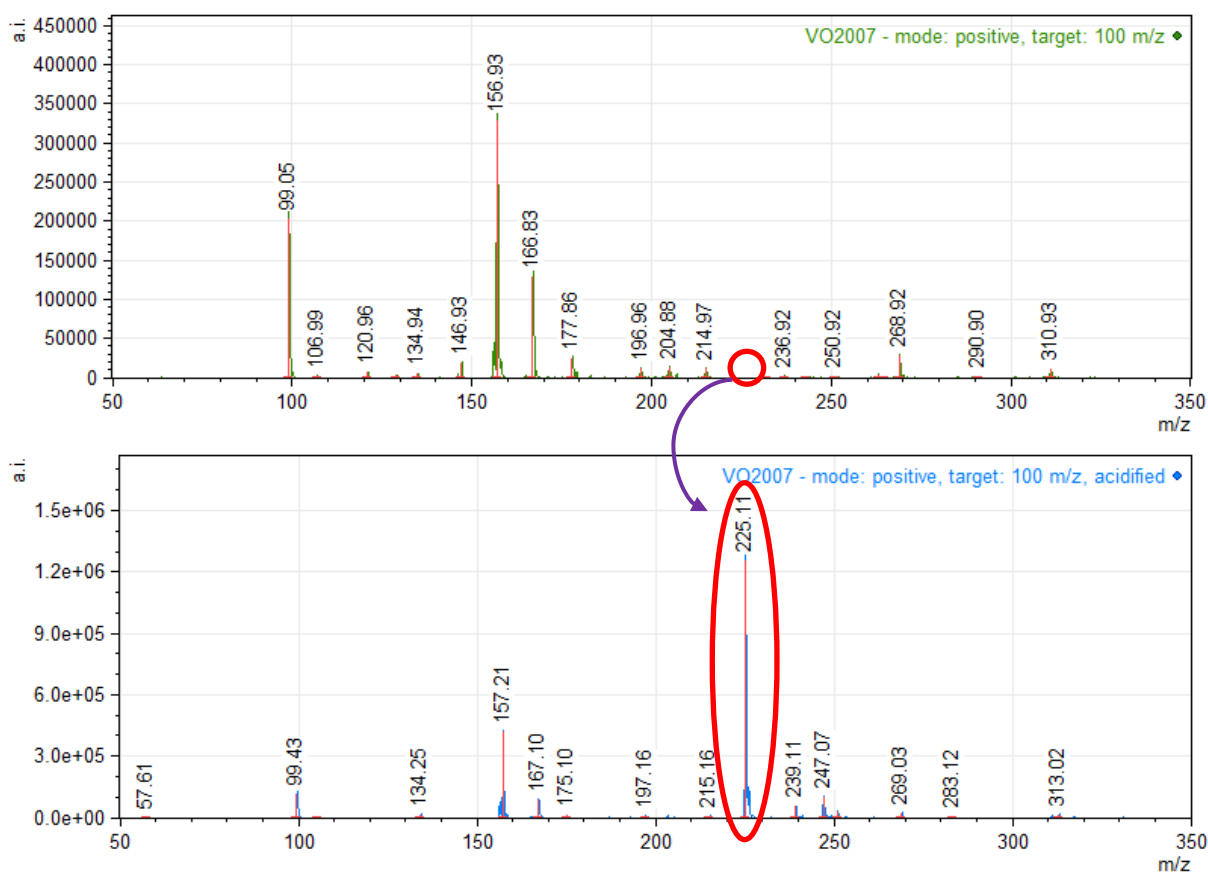
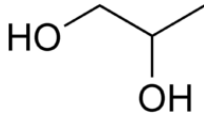
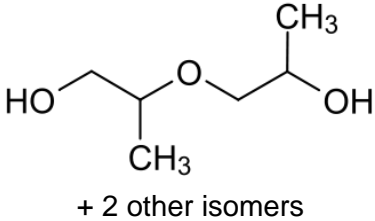
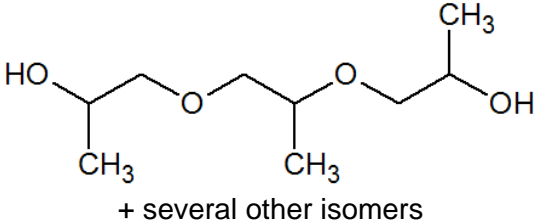
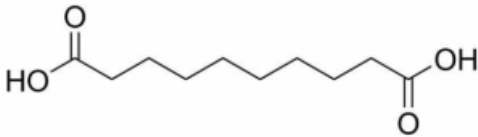
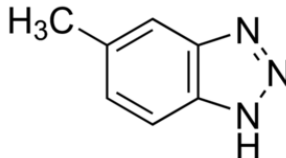
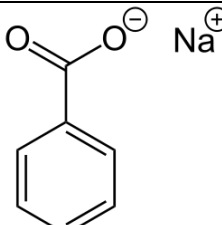


Fig. 6-20 Intensity enhancement of sebacic acid by acidifying – protonating

Table 6-11. Identified chemicals in the examined samples

Substance	CAS	Molecular weight	Structural formula
Propane-1,2-diol	57-55-6	76.1	
Dipropylene glycol	25265-71-8	134.17	
Tripropylen glycol	24800-44-0	192.252	
Sebacic acid	111-20-6	202.25	
Tolyltriazole	29385-43-1	159.19	
Sodium Benzoate	532-32-1	144.11	

It was already mentioned in the chapter 6.1.1 that the aging process is accompanied by physical changes of the fluid. Although, the main factor, freezing protection, is changed only a little, density and viscosity was changed much more visible. That is especially interesting finding, because this will greatly help to better assess failure potential (risk assessment) of some mechanical parts inside the system, such as the circulator pump. The main factor for the changes in the density and viscosity was so far deemed to be connected to creation of dipropylene or possibly tripropylene glycol, however, it is also possible that these substances are introduced to the system together with the original fluid, because the dipropylene and tripropylene glycol are secondary products in the process of propane-1,2-diol production⁵⁴ and their content is usually affected by the degree of the refining process (fractional distillation). The change in the intensity is then more connected to the pH of the sample and therefore to the chemical activity

of these substances. If that is the case, it is necessary to look also for other possible causes for these changes.

To effectively analyse the samples, identifying and eliminating some known substances was necessary as was explained before. After addition of acetic acid, the substances from Table 6-11 were found in the MS spectra in relatively high intensities.

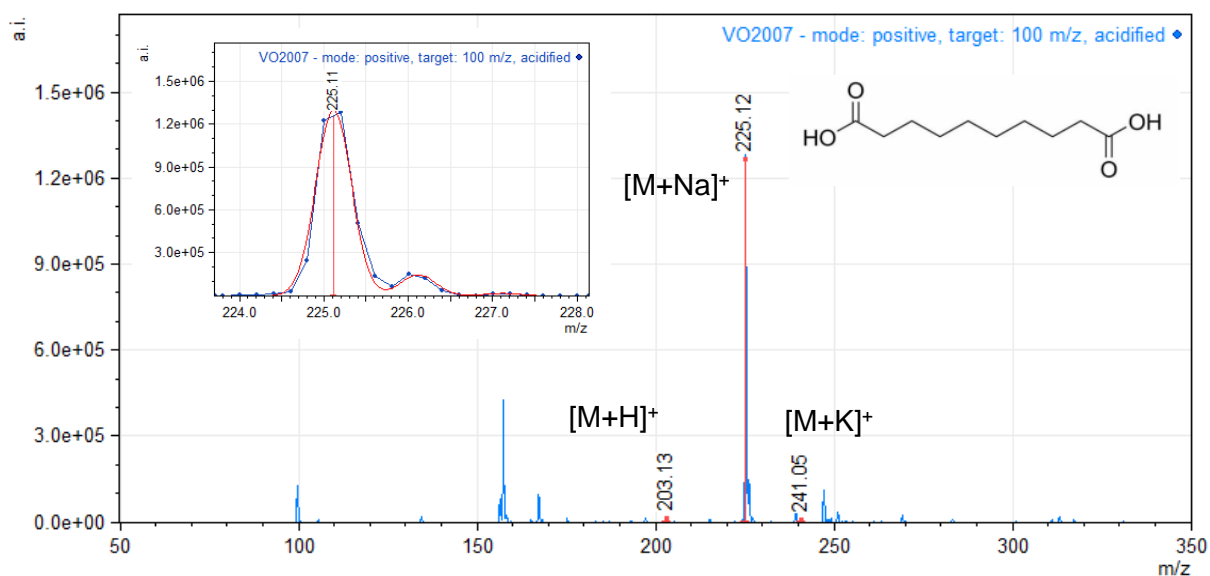


Fig. 6-21 Sebacic acid detection and isotopic distribution

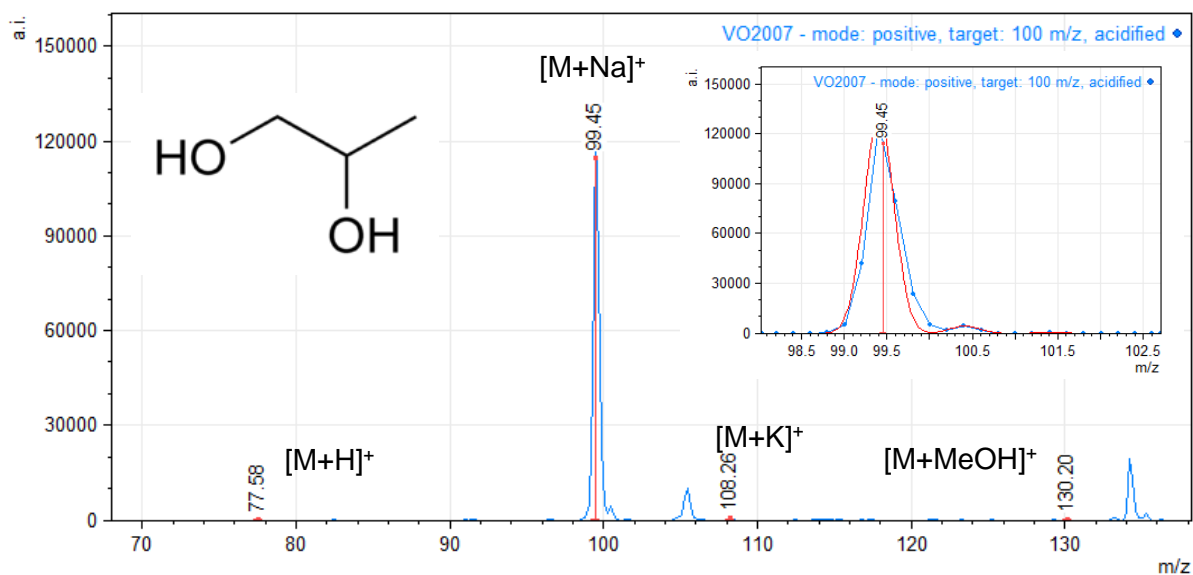


Fig. 6-22 Propane-1,2-diol detection and isotopic peak distribution

On the Fig. 6-21 detection of sebacic acid as the most intensive peak (basic peak) in the spectrum is shown. The isotopic distribution is in compliance with the calculated distribution (indicated by a red line on the sub-picture) and other adducts were also found. The sebacic acid was also found in the negative mode as deprotonated $[M-H]^-$. The additional adducts of the sebacic acid were also quite abundant, especially the sodium adducts and the subsequent sodium salts. The overview of additional adducts is provided in appendix A-6.

Interesting is also the rising intensity of the sebacic acid in the negative mode. The intensity is rising chronologically from VO2007 to V2013 in both acidified and not acidified samples. However, this is most likely caused by different pH of the samples and deprotonation rate rather than by actual rise in the concentration of the sebacic acid, which would be rather surprising.

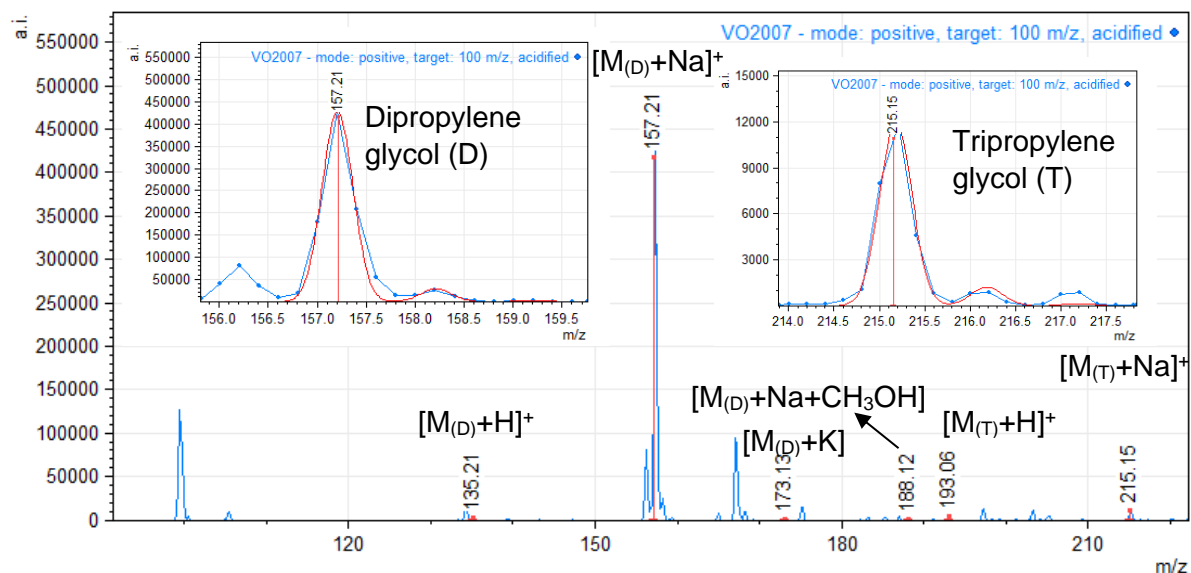


Fig. 6-23 Dipropylene and tripropylene glycol detection and isotopic distribution

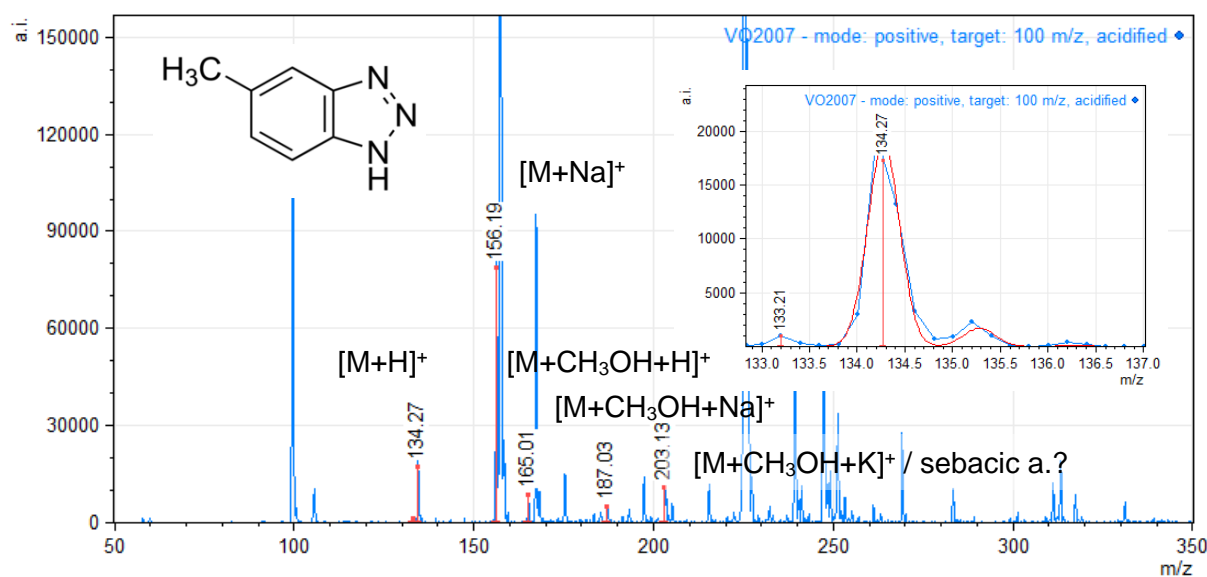


Fig. 6-24 Tolyltriazole detection and isotopic distribution

The propane-1,2-diol was identified with its dominant adduct $[M+Na]^+$ and additional adduct $[M+K]^+$. The protonated $[M+H]^+$ propane-1,2-diol was of very low intensity in every sample together with possible adduct $[M+MeOH+H]^+$. The identification of the propane-1,2-diol is shown on Fig. 6-22. What is important to note is a weight shift of about 0.4 Da of the $[M+Na]^+$ adduct of the propane-1,2-diol. That is caused by the instrument itself and can be observed on basically every ion with increasing tendency from right to left on the m/z axis.

Dipropylene glycol and tripropylene glycol isomers' identification is shown on Fig. 6-23. The intensity of dipropylene glycol is significantly bigger than of the propane-1,2-diol, and what more, the intensity is increasing as it was described before on Fig. 6-8. However, that itself does not prove anything as behind the change of the intensity could be other reasons, such as different pH or possible different concentration of the water, which will be explained later.

Another abundant substance was tolyltriazole which, similarly to sebacic acid, is part of the corrosion inhibitor additives. Tolyltriazole was found with many adduct as can be seen on the Fig. 6-24. In several cases the molecular weight was very similar to other chemicals and it was not possible to distinguish them apart.

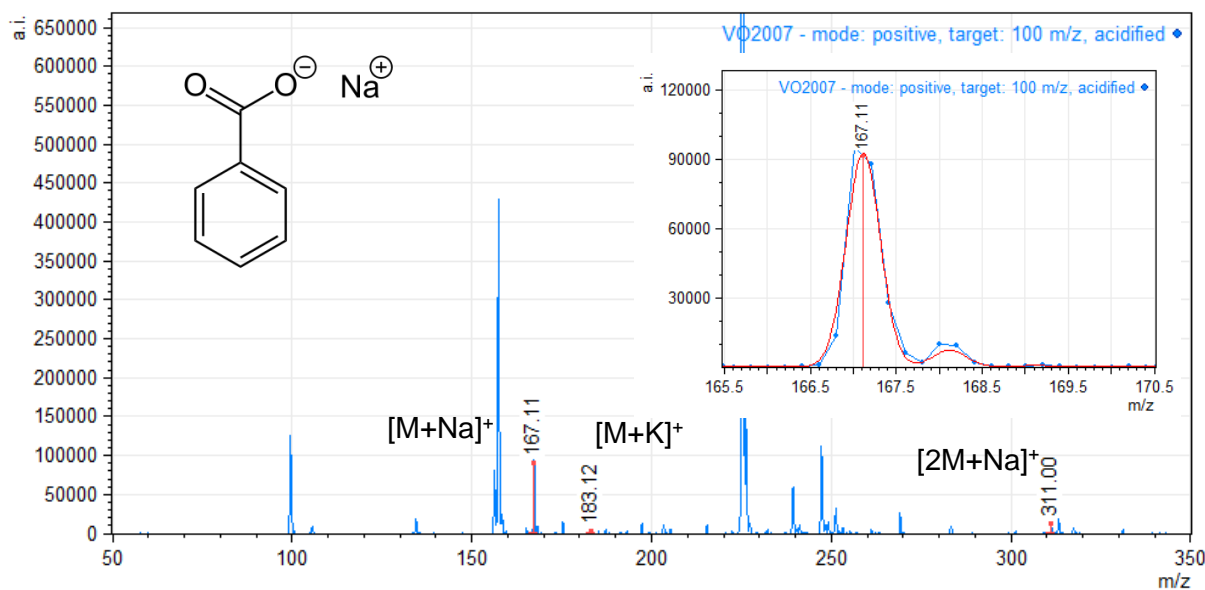


Fig. 6-25 Sodium benzoate detection and isotopic distribution

Positively identified was also sodium benzoate which is, again, added to the mixture as a corrosion inhibitor. Although the sodium benzoate is dissolved in water as an ion, it is found in the spectra in its original molecular form with sodium atom. The MS2 spectrum of the 167 m/z peak can be found in the appendix A-9. The functional part of the molecule is the carboxylic acid base. The sodium salt is used because the solubility of the original benzoic acid in water is very low ($S_{25^{\circ}C} = 3.4 \text{ g}\cdot\text{L}^{-1}$)³⁶ compare to its salt ($S = 556 \text{ g}\cdot\text{L}^{-1}$)²²².

The complete overview of the main components from Table 6-11 is then shown on Fig. 6-27. From the overview and from the detailed analysis available on appendix A-6 is apparent how much is the sebacic acid dominating the spectra. The relative intensity of the sebacic acid can serve as a good indicator of other substances, because the concentration of it seems to be stable, or not dropping, through the time as was explained in the chapter 6.1.1. The comparison of individual peak intensity is provided on Fig. 6-26. As can be seen, the intensity of the peaks does not follow any distinguishable trend and it is assumed that the amount of the corrosion inhibitors does not rapidly changes in the samples from experimental system in Vracov. Quite different situation can be seen on the example from the highly degraded samples SJ and SP which are also originally HTF *Solaren* (VO2007) on Fig. 6-29. In these samples the intensity of the main components significantly differs despite the same original concentration.

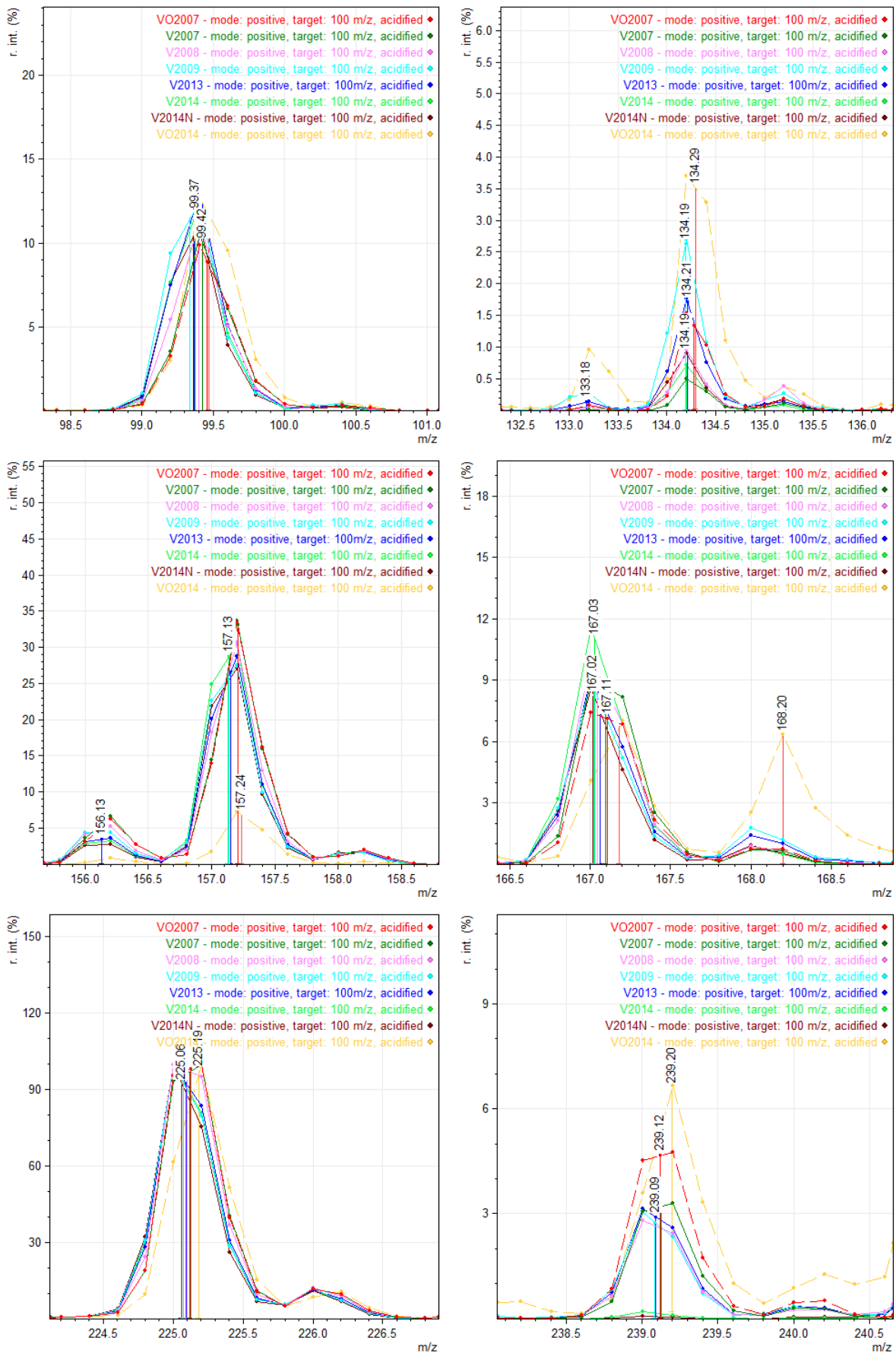


Fig. 6-26 Change of relative peak intensity on traced substances

(dipropylene glycol). The possible causes for such difference is addition of different mixture to the system, however the original inhibitor selection seems to be the same. The important factor stays at the dramatic depletion of sebacic acid and complete depletion of some other inhibitors. The variability of the additional peaks was too great to attempt identification.

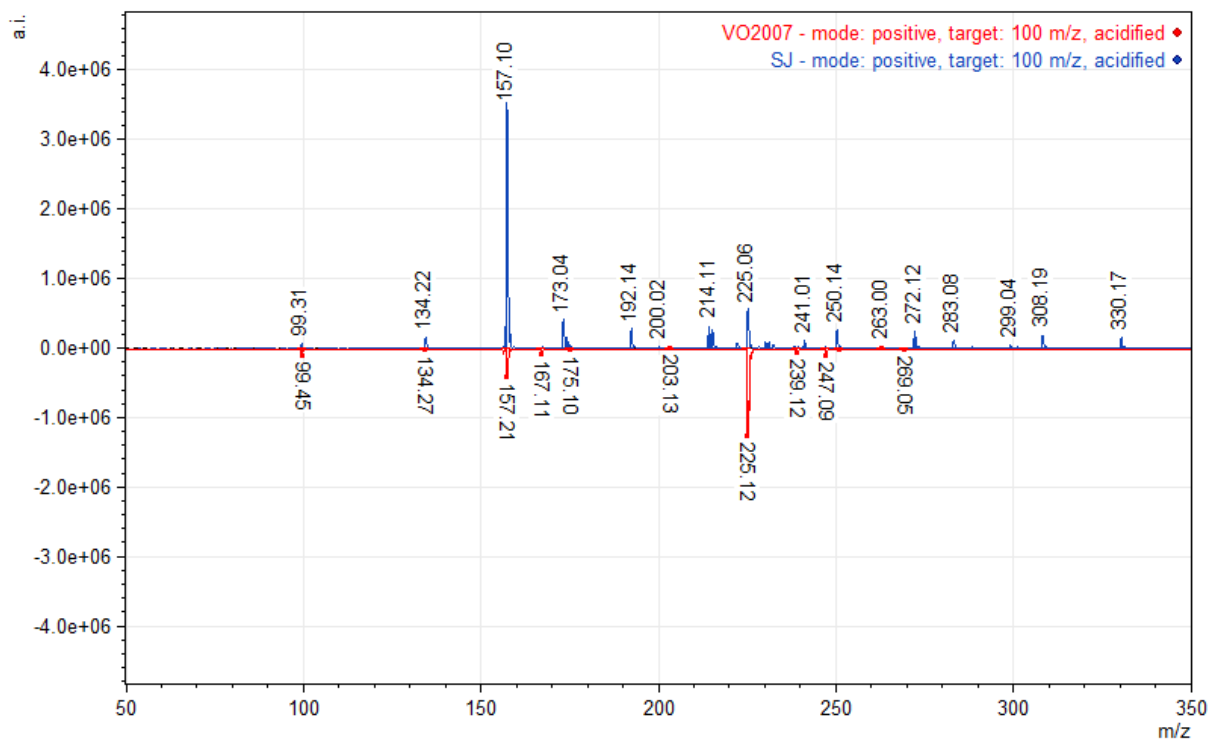
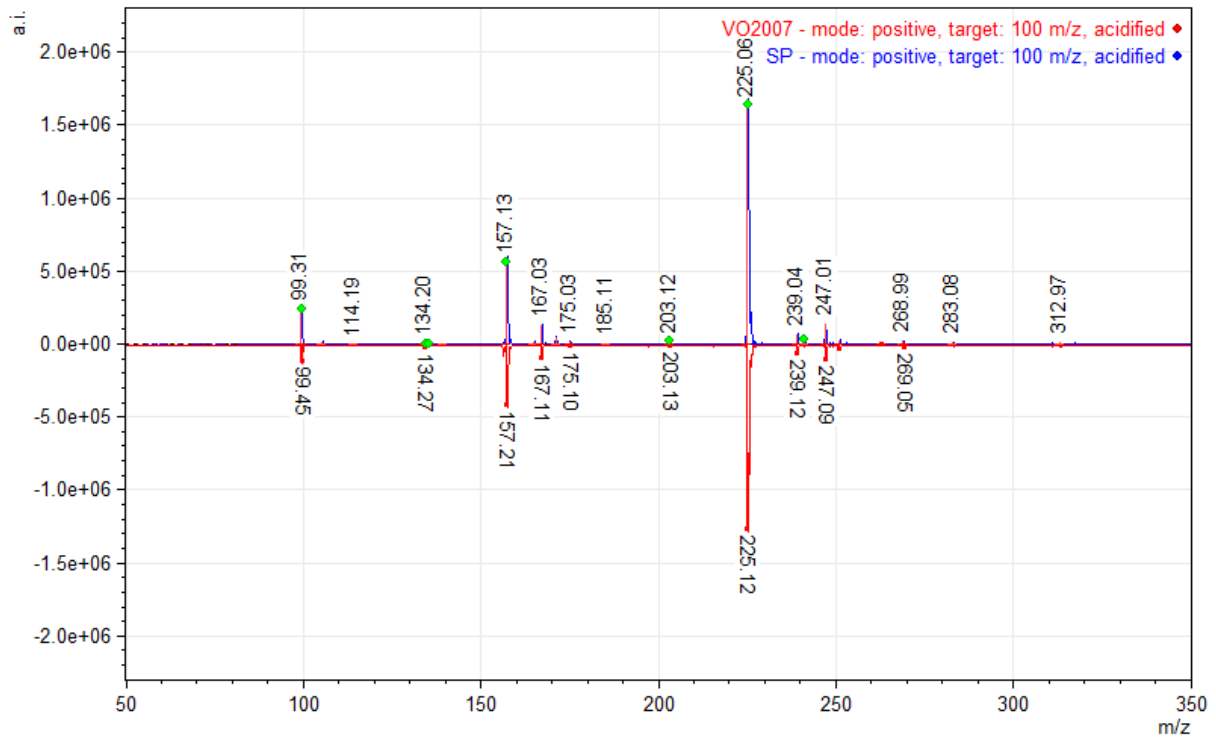


Fig. 6-29 Comparison of highly degraded fluids samples SP and SJ with original

In the internal documents of the DOW company²⁰⁹ another potential degradation products are also mentioned, which are formed in a small quantities. These degradation products belong to the group of acetals/ketals. The main degradation products from this group are shown on Fig. 6-30. Because these products are of a little significance, these degradation products are stated in this work just for completion.

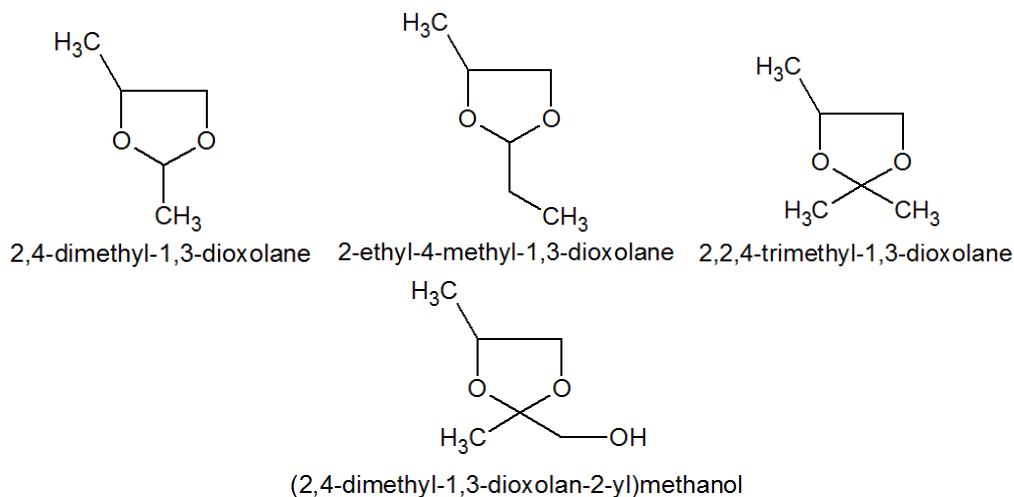


Fig. 6-30 Formation of additional acetal/ketal degradation products

The main problem with organic acid detection by the ion trap MS is their small molecular weight. Although the Agilent 6320 Series Ion Trap used in this work has a working range starting at 50 m/z, the region between 50 m/z and 100 m/z is on the edge of the instrument capabilities and it is difficult to predict its validity. The overview is therefore given only for confirmed acids. The analysis is provided on the sample TS on Fig. 6-31 which has the highest measured amounts of the organic acids (see isotachopheresis method above).

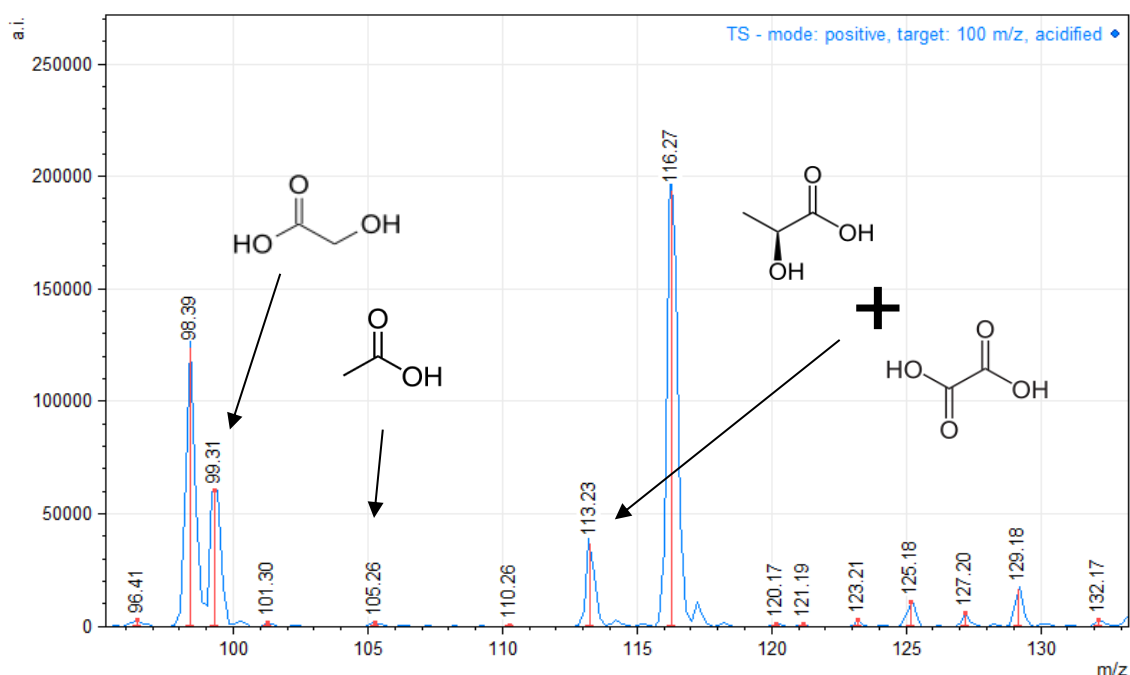
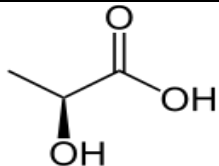
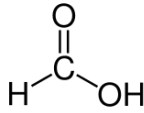
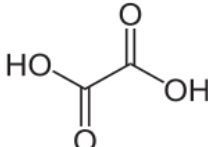
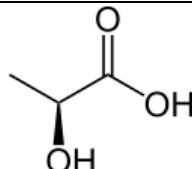
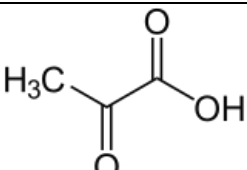
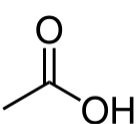


Fig. 6-31 Organic acid products identification on sample TS

Table 6-12. List of organic acid degradation products intended for MS look-up

Substance	Molecular weight	Structural formula
Oxalic acid	90.014	
Formic acid	46.025	
2-hydroxyethanoic acid (Glycolic acid)	76.051	
2-hydroxypropanoic acid (Lactic acid)	90.078	
2-Oxopropanoic acid (Pyruvic acid)	88.062	
Acetic acid	60.052	

6.1.4 Polymerization of propane-1,2-diol based mixtures?

During the measurement with the target of 500 m/z a curious pattern was observed in the middle region of the active range. As can be seen on the Fig. 6-32, the number of peaks of the fluid sampled from the system is incomparable richer than of the original filling. Upon further analysis of the “forest” of peaks was discovered a certain pattern which corresponds to a weight shift of 44 m/z (on Fig. 6-33), which could indicate a polyethylene glycol ($C_{2n}H_{4n+2}O_{n+1}$) row. However, the formation of polyethylene glycol from propane-1,2-diol is not likely to occur even under stagnation conditions. Furthermore, in case a progressing polymerisation a change of the pattern should be visible, however the change between the samples of chronological order from V2007 to V2014 was near to none as can be seen on Fig. 6-33.

The contamination of samples from the plastic containers was ruled out in the previous section, however, the option of contamination²²³ from the system is fully possible. What also support the contamination theory is different outcome for samples SJ and SP which were also tested on the presence of this pattern. The respective spectra are provided in appendix A-8. Similar situation was observed for another glycol-based fluid of sample TS, where no

distinguishable polymeric pattern was observed despite high degradation and high content of organic acids in the sample as was showed in the chapter 6.1.2.

In case of peak-rich spectra of the samples from experimental system in Vracov is actually available another theory explaining such outcome and it is copper complexes with the organic compounds, such as dipropylene glycol or sebacic acid. This theory is partially supported by the shape of some of the isotopic peaks. To positively identify the any copper complexes additional research would be necessary, although it is reasonable to expect them in some amount, even though that the visible peaks in the MS spectra are not made by them. Unfortunately, this option was not available during the creation of this work and it will be a subject of a continuing research.

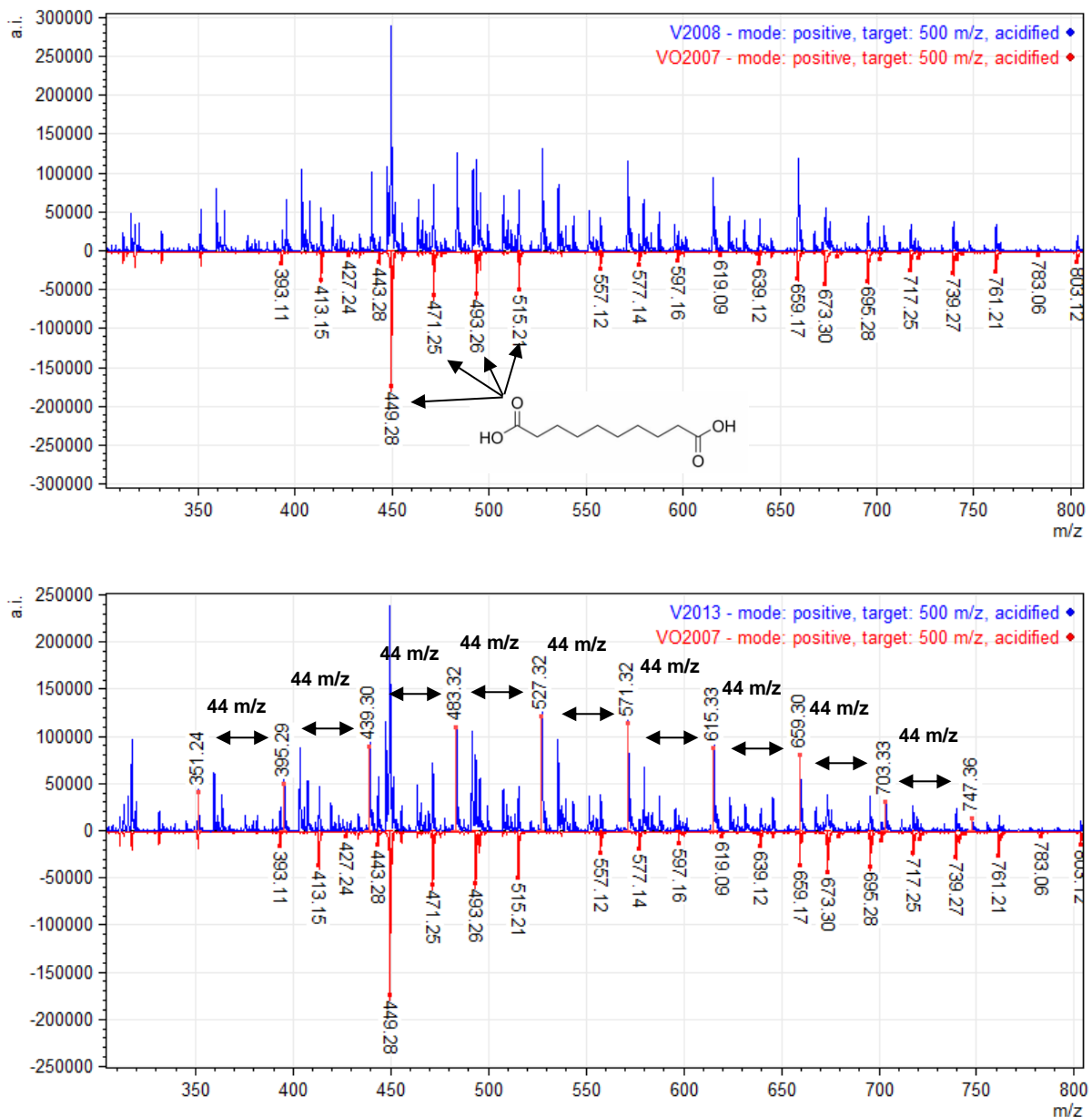


Fig. 6-32 Comparison of original fluid and after 1 and 7 years

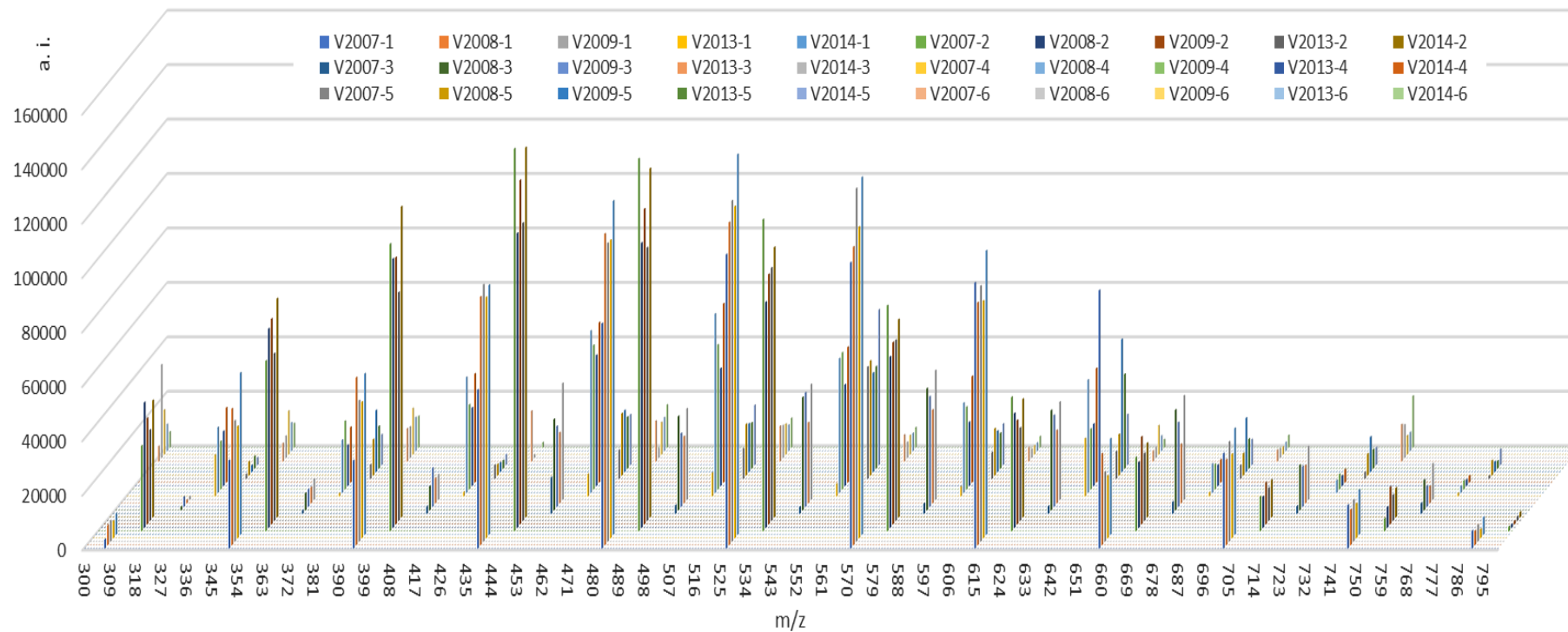


Fig. 6-33 Selected peak rows with identical difference of 44 Da

To further support the theory about the condensation type of polymerisation the Karl Fisher titration was attempted. The data and measurement conditions from the measurement together with the results are shown in Table 6-13 and are visualised on Fig. 6-34. During the process of condensation type of polymerisation (or the creation of dipropylene glycol), the water is released and theoretically the water content should be higher for more degraded/polymerised samples. However, as can be seen from the measured data, the results are exact opposite. The older samples V2007, V2008 and V2009 are showing the smallest amount of water, much smaller than the original mixture, where water should be less than 50 % (48 % of propane-1,2-diol and 3-4 % inhibitors and stabilizing chemicals). Because some higher numbers for newer samples were achieved in the same way, the method itself is presumably correct. The possible cause for this difference would be, with high probability, the manipulation with the samples over the years. As has been mentioned before, the samples were extensively used by several graduate students as well as by author of this thesis for different types of research. During that time, part of the water was probably evaporated which caused this discrepancy. This also means that the originally correct data on some of the physical properties such as density, viscosity and freezing point cannot be repeated with current samples and it would also explain some of the discrepancies in the data from the original measurements after sampling and subsequent measurements. In case of this work, the data were collected gradually and only the mass spectrometry and the Karl-Fisher titration were conducted of the whole range of samples at once after the sampling was completed. This did not have a significant effect on the results of MS analysis, but apparently rendered the Karl-Fisher titration nearly pointless as the only valid data can be considered samples V2014 and V2014N. The reason is that the samples V2014 and V2014N were acquired from the system on the same day and any manipulation was always conducted on both samples. From this point we can see that by adding new, unused fluid the water content dropped a little, which follows the original theory that the water content on the closed system is slowly growing and by adding new fluid this amount is diluted by more concentrated unused mixture.

Table 6-13. Karl Fisher titration results

Sample	V2007	V2008	V2009	V2013	V2014	V2014N
Water content n_1 [%]	44.733	41.9316	47.578	50.19	50.417	50.292
Sample weight m_1 [g]	0.0523	0.1198	0.1126	0.1652	0.1482	0.1366
Titration consumption V_1 [mL]	4.47	9.598	10.236	15.842	14.276	13.126
Titration time t_1 [s]	47.77	43.42	44.46	52.16	89.18	94.42
Water content n_2 [%]	44.546	42.4165	47.869	49.9959	50.503	50.249
Sample weight m_2 [g]	0.1154	0.115	0.0951	0.1095	0.1021	0.1373
Titration consumption V_2 [mL]	9.822	9.32	8.698	10.46	9.852	13.182
Titration time t_2 [s]	80.55	41.69	75.07	44.08	65.75	92.34
Water content n_3 [%]	44.608	42.2989	47.57	50.2445	50.154	50.1965
Sample weight m_3 [g]	0.1239	0.0855	0.1326	0.117	0.1069	0.1134
Titration consumption V_3 [mL]	10.56	6.91	12.052	11.232	10.244	10.876
Titration time t_3 [s]	77.25	64.16	79.14	89.55	80.75	79.95
Water content (avr.) n_a [%]	44.63	42.22	47.67	50.14	50.36	50.25

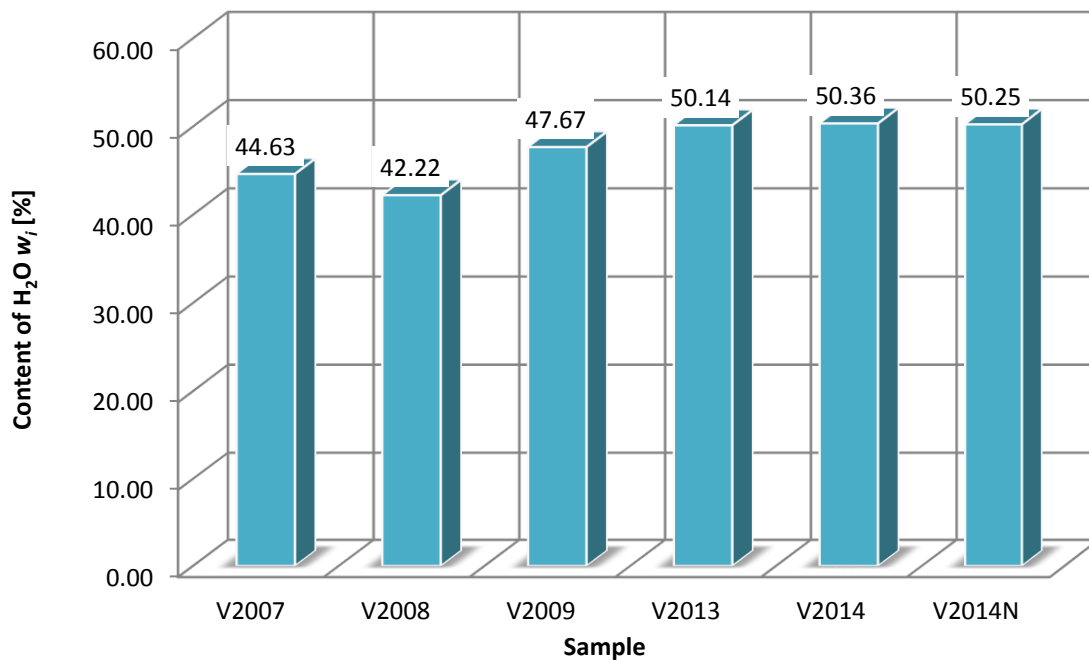


Fig. 6-34 Water content according to Karl Fisher titration

6.2 Aqueous propane-1,3-diol characteristics

Several researchers have already reported some of the physical and chemical data on the pure propane-1,3-diol. However, that applies mainly for pure substance. The data on propane-1,3-diol/water mixtures are severely limited, and they are often lacking necessary temperature range or precision for using as an antifreeze additive. So far, propane-1,3-diol has been reported to be used in several different binary mixtures with various chemicals. Properties of mixture with butane-1,4-diol was reported by Li et al.²²⁴. Densities, viscosities and refractive indices of polyethylene glycol with propane-1,3-diol and butyl lactate with propane-1,3-diol were measured by Bajić et al.^{225,226}, and properties for mixture of pyridine with propane-1,3-diol were provided by Kijevčanin et al.²²⁷. The first data on the propane-1,3-diol/water mixture were prepared by Lee et al.²²⁸ in 2000. The paper contained very basic data on densities, surface tensions and refractive indices in temperature range of 25 °C to 45 °C with only five different dilutions. Other results were published by various researchers focusing on different aspects of the propane-1,3-diol/water system. Density, speed of sound, relative permittivity and viscosity, were reported by George and Sastry²²⁹ together with other water/alkanediols systems. Molar enthalpies was measured by Nagamachi and Franczesconi⁷⁶ and data on heat capacities of some pure α,ω -alkanediols, including PDO, were measured by Góralski and Tkaczyk⁶⁹. The most up to date study of the propane-1,3-diol/water mixture was published by Moosavi and Rostami²³⁰ in 2017 focusing on density, viscosity, refractive index. It is safe to say that for most of the current application of propane-1,3-diol the available data are sufficient, however, for usage such as antifreeze or aircraft deicer it is not nearly enough. For that reason, the following basic data on propane-1,3-diol were prepared in collaboration with a company Classic Oil s.r.o. from Kladno in the Czech Republic. The original raw data were already published in the work of Skolil⁵³ in his thesis from 2016 and selected data were also published on an international conference in Fukuoka Japan²³¹. The following section brings a new and deep analysis of the acquired data and puts them into more profound perspective with literature and explains their physical and chemical meaning creating a basic mathematical apparatus for their description and ease of usage.

6.2.1 Density

The measured data on density of propane-1,3-diol are listed in Table 6-14 and presented on Fig. 6-35. The acquired data of pure PDO are in good agreement with available literature sources²²⁸⁻²³⁰ and the standard deviation does not exceed $\sigma = 0.002$ for the compared range of 20 °C to 65 °C. Broader range of temperatures (15 °C – 80 °C) of experimental data offers only work of Zorębski et al.⁷⁰.

The acquired data of densities of pure propane-1,3-diol were fitted to two different models to cover all temperatures in the range. Furthermore, an attempt to use this model for different dilutions were made as well. For the pressure dependence can be used the Tait equation²³² and its derivatives, however, for the dependence of density on temperature at constant pressure the empirical polynomial model is used in general. The polynomial model can be written as:

$$\rho = A + BT + CT^2 + DT^3 + ET^4, \quad (6.2.1)$$

where ρ is the density, T is the variable temperature and A, B, C, D and E are constants based on experimental data.

Table 6-14. Experimental values of density ρ [$\text{g}\cdot\text{cm}^{-3}$] for propane-1,3-diol

	T [°C]	-20	-15	-10	-5	0	10	20	30	40	50	60	70
	T [K]	253.15	258.15	263.15	268.15	273.15	283.15	293.15	303.15	313.15	323.15	333.15	343.15
w_i	x_i												
0.0000	0.0000					1.0008	1.0006	0.9993	0.9968	0.9932	0.9890	0.9844	0.9786
0.1113	0.0288					1.0097	1.0088	1.0067	1.0041	1.0004	0.9962	0.9911	0.9853
0.2226	0.0635				1.0221	1.0213	1.0192	1.0163	1.0129	1.0083	1.0035	0.9983	0.9924
0.3340	0.1061			1.0352	1.0339	1.0325	1.0292	1.0254	1.0211	1.0163	1.0108	1.0052	0.9993
0.4453	0.1597	1.0537	1.0518	1.0477	1.0457	1.0437	1.0393	1.0345	1.0295	1.0239	1.0181	1.0118	1.0053
0.5010	0.1920	1.0580	1.0559	1.0525	1.0503	1.0481	1.0433	1.0383	1.0330	1.0273	1.0213	1.0148	1.0084
0.6123	0.2721	1.0682	1.0658	1.0621	1.0595	1.0569	1.0514	1.0457	1.0399	1.0338	1.0274	1.0209	1.0141
0.7236	0.3826	1.0749	1.0722	1.0684	1.0656	1.0627	1.0568	1.0509	1.0448	1.0386	1.0321	1.0254	1.0185
0.8349	0.5449	1.0785	1.0755	1.0722	1.0693	1.0663	1.0602	1.0540	1.0478	1.0415	1.0350	1.0283	1.0215
0.9277	0.7523	1.0796	1.0765	1.0732	1.0701	1.0671	1.0610	1.0547	1.0485	1.0422	1.0358	1.0293	1.0226
1.0000	1.0000	1.0782	1.0754	1.0723	1.0690	1.0659	1.0598	1.0536	1.0474	1.0411	1.0348	1.0284	1.0219

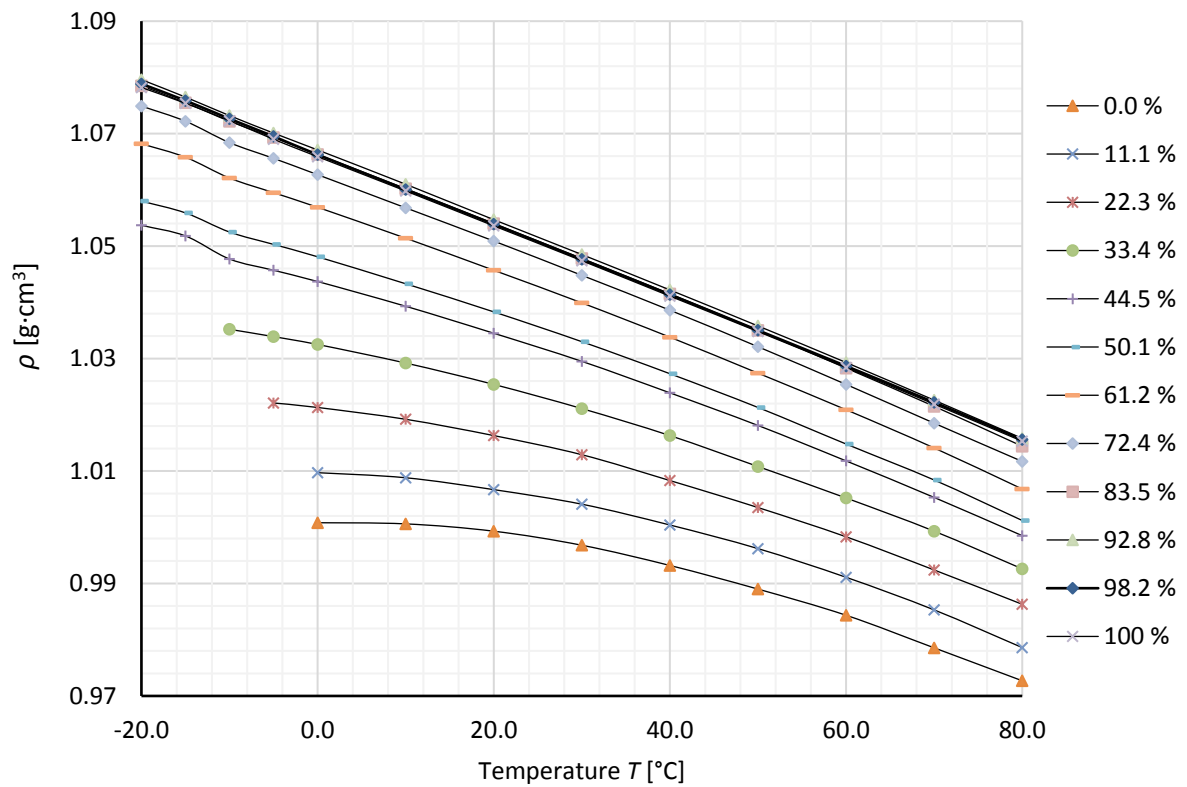
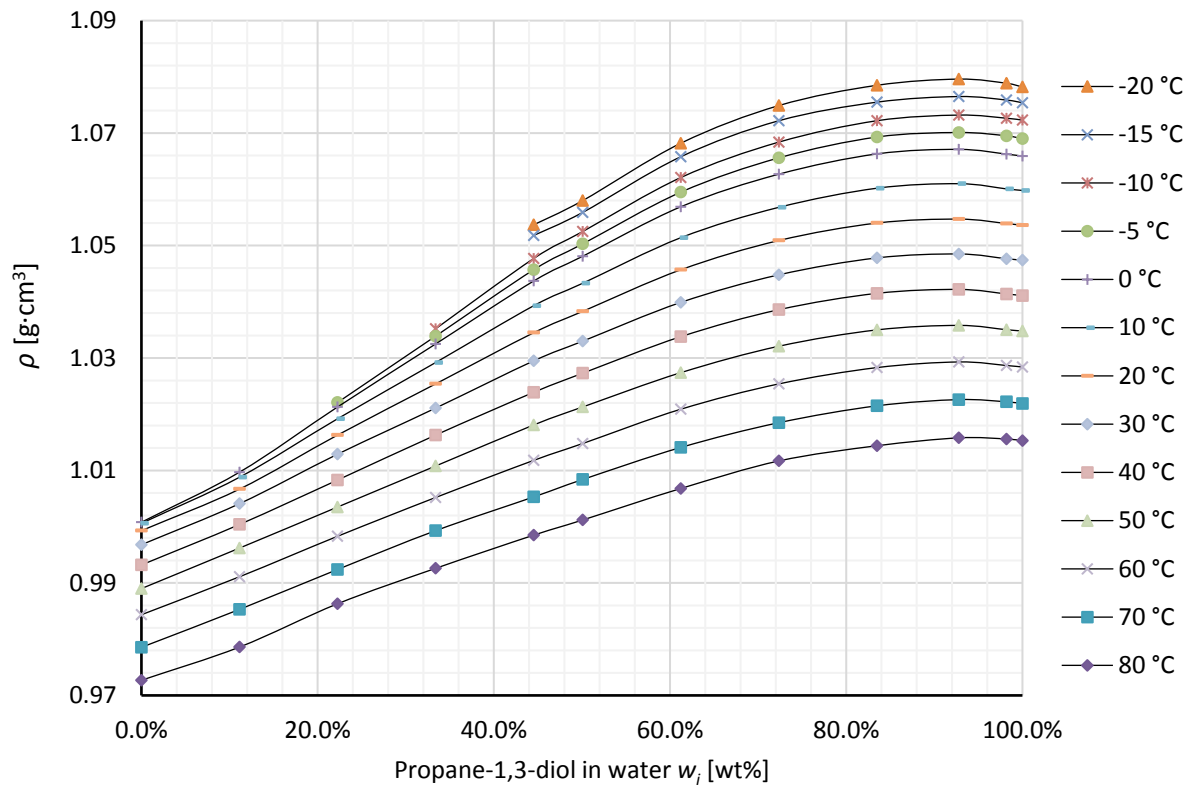


Fig. 6-35 Density of propane-1,3-diol on mass fraction (top) and temperature (bottom)

Another model is proposed by the DIPPR²³³ group and describes the dependence of density on temperature by four constants A , B , C and D as an exponential equation DIPPR-105:

$$\rho = \frac{A}{B^{1+(1-\frac{T}{c})^D}} \quad (6.2.2)$$

The constants of the equations (6.2.1) and (6.2.2) and the deviations for both models for pure propane-1,3-diol are listed in Table 6-15. The root mean-square deviations σ (RMSD) were calculated as:

$$\sigma = \left[\frac{\sum_{i=0}^n (y_{exp} - y_{cal})^2}{n} \right]^{\frac{1}{2}} \quad (6.2.3)$$

where y_{exp} represents the experimental values, y_{cal} states the calculated values and n is the dimension of the correlated set. The models are very precise within the measured range (deviation is less than $\sigma = 0.0002$), however, the polynomial model shows better agreement with the measured data as the variability of the model is naturally higher.

Table 6-15. Density models constants for pure propane-1,3-diol

	A	B	C	D	E	σ (RMSD)
Polynomial	1.02726	0.00227	$-1.513 \cdot 10^{-5}$	$3.537 \cdot 10^{-8}$	$-3.116 \cdot 10^{-11}$	$7.45 \cdot 10^{-5}$
DIPPR	363.87352	0.54489	697.42222	0.52552		$1.44 \cdot 10^{-4}$

To describe the influence of the water dilution on the density of PDO we used the method of excess molar volume. For that purpose, it was necessary to recalculate the mass fractions from the original data set to molar fractions. The excess molar volume for the propane-1,3-diol/water mixture described as V^E [$\text{cm}^3 \cdot \text{mol}^{-1}$] was calculated by the following equation:

$$V^E = \sum_{i=1}^n x_i M_i \left[\left(\frac{1}{\rho} \right) - \left(\frac{1}{\rho_i} \right) \right], \quad (6.2.4)$$

where x_i is the mole fraction, M_i is the molar weight and the ρ_i is the density of the pure substances. The density ρ without the index i then states the measured density at different mole fractions. The calculated excess molar volumes were then fitted to Redlich-Kister^{234,235} (R-K) equation (expansion) described as:

$$Y^E = x_i x_j \sum_{n=0}^k A_n (x_i - x_j)^n, \quad (6.2.5)$$

where the Y^E states for the specific excess property, x_i and x_j are representing the respective mole fractions of the components of the binary fluid and the A_k is used for expansion fitted parameters. The number of fitted parameters was chosen as $k = 4$, which means 5 fitted parameters together. The calculated parameters A_0 to A_4 and the calculated deviations according to Eq. (6.2.3) are listed in Table 6-17. The original values of excess molar volume are then shown in Table 6-16.

Table 6-16. Excess molar volumes V^E [$\text{cm}^3 \cdot \text{mol}^{-1}$] for aqueous propane-1,3-diol

T [°C]		0	10	20	30	40	50	60	70	80
w_i	x_i									
0	0	0	0	0	0	0	0	0	0	0
0.111	0.029	-0.040	-0.038	-0.032	-0.037	-0.041	-0.046	-0.041	-0.043	-0.027
0.223	0.064	-0.140	-0.126	-0.114	-0.112	-0.103	-0.101	-0.098	-0.100	-0.099
0.334	0.106	-0.249	-0.221	-0.199	-0.186	-0.179	-0.166	-0.158	-0.163	-0.150
0.445	0.160	-0.379	-0.337	-0.302	-0.281	-0.261	-0.245	-0.223	-0.215	-0.201
0.501	0.192	-0.424	-0.377	-0.343	-0.317	-0.298	-0.279	-0.253	-0.249	-0.223
0.612	0.272	-0.530	-0.477	-0.434	-0.403	-0.378	-0.351	-0.329	-0.314	-0.284
0.724	0.383	-0.565	-0.513	-0.475	-0.443	-0.422	-0.396	-0.369	-0.351	-0.339
0.835	0.545	-0.518	-0.475	-0.441	-0.415	-0.398	-0.376	-0.352	-0.336	-0.310
0.928	0.752	-0.337	-0.315	-0.291	-0.278	-0.269	-0.257	-0.247	-0.235	-0.222
0.982	0.928	-0.101	-0.089	-0.087	-0.079	-0.079	-0.073	-0.074	-0.077	-0.076
1	1	0	0	0	0	0	0	0	0	0

Table 6-17. Redlich-Kister fitting variables for excess molar volume

T [°C]	A_0	A_1	A_2	A_3	A_4	σ
0	-2.13815	-1.04474	-1.00299	0.66726	1.73058	0.008
10	-1.96135	-0.84526	-0.85436	0.47921	1.59933	0.006
20	-1.83147	-0.79354	-0.45801	0.53301	1.04601	0.006
30	-1.71824	-0.62566	-0.49776	0.30613	1.05976	0.004
40	-1.64783	-0.53979	-0.35839	0.26038	0.80534	0.002
50	-1.55728	-0.43815	-0.27570	0.11339	0.65961	0.001
60	-1.46133	-0.36979	-0.21233	0.12763	0.46425	0.003
70	-1.39219	-0.35020	-0.15933	0.08362	0.17932	0.003
80	-1.30987	-0.33974	-0.03945	0.19667	-0.01046	0.007

The aqueous propane-1,3-diol shows the highest excess molar volumes naturally at lower temperatures. The actual minimum is changing with temperature around $x_i \sim 0.4$ ($w_i = 0.7 \sim 0.8$) uncovering the propane-1,3-diol as the main driving force for the change. The shift in the excess molar volume is mainly caused by the fact that the density is in practice higher than of the pure substances, reaching its minimum around equimolar quantity, as can be seen on Fig. 6-35. This behaviour is caused by the hydroxyl-water interaction and it is typical for some α, ω -alkanediols

such as propane-1,3-diol and butane-1,4-diol. This unique property has been demonstrated and explained in the works of Nagamachi and Francesconi⁷⁶ and Takahashi and Nishi²³⁶. The terminal positions of the hydroxyl groups with only one connected methyl group gives the aqueous α,ω -alkanediols specific properties when the hydrophilic hydration governs over the hydrophobic hydration. Therefore, when introducing a small amount of water into the propane-1,3-diol, the water molecules primarily interact with the hydroxyl groups of the alcohol and subsequently influencing the interaction between the propane-1,3-diol molecules itself. The combination of few water molecules inside the propane-1,3-diol molecules fills up the space more efficiently and that leads to temporarily rise in the mixture's density. When the number of molecules become more equal, the hydrophobic hydration begins to influence the overall interaction patterns more, creating an aberration in the concentration region of $x_i = (0.5 \text{ to } 1.0)$ of the molar fraction which is $w_i = (0.8-1.0)$ of the mass fraction.

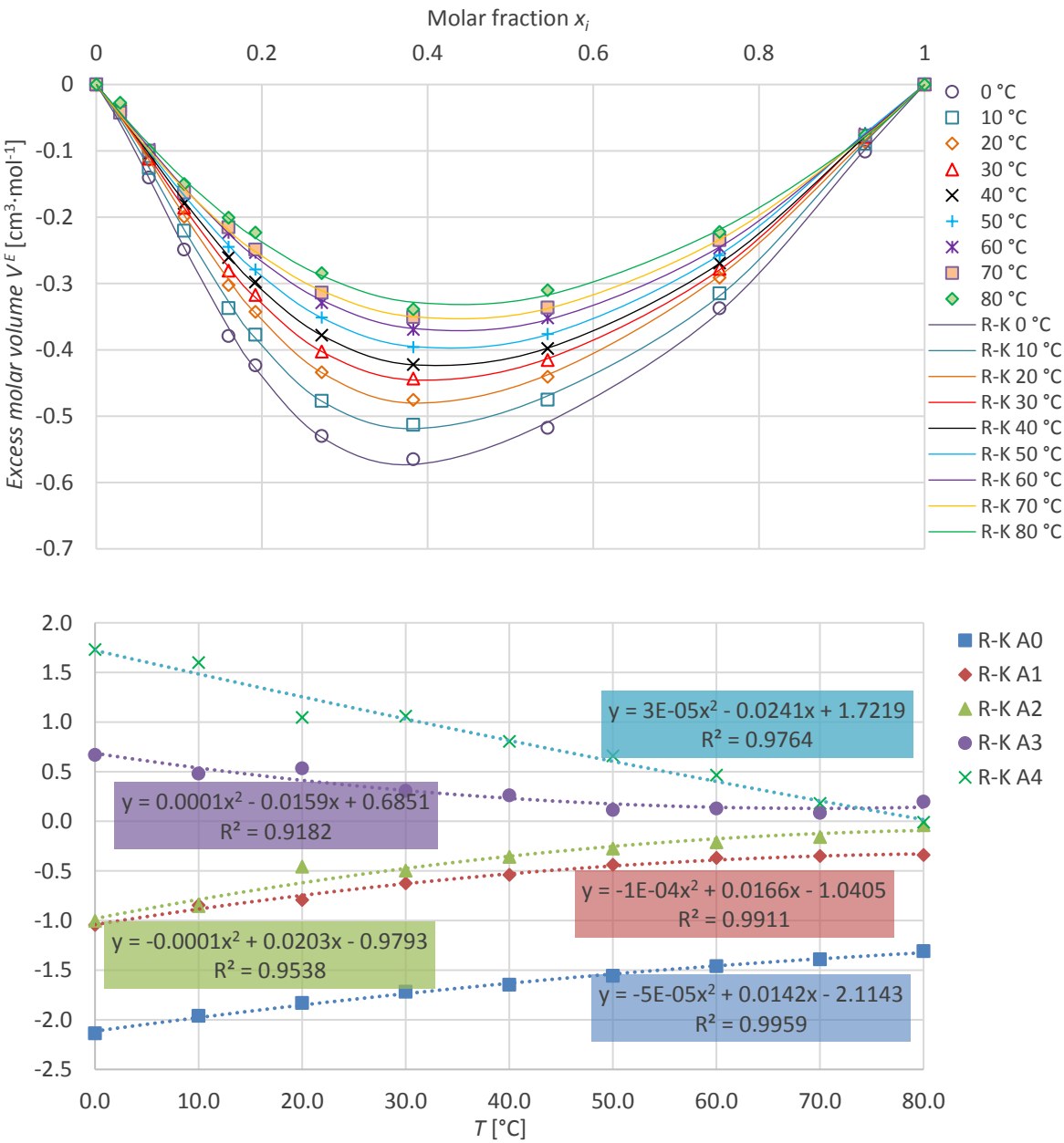


Fig. 6-36 Excess molar volume and R-K fitting (top), R-K parameters (bottom)

6.2.2 Viscosity

Table 6-18. Experimental values of dynamic viscosity η [mPa·s] for propane-1,3-diol

	T [°C]	-20	-15	-10	-5	0	10	20	30	40	50	60	70	80
	T [K]	253.15	258.15	263.15	268.15	273.15	283.15	293.15	303.15	313.15	323.15	333.15	343.15	353.15
w_i	x_i													
0.0000	0.0000					1.8253	1.3453	1.0407	0.8467	0.6997	0.5967	0.5091	0.4355	0.3911
0.1113	0.0288					2.8940	2.0548	1.5287	1.1893	0.9825	0.7887	0.6769	0.5651	0.4871
0.2226	0.0635				5.9079	4.6953	3.1650	2.2507	1.6894	1.3321	1.0758	0.8845	0.7245	0.6668
0.3340	0.1061			12.0210	9.2516	7.2567	4.7484	3.3182	2.4215	1.8575	1.4647	1.1940	0.9821	0.8548
0.4453	0.1597	40.1150	29.0240	19.9140	15.1190	11.7390	7.4508	5.0346	3.5854	2.6594	2.0513	1.6408	1.3015	1.0901
0.5010	0.1920	49.0864	35.2400	24.9700	18.8100	14.5170	9.0999	6.0744	4.3059	3.1485	2.4010	1.8845	1.5117	1.2104
0.6123	0.2721	85.8710	63.1490	44.1980	32.8160	24.8790	15.0980	9.7704	6.7242	4.7253	3.5225	2.6983	2.1229	1.7310
0.7236	0.3826	158.6700	110.6400	76.1810	55.7180	41.5780	24.5710	15.4800	10.3230	7.1844	5.2193	3.8996	3.0098	2.4228
0.8349	0.5449	267.8100	184.1800	132.2900	95.7500	70.7140	40.7640	24.9950	16.2570	11.0490	7.8010	5.7131	4.3029	3.3174
0.9277	0.7523	418.5600	293.3000	206.5300	149.2400	109.6900	62.3200	37.6040	24.0300	16.0440	11.1490	8.0231	5.9334	4.5146
1.0000	1.0000	574.3900	409.8800	289.5000	207.8800	152.7500	86.4830	52.0070	32.9210	21.7910	15.0000	10.7200	7.8549	5.9158

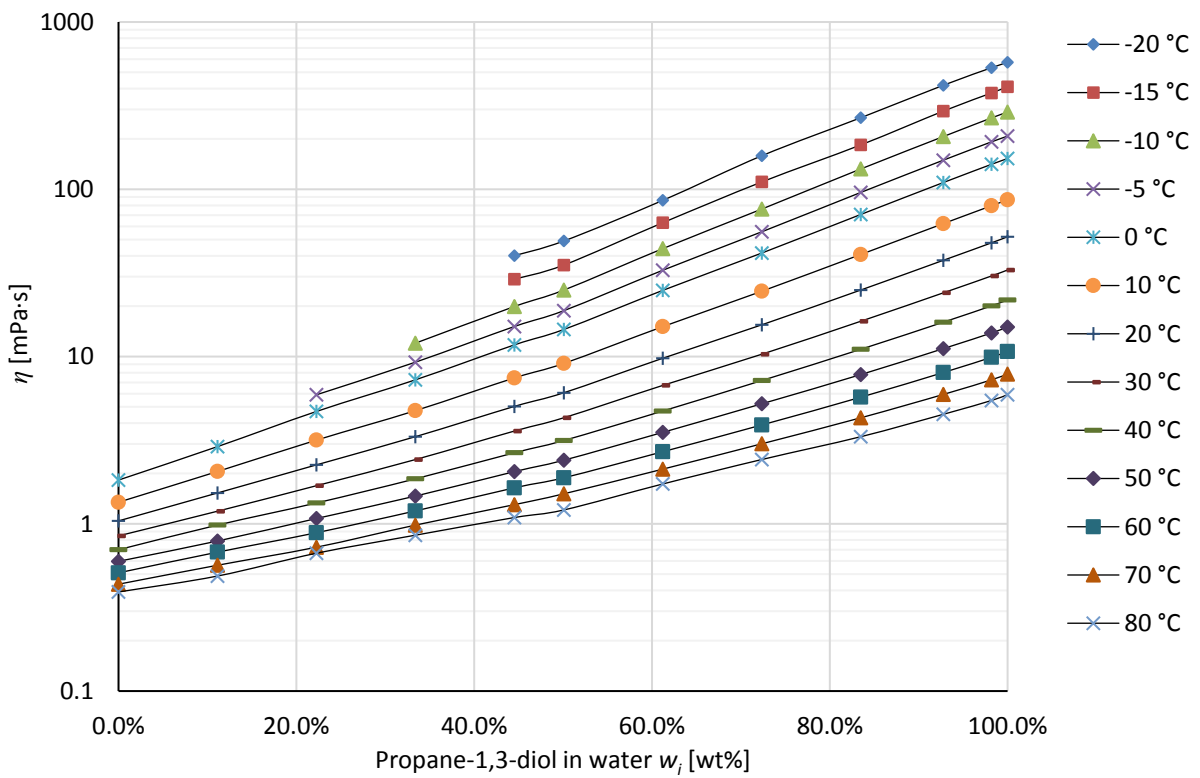
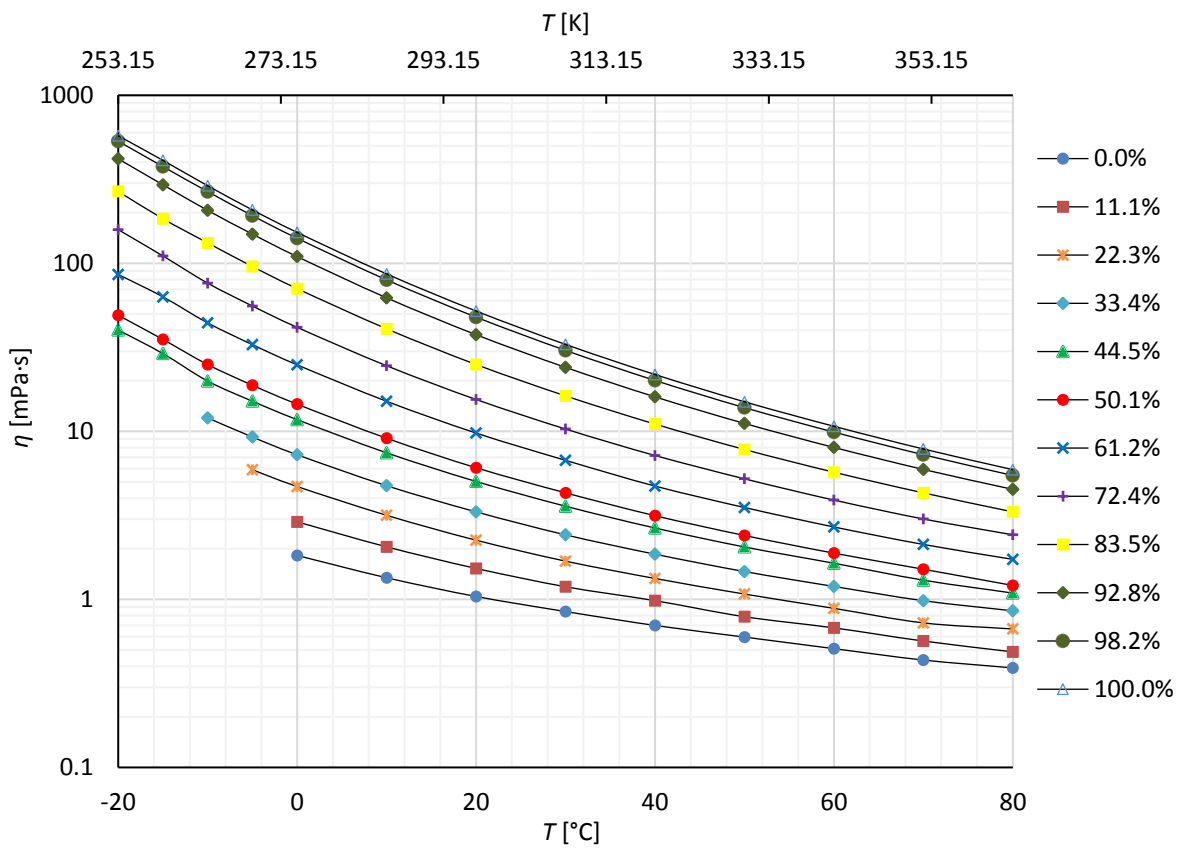


Fig. 6-37 Dynamic viscosity of propane-1,3-diol, temperature (top), w_i (bottom)

The experimental data on viscosity of aqueous propane-1,3-diol are summarized in Table 6-18 with the full graphical representation on Fig. 6-37. To easily compare the viscosity deviation of a real mixture against an ideal mixture and establish the dependence of the viscosity deviation is defined as follows:

$$\Delta\eta = \eta_{12} - (x_1\eta_1 + x_2\eta_2). \quad (6.2.6)$$

In the Eq. (6.2.6) the viscosity deviation $\Delta\eta$ is defined as a difference between the experimental value of dynamic viscosity η_{12} and the linear behaviour of the ideal mixture, where η_1 and η_2 are the viscosities of the pure substances and x_1 and x_2 are their respective mole fractions.

Table 6-19. Dynamic viscosity deviations for propane-1,3-diol

	T [°C]	0	10	20	30	40	50	60	70	80
w_i	x_i									
0	0	0.0	0.0	0.0	0.0	0.0	0.0	0.0	0.0	0.0
0.111	0.029	-3.278	-1.743	-0.980	-0.581	-0.325	-0.223	-0.126	-0.084	-0.063
0.223	0.064	-6.714	-3.587	-2.026	-1.194	-0.707	-0.436	-0.273	-0.182	-0.075
0.334	0.106	-10.584	-5.631	-3.131	-1.829	-1.080	-0.660	-0.399	-0.241	-0.123
0.445	0.160	-14.189	-7.491	-4.145	-2.384	-1.409	-0.846	-0.499	-0.319	-0.183
0.501	0.192	-16.289	-8.594	-4.753	-2.700	-1.601	-0.961	-0.585	-0.348	-0.242
0.612	0.272	-18.017	-9.416	-5.140	-2.851	-1.714	-0.994	-0.589	-0.332	-0.164
0.724	0.383	-17.998	-9.352	-5.063	-2.797	-1.586	-0.889	-0.517	-0.265	-0.082
0.835	0.545	-13.355	-6.976	-3.819	-2.068	-1.144	-0.644	-0.360	-0.176	-0.084
0.928	0.752	-5.682	-3.078	-1.781	-0.947	-0.523	-0.284	-0.168	-0.084	-0.033
0.982	0.928	-0.900	-0.647	-0.489	-0.289	-0.182	-0.125	-0.088	-0.061	-0.056
1	1	0.0	0.0	0.0	0.0	0.0	0.0	0.0	0.0	0.0

The viscosity deviation then can be fitted, similarly to the density, by Redlich-Kister equation (6.2.5). The fitted coefficients of Redlich-Kister equation are listed in Table 6-20. and the comparison against the experimental data is shown on Fig. 6-38. Like in the case of density, the viscosity deviation minimum is shifted towards the propane-1,3-diol. It is important to note that the Redlich-Kister approximation is possible only for temperatures where the pure substances stay in their liquid form. That means, regardless the experimental data of the mixtures expand to -20 °C, the calculation is limited by the freezing point of water to 0 °C.

The dependency of aqueous propane-1,3-diol on temperature, molar and mass fraction is not linear, which is a typical property of aqueous alcohols and diols²³⁷. To describe these dependencies several models are mentioned in literature by various authors. These models are based on theoretical background or empirical findings. Many of these models are based on the ideal mixture calculation originating from Arrhenius equation:

$$\ln \eta_{12} = x_1 \ln \eta_1 + x_2 \ln \eta_2, \quad (6.2.7)$$

where η_{12} is the overall dynamic viscosity and x_1 , x_2 and, η_1 , η_2 are the mole fractions and dynamic viscosities of the pure substances respectively. To get a good agreement with the experimental data several different modifications have been tested.

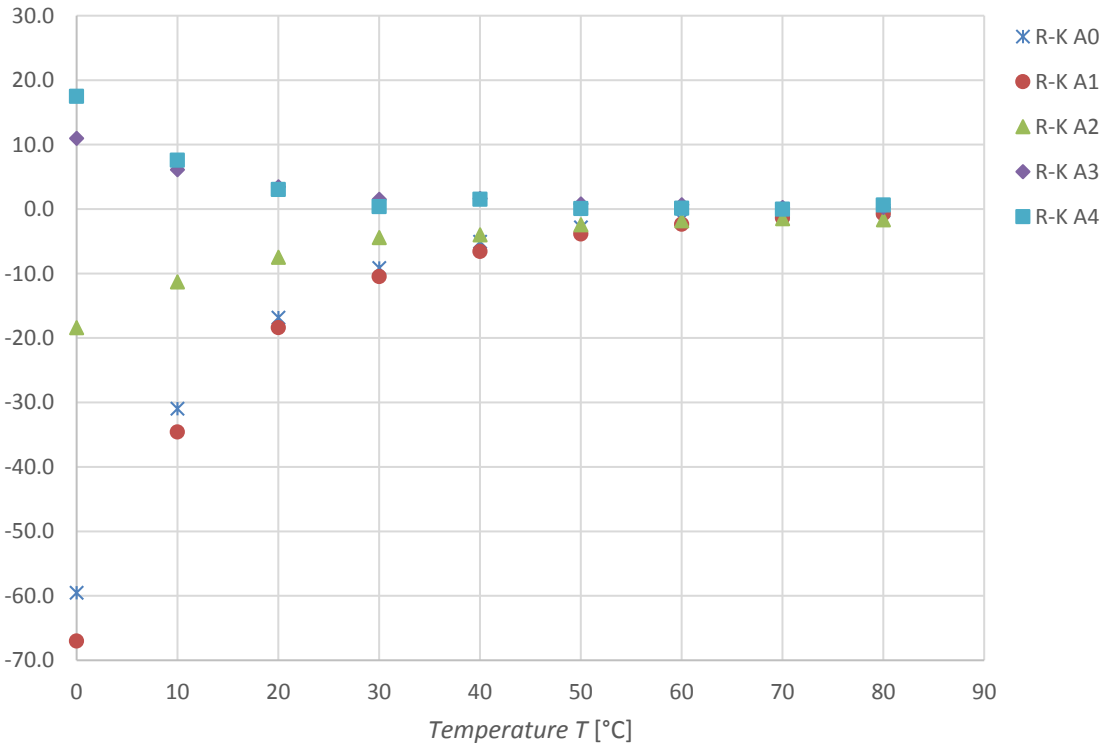
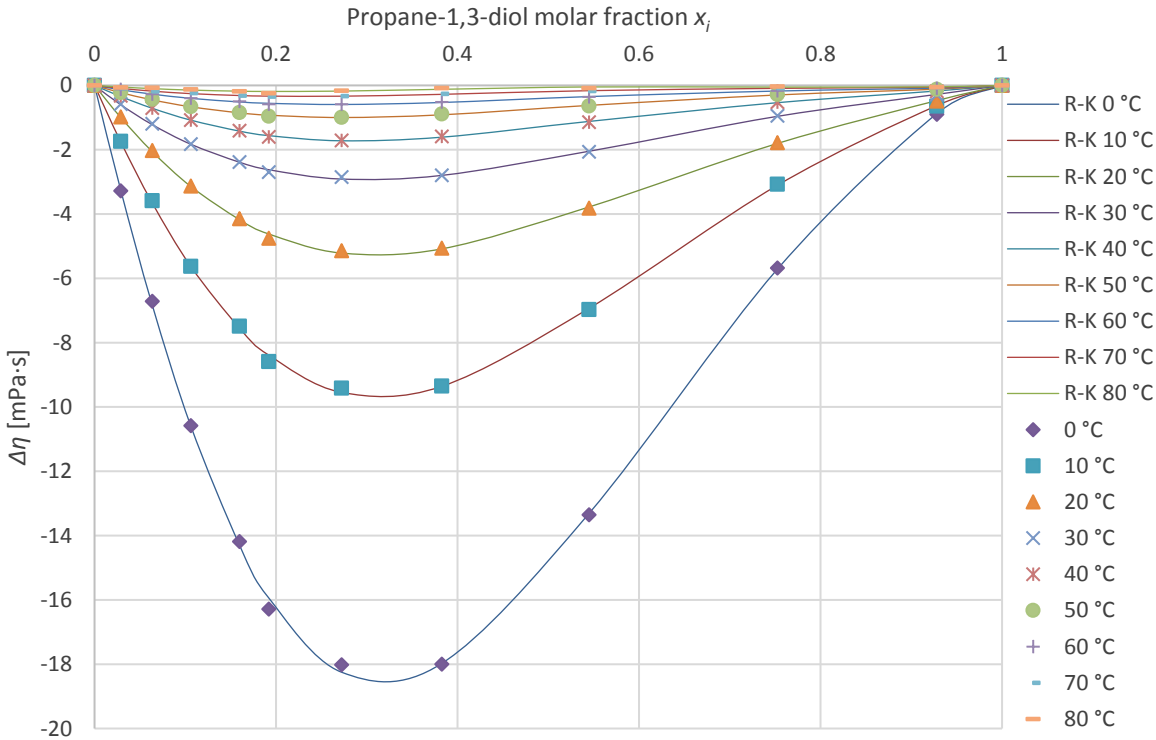


Fig. 6-38 Dynamic viscosity deviation and R-K fitting (top), R-K parameters (bottom)

Table 6-20. Redlich-Kister coefficients for dynamic viscosity deviation

T [°C]	A ₀	A ₁	A ₂	A ₃	A ₄	σ
0	-59.5404	-67.0263	-18.4234	10.9521	17.4700	0.135
10	-30.9695	-34.6122	-11.3212	6.1082	7.5684	0.079
20	-16.8351	-18.4173	-7.4799	3.4410	3.0276	0.051
30	-9.1614	-10.4895	-4.4198	1.5100	0.3515	0.032
40	-5.0749	-6.5922	-4.0212	1.6265	1.4938	0.018
50	-2.8345	-3.8867	-2.4569	0.7721	0.0739	0.016
60	-1.5987	-2.3796	-1.8282	0.6638	0.1173	0.012
70	-0.7713	-1.3829	-1.5010	0.2328	-0.0317	0.009
80	-0.2484	-0.7505	-1.6743	0.2269	0.6008	0.027

Basic and simple modification of the linear Arrhenius model, with significant improvement of the precision, brings Grunberg-Nissan^{238,239} model. The Grunberg-Nissan model introduces the fitting interaction parameter g_{12} to the original Eq. (6.2.7). The interaction fitting parameter g_{12} of the binary mixture is proportional to the interchange energy, therefore, it is proportional to the temperature. The basic form of Grunberg-Nissan (G-N1) equation is written as:

$$\ln \eta_{12} = x_1 \ln \eta_1 + x_2 \ln \eta_2 + g_{12} x_1 x_2. \quad (6.2.8)$$

The Eq. (6.2.8) can be also written in an empirical form, which is further enhancing the precision of the model:

$$\ln \eta_{12} = x_1 \ln \eta_1 + x_2 \ln \eta_2 + \sum_{i=0}^n x_1 x_2 g_i (x_1 - x_2)^i. \quad (6.2.9)$$

In the above Eq. (6.2.9) the interaction parameter g_{12} from the Eq. (6.2.8) (G-N1) than becomes part of a geometric sequence. The introduction of more fitting parameters leads to higher precision of the model, however, calculation becomes more complex, and moreover, the dependence on temperature is significantly decreased. Therefore, the modelling of the dynamic viscosity for different temperatures will turn unreliable. To retain the good dependency on temperature, the maximum number of fitting parameters was selected as $n = 2$, leading to a total number of 3 fitting constants.

Another form of the Eq. (6.2.7) was proposed by Lederer^{240,241}:

$$\ln \eta_{12} = \left(\frac{x_1}{x_1 + x_2 s} \right) \ln \eta_1 + \left(\frac{x_2 s}{x_1 + x_2 s} \right) \ln \eta_2. \quad (6.2.10)$$

Lederer's equation emphasizes the significance of mixing two components with substantially different viscosities²⁴². The more viscous propane-1,3-diol is represented in the Eq. (6.2.10) by its molar (or mass) fraction x_2 . The interaction adjusted by a single empirical constant s , which can be correlated to temperature.

Similar approach to the Grunberg-Nissan was presented in the work of Heric and Brewer²⁴³, often referred only as Heric model or Heric equation. The Heric model expands the original Arrhenius equation by following the Eyring theory^{244,245} of ideal mixture with zero excess of

activation Gibbs free energy ($\Delta G^{*E} = 0$). The model works with molar weights of the mixed liquids M_1 and M_2 and the resulting equation is devised for kinematic viscosity ν_{12} written as a logarithm:

$$\ln \nu_{12} = x_1 \ln(\nu_1 M_1) + x_2 \ln(\nu_2 M_2) - \ln(x_1 M_1 + x_2 M_2) + \left(\sum_{i=0}^n \alpha_i x_1 x_2 (x_1 - x_2)^i \right), \quad (6.2.11)$$

where x_i , ν_i and M_i represent the mole fraction, kinematic viscosity and molar weight of the individual component. The number of power series parameter α_i can vary for different mixtures, although, the literature appearance is commonly stated as $n = 1$ leading to two fitting parameters (also this work).

Similarly to the Heric model, McAllister's²⁴⁶ model also builds on Eyring's theory of absolute rates. The McAllister's describes the binary mixtures by three-body interaction²⁴⁶ involving two different molecules and it is also designed for kinematic viscosity ν_{12} . The model is usually written in its condensed logarithmic form as:

$$\ln \nu_{12} = x_1^3 \ln \nu_1 + 3x_1^2 x_2 \ln \nu_{f1} + 3x_1 x_2^2 \ln \nu_{f2} + x_2^3 \ln \nu_2 - \ln(x_1 + x_2 M_2/M_1) + 3x_1^2 x_2 \ln[(2 + M_2/M_1)/3] + 3x_1 x_2^2 \ln[(1 + 2M_2/M_1)/3] + x_2^3 \ln(M_2/M_1). \quad (6.2.12)$$

Though different in shape, the parameters and variables of the McAllister's equation (6.2.12) are practically identical to the Heric's equation (6.2.11) except for the fitting parameters ν_{f1} and ν_{f2} . These newly introduced parameters can be calculated from the activation entropy and enthalpy energies of the mixing liquids or, like in this case, as an empirical fitting parameter. Both of these methods are further explained in the original work of McAllister²⁴⁶.

The respective fitting parameters of the presented models are summarized in the Table 6-21 and Table 6-22. The percentage models' deviations were calculated according to Eq. (6.2.13). In that equation, η_{exp} is the measured viscosity and η_{cal} is the modelled viscosity. To compensate for the number of fitting parameters, the number of points in the n series is deducted by the number of fitting parameters k for respective model.

$$\sigma(\%) = \sqrt{\frac{1}{n-k} \sum \left(\frac{100(\eta_{exp} - \eta_{cal})}{\eta_{exp}} \right)^2}. \quad (6.2.13)$$

To fit the models to the experimental data a non-linear optimization method in form of generalized reduced gradient algorithm was used. Calculations were repeated several times with different starting values to ensure optimal and true results. However, because the considered models were based on the viscosity of pure components the results are limited to the range of 0 °C to 80 °C.

In general, the models are primarily used for mole fractions, however, based on their empirical validity it is possible to use them for mass fraction modelling, too. When fitting the parameters of aqueous PDO according to mass fraction dependency, a better fitting is usually achieved through the whole data set. As a good example serves the Grunberg-Nissan equation.

The cumulative deviation $\bar{\sigma}$ for molar fraction for G-N1 is $\bar{\sigma} = 17.28 \%$ while for the mass fraction is $\bar{\sigma} = 1.44 \%$. Similar comparison can be seen for other models, too. Exception is the Lederer's model. The model is constructed in a way when the fitting parameter s is directly dependent on the mole or mass fraction and it is therefore mathematically equivalent. Interesting output offer also the McAllister's and Heric's models. As has been proven by Iglesias-Silva²⁴⁷ in case of binary mixtures the McAllister's model and the Heric's model are mathematically equivalent and they should produce identical deviations after fitting, which was also achieved in this work.

Basic shortcoming of the viscosity models is the necessity for large amount of experimental data as the purely theoretical concepts for polar fluids usually lacks some accuracy and are also limited by the measurable temperature range of the pure substances. However, by acquiring sufficiently large set of data sample some of these models can be extended over the whole mole or mass fraction region. That is mainly thanks to the direct dependency of the fitting parameters on temperature. To produce such dependency, above stated models were all used for that purpose with substantial success.

The fitting parameters can be expressed as a dependency on temperature by a standard second order polynomial equation in the form of:

$$y = y_0 + y_1T + y_2T^2, \quad (6.2.14)$$

where y represents the fitting parameter itself, y_0 , y_1 and y_2 are calculated parameters according to the polynomial fitting and T is the temperature. The polynomial regression was conducted on the basis of least squares and the parameters are summarised in Table 6-21 for molar fraction form and in Table 6-22 for mass fraction form of the models. The situation for goodness of fit of these parameters is exactly opposite than for the models. The fitting of the parameters itself is better for mole fractions form of the models than mass fractions.

Another approach was also chosen to further explore the possibilities of utilisation of acquired data. With prepared dependencies of the fitting parameters itself it has been attempted to combine these models with models for pure substances. The reason for that was to create a universal model which would be able to fully predict the viscosity in the selected region of dilutions and temperatures. The base model for the pure substances was used Arrhenius model in the following form:

$$\eta = \eta_0 e^{E_a/RT}, \quad (6.2.15)$$

where η is the viscosity, η_0 is the preexponential (entropic) factor and E_a , R and T are the Arrhenius activation energy, universal gas constant and absolute temperature, respectively. However, the basic form of the Arrhenius equation does not provide necessary accuracy for polar liquids²⁴⁸ and therefore an empirical enhancement was added:

$$\eta = \eta_0 e^{\left[\frac{A}{t_0 + t_1 T + t_2 T^2} \right]}. \quad (6.2.16)$$

In the above equation η is the viscosity, η_0 and A are fitting parameters based on the Arrhenius equation and t_0 - t_2 are the fitted parameters of the temperature dependent geometric sequence. The logarithmic arrangement of the Eq. (6.2.16) will be written as:

$$\ln \eta = \ln \eta_0 + \frac{A}{t_0 + t_1 T + t_2 T^2}. \quad (6.2.17)$$

Through this empirical variation the equations preserve the original shape of the Arrhenius equation while sufficiently compensating for the excess properties. That of course at the cost of adding three more parameters to the whole function. The resulting cumulative percentage deviation (calculated by Eq. (6.2.13)) of the pure liquids according to Eq. (6.2.16) is less than $\sigma < 1\%$ for propane-1,3-diol and $\sigma < 1.5\%$ for water instead of $\sigma < 6.6\%$ and $\sigma < 3.1\%$ for propane-1,3-diol and water, respectively, for the non-adjusted Eq. (6.2.15). From the adjustment, the Arrhenius activation energy can be then still deduced as $A = E_a/R$ while the pre-exponential factor η_0 is the same as in the original equation. The Arrhenius activation energy and pre-exponential factor has been calculated as $E_a = 15.252 \text{ kJ}\cdot\text{mol}^{-1}$ and $\ln(\eta_0) = -13.091$ for water and $E_a = 33.865 \text{ kJ}\cdot\text{mol}^{-1}$ and $\ln(\eta_0) = -16.777$ for propane-1,3-diol, which is in good agreement with available literature data^{36,230}. For comparison, the model of propane-1,3-diol from this work was plotted with the experimental data, and very scarce literature data. The comparison is available on Fig. 6-39. Because the Eq. (6.2.15) is theoretically not dependent on the fusion temperature, it is possible to model the viscosity even beyond the respective fusion points of the liquids.

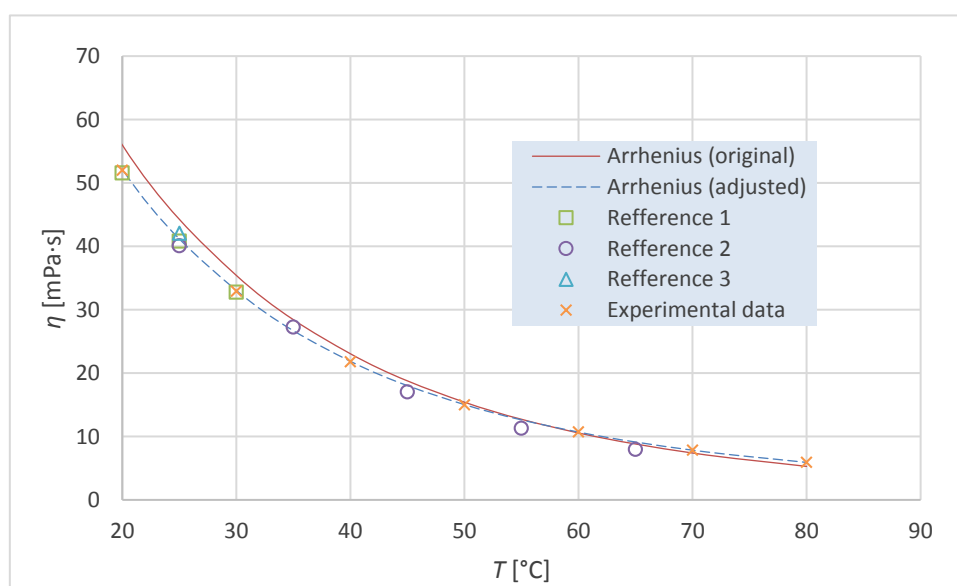


Fig. 6-39 Comparison of viscosity models with literature^{1-230,2-229,3-237}

All the previous models were tried with the adjusted Arrhenius model for pure substances to create a universal combined model with only one set of constants and two variables in form of temperature and molar or mass fraction. The combined equation follows. The Grunberg-Nissan second model equation (6.2.9) (G-N2) in combination with adjusted Arrhenius equation (6.2.16) will be written as:

$$\begin{aligned} \ln \eta_{12} = & x_1 \left(\ln \eta_{10} + \frac{A_1}{t_{10} + t_{11}T + t_{12}T^2} \right) + x_2 \left(\ln \eta_{20} + \frac{A_2}{t_{20} + t_{21}T + t_{22}T^2} \right) \\ & + x_1 x_2 \left((g_{00} + g_{01}T + g_{02}T^2) \right. \\ & + (g_{10} + g_{11}T + g_{12}T^2)(x_1 - x_2) \\ & \left. + (g_{20} + g_{21}T + g_{22}T^2)(x_1 - x_2)^2 \right), \end{aligned} \quad (6.2.18)$$

The combined Lederer's model will be written as:

$$\begin{aligned} \ln \eta_{12} = & \left(\frac{x_1}{x_1 + x_2(s_0 + s_1T + s_2T^2)} \right) \left(\ln \eta_{10} + \frac{A_1}{t_{10} + t_{11}T + t_{12}T^2} \right) \\ & + \left(\frac{x_2(s_0 + s_1T + s_2T^2)}{x_1 + x_2(s_0 + s_1T + s_2T^2)} \right) \left(\ln \eta_{20} + \frac{A_2}{t_{20} + t_{21}T + t_{22}T^2} \right) \end{aligned} \quad (6.2.19)$$

The combined McAllister's model for kinematic viscosity will be written as:

$$\begin{aligned} \ln \nu_{12} = & x_1^3 \left(\ln \nu_{10} + \frac{A_1}{t_{10} + t_{11}T + t_{12}T^2} \right) + 3x_1^2 x_2 \ln(\nu_{f10} + \nu_{11}T + \nu_{f12}T^2) \\ & + 3x_1 x_2^2 \ln(\nu_{f20} + \nu_{f21}T + \nu_{f22}T^2) \\ & + x_2^3 \left(\ln \nu_{20} + \frac{A_2}{t_{20} + t_{21}T + t_{22}T^2} \right) - \ln(x_1 + x_2 M_2/M_1) \\ & + 3x_1^2 x_2 \ln[(2 + M_2/M_1)/3] + 3x_1 x_2^2 \ln[(1 + 2M_2/M_1)/3] \\ & + x_2^3 \ln(M_2/M_1). \end{aligned} \quad (6.2.20)$$

And finally, the Heric's model for $n = 1$ from Eq. (6.2.11) will be written as:

$$\begin{aligned} \ln \nu_{12} = & x_1 \left(\ln \nu_{10} M_1 + \frac{A_1}{t_{10} + t_{11}T + t_{12}T^2} \right) \\ & + x_2 \left(\ln \nu_{20} + \frac{A_2}{t_{20} + t_{21}T + t_{22}T^2} \right) - \ln(x_1 M_1 + x_2 M_2) \\ & + (a_{00} + a_{01}T + a_{02}T^2)x_1 x_2 \\ & + (a_{10} + a_{11}T + a_{12}T^2)x_1 x_2 (x_1 - x_2). \end{aligned} \quad (6.2.21)$$

It may seem that the above combined equations are overly complicated, however their high effectivity is undeniable. The combined models were compared to the experimental data to assess the precision of the models. To assess the precision, absolute average deviations (AAD [%]) between the experimental data and the combined models were calculated. The AAD [%] are listed in Table 6-23 and visual comparison between the models and experimental data is provided on Fig. 6-40 and Fig. 6-41. The AAD [%] was calculated according to Eq. (6.2.22).

$$AAD [\%] = 100 \frac{|\eta_{exp} - \eta_{cal}|}{\eta_{exp}} \quad (6.2.22)$$

On average, the combined models are providing very good fit with the experimental data and they are not exceeding 5 % of absolute average deviation – AAD [%]. Especially good results are showing the Grunberg – Nissan's second model (G-N2) and Lederer's model, when

they are reaching around AAD [%] = 1 % on average. However, it is necessary to point out that the complexity of this modelling does not lie in the average fit but rather in local deviations. Therefore, in the Table 6-23 are also stated the maxima AAD [%] of the individual models. From the Table 6-23 can be seen that the maxima can easily reach 10 % or more. Such models than has limited application as the deviation is exceeding safety margins. To compensate for this effect, we have two options. The more usual is to state for each model the application range (temperature, dilution) or broaden the safety margins for the application itself. The AAD [%] is basically increasing with decreasing temperature but the naturally highest deviations are around the boundary conditions, such as fusion temperature or boiling point.

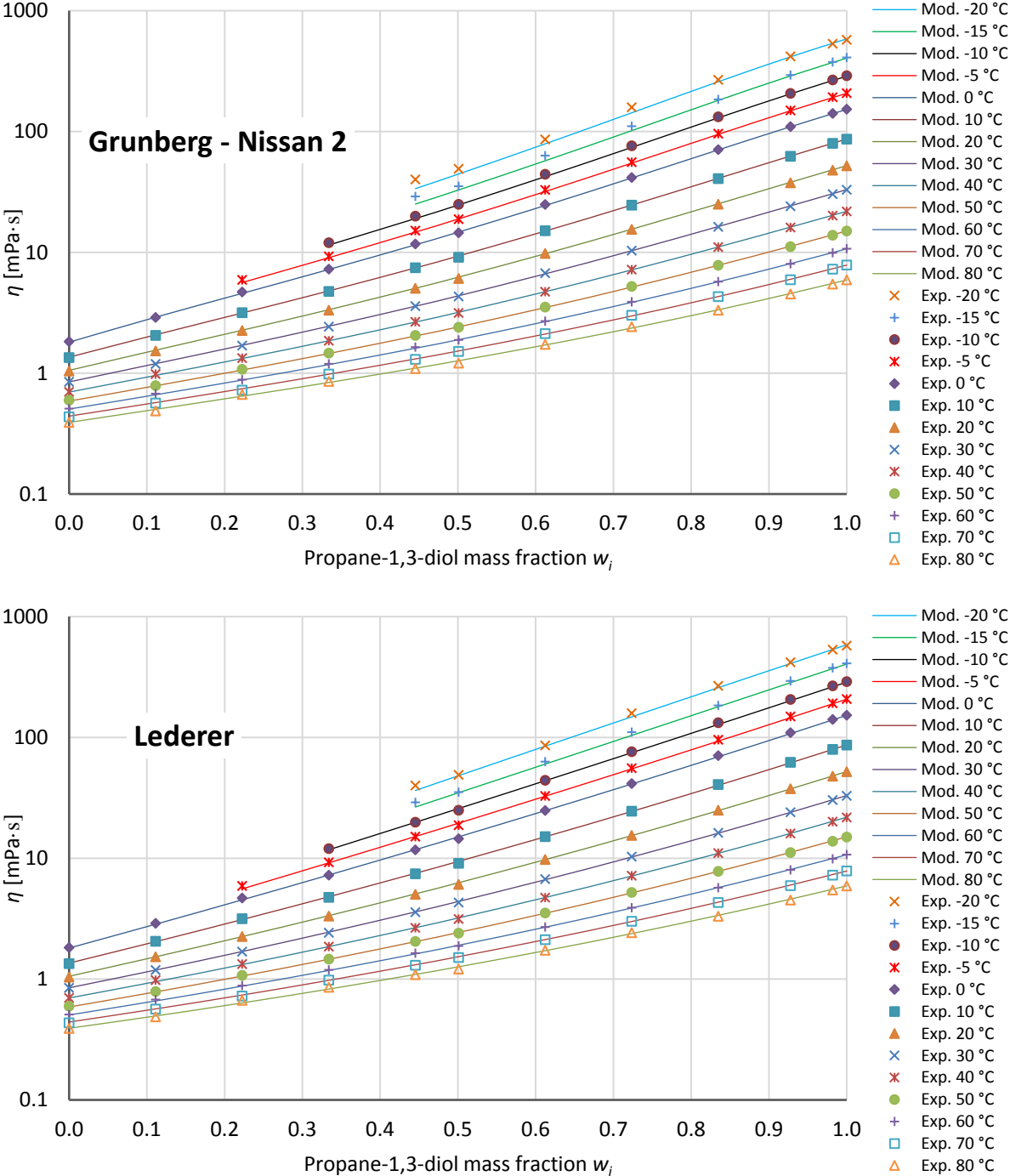


Fig. 6-40 Combined viscosity models (I) in comparison with experimental data

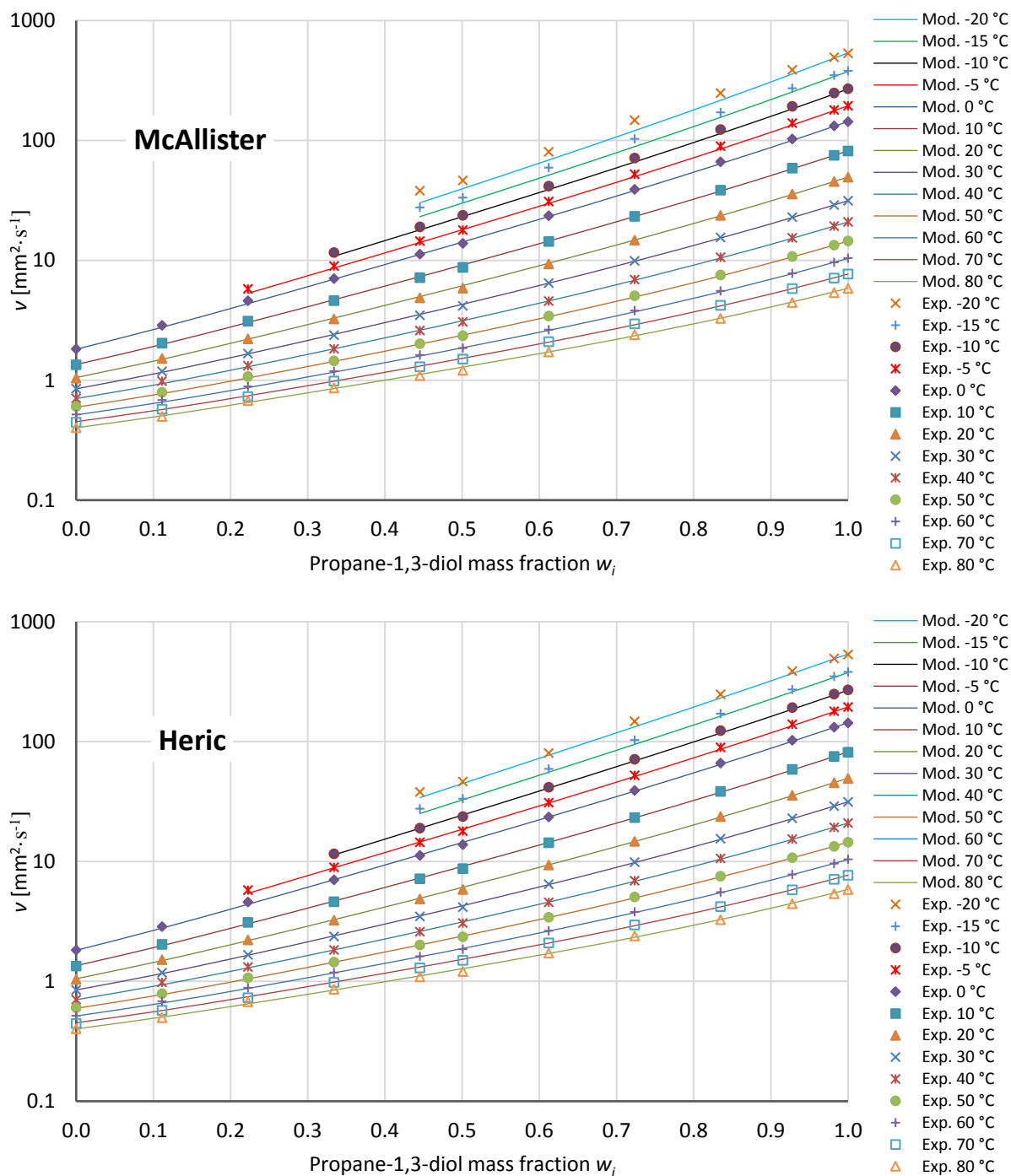


Fig. 6-41 Combined viscosity models (II) in comparison with experimental data

Comparison with available literature data was conducted on Lederer's model, which achieved the best overall fit to the experimental data. The comparison is shown on Fig. 6-43. The absolute average deviations for the work of Moosavi and Rostami²³⁰ with the combined Lederer's models were 7.76 % at 20 °C, 7.30 % at 25 °C and 5.55 % at 30 °C. For the work of George and Sastry²²⁹ the deviations are 7.76 % at 25 °C, 5.16 % at 35 °C, 6.59 % at 45 °C, 13.89 % at 55 °C and 5.16 % at 65 °C. The work of Maximino²³⁷ states only one temperature of 25 °C, when the absolute average deviation with the Lederer's combined model is 4.44 %.

Table 6-21. Fitting parameters for viscosity models: molar-fraction

Fitting parameters for molar fraction x_i														
	G-N1		G-N2				Lederer		McAllister			Heric		
$T [^{\circ}\text{C}]$	g_{12}	σ [%]	g_0	g_1	g_2	σ [%]	s	σ [%]	ν_{f1}	ν_{f2}	σ [%]	α_0	α_1	σ [%]
0	5.74	24.56	5.14	-3.24	2.75	3.47	0.26	1.85	54.10	214.92	8.22	6.35	-4.35	8.22
10	5.30	22.08	4.73	-2.92	2.36	2.92	0.27	1.55	33.17	109.40	7.14	5.90	-3.94	7.14
20	4.88	19.93	4.35	-2.65	2.01	2.31	0.28	1.15	21.29	60.69	6.15	5.49	-3.59	6.15
30	4.48	17.67	4.01	-2.39	1.62	1.46	0.29	0.94	14.58	35.69	4.96	5.11	-3.24	4.96
40	4.14	16.24	3.68	-2.16	1.56	2.13	0.30	1.18	10.16	22.62	5.04	4.77	-2.99	5.04
50	3.82	14.62	3.41	-1.99	1.27	1.24	0.31	0.69	7.39	15.05	4.06	4.47	-2.75	4.06
60	3.58	14.12	3.15	-1.89	1.32	1.58	0.31	0.91	5.35	10.92	4.29	4.23	-2.67	4.29
70	3.39	13.31	3.00	-1.81	1.12	1.20	0.31	0.82	4.07	8.07	3.67	4.05	-2.54	3.67
80	3.16	13.02	2.77	-1.72	1.13	3.10	0.31	2.57	3.14	6.20	4.57	3.83	-2.45	4.57
$\bar{\sigma}$ [%]		17.28				2.16		1.30			5.35			5.35
Regression constants														
	G-N1		G-N2				Lederer		McAllister			Heric		
$T [^{\circ}\text{C}]$	g_{12}		g_0	g_1	g_2		s		ν_{f1}	ν_{f2}		α_0	α_1	
y_0	33.726		29.915	-27.095	35.375		-0.697		28.530	46.271		34.295	-35.732	
y_1	-0.157		-0.138	0.140	-0.197		0.006		-0.132	-0.232		-0.157	0.186	
y_2	2.0E-04		1.7E-04	-1.9E-04	2.8E-04		-8.0E-06		1.5E-04	3.0E-04		2.0E-04	-2.6E-04	
R^2	99.97 %		99.96 %	99.89 %	98.80 %		99.72 %		99.98 %	99.98 %		99.98 %	99.88 %	

Table 6-22. Fitting parameters for viscosity models: mass-fraction

Fitting parameters for mass fraction w_i														
	G-N1		G-N2				Lederer		McAllister			Heric		
T [°C]	g_{12}	σ [%]	g_0	g_1	g_2	σ [%]	s	σ [%]	ν_{f1}	ν_{f2}	σ [%]	α_0	α_1	σ [%]
0	-0.43	1.84	-0.49	-0.01	0.49	1.22	1.10	1.85	27.99	8.44	2.58	0.50	-0.48	2.58
10	-0.56	1.54	-0.62	-0.03	0.42	0.99	1.15	1.55	16.50	5.50	2.27	0.37	-0.50	2.27
20	-0.67	1.17	-0.71	-0.05	0.28	0.86	1.19	1.15	10.42	3.82	1.83	0.27	-0.52	1.83
30	-0.76	0.76	-0.77	0.00	0.13	0.73	1.23	0.94	7.12	2.74	1.36	0.19	-0.47	1.36
40	-0.80	1.39	-0.83	-0.13	0.30	0.78	1.26	1.18	4.84	2.18	1.88	0.15	-0.59	1.88
50	-0.83	0.80	-0.84	-0.07	0.05	0.70	1.29	0.69	3.62	1.69	1.09	0.12	-0.54	1.09
60	-0.81	1.42	-0.81	-0.18	0.07	0.81	1.30	0.91	2.69	1.43	1.26	0.15	-0.65	1.26
70	-0.78	1.20	-0.78	-0.13	-0.05	0.90	1.31	0.82	2.14	1.16	1.08	0.17	-0.60	1.08
80	-0.74	2.88	-0.75	-0.25	0.09	2.65	1.32	2.57	1.68	1.04	2.63	0.21	-0.71	2.63
$\bar{\sigma}$ [%]		1.44				1.07		1.30			1.77			1.77
Regression constants														
	G-N1		G-N2				Lederer		McAllister			Heric		
T [°C]	g_{12}		g_0	g_1	g_2		s		ν_{f1}	ν_{f2}		α_0	α_1	
y_0	13.722		12.582	-2.115	9.357		-2.944		32.952	28.548		14.344	-2.514	
y_1	-0.089		-0.083	0.016	-0.053		0.024		-0.166	-0.152		-0.087	0.015	
y_2	1.36E-04		1.27E-04	-2.93E-05	7.53E-05		-3.40E-05		2.09E-04	2.01E-04		1.34E-04	-2.85E-05	
R^2	99.61 %		98.98 %	79.23 %	83.22 %		99.72 %		99.96 %	99.91 %		99.59 %	80.11 %	

Table 6-23. Absolute average deviation – AAD [%] of combined viscosity models

T [°C]	Grunberg - Nissan 2		Lederer		McAllister		Heric	
	AAD [%]		AAD [%]		AAD [%]		AAD [%]	
	x_i	w_i	x_i	w_i	x_i	w_i	x_i	w_i
-20	7.31	7.04	3.84	3.84	12.05	12.73	7.08	5.80
-15	5.87	6.03	3.90	3.90	9.52	9.95	6.69	5.11
-10	3.17	2.58	1.93	0.16	6.89	5.08	6.48	2.42
-5	3.13	1.86	1.98	1.98	6.87	3.54	7.03	2.33
0	2.49	0.99	1.48	1.48	6.00	2.15	7.45	1.83
10	1.89	0.77	1.13	1.13	5.32	1.67	5.24	1.61
20	1.59	0.97	0.82	0.82	4.66	1.44	4.51	1.27
30	0.98	0.68	0.64	0.64	3.73	1.03	3.64	1.07
40	1.42	0.66	0.75	0.75	3.79	1.24	3.78	1.24
50	1.29	0.77	0.73	0.73	3.36	1.31	3.37	1.08
60	1.42	0.96	0.95	0.95	3.39	1.53	3.41	1.20
70	0.91	0.93	0.80	0.80	2.48	0.95	2.53	0.98
80	1.85	1.80	1.86	1.86	3.44	1.78	3.32	1.75
AAD_{Average}	1.54	0.95	1.02	1.02	4.02	1.45	4.14	1.34
AAD_{Max}	15.48	16.02	9.34	9.34	15.48	20.58	17.61	10.43

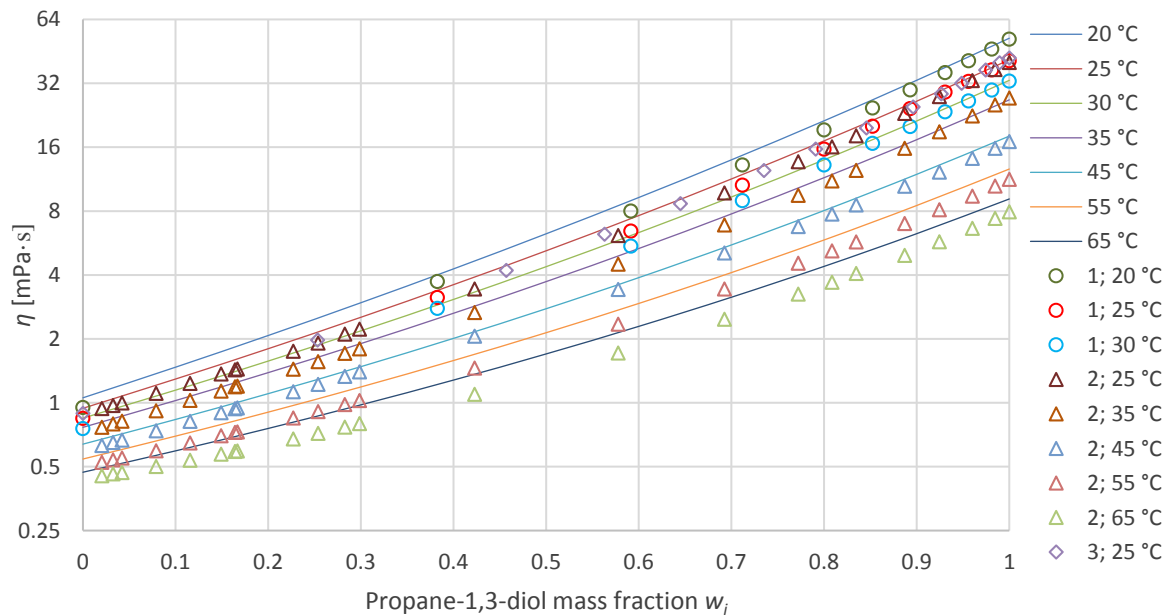


Fig. 6-42 Comparison of the Lederer's combined model with literature^{1-230, 2-229, 3-237}

If we approximate the literature data to experimental data from this work, the relative differences of the experimental data and the combined model follow similar trend. However, because the literature data are highly limited it is very hard to produce any clear conclusion. This is mostly apparent in comparison to the work of George and Sastry²²⁹, where the absolute

average deviation differs from values low as 5.16 % to high as 13.89 %. From this perspective it is necessary to note that their work used different method of measurement. George and Sastry²²⁹ used primarily Ubbelohde viscometer and in this work the primary instrument was rotational viscometer. The works of Moosavi and Rostami²³⁰ and Maximino²³⁷ offers much better agreement with experimental data from this work and better agreement towards the Lederer's combined model, however, the amount and range of the data is limited to 3 datasets for three different temperatures in case of Moosavi and Rostami²³⁰ and only one in case of Maximino²³⁷.

6.2.3 Refractive index

Data on refractive indices are summarized in Table 6-24 and shown on Fig. 6-43. As a basis to create a connection between optical and volumetric properties the Clausius-Mossotti equation was used. This equation describes the relative permittivity ϵ_r (dielectric constant) of a material, or a mixture this way:

$$\frac{\epsilon_r - 1}{\epsilon_r + 2} = \frac{N\alpha'}{3\epsilon_0} \quad (6.2.23)$$

In the above equation N represents the number of particles per volume, ϵ_0 is vacuum permittivity and α' is polarizability volume. The polarizability volume α' expressed in SI units will give polarizability as $\alpha = 4\pi\epsilon_0\alpha'$. In case of a mixture, the right side of the previous equation becomes a sum of calculated individual bodies dependent on the number of particles. To connect the refractive index n_D and relative permittivity was used the Lorenz-Lorenz equation by the Maxwell relation:

$$\frac{n_D^2 - 1}{n_D^2 + 2} = \frac{4\pi}{3} N\alpha, \quad (6.2.24)$$

where the refractive index n_D is expressed as $n_D^2 = \epsilon_r$, N states the number of particles in the volume and α is the polarizability from the abovementioned relation to polarizability volume α' . From that relation we can deduce the molar refraction R_m [mol^{-1}] as:

$$R_m = \frac{n^2 - 1}{n^2 + 2} \frac{M}{\rho} = \frac{4\pi}{3} N_A \alpha, \quad (6.2.25)$$

where M is calculated average molar mass, ρ is density and N_A is the Avogadro constant.

The propane-1,3-diol's polarizability α is higher than that of the water. That means that the light is slower inside it and the refraction is stronger. Naturally the same applies for molar refraction as it is directly dependent on the polarizability. The polarizability and molar refraction values according to temperature are shown on Fig. 6-44. The polarizability of water at 20 °C was calculated as $\alpha = 1.47 \times 10^{-24} \text{ cm}^3 \cdot \text{mol}^{-1}$, which agrees with values from literature²⁴⁹. The polarizability of propane-1,3-diol was find out as $\alpha = 7.54 \times 10^{-24} \text{ cm}^3 \cdot \text{mol}^{-1}$ and it agrees with values find out by Moosavi and Rostami²³⁰. Notable are also the respective trends of the polarizability and molar refraction. In case of water, the values are dropping with the rising temperature, however the values for propane-1,3-diol are rising. The respective differences are $\Delta\alpha = 0.1 \times 10^{-24} \text{ cm}^3 \cdot \text{mol}^{-1}$ for propane-1,3-diol and $\Delta\alpha = 0.02 \times 10^{-24} \text{ cm}^3 \cdot \text{mol}^{-1}$ for water in the range of 10 °C to 40 °C. That shows higher dependency of activity on temperature for propane-1,3-diol.

Table 6-24. Experimental values of refractive indices for propane-1,3-diol

T [°C] / T [K]		5 °C	10 °C	15 °C	20 °C	25 °C	30 °C	35 °C	40 °C	45 °C
w_i	x_i	278.15 K	283.15 K	288.15 K	293.15 K	298.15 K	303.15 K	308.15 K	313.15 K	318.15 K
0.0000	0.0000	1.3341	1.3338	1.3335	1.3331	1.3326	1.3320	1.3313	1.3306	1.3298
0.1113	0.0288	1.3466	1.3462	1.3457	1.3452	1.3446	1.3440	1.3434	1.3426	1.3418
0.2226	0.0635	1.3599	1.3592	1.3586	1.3579	1.3572	1.3564	1.3558	1.3550	1.3541
0.3340	0.1061	1.3740	1.3729	1.3719	1.3710	1.3702	1.3693	1.3684	1.3676	1.3668
0.4453	0.1597	1.3866	1.3856	1.3845	1.3835	1.3825	1.3815	1.3804	1.3793	1.3782
0.5010	0.1920	1.3931	1.3921	1.3910	1.3899	1.3888	1.3876	1.3865	1.3854	1.3845
0.6123	0.2721	1.4066	1.4055	1.4041	1.4029	1.4015	1.4002	1.3989	1.3977	1.3965
0.7236	0.3826	1.4181	1.4169	1.4157	1.4145	1.4133	1.4118	1.4103	1.4089	1.4075
0.8349	0.5449	1.4289	1.4276	1.4263	1.4250	1.4237	1.4224	1.4211	1.4197	1.4182
0.9277	0.7523	1.4371	1.4358	1.4345	1.4332	1.4319	1.4304	1.4289	1.4275	1.4261
1.0000	1.0000	1.4436	1.4423	1.4409	1.4395	1.4381	1.4368	1.4354	1.4340	1.4325

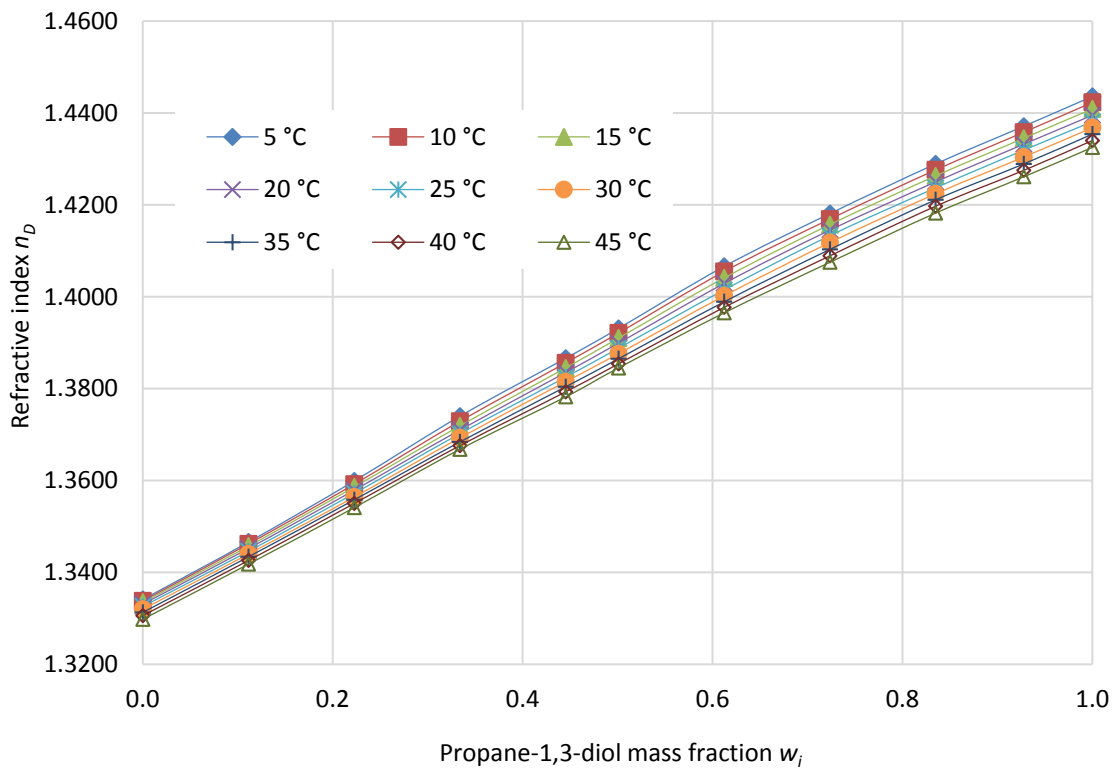
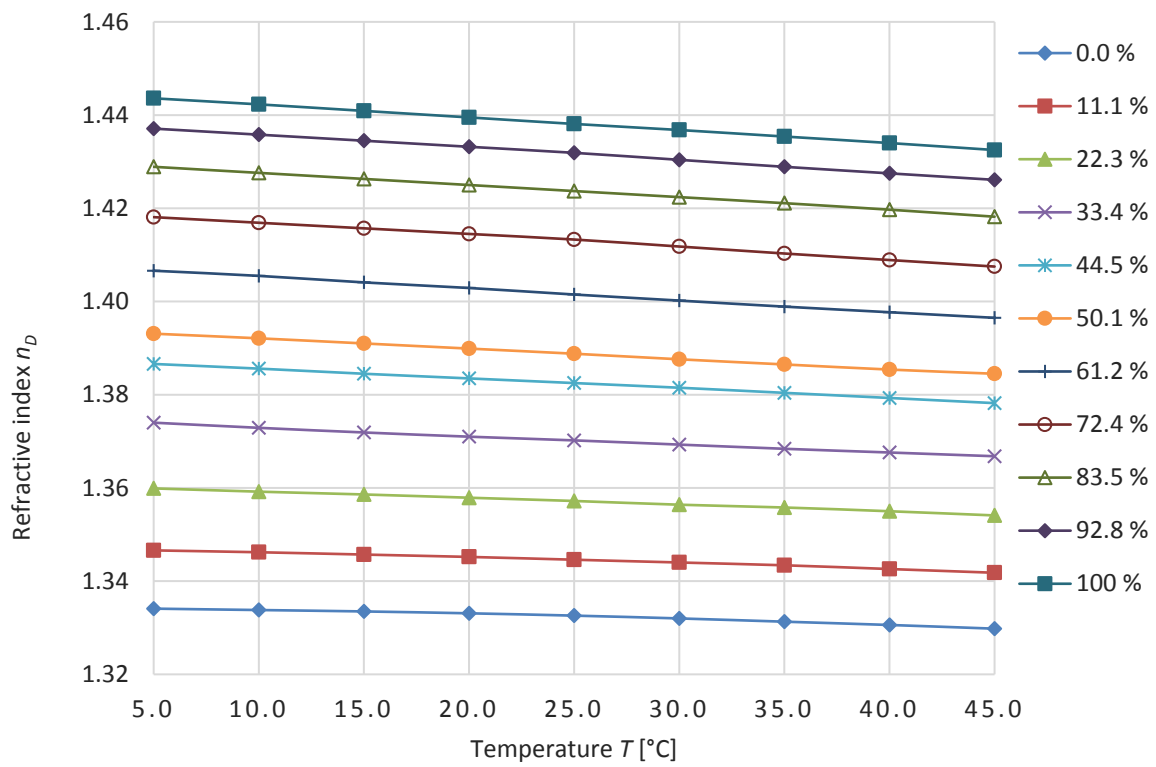


Fig. 6-43 Refractive index of aqueous propane-1,3-diol

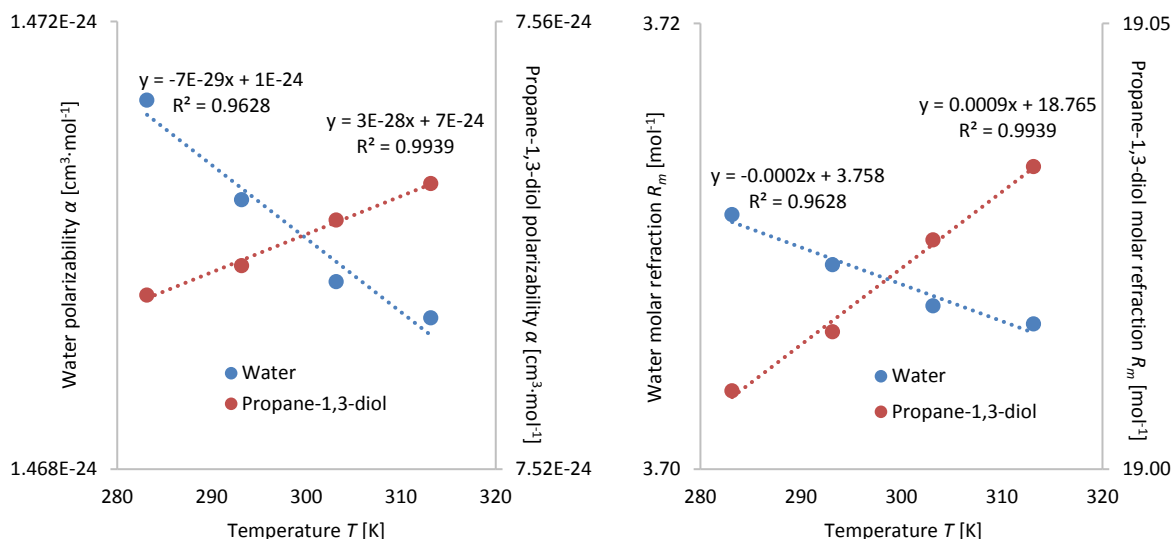


Fig. 6-44 Polarizability (left) and molar Refraction of water and propane-1,3-diol

6.2.4 Freezing point

One of the key properties for using propane-1,3-diol as an antifreeze additive is its capability of depressing freezing point (fusion point) of water. The results of the freezing point depression of the aqueous propane-1,3-diol are listed in Table 6-25 and shown on Fig. 6-45.

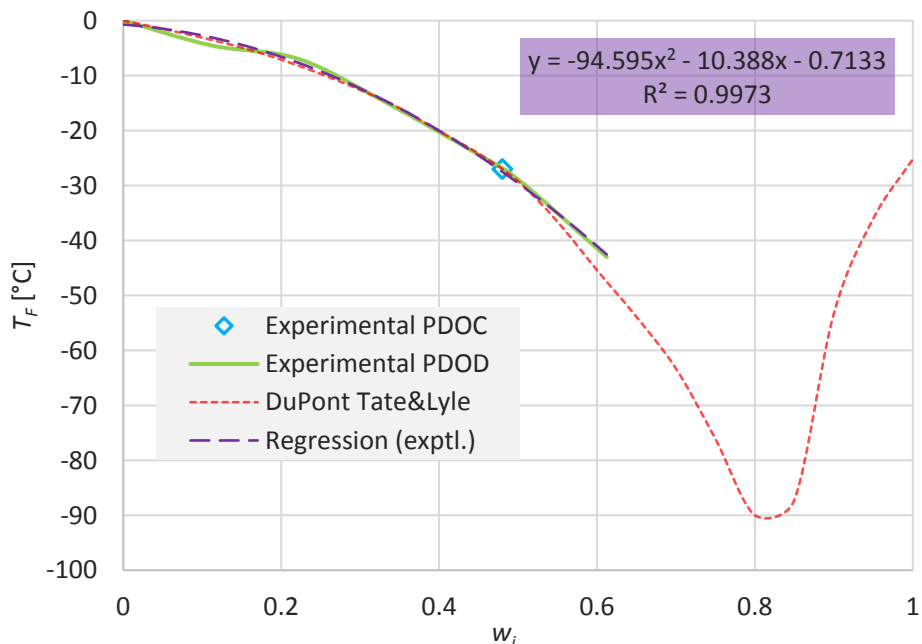


Fig. 6-45 Freezing point of aqueous propane-1,3-diol in comparison with literature²⁵⁰

Comparison of the freezing point is provided on the available data of Sunterra bio-propane-1,3-diol of high purity. The literature reference from the Fig. 6-45 (Ref.²⁵⁰) is using for measurement the same bio-produces propane-1,3-diol as was used in this work as sample PDOD. For comparison was also measured a sample from Chinese manufacturer with stated

purity of 99 %. All the results are in good agreement with literature and between each other, proving good quality of the examined chemicals and possibly good repeatability of the method.

Table 6-25. Freezing points of aqueous propane-1,3-diol

Propane-1,3-diol mass fraction w_i Sample PDOD	Freezing point T_F [°C]
0.0000	0
0.1113	-4.5
0.2226	-7
0.3340	-15
0.4453	-24
0.5010	-29
0.6123	-43
Propane-1,3-diol mass fraction w_i Sample PDOC	Freezing point T_F [°C]
0.4800	-27

In the region of $w_i = (0 \text{ to } 0.6)$ of propane-1,3-diol in water is applicable polynomial regression of the second order to simplify the dilution process. The regression has a shape of

$$T_F = -94.595w_i^2 - 10.388w_i - 0.7133, \quad (6.2.26)$$

where T_F is the freezing point and w_i is the mass fraction in the region of (0 to 0.6). For better precision, the constant -0.7133 should be omitted in the lower concentrations to avoid theoretical undercooling of the mixture.

When comparing the data on freezing depression of propane-1,3-diol with other glycols from Fig. 4-2 it is apparent that propane-1,3-diol does not have such strong freezing point depression for water as propane-1,2-diol and ethane-1,2-diol and for the same freezing protection of water is necessary higher concentration of propane-1,3-diol. That gives another blow to the feasibility of already over-expensive use of propane-1,3-diol. To achieve the same freezing protection, it is necessary additional 5-10 % of propane-1,3-diol. But even this added amount can be sufficiently reasoned through other advantageous properties of propane-1,3-diol which will be explained later.

6.3 Heat transfer fluid based on propane-1,3-diol

6.3.1 Thermal degradation processes

The thermal degradation process of propane-1,3-diol is yet to be properly studied, but some of the basic information are already available. The stability of the aqueous propane-1,3-diol was for the first time studied by Eaton and co-workers⁵⁷ when comparing it to the ethane-1,2-diol for usage in exhaust gas recirculation devices use. The premise for their research for seemingly higher thermal stability of propane-1,3-diol compared to the common

systems using propane-1,2-diol and ethane-1,2-diol. The results were promising, however the whole research was presented only on basis of testing the prepared fluid through a series of ASTM standards and it was not intended as a full investigation of the degradation process of the fluid based on propane-1,3-diol. The main setting for the experiment was oxidative degradation of the aqueous propane-1,3-diol, when most of the modern systems are not exposed to direct oxidative stress through dissolved oxygen. Nevertheless, this work proves propane-1,3-diol superiority over the current systems.

Another study was provided by one the biggest manufacturer of bio propane-1,3-diol DuPont Tate&Lyle^{250,251}. The aqueous propane-1,3-diol was again compared to the common systems of propane-1,2-diol and ethane-1,2-diol. The three samples of 50 wt% solutions were inhibited by addition of 2.2 wt% of standard heavy-duty inhibitor system Penray 2792²⁵² and the formation of glycolate, formate and inhibitor depletion was studied. The temperature of the test was chosen to be 192 ± 10 °C and the test was conducted for 16 hours (instead of 150 °C and 336 hours in case of Eaton⁵⁷). Though results in case of Eaton were just better in case of uninhibited systems, the results of the Dupont team can be described as astonishingly good. The amount of glycolate in the propene-1,3-diol system after experiment is 10 times lower than that of propane-1,2-diol and even more in case of ethane-1,2-diol. Similarly, the depletion of inhibitor additives was significantly lower. However, several things in this study is questionable. The experiment was conducted in glassware only without adding any standard metals that can be encountered in standard systems. Only glycolate and formate degradation products were studied and no information on change of pH or conductivity was given. Therefore, even though that the results are very intriguing, the validity of this study is somehow questionable, adding to it the very short time of the actual experiment.

6.3.2 Corrosivity properties

To test the actual corrosion properties a standard ASTM D1384¹¹⁵ corrosivity test for antifreeze glycol-based mixtures was conducted. Test was conducted in the laboratory of Classic Oil s.r.o. and the data were kindly provided by Dr. Jan Skolil. The used inhibitor was a hybrid inhibitor system Cemkor C33²⁵³ based on silicates from Slochem Trade s.r.o.

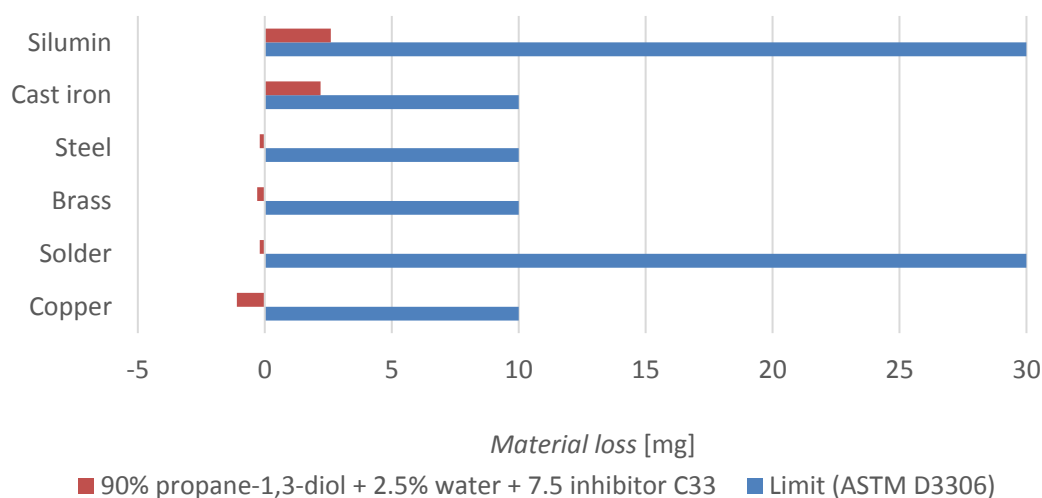


Fig. 6-46 Corrosion test of aqueous propane-1,3-diol according to ASTM D1384

As it was expected, the propane-1,3-diol is stable and shows only a limited amount of corrosion basically on the verge of measurement and method error. However, it is necessary to note, that this method is intended only as a basic information source about its corrosivity and the actual situation in the real system can significantly vary from these results as it is directly described in the standard itself. Although, because the chemical quality is very similar to the other glycols, which are highly tested in many applications, we can safely assume that the propane-1,3-diol would perform very well with any corrosion inhibitor system intended for use with propane-1,2-diol or ethane-1,2-diol. Still, any comparative study has yet been published to confirm this assumption according to the best knowledge of this thesis' writer.

6.3.3 Perspectives of utilisation of propane-1,3-diol as a novel antifreeze additive

Despite all the positive properties of propane-1,3-diol, its simple utilisation as novel antifreeze additive is a different problem. The main setbacks so far is its high price around 1500-2000 \$ per ton (based on survey on Alibaba.com) when propane-1,2-diol is in the range of 800-1400 \$²⁵⁴ per ton (Fig. 6-48) and ethane-1,2-diol in the range of 500-1000 \$²⁵⁵ per ton (Fig. 6-47), depending on quality and season. The market is strongly influenced by Chinese manufacturers as China is becoming the largest single consumer and producer of glycols in the world²⁵⁶. Furthermore, the price for propane-1,3-diol is only an estimation for limited quantity. That is because the global market of propane-1,3-diol is yet to be established, the number of actual producers is highly limited, and therefore, the price varies significantly according to manufacturer and ordered amount. The biggest producer so far, DuPont Tate&Lyle²⁵⁷, is producing propane-1,3-diol mainly for its own manufacturing purposes (see chapter 4.5.2 for more information) and in general, acquiring any stable supply of propane-1,3-diol for a continuous production is a difficult task.

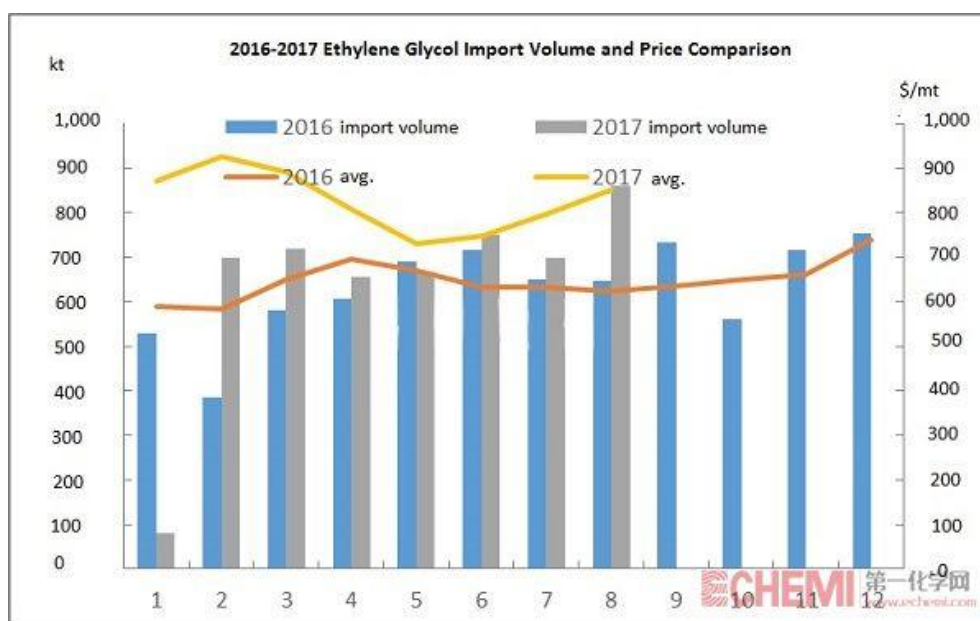


Fig. 6-47 Ethane-1,2-diol import volume (China) and average market price²⁵⁵

Another problem is also limited options for economically feasible production. The major producers have their own manufacturing processes patent protected and any new producer,

which would put some pressure on the market price, would have to come with a breakthrough manufacturing process to be competitive.

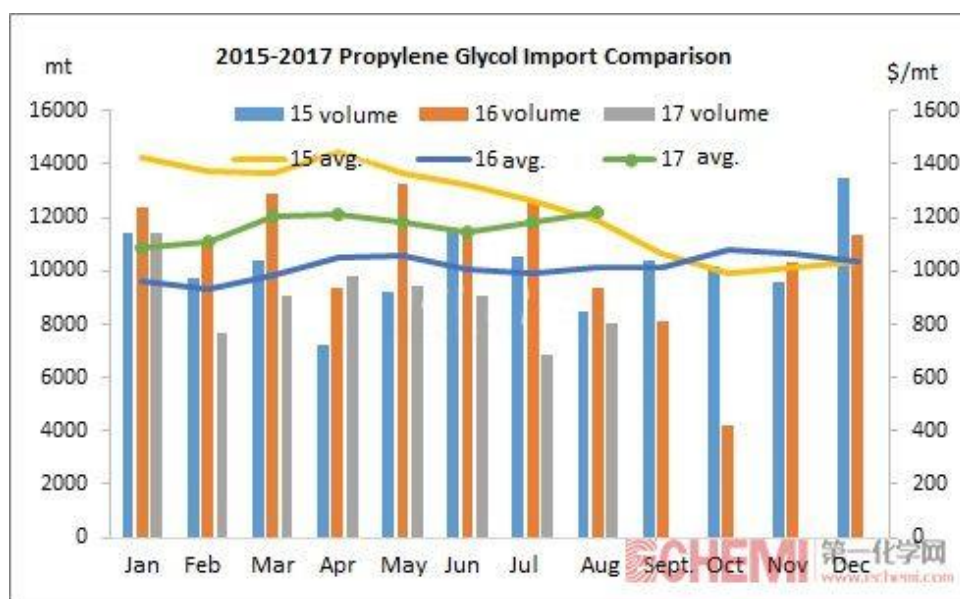


Fig. 6-48 Propane-1,2-diol import volume (China) and average market price²⁵⁴

The situation in favour for propane-1,3-diol as a novel antifreeze was changing only very slowly during the last decade⁴⁶. It was mainly caused by the limited production capacities, and therefore high price, and very limited amount of available information on the physical and chemical properties of propane-1,3-diol. The main producer DuPont Tate&Lyle is advertising propane-1,3-diol as novel antifreeze additive for couple of years now^{250,258}, however, on the actual market is nearly impossible to find any developed product. That is despite the fact that propane-1,3-diol-based engine coolant has already its own ASTM standards for quality specification ASTM D7388²⁵⁹, test method for purity assessment ASTM D7515²⁶⁰ and standard specifications for engine coolant ATSM D7517²⁶¹ and automobile and light-duty service ASTM D7518¹⁹².

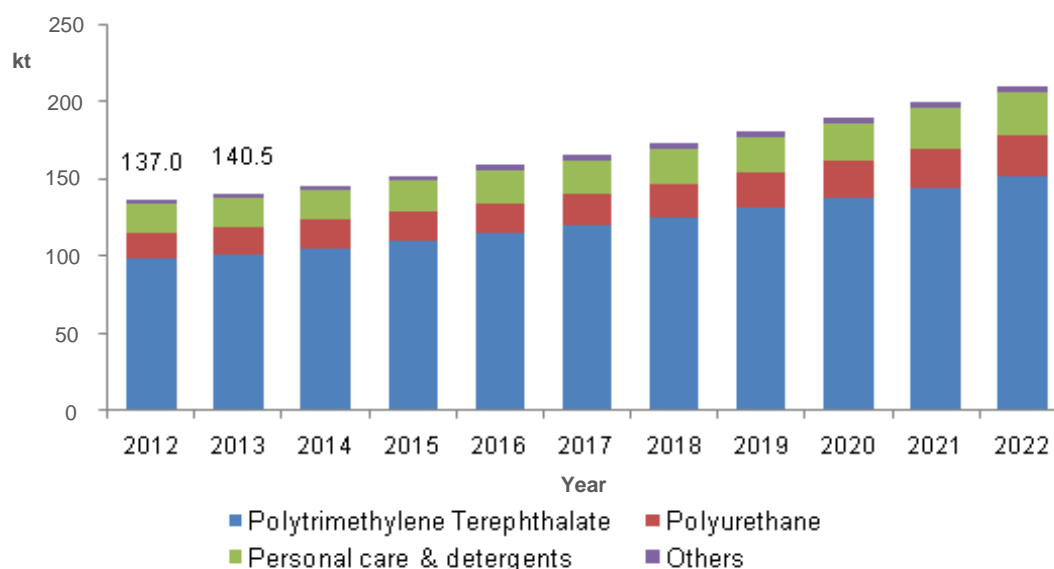


Fig. 6-49 Market volume of propane-1,3-diol by application (prediction 2015+)²⁶²

Theoretically in the current situation by just publishing more information about propane-1,3-diol could change awareness about this chemical and support the interest of antifreeze manufacturers. That is especially in connection with the high social demand for new green technologies²⁶³⁻²⁶⁵. However, the prognosis for other applications except polymer industry is somehow dim as can be seen from the prediction from Fig. 6-49. That prediction is made on the basis of the market development so far and the demand for green technologies is not fully accounted or understood.

The propane-1,3-diol has great potential to become the third big antifreeze additive in spite of its high price. That is, however, only in case of continuing research on its possibly superior thermal stability and low corrosivity. Only in that case it can be reasonably used even though the price is higher than the common propane-1,2-diol and ethane-1,2-diol.

7 CONCLUSION

An experimental thermal solar system in Vracov, Czech Republic was observed over a time span of 7 years with periodically sampling of the heat transfer fluid based on propane-1,2-diol for chemical and physical analysis. The results of the analysis show that even after seven years of continuous operation, the fluid is in relatively good condition and can be used unaltered further on. Such a good state of the fluid can be seen as little bit surprising, because the manufacturers of the heat transfer fluids recommend to change the fluid every five years on a general basis. The main factor of the fluid, freezing point was not affected, and if, it was in an amount which is negligible and will not affect the performance of the fluid. The data of pH and conductivity are showing reaching a pseudo-equilibrium and possible slowing down of the fatal degradation process. The prefix “pseudo” is used in this context rightfully as it is not reasonable to expect this state to hold out forever, even though all the measurements indicate a significantly prolonged time of operation of the fluid in the Vracov system without the necessity of replacement.

This state is further on supported by the mass spectrometry analysis on the presence of the corrosion inhibitors in the mixture. During the whole monitored time, the amount seems to be constant without significant drop of their concentration and sustained effective protection of the system. The samples from Vracov were also tested on presence of organic acids as one the typical products of degradation. During the whole period of observation from 2007 to 2014 the amount of monitored organic acids, known to be formed in the propane-1,2-diol-based antifreeze systems, were not detected in amount more than $1 \text{ mg}\cdot\text{L}^{-1}$. This also proves very good condition of the fluid and expected prolonged life-span of the fluid.

But some change was detected after all. If we look at the results for density a clear trend of continuous density drop can be observed. There may be two reasons for this change. First is connected to change of the concentration of propane-1,2-diol and water. During the operation the temperatures exceed $120 \text{ }^\circ\text{C}$ from time to time (boiling point of water at 2 bars) and part of the water is evaporated and if the pressure exceeds 6 bar the steam is vented to the atmosphere through the safety pressure relief valve. However, this situation was not detected during the operation of the Vracov system and what more, this would cause a density rise not a decrease like in this case. Therefore, a different explanation is necessary. A possible cause of this change could be actual change in the chemical makeup of the mixture. By additional mass spectrometry analysis, a seemingly increasing concentration of dipropylene glycol isomers was observed. This would completely explain the drop of the density, rise of the viscosity and at the same time preservation of some of the key properties of the fluid such as freezing point. What more, this change seems to be gradual and no serious harm to the system is expected by the means of this change. However, this discovery is very important for further manipulation with the spent fluid, especially in case of intended recycling. If the concentration of the dipropylene glycol become too high, the change of viscosity could cause some technological problems and would be better to be avoided. To fully support this thesis and establish a reaction kinetics for this change further research is necessary.

Not completely different situation was observed during the analysis of samples from several other systems which were using the same original fluid for their operation or, in case of sample TS, the same organic base propane-1,2-diol. The samples were collected from several thermal solar systems from the region of South Moravia and North Moravia. The samples were selected on the basis of their highly progressed degradation and that none of them was in operation

longer than the experimental system in Vracov. The biggest difference of these samples was therefore not the fluid composition but their operating conditions. All of the samples were taken from systems that went through a series of system stagnation resulting in high thermal stress on the fluid and consequent system damage. The main purpose of this measurement of observation of the acidic degradation product formation in anoxic conditions. According to current knowledge, the degradation of propane-1,2-diol is complicated process consisting mainly from formation of organic acid products which are reducing the pH of the fluid and supporting corrosive properties of the fluid. However, this process was mainly studied in environments rich on dissolved oxygen and any comparative studies for modern systems are not available. This work shows, that these products are formed even in environment depleted of oxygen and are directly connected to the temperature. The highest concentrations of the organic acids were found in the sample TS equipped with evacuated tube collectors and with the highest stagnation temperatures. An interesting finding was the high concentration of acetate in case of the TS sample which goes against the current knowledge stating the main degradation product of propane-1,2-diol to be 2-hydroxypropionate (lactate). However, the possibility of some catalytic influence cannot be ruled out, thanks to different inhibitor system, because the samples SD and SJ, of the same origin, developed according to known preferences. Another finding was relatively low concentration of the monitored organic acids. In the available studies conducted usually over a short period of time, the concentrations of the main products (2-hydroxypropionate in case of propane-1,2-diol and 2-hydroxyethanoate in case of ethane-1,2-diol) is in range of grams per litre but this work shows milligram concentrations. The cause for such discrepancy may lie exactly in the time difference. In the case of the laboratory test, the samples are tested almost immediately for the monitored organic acids, however, in the real systems the acids are continuously interacting with the environment and causing corrosion. The result is, as shown in the work of Brown et al.¹⁹⁸, formation of several copper complexes with the organic acids and their precipitation from the mixture. The precipitate in the continuously circulating system sediments in hydrodynamically suitable places or it is filtered out by the system's filter. That is also a reason why in the working systems the precipitate is hard to find in the fluid itself and why it could have been found in a great quantity in the sample SD. Because the stagnation of the system of sample SD was caused by pump malfunction, the fluid was not circulating, the sedimentation occurred only freely, and the precipitate was also not filtered out by the system filter. Therefore, during the sampling when the fluid was moved for the first time after several days of stagnation, the lightly sedimented precipitate was easily agitated and could be sampled with the rest of the fluid. This means that only the measurement of pH does not have to be sufficient to assess the system state as it does not describe the actual damage but only its current rate, especially in systems, which underwent stagnation conditions.

Comparing the experimental system in Vracov with the results of the highly degraded samples an obvious conclusion offers itself. The degradation process is more connected to the system design and control than the chemical makeup of the fluid itself. Poorly designed systems are prone to overheating and stagnation, which according to this work is the main cause for the heat transfer fluid collapse. This results in shortened life-span of the system and economical losses. With proper design and robust control, the lifespan of the fluid can be significantly extended together with the lifespan of the system.

In the second half of this thesis a full investigation of selected physical properties on the aqueous propane-1,3-diol was conducted. The goal of this investigation was to establish a basic

model tool, which can be used as an engineering base for further testing and progress of development of a novel antifreeze fluid based on propane-1,3-diol. The mathematical analysis included a creation of a new combined viscosity model combining three mathematical expression of water, propane-1,3-diol and standard viscosity model. Several different models were established with various level of agreement with the experimental data. The simplest model, and also one of the best fits, was produced by combined Lederer's model with adjusted Arrhenius viscosity expression for pure liquids. For better agreement, the Arrhenius model was refined by second polynomial sequence. Thanks to this adjustment, the resulting absolute average deviation (AAD [%]) for the whole data set was equal to ~1 % in case of Lederer model. Other models' deviations were higher, however, they did not exceed 5 %. But the problem of these models was not in the overall average deviations but in the local deviations which could reach up to 10-15 %. This situation was observed in case of all models. Though, it was strictly localised near the freezing point of the mixtures which means, that these models can be comfortably used in most of the range and the caution should be taken near the boundary conditions.

As the data shows, the viscosity and density are not that different compared to the common propane-1,2-diol and ethane-1,2-diol. Though, the viscosity is lower in case of aqueous propane-1,3-diol, the substance is little bit losing in terms of freezing protection. To achieve the same level of protection 5-10 % more of the propane-1,3-diol must be added to the mixture, which consequently rises the viscosity of the mixture as well. Connecting this with the higher price of the propane-1,3-diol, the competitiveness of this chemical is still limited. However, the results on the thermal stability and corrosivity show far better qualities than these of propane-1,2-diol and ethane-1,2-diol which possibly could overrule the higher costs connect with the use of antifreeze mixtures based on propane-1,3-diol.

8 LITERATURE CITED

1. FAO. *State of the World 's Forests 2012* [online]. Rome : Food and Agriculture Organization of the United Nations, 2012. ISBN 978-92-5-107292-9. Available from: <http://ccafs.cgiar.org/news/press-releases/agriculture-and-food-production-contribute-29-percent-global-greenhouse-gas>
2. FAO. *State of the World 's Forests 2016*. Rome : Food and Agriculture Organization of the United Nations, 2016. ISBN 978-92-5-109208-8.
3. LIGHTFOOT, H. Douglas, MANHEIMER, Wallace, MENELEY, Daniel A., PENDERGAST, Duane and STANFORD, George S. Nuclear fission fuel is inexhaustible. In : *2006 IEEE EIC Climate Change Technology Conference, EICCCC 2006*. 2007. ISBN 1424402182.
4. IEA. World Energy Outlook 2016. *World Energy Outlook* [online]. 2016. P. 1–8. DOI http://www.iea.org/publications/freepublications/publication/WEB_WorldEnergyOutlook2015ExecutiveSummaryEnglishFinal.pdf. Available from: http://www.iea.org/publications/freepublications/publication/WEB_WorldEnergyOutlook2015ExecutiveSummaryEnglishFinal.pdf
5. INTERNATIONAL ENERGY AGENCY. IEA - Statistics. [online]. 2017. Available from: <https://www.iea.org/statistics/>
6. ENERGY, U S. *2017-EIA-International energy outlook 2017*. 2017.
7. BALL, Philip. Are there nuclear reactors at Earth's core? *Nature* [online]. 15 May 2008. DOI 10.1038/news.2008.822. Available from: <http://www.nature.com/doifinder/10.1038/news.2008.822>
8. ITER. ITER - the way to new energy. [online]. 2018. Available from: <http://www.iter.org/proj/itermission>
9. FEDERICI, G., BIEL, W., GILBERT, M. R., KEMP, R., TAYLOR, N. and WENNINGER, R. European DEMO design strategy and consequences for materials. *Nuclear Fusion*. 2017. Vol. 57, no. 9. DOI 10.1088/1741-4326/57/9/092002.
10. LEONARDO CORPORATION. The Official E-Cat Website of Leonardo Corporation. [online]. 2018. Available from: <https://ecat.com>
11. FOCARDI, S and ROSSI, A. A new energy source from nuclear fusion. *Energy*. 2010. No. 1, p. 1–9.
12. HAMBLING, David. In Cold Fusion 2.0, Who's Scamming Whom? *Popular Mechanics* [online]. 2016. Available from: <https://www.popularmechanics.com/science/energy/a20454/in-cold-fusion-20-whos-scamming-whom/>
13. NREL. Andasol-1. *NREL SolarPACES* [online]. 2017. Available from: http://www.nrel.gov/csp/solarpaces/project_detail.cfm/projectID=3
14. NREL. Planta Solar 10. *NREL SolarPACES* [online]. 2015. Available from: http://www.nrel.gov/csp/solarpaces/project_detail.cfm/projectID=38
15. EUROPEAN ENVIRONMENT AGENCY. Energy efficiency and energy consumption in the household sector. *Assessment published* [online]. 2012. Available from: <http://www.eea.europa.eu/data-and-maps/indicators/energy-efficiency-and-energy-consumption-5/assessment>

16. TIAN, Y. and ZHAO, C.Y. A review of solar collectors and thermal energy storage in solar thermal applications. *Applied Energy* [online]. April 2013. Vol. 104, p. 538–553. DOI 10.1016/j.apenergy.2012.11.051. Available from: <http://dx.doi.org/10.1016/j.apenergy.2012.11.051>
17. KALOGIROU, Soteris A. *Solar thermal collectors and applications*. 2004. ISBN 3572240646.
18. VOHNICKÝ, Aleš. Racionální využití sluneční energie. *TZB-info* [online]. 2004. Available from: <http://oze.tzb-info.cz/solarni-kolektory/2072-racionalni-vyuziti-slunecni-energie>
19. EUROSTAT. Housing statistics. [online]. 2015. Available from: <http://www.homesandcommunities.co.uk/housing-statistics>
20. ESTIF. Solar Thermal Markets in Europe. . 2012. No. June, p. 1–20.
21. FARZANEH, Amir and MOHAMMADI, Maysam. Aluminium Alloys - New Trends in Fabrication and Applications. In : AHMAD, Z. (ed.), *Aluminium Alloys in Solar Power – Benefits and Limitations* [online]. InTech Open Access Publisher, 2012. p. 325–359. ISBN 978-953-51-0861-0. Available from: <http://www.intechopen.com/books/aluminium-alloys-new-trends-in-fabrication-and-applications>
22. ALGHOUL, M.A., SULAIMAN, M.Y., AZMI, B.Z. and WAHAB, M.Abd. Review of materials for solar thermal collectors. *Anti-Corrosion Methods and Materials* [online]. 2005. Vol. 52, no. 4, p. 199–206. DOI 10.1108/00035590510603210. Available from: <http://www.emeraldinsight.com/doi/10.1108/00035590510603210>
23. EXERGIA S.A. *Materials used for manufacturing solar domestic hot water systems & comments on their reliability* [online]. Athens, 2004. Available from: <http://exergia.gr/wp-content/uploads/materials-domestic-water.pdf>
24. MATUŠKA, Tomáš. Prvky solárních soustav (III). *TZB-info* [online]. 2006. Available from: <http://www.tzb-info.cz/3517-prvky-solarnich-soustav-iii>
25. MATUŠKA, Tomáš. Potrubí solárních soustav. *TZB-info* [online]. 2010. Available from: <http://oze.tzb-info.cz/solarni-kolektory/150-potrubi-solarnich-soustav>
26. DEUTCHES KUPFERINSTITUT. *Die Fachrechte Kupferrohr Installation* [online]. DKI-i158-0. Düsseldorf : Deutsches Kupferinstitut, 2012. Available from: www.kupferinstitut.de
27. ISO. *ISO 10380: Pipework – Corrugated metal hoses and hose assemblies*. 2014.
28. BECHYNĚ, Milan. Spojování potrubí. *TZB-info* [online]. 2001. Available from: <http://vytapani.tzb-info.cz/potrubi-a-armatury/551-spojovani-potrubi>
29. AMERICAN IRON AND STEEL INSTITUTE. *Welding Processes for Stainless Steels. Welding of Stainless Steels and Other Joining Methods*. 1988. P. 15–32. DOI 10.4262/denkiseiko.40.117.
30. AEL HEATING. Plate Heat Exchangers from AEL Heating. [online]. 2018. [Accessed 2 March 2018]. Available from: <https://www.aelheating.com/heat-exchangers/>
31. WILO. Wilo - product finder. *Wilo* [online]. 2018. Available from: <http://productfinder.wilo.com/com/en/Wilo/home.html>

32. MIKŠÍK, František and KOTLÍK, Josef. Kombinované solární systémy v RD - energeticky rovnovážná soustava. *Energetika*. 2013. Vol. 63, no. 12, p. 716–719.
33. MIKŠÍK, František and KOTLÍK, Josef. Perspektivy využití kombinovaných solárních systémů v rodinných domech. *Energetika*. 2013. Vol. 63, no. 1, p. 20–22.
34. MINGOTTI, Nicola, CHENVIDYAKARN, Torwong and WOODS, Andrew W. The fluid mechanics of the natural ventilation of a narrow-cavity double-skin facade. *Building and Environment* [online]. April 2011. Vol. 46, no. 4, p. 807–823. DOI 10.1016/j.buildenv.2010.09.015. Available from: <http://linkinghub.elsevier.com/retrieve/pii/S0360132310003239>
35. ALKILANI, Mahmud M., SOPIAN, K., ALGHOUL, M.A., SOHIF, M. and RUSLAN, M.H. Review of solar air collectors with thermal storage units. *Renewable and Sustainable Energy Reviews* [online]. April 2011. Vol. 15, no. 3, p. 1476–1490. DOI 10.1016/j.rser.2010.10.019. Available from: <http://linkinghub.elsevier.com/retrieve/pii/S1364032110003692>
36. LIDE, David R. *CRC Handbook of Chemistry and Physics 88th Edition* [online]. 2007. ISBN 0849304881. Available from: <http://books.google.com/books?id=gb8OAwAACAAJ&printsec=frontcover>
37. MOSS, G. P., SMITH, P. A. S. and TAVERNIER, D. *Glossary of class names of organic compounds and reactivity intermediates based on structure (IUPAC Recommendations 1995)* [online]. 1995. ISBN 0-521-51150-X. Available from: <https://www.degruyter.com/view/j/pac.1995.67.issue-8-9/pac199567081307/pac199567081307.xml>
38. WERLE, Peter and MORAWIETZ, Marcus. Alcohols, Polyhydric. In : *Ullmann's Encyclopedia of Industrial Chemistry* [online]. Weinheim, Germany : Wiley-VCH Verlag GmbH & Co. KGaA, 2000. Available from: http://doi.wiley.com/10.1002/14356007.a01_305
39. THE DOW CHEMICAL COMPANY. *A Guide to Glycols*. 2003.
40. IWAMOTO, Reikichi, MATSUDA, Toshihiko and KUSANAGI, Hiroshi. Contrast effect of hydrogen bonding on the acceptor and donor OH groups of intramolecularly hydrogen-bonded OH pairs in diols. *Spectrochimica Acta - Part A: Molecular and Biomolecular Spectroscopy*. 2005. Vol. 62, no. 1–3, p. 97–104. DOI 10.1016/j.saa.2004.12.007.
41. BOSEN, Sidney F., BOWLES, William A., FORD, Emory A. and PERLSON, Bruce D. Antifreezes. In : *Ullmann's Encyclopedia of Industrial Chemistry* [online]. Weinheim, Germany : Wiley-VCH Verlag GmbH & Co. KGaA, 2000. Available from: http://doi.wiley.com/10.1002/14356007.a03_023
42. PATRICK, Bethanne Kelly. and THOMPSON, John M. (John Milliken). *An uncommon history of common things*. 2009. ISBN 1426204205.
43. MATUŠKA, Tomáš. Prvky solárních soustav (I). *TZB-info* [online]. 2006. Available from: <http://www.tzb-info.cz/>
44. HUDGENS, R. Douglas, HERCAMP, Richard D., FRANCIS, Jaime, NYMAN, Dan A. and BARTOLI, Yolanda. An evaluation of glycerin (glycerol) as a heavy duty engine antifreeze/coolant base. *SAE Technical Paper 2007-01-4000* [online]. 2007. No. 724, p. 776–790. DOI 10.4271/2007-01-4000. Available from: <http://www.sae.org/technical/papers/2007-01-4000>

45. THIRUGNANASAMBANDAM, M, INIYAN, S and GOIC, R. A review of solar thermal technologies. *Renewable & Sustainable Energy Reviews*. 2010. Vol. 14, no. 1, p. 312–322. DOI 10.1016/j.rser.2009.07.014.
46. MIKŠÍK, František. *Nemrzoucí teplotnosné kapaliny pro solární systémy*. Brno University of Technology, 2010.
47. RIETJENS, S. J., DE LANGE, D. W. and MEULENBELT, J. Ethylene glycol or methanol intoxication: Which antidote should be used, fomepizole or ethanol? *Netherlands Journal of Medicine*. 2014. Vol. 72, no. 2, p. 73–79.
48. JUGER, Joseph J. and CROOK, Richard F. Heat Transfer Performance of Propylene Glycol Versus Ethylene Glycol Coolant Solutions in Laboratory Testing. In : [online]. 1 March 1999. Available from: <http://papers.sae.org/1999-01-0129/>
49. REBSDAT, Siegfried and MAYER, Dieter. Ethylene Glycol. In : *Ullmann's Encyclopedia of Industrial Chemistry* [online]. Weinheim, Germany : Wiley-VCH Verlag GmbH & Co. KGaA, 2000. Available from: http://doi.wiley.com/10.1002/14356007.a10_101
50. PILLARD, D. A. and DUFRESNE, D. L. Toxicity of formulated glycol deicers and ethylene and propylene glycol to *Lactuca sativa*, *Lolium perenne*, *Selenastrum capricornutum*, and *Lemna minor*. *Archives of Environmental Contamination and Toxicology* [online]. 1999. Vol. 37, no. 1, p. 29–35. DOI 10.1007/s002449900486. Available from: <http://link.springer.com/10.1007/s002449900486>
51. OECD. 11th SIAM: *Propylene glycol: SIDS Initial Assessment Profile* [online]. 2001. OECD SIDS. Available from: <http://www.inchem.org>
52. RUDDICK, Joseph A. Toxicology, metabolism, and biochemistry of 1,2-propanediol. *Toxicology and Applied Pharmacology*. 1972. Vol. 21, no. 1, p. 102–111. DOI 10.1016/0041-008X(72)90032-4.
53. SKOLIL, Jan. *Physicochemical Aspects of Ecological Heat-Transfer Fluids*. Brno University of Technology, 2016.
54. SULLIVAN, Carl J. Propanediols. In : *Ullmann's Encyclopedia of Industrial Chemistry* [online]. Weinheim, Germany : Wiley-VCH Verlag GmbH & Co. KGaA, 2000. Available from: http://doi.wiley.com/10.1002/14356007.a22_163
55. MUSKA, Carl F and ALLES, Carina. A New Platform Chemical For The 21st Century. *BREW Symposium* [online]. 2005. P. 1–38. Available from: <http://brew.geo.uu.nl/BREWsymposiumWiesbaden11mei2005/WEBSITEBrewPresentations51105.PDF>
56. KRAUS, George A. Synthetic methods for the preparation of 1,3-propanediol. *Clean - Soil, Air, Water*. 2008. Vol. 36, no. 8, p. 648–651. DOI 10.1002/clen.200800084.
57. EATON, Edward R., BOON, W. H. and SMITH, Chris J. A Chemical Base for Engine Coolant / Antifreeze with Improved Thermal Stability Properties. In : *Journal of Catalysis* [online]. 5 March 2001. p. 170–177. Available from: <http://papers.sae.org/2001-01-1182/>
58. KURIAN, Joseph V. A New Polymer Platform for the Future — Sorona® from Corn Derived 1,3-Propanediol. *Journal of Polymers and the Environment* [online]. April 2005. Vol. 13, no. 2, p. 159–167. DOI 10.1007/s10924-005-2947-7. Available from: <http://link.springer.com/10.1007/s10924-005-2947-7>

59. US-EPA. *1,3-Propanediol; Exemptions From the Requirement of a Tolerance* [online]. 2013. Available from: <https://www.federalregister.gov/articles/2013/06/12/2013-13823/13-propanediol-exemptions-from-the-requirement-of-a-tolerance>
60. WOOD, David. GRAS exemption claim: 1,3-propanediol. [online]. 2009. P. 1–7. Available from: <https://www.fda.gov/downloads/Food/IngredientsPackagingLabeling/GRAS/NoticeInventory/ucm269352.pdf>
61. GARG, Uttam, FRAZEE, C Clinton, KISCOAN, Mike, SCOTT, David, PETERSON, Bonita and CATHCART, David. A Fatality Involving 1,3-Propanediol and its Implications in Measurement of other Glycols. *Journal of Analytical Toxicology*. 2008. Vol. 32, no. May, p. 324–326.
62. REZENDE, Daniel, VEREZA, Felipe, PEREIRA, Leonardo and AVILA, Ronaldo. Technical evaluation of a glycerol-based automotive cooling fluid. [online]. 2010. Vol. 7, p. 3–10. DOI 10.4271/2010-36-0010. Available from: <http://www.sae.org/technical/papers/2010-36-0010>
63. CHRISTOPH, Ralf, SCHMIDT, Bernd, STEINBERNER, Udo, DILLA, Wolfgang and KARINEN, Reetta. Glycerol. In : *Ullmann's Encyclopedia of Industrial Chemistry* [online]. Weinheim, Germany : Wiley-VCH Verlag GmbH & Co. KGaA, 2006. Available from: http://doi.wiley.com/10.1002/14356007.a12_477.pub2
64. NOBEL, Alfred. Improved explosive compound. US78317A. 1868. USA.
65. OECD. 14th SIAM: *Glycerol: SIDS Initial Assessment Profile* [online]. Paris, 2002. OECD SIDS. Available from: <http://www.inchem.org>
66. WORLD HEALTH ORGANIZATION, WHO. Electronic nicotine delivery systems. *Conference of the Parties to the WHO Framework Convention on Tobacco Control* [online]. 2014. No. October, p. 13. DOI 10.1001/jama.2013.285347.2. Available from: http://apps.who.int/gb/fctc/PDF/cop6/FCTC_COP6_10Rev1-en.pdf?ua=1
67. MATUŠKA, Tomáš. Problematika stagnace u solárních tepelných soustav (I). *TZB-info* [online]. 2006. Available from: <http://www.tzb-info.cz/3462-problematika-stagnace-u-solarnich-tepelných-soustav-i>
68. LINSTROM, P. J. and MALLARD, W. G. NIST chemistry Webbook. *Choice Reviews Online* [online]. 1 January 1998. Vol. 35, no. 05, p. 35–2709. [Accessed 30 July 2017]. DOI 10.5860/CHOICE.35-2709. Available from: <http://choicereviews.org/review/10.5860/CHOICE.35-2709>
69. GÓRALSKI, Pawel and TKACZYK, Mariola. Heat Capacities of Some Liquid α , ω -Alkanediols within the Temperature Range between (293 . 15 and 353 . 15) K. *Journal of Chemical & Engineering Data*. 2008. Vol. 111, no. 53, p. 1932–1934. DOI 10.1021/je800356x.
70. ZOREŃSKI, Edward, DZIDA, Marzena and PIOTROWSKA, Martyna. Study of the Acoustic and Thermodynamic Properties of 1,2- and 1,3-Propanediol by Means of High-Pressure Speed of Sound Measurements at Temperatures from (293 to 318) K and Pressures up to 101 MPa. *Journal of Chemical & Engineering Data* [online]. 12 January 2008. Vol. 53, no. 1, p. 136–144. DOI 10.1021/je7004374. Available from: <http://pubs.acs.org/doi/abs/10.1021/je7004374>
71. ZÁBRANSKÝ, Milan, KOLSKÁ, Zdenka, RŮŽIČKA, Vlastimil and DOMALSKI, Eugene S. Heat capacity of liquids: Critical review and recommended values.

- Supplement ii. *Journal of Physical and Chemical Reference Data*. 2010. Vol. 39, no. 1, p. 3–404. DOI 10.1063/1.3182831.
72. WEINGÄRTNER, Hermann, FRANCK, Ernst Ulrich, WIEGAND, Gabriele, DAHMEN, Nicolaus, SCHWEDT, Georg, FRIMMEL, Fritz H., GORDALLA, Birgit C., JOHANNSEN, Klaus, SUMMERS, R. Scott, HÖLL, Wolfgang, JEKEL, Martin, GIMBEL, Rolf, RAUTENBACH, Robert and GLAZE, William H. Water. In : *Ullmann's Encyclopedia of Industrial Chemistry* [online]. Weinheim, Germany : Wiley-VCH Verlag GmbH & Co. KGaA, 2000. Available from: http://doi.wiley.com/10.1002/14356007.a28_001
 73. MOELBERT, Susanne, NORMAND, B. and DE LOS RIOS, Paolo. Kosmotropes and chaotropes: modelling preferential exclusion, binding and aggregate stability. *Biophysical Chemistry* [online]. December 2004. Vol. 112, no. 1, p. 45–57. DOI 10.1016/j.bpc.2004.06.012. Available from: <http://linkinghub.elsevier.com/retrieve/pii/S0301462204001644>
 74. SOKHAN, Vlad P., JONES, Andrew P., CIPCIGAN, Flaviu S., CRAIN, Jason and MARTYNA, Glenn J. Signature properties of water: Their molecular electronic origins. *Proceedings of the National Academy of Sciences* [online]. 2015. Vol. 112, no. 20, p. 6341–6346. DOI 10.1073/pnas.1418982112. Available from: <http://www.pnas.org/lookup/doi/10.1073/pnas.1418982112>
 75. FRANKS, F. and IVES, D. J. G. The structural properties of alcohol–water mixtures. *Q. Rev. Chem. Soc.* [online]. 1966. Vol. 20, no. 1, p. 1–44. DOI 10.1039/QR9662000001. Available from: <http://xlink.rsc.org/?DOI=QR9662000001>
 76. NAGAMACHI, M. Y. and FRANCESCONI, A. Z. Measurement and correlation of excess molar enthalpy H_{EM} for (1,2-propanediol, or 1,3-propanediol, or 1,4-butanediol + water) at the temperatures (298.15, 323.15, and 343.15) K. *Journal of Chemical Thermodynamics*. 2006. Vol. 38, no. 4, p. 461–466. DOI 10.1016/j.jct.2005.06.018.
 77. TAKAIZUMI, K. and WAKABAYASHI, T. The freezing process in methanol-, ethanol-, and propanol-water systems as revealed by differential scanning calorimetry. *Journal of Solution Chemistry* [online]. 1997. Vol. 26, no. 10, p. 927–939. DOI 10.1007/BF02768051. Available from: http://apps.webofknowledge.com/full_record.do?product=UA&search_mode=General Search&qid=1&SID=Y1YBLiBGjwSabrJyRML&page=1&doc=1
 78. FULLERTON, Gary D., KEENER, Carl R. and CAMERON, Ivan L. Correction for solute/solvent interaction extends accurate freezing point depression theory to high concentration range. *Journal of Biochemical and Biophysical Methods*. 1994. Vol. 29, no. 3–4, p. 217–235. DOI 10.1016/0165-022X(94)90034-5.
 79. CORDRAY, Dennis R., KAPLAN, Lisa R., WOYCIESJES, Peter M. and KOZAK, Theodore F. Solid - liquid phase diagram for ethylene glycol + water. *Fluid Phase Equilibria*. 1996. Vol. 117, no. 1–2 pt 2, p. 146–152. DOI 10.1016/0378-3812(95)02947-8.
 80. HAUSNER, Robert and FINK, Christian. Stagnation behaviour of solar thermal systems. *IEA Task 26*. 2002. No. November.
 81. HARRISON, Stephen and CRUICKSHANK, Cynthia A. A review of strategies for the control of high temperature stagnation in solar collectors and systems. *Energy Procedia* [online]. 2012. Vol. 30, p. 793–804. DOI 10.1016/j.egypro.2012.11.090. Available

from: <http://dx.doi.org/10.1016/j.egypro.2012.11.090>

82. MATUŠKA, Tomáš. Problematika stagnace u solárních tepelných soustav (II). *TZB-info* [online]. 2006. Available from: <http://www.tzb-info.cz/3474-problematika-stagnace-u-solarnich-tepelnych-soustav-ii>
83. DRAGSTED, Janne, FURBO, Simon, CHEN, Ziqian and PERERS, Bengt. Pressure and Temperature Development in a Solar Heating System During Stagnation. In : *Proceedings of the EuroSun 2010 Conference* [online]. Freiburg, Germany : International Solar Energy Society, 2010. p. 1–8. ISBN 978-3-901425-13-4. Available from: <http://proceedings.ises.org/citation?doi=eurosun.2010.07.06>
84. SPÄTE, Frank and LADENER, Heinz. *Solaranlagen, Handbuch der thermischen Solarenergienutzung*. Staufen bei Freiburg : Ökobuch, 2011. ISBN 978-3-936896-40-4.
85. WONG, D., SWETTE, L. and COCKS, F. H. Aluminum Corrosion in Uninhibited Ethylene Glycol-Water Solutions. *Journal of The Electrochemical Society* [online]. 1979. Vol. 126, no. 1, p. 11–15. DOI 10.1149/1.2128966. Available from: <http://jes.ecsdl.org/content/126/1/11%5Cnhttp://jes.ecsdl.org/content/126/1/11.abstract>
86. DOW CHEMICAL COMPANY. *DOWTHERM™ and DOWFROST™ Heat Transfer Fluids : Inhibited vs Uninhibited Glycols*. [no date].
87. DIEGLE, R. B., BEAVERS, J. A. and CLIFFORD, J. E. *Corrosion Problems with aqueous coolants*. 1980.
88. SAJI, Viswanathan S. A Review on Recent Patents in Corrosion Inhibitors. *Recent Patents on Corrosion Science* [online]. 2010. Vol. 2, no. 1, p. 6–12. DOI 10.2174/1877610801002010006. Available from: <http://benthamscience.com/open/openaccess.php?rptcs/articles/V002/6RPTCS.htm>
89. MARCUS, P. *Corrosion mechanisms in theory and practice, Third edition*. 3, revised. CRC Press, 2011. ISBN 9781420094626.
90. FARMER, Joseph, CHOI, Jor Shan, SAW, Cheng, HASLAM, Jeffrey, DAY, Dan, HAILEY, Phillip, LIAN, Tiangan, REBAK, Raul, PEREPEZKO, John, PAYER, Joe, BRANAGAN, Daniel, BEARDSLEY, Brad, D'AMATO, Andy and APRIGLIANO, Lou. Iron-Based amorphous metals: High-performance corrosion-resistant material development. *Metallurgical and Materials Transactions A: Physical Metallurgy and Materials Science*. 2009. Vol. 40, no. 6, p. 1289–1305. DOI 10.1007/s11661-008-9779-8.
91. CONSULTANTS CODE, Inc. Antifreeze Solutions in Home Fire Sprinkler Systems. *SpringerBriefs in Fire* [online]. 2010. DOI 10.1007/978-1-4614-3840-3. Available from: <http://link.springer.com/10.1007/978-1-4614-3840-3>
92. DARIVA, Camila G. and GALIO, Alexandre F. Corrosion Inhibitors – Principles, Mechanisms and Applications. In : *Developments in Corrosion Protection* [online]. InTech, 2014. ISBN 978-953-51-1223-5. Available from: <http://www.intechopen.com/books/developments-in-corrosion-protection/corrosion-inhibitors-principles-mechanisms-and-applications>
93. HOLUB, Luděk, MATĚJKA, Jindřich and HOFMANOVÁ, Helena. Nepěňivá kapalina na bázi 1,2-ethandiolu nebo 1,2-propandiolu a vody k přenosu tepla. 251846. 1987. Czechoslovak Socialist Republic : Úřad pro vynálezy a objevy.
94. HOLUB, Luděk, HOFMANOVÁ, Helena, MATĚJKA, Jindřich and MICHALIČKA, Ladislav. Vícesložková nemrznoucí kapalina pro tepelná čerpadla a solární systémy.

246633. 1987. Czechoslovak Socialist Republic : Úřad pro vynálezy a objevy.
95. KUZNETSOV, Yurii I., MERCER, A. D. and THOMAS, J. G. N. Organic Corrosion Inhibitors for Cooling Systems. In : *Organic Inhibitors of Corrosion of Metals* [online]. Boston, MA : Springer US, 1996. p. 225–246. Available from: http://link.springer.com/10.1007/978-1-4899-1956-4_5
 96. WINKLER, David and A., David. Predicting the Performance of Organic Corrosion Inhibitors. *Metals* [online]. 2017. Vol. 7, no. 12, p. 553. DOI 10.3390/met7120553. Available from: <http://www.mdpi.com/2075-4701/7/12/553>
 97. IPCS. Chemical safety information from intergovernmental organizations. [online]. 2017. [Accessed 3 March 2018]. Available from: <http://www.inchem.org/>
 98. WORLD HEALTH ORGANIZATION (WHO), INTERNATIONAL LABOUR ORGANIZATION (ILO) and EUROPEAN UNION. The International Chemical Safety Cards (ICSC) database. [online]. 2017. [Accessed 3 March 2018]. Available from: <http://www.ilo.org/dyn/icsc/>
 99. OECD. OECD Screening Information DataSet (SIDS) database. *OECD Guidelines for the Testing of Chemicals, Section 3* [online]. 2017. Available from: <http://www.oecd.org/env/hazard/data>
 100. OECD. Ethylene glycol group: SIDS Initial Assessment Profile. [online]. 2004. No. April, p. 20–23. Available from: <http://www.inchem.org>
 101. LISSNER, Heidi, WEHRER, Markus, REINICKE, Martin, HORVÁTH, Nikoletta and TOTSCHKE, Kai Uwe. Constraints of propylene glycol degradation at low temperatures and saturated flow conditions. *Environmental Science and Pollution Research*. 2015. Vol. 22, no. 4, p. 3158–3174. DOI 10.1007/s11356-014-3506-3.
 102. DOBSON, S. *Concise International Chemical Assessment Document 22: Ethylene glycol: Environmental aspects*. Geneva, 2000. ISBN 92-4-153022-7.
 103. OECD. *Test No. 301: Ready Biodegradability* [online]. Paris : OECD Publishing, 1992. OECD Guidelines for the Testing of Chemicals, Section 3. ISBN 9789264070349. Available from: http://www.oecd-ilibrary.org/environment/test-no-301-ready-biodegradability_9789264070349-en
 104. ZHANG, Shaoyan, LIU, Quanyao, FAN, Guoli and LI, Feng. Highly-dispersed copper-based catalysts from Cu-Zn-Al layered double hydroxide precursor for gas-phase hydrogenation of dimethyl oxalate to ethylene glycol. *Catalysis Letters*. 2012. Vol. 142, no. 9, p. 1121–1127. DOI 10.1007/s10562-012-0871-8.
 105. TEUNISSEN, Herman T. and ELSEVIER, Cornelis J. Ruthenium Catalysed Hydrogenation of Dimethyl Oxalate to Ethylene Glycol. *Chemical Communications*. 1997. No. 12 ml, p. 667. DOI 10.1039/a700862g.
 106. KAHLICH, Dietmar, WIECHERN, Uwe and LINDNER, Jörg. Propylene Oxide. In : *Ullmann's Encyclopedia of Industrial Chemistry* [online]. Weinheim, Germany : Wiley-VCH Verlag GmbH & Co. KGaA, 2000. Available from: http://doi.wiley.com/10.1002/14356007.a22_239
 107. PLAHUTA, Joseph M, TEEL, Amy L, AHMAD, Mushtaque, BEUTEL, Mark W, RENTZ, Jeremy A and WATTS, Richard J. Oxidized starch solutions for environmentally friendly aircraft deicers. *Water environment research : a research publication of the Water Environment Federation*. 2011. Vol. 83, no. 9, p. 826–833. DOI 10.2175/106143011X12928814445050.

108. EPA. Managing Aircraft and Airfield Deicing Operations to Prevent Contamination of Drinking Water I. WATER, Office of (ed.), *United States Environmental Protection Agency* [online]. 2010. No. 4606, p. 12. Available from: www.epa.gov/safewater
109. US-EPA. *Source Water Protection Practices Bulletin Managing Stormwater Runoff to Prevent Contamination of Drinking Water* [online]. Washington : USEPA East, 2010. Available from: www.epa.gov/safewater
110. CIRIMINNA, Rosaria, PINA, Cristina Della, ROSSI, Michele and PAGLIARO, Mario. Understanding the glycerol market. *European Journal of Lipid Science and Technology* [online]. October 2014. Vol. 116, no. 10, p. 1432–1439. DOI 10.1002/ejlt.201400229. Available from: <http://doi.wiley.com/10.1002/ejlt.201400229>
111. GARGALO, Carina L., CHEALI, Peam, GERNAEY, Krist V. and SIN, Gürkan. Techno-economic risk analysis of glycerol biorefinery concepts against market price fluctuation. In : *AIChE Annual Meeting 2015*. 2015.
112. CLIFTON, James R, ROSSITER, Walter J. and BROWN, Paul W. Degraded aqueous glycol solutions: pH values and the effects of common ions on suppressing pH decreases. *Solar Energy Materials* [online]. March 1985. Vol. 12, no. 1, p. 77–86. DOI 10.1016/0165-1633(85)90026-7. Available from: <http://linkinghub.elsevier.com/retrieve/pii/0165163385900267>
113. ROSSITER, Walter J., GODETTE, McClure, BROWN, Paul W. and GALUK, Kevin G. An investigation of the degradation of aqueous ethylene glycol and propylene glycol solutions using ion chromatography. *Solar Energy Materials* [online]. January 1985. Vol. 11, no. 5–6, p. 455–467. DOI 10.1016/0165-1633(85)90016-4. Available from: <http://linkinghub.elsevier.com/retrieve/pii/0165163385900164>
114. ROSSITER, Walter J., BROWN, Paul W. and GODETTE, McClure. The determination of acidic degradation products in aqueous ethylene glycol and propylene glycol solutions using ion chromatography. *Solar Energy Materials* [online]. October 1983. Vol. 9, no. 3, p. 267–279. DOI 10.1016/0165-1633(83)90049-7. Available from: <http://linkinghub.elsevier.com/retrieve/pii/0165163383900497>
115. ASTM D1384. *Standard Test Method for Corrosion Test for Engine Coolants in Glassware* [online]. 2004. West Conshohocken, PA : ASTM International. Available from: www.astm.org
116. HILLERNS, Frank. The Behaviour of Heat Transfer Media in Solar Active Thermal Systems in View of the Stagnation Conditions. In : *9. Symposium Thermal Solar Energy in Staffelstein*. 1999. p. 1–3.
117. QUILES, Pedro V., AGUILAR, Francisco J. and ALEDO, Simón. Analysis of the overheating and stagnation problems of solar thermal installations. *Energy Procedia* [online]. 2014. Vol. 48, p. 172–180. DOI 10.1016/j.egypro.2014.02.022. Available from: <http://dx.doi.org/10.1016/j.egypro.2014.02.022>
118. MERCUS, David, DIDELOT, Aurélien, CAPON, Fabien, PIERSON, Jean-François, HAFNER, Bernd, PAZIDIS, Alexandra, FÖSTE, Sebastian and REINEKE-KOCH, Rolf. Innovative Smart Selective Coating to Avoid Overheating in Highly Efficient Thermal Solar Collectors. *Energy Procedia* [online]. June 2016. Vol. 91, p. 84–93. DOI 10.1016/j.egypro.2016.06.177. Available from: <http://linkinghub.elsevier.com/retrieve/pii/S1876610216302752>

119. FÖSTE, Sebastian, PAZIDIS, Alexandra, REINEKE-KOCH, Rolf, HAFNER, Bernd, MERCS, David and DELORD, Christine. Flat Plate Collectors with Thermochromic Absorber Coatings to Reduce Loads during Stagnation. *Energy Procedia* [online]. 2016. Vol. 91, p. 42–48. DOI 10.1016/j.egypro.2016.06.169. Available from: <http://dx.doi.org/10.1016/j.egypro.2016.06.169>
120. SLAMAN, M. and GRIESSEN, R. Solar collector overheating protection. *Solar Energy* [online]. 2009. Vol. 83, no. 7, p. 982–987. DOI 10.1016/j.solener.2009.01.001. Available from: <http://dx.doi.org/10.1016/j.solener.2009.01.001>
121. NATIONAL CENTER FOR BIOTECHNOLOGY INFORMATION. Propanediol. *PubChem Compound database; CID=10442* [online]. 2018. [Accessed 1 May 2018]. Available from: <https://pubchem.ncbi.nlm.nih.gov/compound/10442>
122. HOUCK, Max M, HUFF, Rebecca A, LOWE, Preston C and MENOLD, Ronald E. Poly (Trimethylene Terephthalate): A “New” Type of Polyester Fiber. *Forensic Science Communications* [online]. 2001. Vol. 3, no. 3, p. 1–4. Available from: <http://www.fbi.gov/hq/lab/fsc/backissu/july2001/houck.htm>
123. WANG, Keyi, HAWLEY, Martin C and DEATHOS, Scott J. Conversion of glycerol to 1, 3-propanediol via selective dehydroxylation. *Industrial & engineering chemistry research*. 2003. Vol. 42, no. 13, p. 2913–2923. DOI 10.1021/ie020754h.
124. PAPANIKOLAOU, Seraphim, FAKAS, Stylianos, FICK, Michel, CHEVALOT, Isabelle, GALIOTOU-PANAYOTOU, Maria, KOMAITIS, Michael, MARC, Ivan and AGGELIS, George. Biotechnological valorisation of raw glycerol discharged after bio-diesel (fatty acid methyl esters) manufacturing process: Production of 1,3-propanediol, citric acid and single cell oil. *Biomass and Bioenergy*. 2008. Vol. 32, no. 1, p. 60–71. DOI 10.1016/j.biombioe.2007.06.007.
125. SZYMANOWSKA-POWAŁOWSKA, Daria, DROŹDŹYŃSKA, Agnieszka and REMSZEL, Natalia. Isolation of New Strains of Bacteria Able to Synthesize 1,3-Propanediol from Glycerol *. *Advances in Microbiology* [online]. 2013. Vol. 3, no. June, p. 171–180. DOI 10.4236/aim.2013.32027. Available from: <http://dx.doi.org/10.4236/aim.2013.32027>
<http://www.scirp.org/journal/aim>
126. QUISPE, César A.G., CORONADO, Christian J.R. and CARVALHO JR., João A. Glycerol: Production, consumption, prices, characterization and new trends in combustion. *Renewable and Sustainable Energy Reviews* [online]. November 2013. Vol. 27, p. 475–493. DOI 10.1016/j.rser.2013.06.017. Available from: <http://dx.doi.org/10.1016/j.rser.2013.06.017>
127. RATANAPARIYANUCH, Kornsuree, SHIM, Youn Young, EMAMI, Shahram and REANEY, Martin J. T. Production of Protein Concentrate and 1,3-Propanediol by Wheat-Based Thin Stillage Fermentation. *Journal of Agricultural and Food Chemistry* [online]. 17 May 2017. Vol. 65, no. 19, p. 3858–3867. DOI 10.1021/acs.jafc.7b00772. Available from: <http://pubs.acs.org/doi/abs/10.1021/acs.jafc.7b00772>
128. SAXENA, R. K., ANAND, Pinki, SARAN, Saurabh and ISAR, Jasmine. Microbial production of 1,3-propanediol: Recent developments and emerging opportunities. *Biotechnology Advances* [online]. 2009. Vol. 27, no. 6, p. 895–913. DOI 10.1016/j.biotechadv.2009.07.003. Available from: <http://dx.doi.org/10.1016/j.biotechadv.2009.07.003>
129. ASTM D3306. *Standard Specification for Glycol Base Engine Coolant for Automobile and Light-Duty Service* [online]. 2014. West Conshohocken, PA, PA : ASTM

- International. Available from: www.astm.org
130. ASTM D6210. *Standard Specification for Fully-Formulated Glycol Base Engine Coolant for Heavy-Duty Engines* [online]. 2017. West Conshohocken, PA : ASTM International. Available from: www.astm.org
 131. FRITSCH, R.J. and KRAUSE, I. ELECTROPHORESIS. In : *Encyclopedia of Food Sciences and Nutrition* [online]. Elsevier, 2003. p. 2055–2062. [Accessed 26 March 2018]. ISBN 9780122270550. Available from: <http://linkinghub.elsevier.com/retrieve/pii/B012227055X014097>
 132. KOHLRAUSCH, F. Ueber Concentrations_ Verschiebungen durch Electrolyse in Inneren von Losungen und Losungsgemischen. *Annalen der Physik*. 1897. Vol. 62, p. 209–239.
 133. PASCHKEWITZ, John S., MOLHO, Joshua I., XU, Hui, BHARADWAJ, Rajiv and PARK, C. Charles. Turn-induced isotachophoretic focusing in microfluidic channels. *Electrophoresis*. 2007. Vol. 28, no. 24, p. 4561–4571. DOI 10.1002/elps.200700320.
 134. MOSHER, R A, SAVILLE, D A, THORMANN, W and RADOLA, B J. *The Dynamics of Electrophoresis*. New York : Weinheim, 1992. ISBN 1-56081-192-7.
 135. LIU, Bingwen and IVORY, Cornelius F. Isotachophoresis with counterflow in an open capillary: Computer simulation and experimental validation. *Journal of Separation Science*. 2013. Vol. 36, no. 12, p. 1986–1995. DOI 10.1002/jssc.201300066.
 136. CUI, By Huanchun and IVORY, Cornelius F. Isotachophoresis. *Electrophoresis Society* [online]. 2008. [Accessed 3 March 2018]. Available from: <http://www.aesociety.org/areas/pdfs/IsotachophoresisCuiIvory2-08.pdf>
 137. JUNG, Byoungsok, BHARADWAJ, Rajiv and SANTIAGO, Juan G. On-chip millionfold sample stacking using transient isotachophoresis. *Analytical Chemistry*. 2006. Vol. 78, no. 7, p. 2319–2327. DOI 10.1021/ac051659w.
 138. RECMAN. *Stanovení vybraných organických a anorganických kyselin v cukru a v cukerných roztocích III* [online]. 2003. Available from: http://www.recman.cz/pdf/aplikacni_list_13.pdf
 139. LINSCHIED, Michael. Mass Spectrometry. In : *Ullmann's Encyclopedia of Industrial Chemistry* [online]. Weinheim, Germany : Wiley-VCH Verlag GmbH & Co. KGaA, 2001. Available from: http://doi.wiley.com/10.1002/14356007.b05_515
 140. AGILENT TECHNOLOGIES. *Agilent 6300 Ion Trap LC/MS Systems Concepts Guide* [online]. 2006. Available from: http://www.agilent.com/cs/library/usermanuals/Public/G2440-90096_Concepts_6.1.pdf
 141. YAMASHITA, Masamichi and FENN, John B. Electrospray ion source. Another variation on the free-jet theme. *Journal of Physical Chemistry*. 1984. Vol. 88, no. 20, p. 4451–4459. DOI 10.1021/j150664a002.
 142. TAFLIN, Daniel C., WARD, Timothy L. and DAVIS, E. James. Electrified Droplet Fission and the Rayleigh Limit. *Langmuir*. 1989. Vol. 5, no. 2, p. 376–384. DOI 10.1021/la00086a016.
 143. STAFFORD, George. Ion trap mass spectrometry: A personal perspective. *Journal of the American Society for Mass Spectrometry*. 2002. Vol. 13, no. 6, p. 589–596. DOI 10.1016/S1044-0305(02)00385-9.
 144. HPLC - Mass Spectrometry. *Universidad de Antioquia - Instituto de Química* [online].

- [Accessed 1 March 2018]. Available from:
<http://quimica.udea.edu.co/~carlopez/cromatohplc/hplc-ms.html>
145. SCIENTIFIC INSTRUMENT SERVICES INC. KD Scientific KDS100 Infusion Pump. *KD Scientific Infusion Syringe Pumps for Mass Spectrometry* [online]. 2017. [Accessed 1 March 2018]. Available from: <http://www.sisweb.com/lc/kd-scientific-kds100.htm>
 146. FISCHER, Karl. Neues Verfahren zur maßanalytischen Bestimmung des Wassergehaltes von Flüssigkeiten und festen Körpern. *Angewandte Chemie* [online]. 1935. Vol. 48, no. 26, p. 394–396. DOI 10.1002/ange.19350482605. Available from: <http://doi.wiley.com/10.1002/ange.19350482605>
 147. CEDERGREN, Anders. Comparison between Bipotentiometric and True Potentiometric End-Point Detection Using Rapidly Reacting Karl Fischer Reagents. *Analytical Chemistry*. 1996. Vol. 68, no. 20, p. 3679–3681. DOI 10.1021/ac960047w.
 148. MARGOLIS, Sam A. Source of the difference between the measurement of water in hydrocarbons as determined by the volumetric and coulometric Karl Fischer methods. *Analytical Chemistry*. 1999. Vol. 71, no. 9, p. 1728–1732. DOI 10.1021/ac981137z.
 149. HONEYWELL. Volumetric KF Titration. *Research Chemicals Shop* [online]. 2018. [Accessed 8 March 2018]. Available from: <https://shop-lab-honeywell.com/products/featured-hydranal/volumetric-kf-titration>
 150. METROHM. *Determination of the water content in tooth paste with MATi 10*. Metrohm.
 151. SCHOLZ, Eugen. *Karl Fischer Titration: Determination of Water* [online]. 2012. ISBN 3642699898. Available from: <https://books.google.com/books?id=bbL0CAAQBAJ&pgis=1>
 152. ASTM D1123 - 99. *Standard Test Methods for Water in Engine Coolant Concentrate by the Karl Fischer* [online]. 2015. West Conshohocken, PA : ASTM International. Available from: www.astm.org
 153. BROEKAERT, José A. C. and HYWEL EVANS, E. Atomic Spectroscopy. In : *Ullmann's Encyclopedia of Industrial Chemistry* [online]. Weinheim, Germany : Wiley-VCH Verlag GmbH & Co. KGaA, 2003. Available from: http://doi.wiley.com/10.1002/14356007.b05_559
 154. KOIRTYOHANN, S. R. A history of atomic absorption spectroscopy. *Spectrochimica Acta Part B: Atomic Spectroscopy*. 1980. Vol. 35, no. 11–12, p. 663–670. DOI 10.1016/0584-8547(80)80006-1.
 155. Methods used in detecting and monitoring mercury. [online]. 2010. Available from: <http://health-hazard-mercury.blogspot.jp/2010/08/methods-used-in-detecting-and.html>
 156. LAMBERT, J H. Photometria sive de mensura de gratibus luminis, colorum umbrae (1760). *Eberhard Klett* [online]. 1892. P. 141. Available from: http://books.google.com/books?id=zmpJAAAAYAAJ&hl=&source=gbs_api
 157. BEER. Bestimmung der Absorption des rothen Lichts in farbigen Flüssigkeiten. *Annalen der Physik*. 1852. Vol. 162, no. 5, p. 78–88. DOI 10.1002/andp.18521620505.
 158. COVINGTON, A. K., BATES, R. G. and DURST, R. A. Definition of pH scales, standard reference values, measurement of pH and related terminology (Recommendations 1984). *Pure and Applied Chemistry* [online]. 1 January 1985.

- Vol. 57, no. 3, p. 531–542. DOI 10.1351/pac198557030531. Available from: <http://www.degruyter.com/view/j/pac.1985.57.issue-3/pac198557030531/pac198557030531.xml>
159. ISO. *ISO 80000-9: 2009 Quantities and units - Part 9: Physical chemistry and molecular physics*. 2009. Technical Committee : ISO/TC 12 Quantities and units.
 160. BATES, R G and GUGGENHEIM, E A. Report on the standardization of pH and related terminology. *Pure and Applied Chemistry* [online]. 1 January 1960. Vol. 1, no. 1, p. 163–168. DOI 10.1351/pac196001010163. Available from: <http://www.degruyter.com/view/j/pac.1960.1.issue-1/pac196001010163/pac196001010163.xml>
 161. ATKIN, Emma. What is the difference between a single junction and double junction pH electrode? [online]. 2017. [Accessed 1 April 2018]. Available from: <http://camblab.info/wp/index.php/what-is-the-difference-between-a-single-junction-and-double-junction-ph-electrode/>
 162. WTW. *inoLab pH Level 2 Laboratory pH meter - Operating Manual*. 2002.
 163. KITTEL, Charles. *Introduction to solid state physics*. 7th editio. Wiley India Pvt. Limited, 2007. ISBN 9788126510450.
 164. NEAMEN, Donald A. *Semiconductor physics and devices Basic principles*. 3rd Editio. McGraw-Hill, 2003. ISBN 0-07-1 19862-8.
 165. CECIL, B Y, DAVIES, Whitfield and DAVIES, C W. The Conductivity of Electrolytes. *The Journal of Physical Chemistry* [online]. 1924. Vol. 29, no. 4, p. 473–481. DOI 10.1021/j150250a011. Available from: <http://dx.doi.org/10.1021/j150250a011>
 166. BEŠTER-ROGAČ, Marija and HABE, Dušan. Modern advances in electrical conductivity measurements of solutions. *Acta Chimica Slovenica*. 2006. Vol. 53, no. 3, p. 391–395.
 167. VIANA, M., JOUANNIN, P., PONTIER, C. and CHULIA, D. About pycnometric density measurements. *Talanta*. 2002. Vol. 57, no. 3, p. 583–593. DOI 10.1016/S0039-9140(02)00058-9.
 168. LABOTIENDA. Pycnometer of Gay Lussac 25ml. [online]. [Accessed 3 April 2018]. Available from: <https://www.labotienda.com/en/laboratory-equipment/pycnometer-of-gay-lussac-25ml/>
 169. ACTTR INC. What Is The Principle of A Density Meter? [online]. 2017. [Accessed 5 April 2018]. Available from: <http://www.acttr.com/en/en-faq/en-faq-laboratory/259-en-faq-what-principle-of-density-meter.html>
 170. FURTADO, A, BATISTA, E, SPOHR, I and FILIPE, E. Measurement of density using oscillation-type density meters. Calibration, traceability and uncertainties. *Instituto Portugues da Qualidade* [online]. 2009. No. June, p. 3. Available from: <http://www.ipq.pt/backfiles/mesuremassevolumique.pdf>
 171. INTERNATIONAL ORGANIZATION FOR STANDARDIZATION. *ISO 15212: Oscillation-type density meters -- Part 1: Laboratory instruments* [online]. 1998. International Standard Organization. Available from: <https://www.iso.org/standard/28482.html>
 172. INTERNATIONAL ORGANIZATION FOR STANDARDIZATION. *ISO/IEC 17025*

- General requirements for the competence of testing and calibration laboratories*. 2005. ISBN IEC 17025.
173. INTERNATIONAL ORGANIZATION FOR STANDARDIZATION. *GUIDE 34. General requirements for the competence of reference material producers*. 2009. ISBN ISO Guide 34.
 174. ASTM D1480. *Standard Test Method for Density and Relative Density (Specific Gravity) of Viscous Materials by Bingham Pycnometer* [online]. 2015. West Conshohocken, PA : ASTM International. Available from: www.astm.org
 175. FITCH, Bennett. Anatomy of a Viscometer. *Machinery Lubrication* [online]. March 2013. P. 1–2. Available from: <http://www.machinerylubrication.com/Read/29451/anatomy-of-viscometer>
 176. UBBELOHDE, Leo. The Principle of the Suspended Level: Applications to the Measurement of Viscosity and Other Properties of Liquids. *Industrial and Engineering Chemistry - Analytical Edition*. 1937. Vol. 9, no. 2, p. 85–90. DOI 10.1021/ac50106a015.
 177. IUPAC. *Recommended Reference Materials for the Realization of Physicochemical Properties*. 1st editio. IUPAC International Union of Pure and Applied Chemistry, 1987. ISBN 9780632017188.
 178. DONTULA, Prasannarao, MACOSKO, Christopher W. and SCRIVEN, L. E. Origins of concentric cylinders viscometry. *Journal of Rheology* [online]. 2005. Vol. 49, no. 4, p. 807–818. DOI 10.1122/1.1940640. Available from: <http://sor.scitation.org/doi/10.1122/1.1940640>
 179. G.F.C SEARLE. A simple viscometer for very viscous liquids. *Mathematical Proceedings of the Cambridge Philosophical Society*. 1912. Vol. 16, p. 600–606.
 180. AUTIO, K. and HOUSKA, M. Measurement of flow curves for model liquids and real food systems with two commercial viscometers. *Journal of Food Engineering*. 1991. Vol. 13, no. 1, p. 57–66. DOI 10.1016/0260-8774(91)90037-S.
 181. FISHER, Jelena. New Viscometry: The Top 10 Benefits for Kinematic Viscosity Measurement. *Anton Paar Blog* [online]. 2017. [Accessed 4 April 2018]. Available from: <https://blog.anton-paar.com/new-viscometry-top-10-benefits-kinematic-viscosity-measurements/>
 182. Hydrodynamic Lubrication. In : *Tribology Series* [online]. 1993. p. 121–240. Available from: <http://linkinghub.elsevier.com/retrieve/pii/S0167892208705789>
 183. ASTM D7042. *Standard Test Method for Dynamic Viscosity and Density of Liquids by Stabinger Viscometer (and the Calculation of Kinematic Viscosity)* [online]. 2016. West Conshohocken, PA : ASTM International. Available from: www.astm.org
 184. ASTM D2162. *Standard Practice for Basic Calibration of Master Viscometers and Viscosity Oil Standards* [online]. 2017. West Conshohocken, PA : ASTM International. Available from: www.astm.org
 185. HECHT, Eugene. *Optics*. 4th, illus. Addison-Wesley, 2002. ISBN 9780321188786.
 186. YUNUS, W M and RAHMAN, a B. Refractive index of solutions at high concentrations. *Applied optics* [online]. 1988. Vol. 27, no. 16, p. 3341–3. DOI 10.1364/AO.27.003341. Available from: <http://www.ncbi.nlm.nih.gov/pubmed/20539378>

187. RIOBÓO, R. J., PHILIPP, M., RAMOS, M. A. and KRÜGER, J. K. Concentration and temperature dependence of the refractive index of ethanol-water mixtures: influence of intermolecular interactions. *The European physical journal. E, Soft matter*. 2009. Vol. 30, no. 1, p. 19–26. DOI 10.1140/epje/i2009-10496-4.
188. ANTON PAAR. *Abbat Universal Refractometer Series* [online]. 2013. Graz, Austria : Anton Paar GmbH. Available from: <http://www.sanicoarg.com.ar/public/files/574311be5e50e.pdf>
189. ANTON PAAR. Abbat Performance and Performance Plus Line. *Anton-Paar.com - Products* [online]. 2017. [Accessed 5 April 2018]. Available from: <https://www.anton-paar.com/corp-en/products/details/abbat-performance-and-performance-plus-line/>
190. ASTM D3321. *Standard Test Method for Use of the Refractometer for Field Test Determination of the Freezing Point of Aqueous Engine Coolants* [online]. 2013. West Conshohocken, PA : ASTM International. Available from: www.astm.org
191. ASTM D1177. *Standard Test Method for Freezing Point of Aqueous Engine Coolants* [online]. 2016. West Conshohocken, PA : ASTM International. Available from: www.astm.org
192. ASTM D7518. *Standard Specification for 1,3 Propanediol (PDO) Base Engine Coolant for Automobile and Light-Duty Service* [online]. 2015. West Conshohocken, PA, PA : ASTM International. Available from: www.astm.org
193. ASTM D2570. *Standard Test Method for Simulated Service Corrosion Testing of Engine Coolants* [online]. 2016. West Conshohocken, PA, PA : ASTM International. Available from: www.astm.org
194. ASTM D2758 - 94. *Standard Test Method for Engine Coolants by Engine Dynamometer* [online]. 2009. West Conshohocken, PA, PA : ASTM International. Available from: www.astm.org
195. SI ANALYTICS. *Visco handbook: Theory and Application of Viscometry with Glass Capillary Viscometers* [online]. 2015. Mainz, Germany : Xylem, inc., 2015. Available from: http://www.si-analytcs.com/fileadmin/upload//Broschueren_und_flyer/Kapillarviskosimetrie/INT/Handbook_Viscometry_2.7MB_PDF-English.pdf
196. ATMEL. *ATmega32A DATASHEET COMPLETE*. 2016. Atmel.
197. BROWN, Paul W., ROSSITER, Walter J. and GALUK, Kevin G. A mass spectrometric investigation of the thermal oxidative reactivity of ethylene glycol. *Solar Energy Materials* [online]. April 1986. Vol. 13, no. 3, p. 197–202. DOI 10.1016/0165-1633(86)90018-3. Available from: <http://linkinghub.elsevier.com/retrieve/pii/0165163386900183>
198. BROWN, Paul Wencil, GALUK, Kevin G. and ROSSITER, Walter J. Characterization of potential thermal degradation products from the reactions of aqueous ethylene glycol and propylene glycol solutions with copper metal. *Solar Energy Materials*. 1987. Vol. 16, no. 4, p. 309–313. DOI 10.1016/0165-1633(87)90079-7.
199. VELVANA A.S. *Solaren P Plus -30 °C - Technický list*. 2006. Velvary, Czech Republic : Velvana a.s.
200. VELVANA A.S. *Solaren P Plus -30 °C - Technický list*. 2011. Velvary, Czech Republic : Velvana a.s.

201. VELVANA A.S. *Solaren P PLUS -30 °C - Safety Data Sheet*. 2015. Velvary, Czech Republic : Velvana a.s.
202. GRÄFEN, Hubert, HORN, Elmar-Manfred, SCHLECKER, Hartmut and SCHINDLER, Helmut. Corrosion. In : *Ullmann's Encyclopedia of Industrial Chemistry* [online]. Weinheim, Germany : Wiley-VCH Verlag GmbH & Co. KGaA, 2000. Available from: http://doi.wiley.com/10.1002/14356007.b01_08
203. MONTICELLI, C., BRUNORO, G., TRABANELLI, G. and FRIGNANI, A. Corrosion in solar heating systems. I. Copper behaviour in water/glycol solutions. . 1986. Vol. 37, p. 479–484.
204. MACBETH, Gordon and RALPH THOMPSON, A. Densities and Refractive Indexes for Propylene Glycol-Water Solutions. *Analytical Chemistry*. 1951. Vol. 23, no. 4, p. 618–619. DOI 10.1021/ac60052a019.
205. SUN, T and TEJA, a S. Density, viscosity and thermal conductivity of aqueous solutions of propylene glycol, dipropylene glycol, and tripropylene glycol between 290~{K} and 460~{K}. *J. Chem. Eng. Data*. 2004. Vol. 49, p. 1311–1317.
206. THE DOW CHEMICAL COMPANY. What are the density values for glycols and glycol-water solutions? [online]. 2017. [Accessed 10 April 2018]. Available from: https://dowac.custhelp.com/app/answers/detail/a_id/7471
207. RHYS, Natasha H., GILLAMS, Richard J., COLLINS, Louise E., CALLEAR, Samantha K., LAWRENCE, M. Jayne and MCLAIN, Sylvia E. On the structure of an aqueous propylene glycol solution. *Journal of Chemical Physics*. 2016. Vol. 145, no. 22, p. 1–12. DOI 10.1063/1.4971208.
208. MONTICELLI, C., BRUNORO, G., FRIGNANI, A. and ZUCCHI, F. Corrosion behaviour of the aluminium alloy AA 6351 in glycol/water solutions degraded at elevated temperature. *Materials and Corrosion*. 1988. Vol. 39, no. 8, p. 379–384. DOI 10.1002/maco.19880390805.
209. THE DOW CHEMICAL COMPANY. What are the thermal degradation products of glycol based fluids such as DOWCAL™, DOWTHERM™ SR-1, DOWTHERM™ 4000 and DOWFROST™? *Dow Answer Center* [online]. 2017. [Accessed 10 April 2018]. Available from: https://dowac.custhelp.com/app/answers/detail/a_id/11979/related/1
210. WATANABE, Shoji. Preparations and properties of anti-corrosion additives of water-soluble metal working fluids for aluminum alloy materials. *Journal of Oleo Science* [online]. 2008. Vol. 57, no. 1, p. 1–10. DOI 10.5650/jos.57.1. Available from: <http://www.scopus.com/inward/record.url?eid=2-s2.0-40949165402&partnerID=tZOtx3y1>
211. BASHKIRCEVA, N. Y., SLADOVSKYA, O. Y., OVCHINNIKOVA, Y. S. and VAGAPOV, B. R. ANTI-CORROSION PROPERTIES OF CARBOXYLIC ACID IN WATER-GLYCOL SOLUTIONS. *Международный научно-исследовательский журнал*. 2012. Vol. 5–2, p. 73–76. DOI 10.18454/IRJ.2227-6017.
212. VELVANA A.S. SOLAREN® P PLUS -30°C. *Production list* [online]. 2018. [Accessed 2 April 2018]. Available from: <http://www.velvana.cz/produkt/solaren-p-plus-30-c>
213. SEITZ, Ulrike, BONN, Günther, OEFNER, Peter and POPP, Michael. Isotachophoretic analysis of flavonoids and phenolcarboxylic acids of relevance to phytopharmaceutical

- industry. *Journal of Chromatography A*. 1991. Vol. 559, no. 1–2, p. 499–504. DOI 10.1016/0021-9673(91)80097-Z.
214. MASÁR, Marián, KANIANSKY, Dušan, BODOR, Róbert, JÖHNCK, Matthias and STANISLAWSKI, Bernd. Determination of organic acids and inorganic anions in wine by isotachopheresis on a planar chip. *Journal of Chromatography A*. 2001. Vol. 916, no. 1–2, p. 167–174. DOI 10.1016/S0021-9673(00)01094-3.
215. MALÁ, Zdena, GEBAUER, Petr and BOČEK, Petr. Recent progress in analytical capillary isotachopheresis. *Electrophoresis*. 2015. Vol. 36, no. 1, p. 2–14. DOI 10.1002/elps.201400337.
216. JESZKA-SKOWRON, Magdalena and ZGOŁA-GRZEŚKOWIAK, Agnieszka. Usage of Capillary Isotachopheresis and Antioxidant Capacity Measurement in Analysis of Changes in Coffee Properties After Roasting, Steaming and Decaffeination. *Food Analytical Methods*. 2017. Vol. 10, no. 5, p. 1245–1251. DOI 10.1007/s12161-016-0679-z.
217. STROHALM, Martin, HASSMAN, Martin, KOŠATA, Bedřich and KODÍČEK, Milan. mMass data miner: an open source alternative for mass spectrometric data analysis. *Rapid Communications in Mass Spectrometry* [online]. 30 March 2008. Vol. 22, no. 6, p. 905–908. DOI 10.1002/rcm.3444. Available from: <http://doi.wiley.com/10.1002/rcm.3444>
218. STROHALM, Martin, KAVAN, Daniel, NOVÁK, Petr, VOLNÝ, Michael and HAVLÍČEK, Vladimír. mMass 3: A Cross-Platform Software Environment for Precise Analysis of Mass Spectrometric Data. *Analytical Chemistry* [online]. June 2010. Vol. 82, no. 11, p. 4648–4651. DOI 10.1021/ac100818g. Available from: <http://pubs.acs.org/doi/abs/10.1021/ac100818g>
219. NIEDERMEYER, Timo H. J. and STROHALM, Martin. mMass as a Software Tool for the Annotation of Cyclic Peptide Tandem Mass Spectra. KOOMEN, John Matthew (ed.), *PLoS ONE* [online]. 13 September 2012. Vol. 7, no. 9, p. e44913. DOI 10.1371/journal.pone.0044913. Available from: <http://dx.plos.org/10.1371/journal.pone.0044913>
220. KRUBE, Anneli, KAUPMEES, Karl, LIIGAND, Jaanus, OSS, Merit and LEITO, Ivo. Sodium adduct formation efficiency in ESI source. *Journal of Mass Spectrometry*. 2013. Vol. 48, no. 6, p. 695–702. DOI 10.1002/jms.3218.
221. HOLČAPEK, Michal, JIRÁSKO, Robert and LÍSA, Miroslav. Basic rules for the interpretation of atmospheric pressure ionization mass spectra of small molecules. *Journal of Chromatography A*. 2010. Vol. 1217, no. 25, p. 3908–3921. DOI 10.1016/j.chroma.2010.02.049.
222. NATIONAL CENTER FOR BIOTECHNOLOGY INFORMATION. Sodium Benzoate. *PubChem Compound Database; CID=517055* [online]. 2018. [Accessed 30 April 2018]. Available from: <https://pubchem.ncbi.nlm.nih.gov/compound/517055>
223. KELLER, Bernd O., SUI, Jie, YOUNG, Alex B. and WHITTAL, Randy M. Interferences and contaminants encountered in modern mass spectrometry. *Analytica Chimica Acta*. 2008. Vol. 627, no. 1, p. 71–81. DOI 10.1016/j.aca.2008.04.043.
224. LI, Qun-Sheng, TIAN, Yuan-Ming and WANG, Shui. Densities and excess molar volumes for binary mixtures of 1, 4-butanediol+ 1, 2-propanediol, + 1, 3-propanediol,

- and+ ethane-1, 2-diol from (293.15 to 328.15) K. *Journal of Chemical & Engineering Data*. 2007. Vol. 53, no. 1, p. 271–274.
225. BAJIĆ, Divna M., IVANIŠ, Gorica R., VISAK, Zoran P., ŽIVKOVIĆ, Emila M., ŠERBANOVIĆ, Slobodan P. and KIJEVČANIN, Mirjana Lj. Densities, viscosities, and refractive indices of the binary systems (PEG200 + 1,2-propanediol, +1,3-propanediol) and (PEG400 + 1,2-propanediol, +1,3-propanediol) at (288.15 to 333.15) K and atmospheric pressure: Measurements and modeling. *Journal of Chemical Thermodynamics*. 2013. Vol. 57, p. 510–529. DOI 10.1016/j.jct.2012.07.024.
226. BAJIĆ, Divna M., ŽIVKOVIĆ, Emila M., ŠERBANOVIĆ, Slobodan P. and KIJEVČANIN, Mirjana Lj. Experimental measurements and modelling of volumetric properties, refractive index and viscosity of selected binary systems with butyl lactate at 288.15-323.15 K and atmospheric pressure. New UNIFAC-VISCO interaction parameters. *Thermochimica Acta*. 2013. Vol. 562, p. 42–55. DOI 10.1016/j.tca.2013.03.025.
227. KIJEVČANIN, Mirjana Lj, ŽIVKOVIĆ, Emila M., DJORDJEVIĆ, Bojan D., RADOVIĆ, Ivona R., JOVANOVIĆ, Jovan and ŠERBANOVIĆ, Slobodan P. Experimental determination and modeling of excess molar volumes, viscosities and refractive indices of the binary systems (pyridine + 1-propanol, +1,2-propanediol, +1,3-propanediol, and +glycerol). New UNIFAC-VISCO parameters determination. *Journal of Chemical Thermodynamics*. 2013. Vol. 56, p. 49–56. DOI 10.1016/j.jct.2012.06.031.
228. LEE, J. W., PARK, S. B. and LEE, H. Densities, surface tensions, and refractive indices of the water + 1,3-propanediol system. *Journal of Chemical and Engineering Data*. 2000. Vol. 45, no. 2, p. 166–168. DOI 10.1021/je990196m.
229. GEORGE, John and SASTRY, Nandhibatla V. Densities, Dynamic Viscosities, Speeds of Sound, and Relative Permittivities for Water + Alkanediols (Propane-1,2- and -1,3-diol and Butane-1,2-, -1,3-, -1,4-, and -2,3-Diol) at Different Temperatures. *Journal of Chemical and Engineering Data*. 2003. Vol. 48, no. 6, p. 1529–1539. DOI 10.1021/je0340755.
230. MOOSAVI, Mehrdad and ROSTAMI, Abbas Ali. Densities, viscosities, refractive indices, and excess properties of aqueous 1,2-ethanediol, 1,3-propanediol, 1,4-butanediol, and 1,5-pentanediol binary mixtures. *Journal of Chemical and Engineering Data*. 2017. Vol. 62, no. 1, p. 156–168. DOI 10.1021/acs.jced.6b00526.
231. MIKŠÍK, František, SKOLIL, Jan, KOTLÍK, Josef, ČÁSLAVSKÝ, Josef, MIYAZAKI, Takahiko, KOYMA, Shigeru and LEVEK, Petr. Antifreeze heat transfer fluid based on Propane-1,3-diol. In : *IEICES2017 Proceedings and Program*. Fukuoka : Kyushu University, 2017. p. 117–120.
232. DYMOND, J. H. and MALHOTRA, R. The Tait equation: 100 years on. *International Journal of Thermophysics*. 1988. Vol. 9, no. 6, p. 941–951. DOI 10.1007/BF01133262.
233. DESIGN INSTITUTE FOR PHYSICAL PROPERTIES. DIPPR 801: Chemical Database. [online]. 2018. Available from: <https://www.aiche.org/dippr>
234. REDLICH, Otto and KISTER, A. T. Thermodynamics of Nonelectrolyte Solutions - x-y-t relations in a Binary System. *Industrial & Engineering Chemistry* [online]. 1948. Vol. 40, no. 2, p. 341–345. DOI 10.1021/ie50458a035. Available from: <http://pubs.acs.org/doi/abs/10.1021/ie50458a035>

235. DE OLIVEIRA, Jaime D Gomes and REIS, João Carlos R. The two faces of the Redlich-Kister equation and the limiting partial molar volume of water in 1-aminopropan-2-ol. *Thermochimica Acta*. 2008. Vol. 468, no. 1–2, p. 119–123. DOI 10.1016/j.tca.2007.12.002.
236. TAKAHASHI, Satoru and NISHI, Nobuyuki. Hydrate Cluster Formation of Diol Compounds in Aqueous Solution. *Bulletin of the Chemical Society of Japan*. 1995. Vol. 68, no. 2, p. 539–546. DOI <https://doi.org/10.1246/bcsj.68.539>.
237. BELDA MAXIMINO, R. Viscosity and density of binary mixtures of alcohols and polyols with three carbon atoms and water: Equation for the correlation of viscosities of binary mixtures. *Physics and Chemistry of Liquids*. 2009. Vol. 47, no. 5, p. 515–529. DOI 10.1080/00319100802372114.
238. GRUNBERG, L and NISSAN, A H. The energies of vaporisation, viscosity and cohesion and the structure of liquids. *Transactions of the Faraday Society* [online]. 1949. Vol. 45, p. 125–137. DOI 10.1039/tf9494500125. Available from: <https://www.scopus.com/inward/record.uri?eid=2-s2.0-0001549023&partnerID=40&md5=519954731e84a47809dbf3e59bd28123>
239. GRUNBERG, L and NISSAN, A. Mixture law for viscosity. *Nature*. 1949. Vol. 164, no. 4175, p. 799–800. DOI 10.1038/164799b0.
240. LEDERER, E.L. Viscosity of mixtures with and without diluents. In : *Proceedings of the First World Petroleum Congress London*. London, 1933. p. 526–528.
241. LEDERER, E. L. Viscosity of Binary Mixtures. *Nature* [online]. 2 January 1937. Vol. 139, no. 3505, p. 27–28. DOI 10.1038/139027c0. Available from: <http://www.nature.com/articles/139027c0>
242. ZHMUD, Boris, PH, D and PROF, Assoc. Viscosity Blending Equations. *Lube Magazine*. June 2014. No. 5, p. 2–5.
243. HERIC, E. L. and BREWER, J. G. Viscosity of Some Binary Liquid Nonelectrolyte Mixtures. *Journal of Chemical and Engineering Data*. 1967. Vol. 12, no. 4, p. 574–583. DOI 10.1021/je60035a028.
244. ONKEN, Ulfert, FISCHER, Kai and RAREY, Jürgen. Estimation of Physical Properties. In : *Ullmann's Encyclopedia of Industrial Chemistry* [online]. Weinheim, Germany : Wiley-VCH Verlag GmbH & Co. KGaA, 2000. Available from: http://doi.wiley.com/10.1002/14356007.b01_06
245. EYRING, Henry. and HIRSCHFELDER, Joseph. The Theory of the Liquid State. *The Journal of Physical Chemistry* [online]. February 1937. Vol. 41, no. 2, p. 249–257. DOI 10.1021/j150380a007. Available from: <http://pubs.acs.org/doi/abs/10.1021/j150380a007>
246. MCALLISTER, R. A. The viscosity of liquid mixtures. *AIChE Journal*. 1960. Vol. 6, no. 3, p. 427–431. DOI 10.1002/aic.690060316.
247. IGLESIAS-SILVA, Gustavo A. and HALL, Kenneth R. Equivalence of the mcallister and heric equations for correlating the liquid viscosity of multicomponent mixtures. *Industrial and Engineering Chemistry Research*. 2010. Vol. 49, no. 13, p. 6250–6254. DOI 10.1021/ie1002763.
248. KACEM, R.B.H., ALZAMEL, N.O. and OUERFELLI, N. Sensitivity of viscosity Arrhenius parameters to polarity of liquids. *Russian Journal of Physical Chemistry A*. 2017. Vol. 91, no. 9, p. 1654–1659. DOI 10.1134/S0036024417090138.

249. ANSLYN, Eric V and DOUGHERTY, Dennis A. *Modern Physical Organic Chemistry* [online]. 2006. ISBN 9781891389313. Available from: <http://iupac.org/publications/pac/69/2/0259/>
250. DUPONT TATE&LYLE. *Susterra 1,3 Propanediol For Brewery Heat Transfer Fluids* [online]. 2016. DuPont Tate&Lyle. Available from: [http://www.duponttateandlyle.com/sites/default/files/Susterra for Brewery Heat Transfer Fluids_5 30 14_Brewery.pdf](http://www.duponttateandlyle.com/sites/default/files/Susterra%20for%20Brewery%20Heat%20Transfer%20Fluids_5%2030%2014_Brewery.pdf)
251. DUPONT TATE&LYLE. *Susterra® Propanediol : Heat Transfer Fluid is Advantaged for High Temperature Applications*. 2016. Loudon : DuPont Tate&Lyle.
252. PENRAY. HEAVY-DUTY CONVENTIONAL INHIBITOR 2792. [online]. 2018. [Accessed 1 May 2018]. Available from: <http://penray.com/products/fully-formulated-for-eg-2792/>
253. SLOCHEM TRADE S.R.O. *Bezpečnostní list Cemkor C33*. 2014. Trnava.
254. ECHEMI.COM. Propylene Glycol Market in Q3, 2017: Increased Prices and Declined Supply. *Echemi Analysis* [online]. 2017. [Accessed 1 May 2018]. Available from: <http://info.echemi.com/en-price/9031.html>
255. ECHEMI.COM. Analysis of the Ethylene Glycol Market in Q3, 2017. *Echemi Analysis* [online]. 2017. [Accessed 1 May 2018]. Available from: <http://info.echemi.com/en-price/9069.html>
256. GRAND VIEW RESEARCH, Inc. Glycols Market Analysis By Product, By Application (Automotive, HVAC, Textiles, Airline, Medical, Pipeline Maintenance Polyester Fibers & Resin, And Food & Beverage Processing), By Region, And Segment Forecasts, 2018 - 2025. *Report ID: GVR-1-68038-402-4* [online]. 2017. [Accessed 1 May 2018]. Available from: <https://www.grandviewresearch.com/industry-analysis/glycols-market>
257. MARKETSandMARKETS.COM. 1 , 3 - Propanediol (PDO) Market by Applications (PTT , Polyurethane , Cosmetic , Personal Care & Home Cleaning & Others) & Geography - Global Market Trends & Forecasts to 2021. [online]. 2015. [Accessed 3 February 2018]. Available from: <http://www.marketsandmarkets.com/Market-Reports/1-3-propanediol-pdo-market-760.html>
258. DUPONT TATE&LYLE. Susterra® 1,3-Propanediol, High-Performance, Biobased Glycol Antifreeze and Coolant. *Engine Coolants* [online]. 2016. [Accessed 2 May 2018]. Available from: http://www.duponttateandlyle.com/susterra/engine_coolant_glycol_antifreeze
259. ASTM D7388 - 08. *Standard Specification for Engine Coolant Grade 1,3-Propanediol (PDO)* [online]. 2013. West Conshohocken, PA : ASTM International. Available from: www.astm.org
260. ASTM D7515 - 09. *Standard Test Method for Purity of 1,3-Propanediol (Gas Chromatographic Method)* [online]. 2014. West Conshohocken, PA : ASTM International. Available from: www.astm.org
261. ASTM D7517 - 09. *Standard Specification for Fully-Formulated 1,3 Propanediol (PDO) Base Engine Coolant for Heavy-Duty Engines* [online]. 2014. West Conshohocken, PA : ASTM International. Available from: www.astm.org
262. GRAND VIEW RESEARCH, Inc. 1,3 Propanediol (PDO) Market Analysis By

- Application (Polytrimethylene Terephthalate (PTT), Polyurethane, Personal Care & Detergents) And Segment Forecasts To 2022. *Report ID: 978-1-68038-385-0* [online]. 2015. Available from: <https://www.grandviewresearch.com/industry-analysis/1-3-propanediol-pdo-market>
263. WILLIAMS, Robin and EDGE, David. The social shaping of technology. *ELSEVIER Research Policy*. 1996. Vol. 25, p. 865–899. DOI 10.1016/0048-7333(96)00885-2.
264. FEHER, Lambert. How will the demand for innovative, green technologies affect the future of materials and natural resources? *Materials & Natural Resources* [online]. September 2015. Available from: <https://atheneum-partners.com/how-will-the-demand-for-innovative-green-technologies-affect-the-future-of-materials-and-natural-resources/>
265. JØRGENSEN, Michael Søgaard and JØRGENSEN, Ulrik. Green technology foresight of high technology: a social shaping of technology approach to the analysis of hopes and hypes. *Technology Analysis & Strategic Management* [online]. 2009. Vol. 21, no. 3, p. 363–379. DOI 10.1080/09537320902750764. Available from: <http://www.tandfonline.com/doi/abs/10.1080/09537320902750764>

9 SYMBOLS, UNITS AND ABBREVIATIONS

9.1 Symbols and units

Mtoe	Million tons oil equivalent	V	Volume
PJ	Petajoule	C	Spring constant
kW	Kilowatt	π	Pi
MW	Megawatt	τ	Shear stress
pH	Potential of hydrogen - acidity scale	u	Flow velocity
m^2	Square meter	ν	Kinematic viscosity
kPa	Kilopascal	N	Newton
wt%	Weight percentage - mass fraction	cP	Centipoise
bar	1 bar (= 100 kPa)	cSt	Centistokes
mg	Milligram	t	Volume flow
h	Hour	v	Mean flow velocity
kg	Kilogram	R	Capillary radius
LD ₅₀	Lethal dose, 50 % (median lethal dose)	ΔP	Applied pressure – average
m^3	Cubic meter	L	Length of capillary
Mr	Molar mass	ΔH	Average head of the liquid
ρ	Density	g	Gravitational constant
mol	Mol	t	Time
g	Gram	K	Combined viscometer constant
Pa	Pascal	n	Speed of rotation
mPa	Millipascal	M	Torque
s	Second	K_D	System driving constant
T_F	Fusion/freezing point	K_R	System retarding constant
T_B	Boiling point	K	System combining constant
η	Dynamic viscosity	v	Speed of light inside a medium
n_D	Refractive index	θ	Angle of light to normal
μ	Electrophoretic mobility	f	Frequency
V	Volt	ΔG	Gibbs free energy
v	Rate of migration	ΔH	Enthalpy
E	Electric field strength	ΔS	Entropy
c	Concentration	Q	Transported energy
z	Charge	h	Step height
I_S	Working current – starting	pK_a	Dissociation constant
I_T	Working current – terminating	U	Voltage
mmol	Millimole	ΔU	Voltage change / difference
μA	Microampere	t	Time
mm	Millimetre	Δt	Time difference
ρ	Resistivity	m/z	Weight charge ration
m	Weight	kV	Kilovolt
τ	Oscillation period	vol%	Volumetric percent

q	Flow	σ	Standard deviation
L	Litre	w_i	Mass fraction
mL	Millilitre	x_i	Mole fraction
μL	Microlitre	V^E	Excess molar volume
λ	Wavelength	Y^E	Excess property (Redlich Kister)
h	Planck constant	A_k	Redlich Kister expansion fitting parameters
c	Speed of light	$\Delta\eta$	Viscosity deviation
E	Energy	g_i	Grunberg Nissan fitting parameters, interaction parameter
T	Transmittance	s	Empirical constant in Lederer's model
τ	Optical depth	ΔG^{*E}	Activation Gibbs free energy
A	Absorbance	α_i	Fitting parameters for Heric's model
e	Euler's number	ν_f	Fitting parameter for McAllister's model
Φ_e^i	Radiant flux received	$\bar{\sigma}$	Cumulative deviation
Φ_e^t	Radiant flux transmitted	η_0	Viscosity preexponential (entropic) factor
I	Intensity of transmitted light	E_a	Arrhenius activation energy
I_0	Intensity of transmitted light through blank	ε_r	Relative permittivity
l	Optical path length	N	Number of particles per volume
ε_i	Absorptivity	ε_0	Permittivity of vacuum
nm	Nanometres	α'	Polarizability volume
a_{H^+}	Hydrogen ion relative activity	α	Polarizability
E	Electrode potential	R_m	Molar refraction
E^0	Standard electrode potential	N_A	Avogadro constant
R	Gas constant	T	Temperature
F	Faraday constant	κ	Conductivity
Da	Dalton	S	Siemens
n	Water content	J	Current density

9.2 Abbreviations

AAD	Absolute average deviation
AAS	Atomic absorption spectrometry
AC	Alternating current
ASTM	American Section of the International Association for Testing Materials
BUT	Brno University of Technology
CAS	Chemical Abstracts Service
DC	Direct current
DEMO	DEMOstration Power Station
DHW	Domestic hot water
DIN	Deutsches Institut für Normung

DKI	Deutsches Kupferinstitut
E-CAT	The Energy Catalyzer
EG	Ethylene glycol (ethane-1,2-diol)
ESI	Electrospray
EU	European Union
G-N	Grunberg Nissan
HTF	Heat transfer fluid
ICSC	The International Chemical Safety Cards
IPCS	International Programme on Chemical Safety
ISO	International standard organisation
ITER	International Thermonuclear Experimental Reactor
ITP	Isotachophoresis
IUPAC	International Union of Pure and Applied Chemistry
K-F	Karl Fisher
LE	Leading electrolyte
LED	Light emitting diode
LENR	Low-energy nuclear reactions
MBT	Merkaptobenzothiazole
MEG	Monoethylene glycol (ethane-1,2-diol)
MPG	Monopropylene glycol (propane-1,2-diol)
MS	Mass spectrometry
NASA	National Aeronautics and Space Administration
OCI	Organic corrosion inhibitor
OECD	The Organisation for Economic Co-operation and Development
PDO	Propanediol (propane-1,3-diol)
PET	Polyethylene terephthalate
PG	Propylene glycol (propane-1,2-diol)
PTT	Polytrimethylene terephthalate
PUR	Polyurethane
PV	Photovoltaic
RES	Renewable energy source
RF	Radiofrequency
R-K	Redlich Kister
RSH	Relative step height
SI	International System of Units
TE	Terminating electrolyte
TOKAMAK	Toroidal'naya kamera s magnitnymi katushkami (fusion reactor)
TSS	Thermal solar system
UV	Ultraviolet

10 LISTS OF TABLES AND FIGURES

10.1 List of tables

Table 3-1. Materials mostly used for the fabrication of the solar collectors.....	19
Table 4-1. Physical properties of antifreeze additives in their pure state.....	29
Table 4-2. LD ₅₀ of the selected substances	36
Table 4-3. Approximate stagnation temperatures for different collector types ^{17,67}	39
Table 4-4. Basic physical and chemical data on propane-1,3-diol.....	41
Table 5-1. Characteristics of the experimental system Vracov.....	43
Table 5-2. Main components of the experimental system Vracov.....	44
Table 5-3. Samples from experimental thermal solar system in Vracov	44
Table 5-4. Selected samples of highly degraded HTF	45
Table 5-5. Samples of propane-1,3-diol.....	45
Table 5-6. Chemicals used for isotachopheresis	45
Table 5-7. Chemicals used for mass spectrometry	46
Table 5-8. Chemicals used for Karl Fisher titration	46
Table 5-9. Chemicals used for atomic absorption spectrometry	46
Table 5-10. Chemicals used for determination of pH	47
Table 5-11. Chemicals used for determination of conductivity	47
Table 5-12. Chemicals used for pycnometry.....	47
Table 5-13. Chemicals used for Oscillating U-tube Densitometry	47
Table 5-14. Chemicals used for Capillary Viscometry	47
Table 5-15. Chemicals used for Rotational Viscometry	47
Table 5-16. Chemicals used for refractive index measurement	48
Table 5-17. Chemicals used for freezing point measurement	48
Table 5-18. Chemicals used for corrosivity quantification	48
Table 5-19. Machine and Equipment used according to method	48
Table 5-20. Isotachopheretic analysis setting	53
Table 5-21. Mass spectrometer analysis setting.....	56
Table 5-22. Atomic absorption spectroscopy analysis setting	61
Table 5-23. Absorbance of the calibration solutions.....	62
Table 5-24. Constants for pycnometry at T = 20 °C	65
Table 5-25. Corrosion limits expressed as weight loss according to ASTM D3306	78
Table 6-1. pH measurement results	83
Table 6-2. Conductivity measurement results	84
Table 6-3. Density measurement results	85
Table 6-4. Copper concentration Results	88
Table 6-5. Selected acidic products and their Relative Step Height (RSH ₀) coefficients ..	91
Table 6-6. Results of quantitative and qualitative analysis of standard mixtures	94
Table 6-7. pH measurement for highly degraded samples SD, SJ, TS and SP.....	97
Table 6-8. Collected data and step finding results of isotachopheretic analysis.....	98
Table 6-9. Isotachopheretic quantitative analysis - results.....	102
Table 6-10. Some common adducts created by electrospray ²²¹	104
Table 6-11. Identified chemicals in the examined samples.....	106
Table 6-12. List of organic acid degradation products intended for MS look-up.....	114

Table 6-13. Karl Fisher titration results	117
Table 6-14. Experimental values of density ρ [$\text{g}\cdot\text{cm}^{-3}$] for propane-1,3-diol	120
Table 6-15. Density models constants for pure propane-1,3-diol	122
Table 6-16. Excess molar volumes V^E [$\text{cm}^3\cdot\text{mol}^{-1}$] for aqueous propane-1,3-diol	123
Table 6-17. Redlich-Kister fitting variables for excess molar volume	123
Table 6-18. Experimental values of dynamic viscosity η [$\text{mPa}\cdot\text{s}$] for propane-1,3-diol ..	125
Table 6-19. Dynamic viscosity deviations for propane-1,3-diol	127
Table 6-20. Redlich-Kister coefficients for dynamic viscosity deviation	129
Table 6-21. Fitting parameters for viscosity models: molar-fraction	136
Table 6-22. Fitting parameters for viscosity models: mass-fraction	137
Table 6-23. Absolute average deviation – AAD [%] of combined viscosity models	138
Table 6-24. Experimental values of refractive indices for propane-1,3-diol	140
Table 6-25. Freezing points of aqueous propane-1,3-diol	143

10.2 List of figures

Fig. 3-1 Primary energy sources by fuel - global composition 2000 and 2014 ⁴	9
Fig. 3-2 Electricity sources - global composition ⁴	10
Fig. 3-3 Energy sources by their origin	10
Fig. 3-4 Structure and use of planetary forces	11
Fig. 3-5 Structure and use of nuclear energy	12
Fig. 3-6 Structure and use of solar energy	13
Fig. 3-7 Concentrating solar power plant Planta Solar 10 (11 MWp) in Seville, Spain ¹⁴ ...	15
Fig. 3-8 Structure of energy consumption in the European household ¹⁵	16
Fig. 3-9 Structure of energy consumption in the European households by country ¹⁵	16
Fig. 3-10 Schema of a basic two-circuit thermal solar system	17
Fig. 3-11 The structure of a flat-type solar collector	19
Fig. 3-12 Transfer pipe (corrugated stainless-steel pipe) encased in insulating material...	20
Fig. 3-13 Plate exchanger design	21
Fig. 3-14 The circulator pump ³¹	22
Fig. 4-1 Structural formula of selected glycols.	26
Fig. 4-2 Comparison of fusion point of some antifreeze additives.	30
Fig. 4-3 Efficiency of solar systems, depending on the heat transfer medium ⁴³	31
Fig. 4-4 Kinematic viscosity of binary mixture propane-1,2-diol/water ⁴³	31
Fig. 4-5 Ethane-1,2-diol production from ethene	37
Fig. 4-6 Propane-1,2-diol production from 2-methyloxirane	37
Fig. 4-7 Evacuation ability of different design solution, good (top), bad (bottom) ⁸²	39
Fig. 4-8 Propane-1,3-diol 3D structural model	41
Fig. 4-9 Poly(trimethylene terephthalate)	42
Fig. 5-1 Position of Vracov, Czech Republic	43
Fig. 5-2 Isotachophoresis - principle diagram	51
Fig. 5-3 Isotachophoresis - quantitative and qualitative analysis	52
Fig. 5-4 MS – Electrospray ionization diagram and principle (Agilent) ¹⁴⁴	55
Fig. 5-5 MS – Spherical Ion Trap schema ¹⁴⁰ and Mathieu stability diagram ¹⁴³	55
Fig. 5-6 Mass spectrometry – Agilent 6300 series system diagram ¹⁴⁰	56
Fig. 5-7 Syringe infusion pump KDS 100 ¹⁴⁵	57
Fig. 5-8 Karl Fisher titration – basic apparatus ¹⁴⁹ and titration progress diagram ¹⁵⁰	58

Fig. 5-9 Atomic Absorption Spectroscopy – system diagram ¹⁵⁵	59
Fig. 5-10 AAS - calibration dependences for Cu, Fe and Pb	61
Fig. 5-11 Schema of a typical combined glass electrodes for pH determination ¹⁶¹	63
Fig. 5-12 Pycnometer – 25 mL/20 °C ¹⁶⁸	65
Fig. 5-13 Oscillating U-tube density meter – principle of function ¹⁶⁹	66
Fig. 5-14 Parallel flow in a straight pipe	68
Fig. 5-15 Common U-tube viscometers ¹⁷⁵	69
Fig. 5-16 Ubbelohde viscometer according to DIN 51 562 Part 1 and ISO DIS 3105	70
Fig. 5-17 Stabinger Viscometer™ viscosity measuring principle ¹⁸¹	71
Fig. 5-18 Refraction in water and Refractive index definition.....	74
Fig. 5-19 Refractometry – principle of measurement ¹⁸⁸	75
Fig. 5-20 Freezing point measurement – temperature development over time	76
Fig. 5-21 Corrosion test apparatus as described in the ASTM D1384 ¹¹⁵	77
Fig. 5-22 Automatic Ubbelohde viscometer – IR pair sensor positioning	80
Fig. 6-1 Cumulative energy production (transported) in Vracov system	81
Fig. 6-2 Weekly energy production (transported) in Vracov system	82
Fig. 6-3 pH comparison of unused and used HTFs from experimental system	83
Fig. 6-4 Conductivity comparison of unused and used HTFs from experimental system ..	84
Fig. 6-5 Density comparison of unused and used HTFs from the experimental system.....	86
Fig. 6-6 Kinematic viscosity of the unused and used HTFs from the experimental system	86
Fig. 6-7 Dipropylene glycol isomers - products of condensation reaction of MPG.....	87
Fig. 6-8 MS peak of dipropylene glycol (top) and its isotopic pattern (bottom).....	87
Fig. 6-9 Development of copper concentration and comparison to unused samples	89
Fig. 6-10 Isotachophoregrams of individual standards of organic acids for analysis	92
Fig. 6-11 Isotachophoregrams of mixed standard, u* - unknown/impurities.....	93
Fig. 6-12 Degradation process of propane-1,2-diol through C ₂ thermal oxidation.....	95
Fig. 6-13 Degradation process of propane-1,2-diol through C ₁ thermal oxidation.....	95
Fig. 6-14 Examples of real samples analysis results	96
Fig. 6-15 ITP step detection times of sample SD for different standard additions	99
Fig. 6-16 ITP step detection times of sample SJ for different standard additions.....	100
Fig. 6-17 ITP step detection times of TS for different standard additions (to 1 µL).....	101
Fig. 6-18 Organic acid content - comparison of analysed samples	103
Fig. 6-19 Comparison of the same sample with and without acetic acid addition	104
Fig. 6-20 Intensity enhancement of sebacic acid by acidifying – protonating.....	105
Fig. 6-21 Sebacic acid detection and isotopic distribution.....	107
Fig. 6-22 Propane-1,2-diol detection and isotopic peak distribution	107
Fig. 6-23 Dipropylene and tripropylene glycol detection and isotopic distribution.....	108
Fig. 6-24 Tolyltriazole detection and isotopic distribution	108
Fig. 6-25 Sodium benzoate detection and isotopic distribution	109
Fig. 6-26 Change of relative peak intensity on traced substances.....	110
Fig. 6-27 Overview of main components in Solaren HTF	111
Fig. 6-28 Comparison of new and old formula	111
Fig. 6-29 Comparison of highly degraded fluids samples SP and SJ with original	112
Fig. 6-30 Formation of additional acetal/ketal degradation products.....	113
Fig. 6-31 Organic acid products identification on sample TS.....	113
Fig. 6-32 Comparison of original fluid and after 1 and 7 years	115

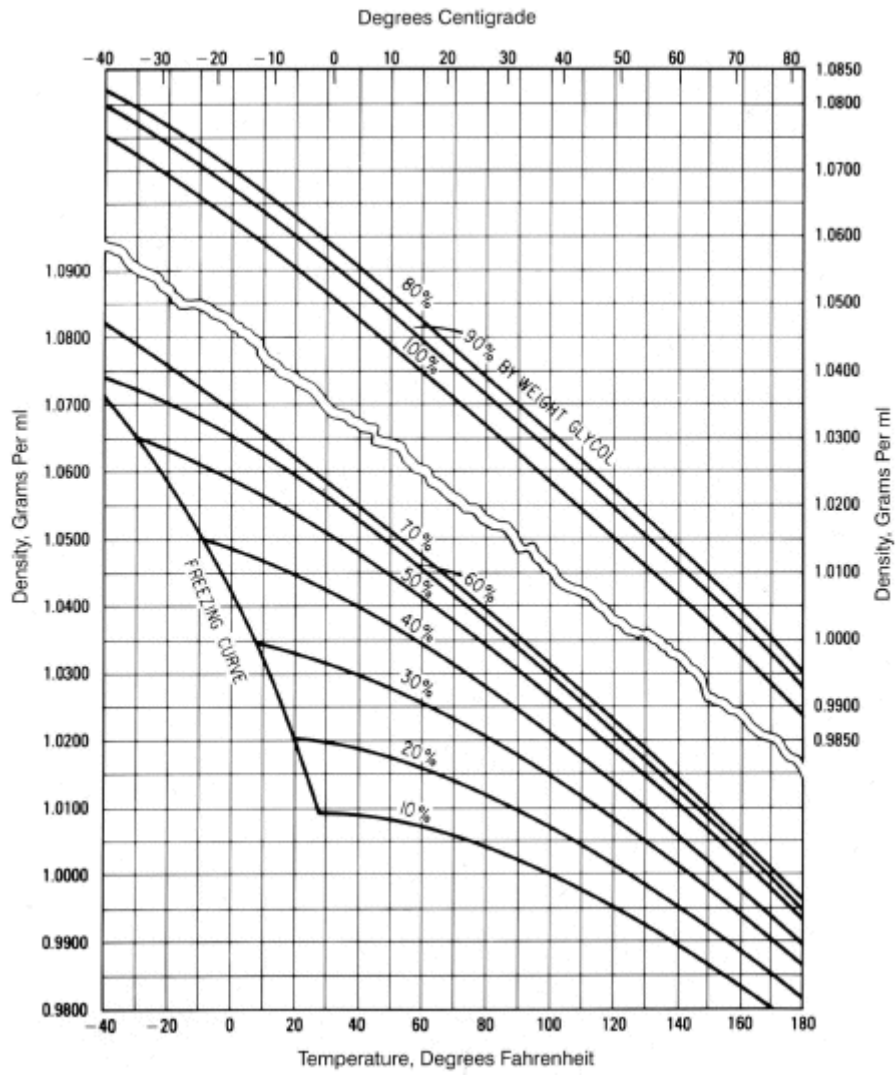
Fig. 6-33 Selected peak rows with identical difference of 44 Da.....	116
Fig. 6-34 Water content according to Karl Fisher titration	118
Fig. 6-35 Density of propane-1,3-diol on mass fraction (top) and temperature (bottom). 121	
Fig. 6-36 Excess molar volume and R-K fitting (top), R-K parameters (bottom)	124
Fig. 6-37 Dynamic viscosity of propane-1,3-diol, temperature (top), w_i (bottom).....	126
Fig. 6-38 Dynamic viscosity deviation and R-K fitting (top), R-K parameters (bottom). 128	
Fig. 6-39 Comparison of viscosity models with literature ^{1-230,2-229,3-237}	132
Fig. 6-40 Combined viscosity models (I) in comparison with experimental data.....	134
Fig. 6-41 Combined viscosity models (II) in comparison with experimental data	135
Fig. 6-42 Comparison of the Lederer's combined model with literature ^{1-230, 2-229, 3-237}	138
Fig. 6-43 Refractive index of aqueous propane-1,3-diol.....	141
Fig. 6-44 Polarizability (left) and molar Refraction of water and propane-1,3-diol	142
Fig. 6-45 Freezing point of aqueous propane-1,3-diol in comparison with literature ²⁵⁰ ...	142
Fig. 6-46 Corrosion test of aqueous propane-1,3-diol according to ASTM D1384.....	144
Fig. 6-47 Ethane-1,2-diol import volume (China) and average market price ²⁵⁵	145
Fig. 6-48 Propane-1,2-diol import volume (China) and average market price ²⁵⁴	146
Fig. 6-49 Market volume of propane-1,3-diol by application (prediction 2015+) ²⁶²	146

11 LIST OF APPENDICES

A-1 Propane-1,2-diol density diagram	181
A-2 Samples visualization – Vracov experimental system	182
A-3 Samples visualisation – Highly degraded samples	183
A-4 Corrosion examples	184
A-5 Automatic Ubbelohde viscometer – photodocumentation	185
A-6 Sebacic acid additional adducts.....	186
A-7 Detailed MS analysis of VO2007.....	187
A-8 Additional MS spectra for polymer-like contamination	188
A-9 Additional MS spectra.....	189

12 APPENDICES

A-1 PROPANE-1,2-DIOL DENSITY DIAGRAM



A-2 SAMPLES VISUALIZATION – VRACOV EXPERIMENTAL SYSTEM



Sample VO2007



Sample V2007



Sample V2008



Sample V2009



Sample V2013



Sample V2014

A-3 SAMPLES VISUALISATION – HIGHLY DEGRADED SAMPLES



Sample SD



Sample SD - settled



Sample SJ



Sample SP



Sample TS

A-4 CORROSION EXAMPLES

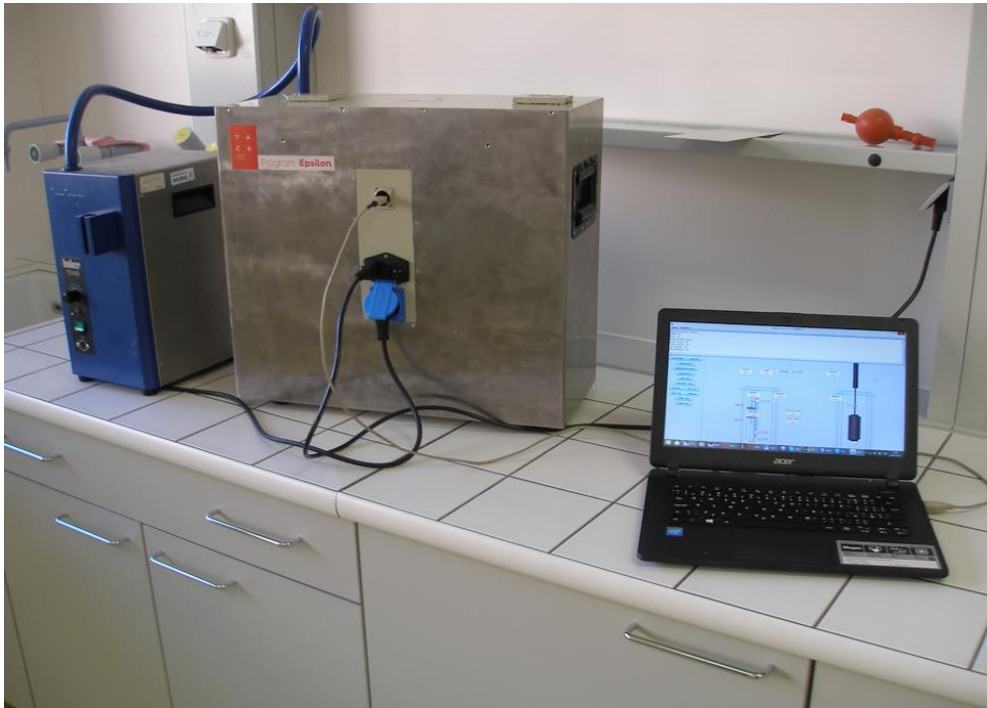


Pitting corrosion – Diesel motor cylinder liner

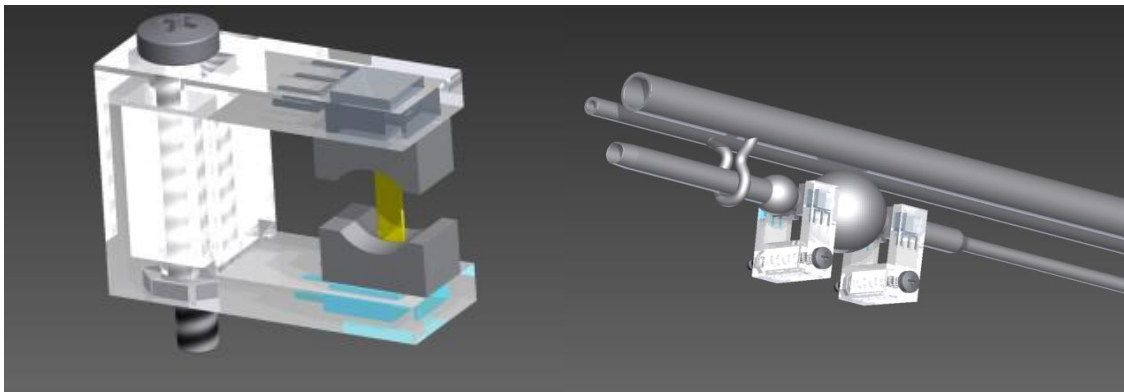


Corrosion – areal corrosion – Diesel motor cylinder liner

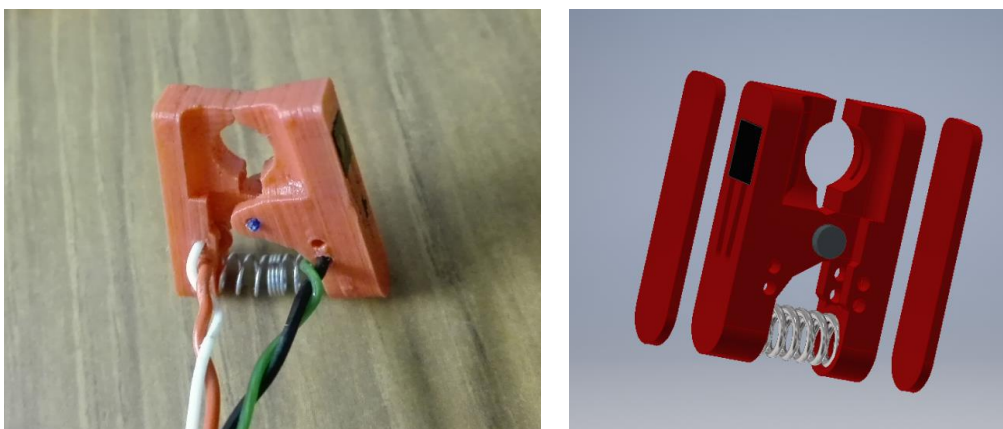
A-5 AUTOMATIC UBBELOHDE VISCOMETER – PHOTODOCUMENTATION



Automatic Ubbelohde viscometer – connected to immersion cooler Huber

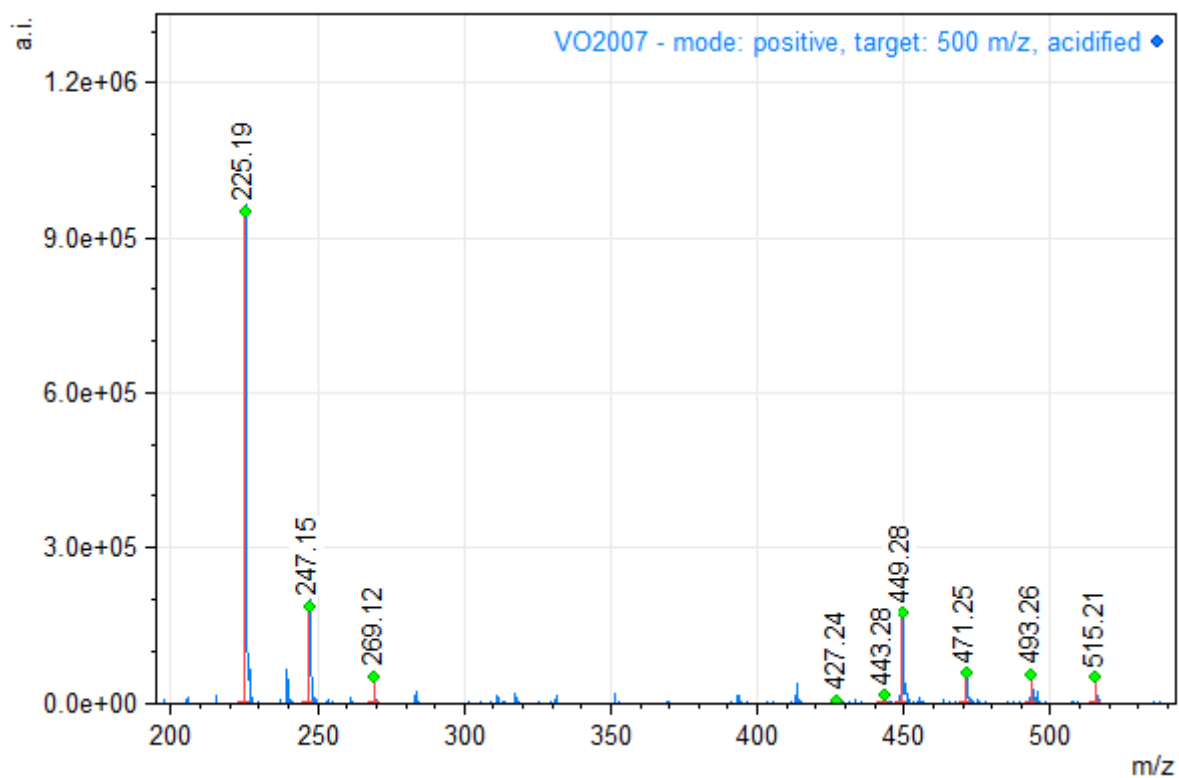


First version of IR sensor pair and its position on the Ubbelohde viscometer



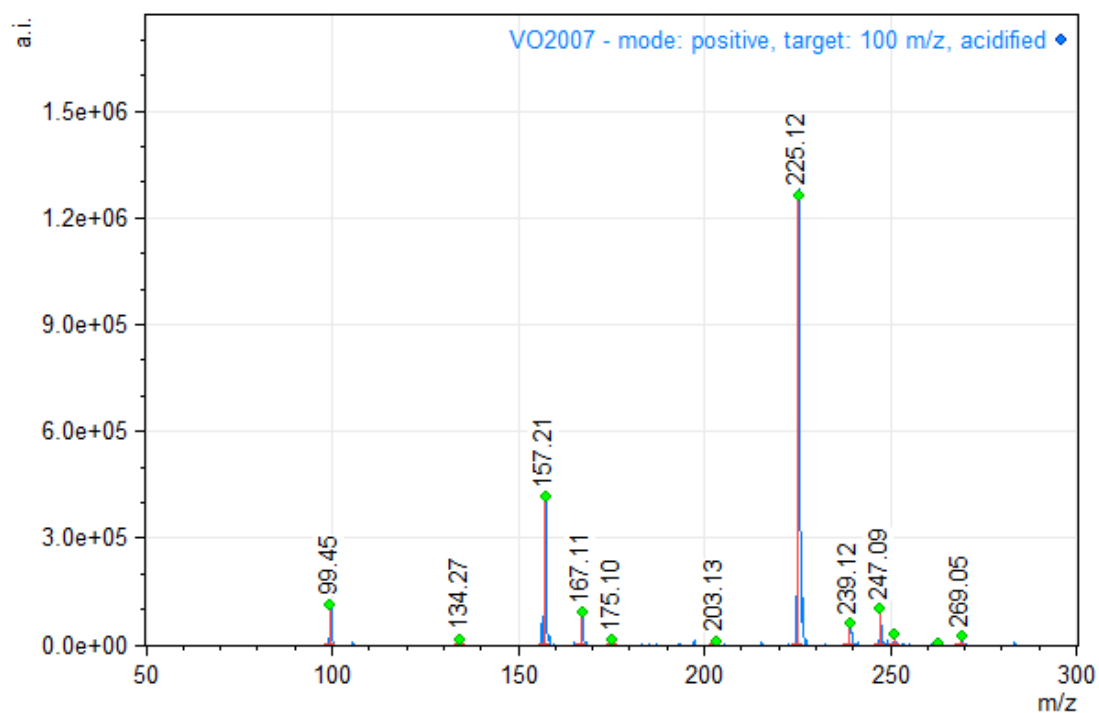
Second version of IR sensor pair

A-6 SEBACIC ACID ADDITIONAL ADDUCTS



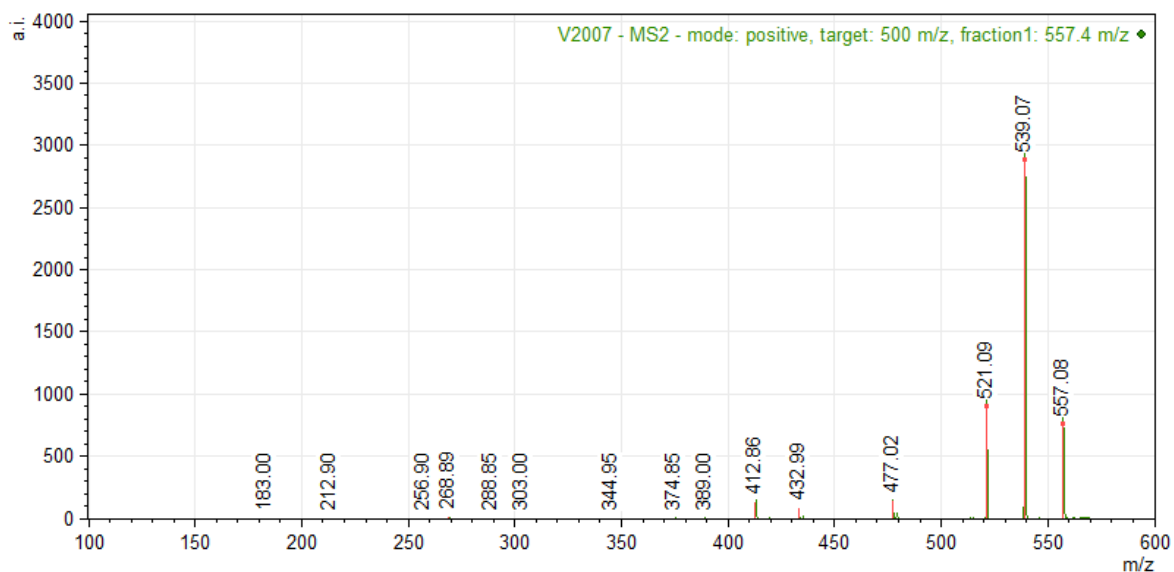
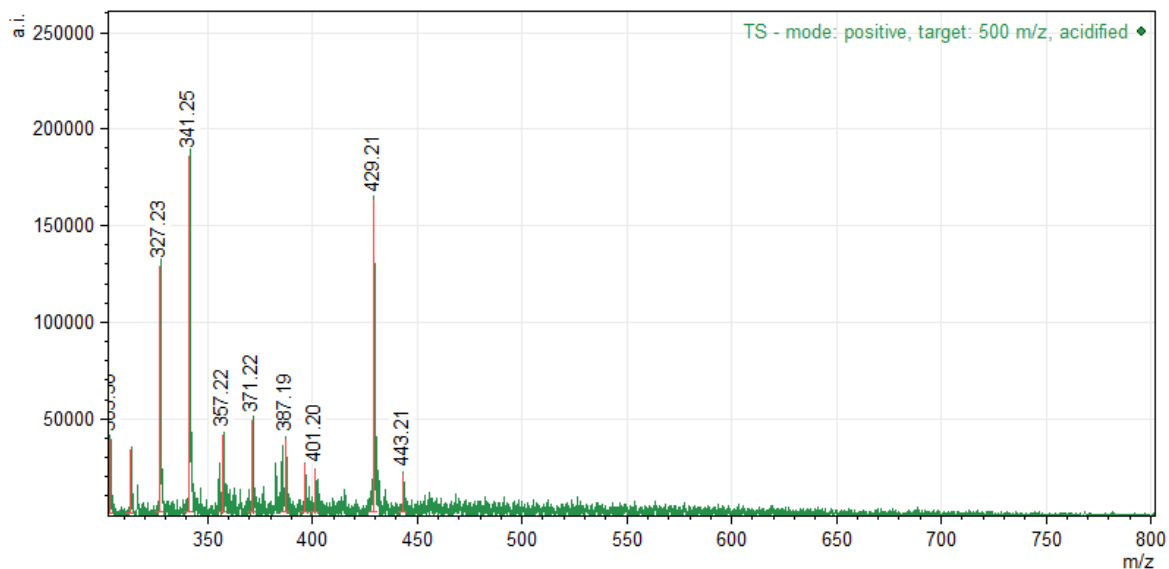
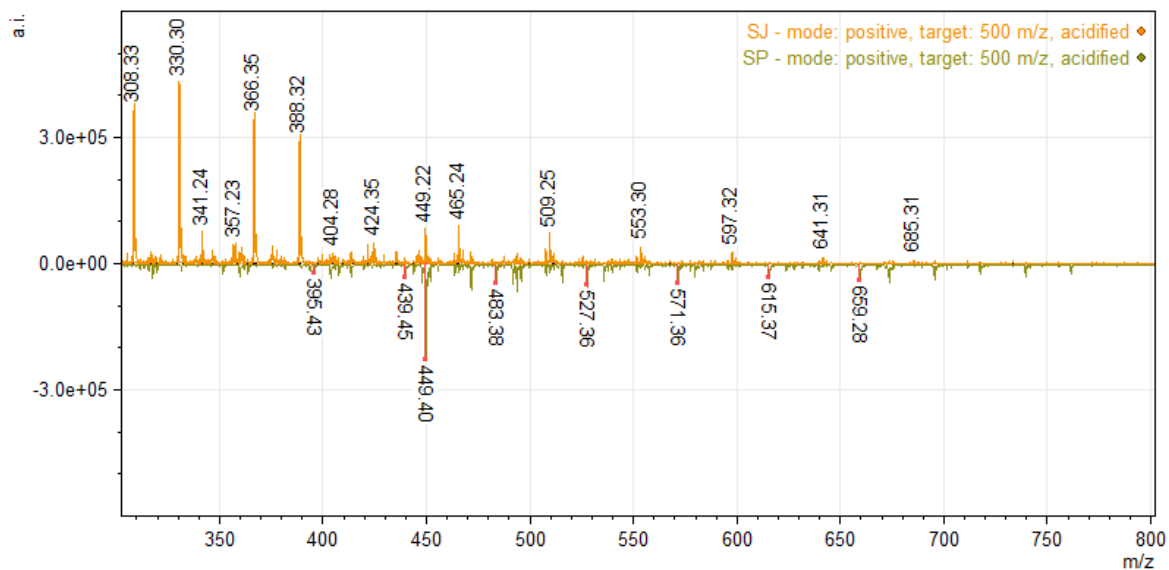
Meas. m/z	Calc. m/z	δ (Da)	δ (ppm)	Int.	Rel. Int. (%)	z	Annotation	Formula
225.19	225.11	0.08	368.2	951352	100.00	1	Sebacic acid + Sodium Sebacate	C10H16O4NaH
247.15	247.09	0.06	238.6	187973	19.76	1	Sodium Sebacate + Disodium Sebacate	C10H16O4Na2
269.12	269.07	0.05	187.6	51945	5.46	1	Disodium Sebacate	C10H15O4Na3
427.24	427.23	0.01	13.3	5196	0.55	1	Sebacic acid 2xM	(C10H18O4)2Na(H-1)
443.28	443.20	0.08	182.0	14691	1.54	1	Sebacic acid 2xM	(C10H18O4)2K(H-1)
449.28	449.21	0.07	155.1	173830	18.27	1	Sodium Sebacate 2xM	(C10H17O4Na)2
471.25	471.19	0.06	127.5	56526	5.94	1	Sodium Sebacate 2xM	(C10H17O4Na)2Na(H-1)
493.26	493.18	0.08	165.2	55276	5.81	1	Disodium Sebacate 2xM	(C10H16O4Na2)2
515.21	515.16	0.05	98.5	49984	5.25	1	Disodium Sebacate 2xM	(C10H16O4Na2)2Na(H-1)

A-7 DETAILED MS ANALYSIS OF VO2007



Meas. m/z	Calc. m/z	δ (Da)	δ (ppm)	Int.	Rel. Int. (%)	z	Annotation	Formula
99.45	99.04	0.41	4167.4	114419	9.06	1	Propane-1,2-diol (Na)	C3H8O2(Na)(H-1)
134.27	134.07	0.20	1517.4	17315	1.37	1	Tolyltriazol	C7H7N3
157.21	157.08	0.13	814.3	416704	32.99	1	2-(2-hydroxypropoxy)propan-1-ol (Na)	C6H14O3(Na)(H-1)
167.11	167.01	0.10	602.6	91433	7.24	1	Sodium Benzoate (Na)	C7H5O2Na(Na)(H-1)
175.10	175.09	0.01	60.7	14761	1.17	1	2x(Propane-1,2-diol) (Na)	(C3H8O2)2(Na)(H-1)
203.13	203.13	0.00	4.2	10633	0.84	1	Sebacic acid	C10H18O4
225.12	225.11	0.01	60.1	1263054	100.00	1	Sodium Sebacate	C10H17O4Na
225.12	225.11	0.01	60.1	1263054	100.00	1	Sebacic acid (Na)	C10H18O4(Na)(H-1)
239.12	239.10	0.02	68.2	59941	4.75	1	2x(Benzotriazole)	(C6H5N3)2
247.09	247.09	-0.00	-20.1	101236	8.02	1	Disodium Sebacate	C10H16O4Na2
247.09	247.09	-0.00	-20.1	101236	8.02	1	Sodium Sebacate (Na)	C10H17O4Na(Na)(H-1)
251.04	251.15	-0.11	-433.0	31223	2.47	1	3x(Propane-1,2-diol) (Na adduct)	(C3H8O2)3(Na)(H-1)
263.02	263.07	-0.05	-184.4	2725	0.22	1	Sodium Sebacate (K)	C10H17O4Na(K)(H-1)
269.05	269.07	-0.03	-95.8	25211	2.00	1	Disodium Sebacate (Na)	C10H16O4Na2(Na)(H-1)
269.05	269.20	-0.15	-549.9	25211	2.00	1	2x(2-(2-hydroxypropoxy)propan-1-ol)	(C6H14O3)2

A-8 ADDITIONAL MS SPECTRA FOR POLYMER-LIKE CONTAMINATION



A-9 ADDITIONAL MS SPECTRA

